Spring 4-28-2020

Modeling and Simulation of Stochastic Neutron and Cumulative Deposited Fission Energy Distributions

Patrick O'Rourke
Doctoral Student, Nuclear Engineering

Patrick Francis O'Rourke

Candidate

Nuclear Engineering

Department

This dissertation is approved, and it is acceptable in quality and form for publication:

Approved by the Dissertation Committee:

Prof. Anil Prinja — Chair

Dr. Forrest Brown

Prof. Christopher Perfetti

Prof. Dimiter Petsev

Dr. Erin Davis

Modeling and Simulation of Stochastic Neutron and Cumulative Deposited Fission Energy Distributions

by

Patrick F. O'Rourke

B.S., Nuclear Engineering, University of New Mexico, 2015

DISSERTATION

Submitted in Partial Fulfillment of the

Requirements for the Degree of

Doctor of Philosophy

Engineering

The University of New Mexico

Albuquerque, New Mexico

May, 2020

Dedication

To mom.

"And in the end, the love you take is equal to the love you make"

Acknowledgments

Foremost, I would like to thank Dr. Anil Prinja for imparting on me a fragment of his boundless knowledge regarding stochastic neutron transport and many topics on life. Dr. Prinja's patience, teaching ability, and mentorship were essential in helping me to produce this dissertation. I am grateful to Erin Davis for her mentorship at LANL and for teaching me neutron transport and many of the numerical methods used throughout this document. I wish to thank my committee for their insight, guidance, and willingness to study this dissertation. I am indebted to Scott Ramsey of LANL for providing me with a workspace which undoubtedly increased the quality of this dissertation. I am beholden to the unconditional support of my mother, Christina Aulbach, my grandmothers, Barbara and Margaret, my siblings, Brigid, Thomas, Lexy, and Erin and my closest friends, James Cole and Randy Light. I must thank my grandfather, Albert Aulbach, for inspiring me to become an engineer in the first place and for whom I would not be the man I am today. Finally, I simply wish to say I miss you, grandpa Michael.

Modeling and Simulation of Stochastic Neutron and Cumulative Deposited Fission Energy Distributions

by

Patrick F. O'Rourke

B.S., Nuclear Engineering, University of New Mexico, 2015

Ph.D., Engineering, University of New Mexico, 2020

Abstract

Methods of stochastic neutron transport are investigated and applied to novel formulations for the neutron number distribution and the cumulative fission energy deposition distribution. We utilize two Monte Carlo algorithms: the event-based Monte Carlo (EBMC) method and the Stochastic Simulation Algorithm (SSA) to benchmark and analyze systems. We show that the SSA outperforms the EBMC for the parameter space we are interested in. We then utilize the SSA to analyze systems composed of multiple spherical regions with fast and thermal neutrons with time-dependent reactivity insertions and determine whether group-dependent number distributions approach a gamma distribution. We develop two methods for calculating the geometry-dependent transfer probabilities, the View Factor Approximation and the Sphere Point Picking Monte Carlo Method, and compare the parametric space for which the computationally superior VF approximation holds.

We discuss several numerical solution methods that have been developed for solving the nonlinear adjoint transport equation satisfied by the neutron survival

probability. We show the primary competitive direct solution referred to as the λ-Acceleration Method (λAM), and introduce a new indirect solution method called the Eigenfunction Expansion Method (EFE). The space-angle shape of the solution in a nonhomogeneous planar medium equilibrate rapidly after the initiation of a chain and for practical purposes 3 modes are sufficient to accurately capture the time variation of the survival probability, with a full fission neutron multiplicity distribution, while just 1 mode gives acceptable accuracy in steady state. The order of the nonlinearity, correlated to the induced fission chain branching, has a larger effect on the solution than the number of modes retained in the expansion. In particular, the quadratic approximation, corresponding to truncation order 2 in the nonlinear fission branching terms, is accurate for near critical systems but nonlinearity orders of 4 to 5 are necessary for more strongly supercritical media. Comparison of numerical results against the λAM establish the quantitative accuracy and computational efficiency achievable with the EFE approach.

We derive space, angle, and time-dependent single chain a source equations for the cumulative energy deposition distribution (the FPDF) in a system via the backward Master equation formulation; from which, equations of the moments are also derived. This new formulation has the benefit of not requiring knowledge of the neutron number distribution. We then compare results of the EBMC method with the direct numerical solution of the moment equations and show excellent agreement. We then show that by altering the induced fission energy deposition distribution, the first four moments are virtually the same for supercritical systems. It is shown that the FPDF itself does indeed have noticeable alterations in the high energy deposition tails of the distribution, suggesting that one may need to consider higher order moments in order to witness a noticeable difference in the respective profile. It was also shown that the multiplicity distribution model being used, where we compared the full distribution with the MCNP mean-preserving model, has an effect on the higher energy deposition region of the single chain FPDF.

Finally, we formulate the Boltzmann Master equation- a novel nonlinear adjoint transport equation satisfied by the neutron number density distribution. In a lumped system setting, we consider several numerical discretization schemes for the number distribution, which show that typical basis and test functions used in transport methods are not robust. We apply the collocation method as well as derive an analytical generalization of Bell's distribution via solution ansatz. We then expand our scope to include space and angle dependence, derived systems of equations for the aforementioned discretization schemes, and compared the results, showing excellent agreement for long enough times in supercritical systems with the Quadratic Approximation applied.

Contents

List of Figures

List of Tables

Chapter 1

Introduction

Throughout the design process of any system containing fissile material, one must address the possibility that such a system may unpredictably occupy undesirable states that may pose a threat to a system's integrity and, more importantly, to human life. The primary mechanism that will usher a neutron-multiplying system into an undesirable state is usually due to the unpredictable growth of the neutron population and the ensuing induced fission reactions which propagate the fission chain as well as deposit thermal energy into the system. The topics of this dissertation concern the characterization of such systems- systems for which the neutron population behaves stochastically; i.e., for which the mean of the neutron population is not necessarily representative of the true population at a given moment in time. To characterize these types of systems, we must consider methods for determining the probability distribution function (PDF) of the neutron population number and a related quantity of interest referred to as the cumulative fission energy deposition distribution. Systems for which the studies herein are applicable include: criticality excursions in spent fuel storage and in the handling of fissile solutions in fuel fabrication and reprocessing; approach to critical under suboptimal reactor start-up conditions; preinitiation in fast burst research reactors; and weak nuclear signatures in the passive detection of nuclear materials.

In his classic 1963 paper, Bell obtained analytical expressions for the PDF of the neutron number in a zero-dimensional supercritical multiplying assembly for a single neutron chain as well as for a system containing a constant randomly emitting neutron source [3]. In short, these expressions were obtained under the assumption that the population was large and could therefore be treated as a continuous variable and the nonlinear terms of the dictating equation need not be greater than second order (known as the Quadratic Approximation). Later, Prinja and Souto derived single chain and source neutron number PDFs for the discrete neutron number using the Quadratic Approximation- generalizing Bell's distributions [11, 12]. These lumped model distributions, and others that have been developed [13, 14, 15], are utilized as benchmarks for codes that have been developed to analyze systems of interest, for example in the development of a Monte Carlo code to verify a deterministic code [16].

In Chapter 2, we introduce the lumped forward Master equation formulation and the analytical solution process as outlined by Bell and Prinja and Souto, providing the analytical PDFs used in practice. Further, we obtain analytical solutions without using the Quadratic Approximation, which is a mathematical approximation, but rather by restricting the fundamental physics of the neutron multiplicity. This novel PDF is useful for benchmarking codes for systems in which the Quadratic Approximation is invalid due to low neutron numbers and/or short time intervals.

In Chapter 3, we cover two Monte Carlo methods that may be employed in simulating the evolution and behavior of the neutron population in systems of interest referred to as the Event-Based Monte Carlo (EBMC) method and the Stochastic Simulation Algorithm (SSA). The EBMC method is widely used in production codes, such as MCNP, and the SSA was developed by Gillespie for the study of the dynamics of chemical reactions [37], although the fundamentals had been known since the 1940s with work done by Bartlett [38]. The SSA samples time intervals between interactions and the resultant outcomes based on the reaction rates of the particle populations, whereas the EBMC simulates a single particle's random walk by sampling time

intervals to collision events. Both methods are used throughout this document to study systems or to verify/benchmark other methods we explore.

In Chapter 4, we investigate systems that are composed of regions that are physically separated and we allow the neutron populations to populate different energy groups. We begin the chapter by deriving the relevant coupled first-order ODEs for the moments of the respective neutron populations. We then develop several methods for calculating the probability that the neutrons will leak and transfer from one region to another. Of particular interest is determining if systems that are in close enough proximity will drive each other's neutron populations and if those populations may be modeled using known distribution types, such as Bell's distribution, which is a gamma distribution. We conclude the chapter by simulating systems that have a time-dependent reactivity insertion and the behavior of the neutron number distribution for such scenarios.

In Chapter 5, we replicate Bell's expansive 1965 work which incorporated spatial, angular, and energy dependence, along with time-dependence, on the neutron number PDF [18]. By conducting a probability balance in the first collisional interval, referred to as the Backward Formulation, and applying the probability generating function transform, Bell obtained a nonlinear adjoint Boltzmann-like transport equation, from which several probabilistic quantities of interest may be extracted, namely the probability of extinction of a neutron chain, it's complement, the probability of survival, and the time-asymptotic limit of the survival probability, the probability of initiation, or POI. Unbeknownst to Bell at the time, Pál had also derived a similar equation [19], a few years prior in Hungarian, but he favored using a moment generating function rather than the probability generating function. Originally procured by Feynman, equations for the POI were shown to satisfy a special case of the nonlinear generating function equation [23], and, with the advent of the S_N method devised by Carlson [24], in 1955 Goad implemented a one-speed code to

numerically obtain the POI, which was a straightforward adaptation of the DSN code [25]. Unfortunately, this solution method is slowly convergent for small POI values corresponding to slightly supercritical systems. Therefore, Bell and Lee then chronicled their development of an acceleration scheme [26, 27] for the solution of the multigroup POI equation based on stringent global probability conservation, resulting in the SNP code. This acceleration scheme was then generalized to efficiently solve the time-dependent survival probability equation by Baker [28], allowing for detailed calculations of systems with transient reactivity insertions in the PARTISN code [35]. We cover these principle equations of interest in the phase-space setting in Chapter 5, followed by several numerical solution methods in Chapter 6.

Work has recently been conducted in determining the full phase-space cumulative fission number PDF following the backward formulation [45], as well as the correlated moments and coupled analytical solutions in lumped systems [15, 44]. We demonstrate in Chapter 7 that an equation for the cumulative fission energy deposited due to neutron interactions, referred to as the FPDF, may be obtained using the backward formulation which is decoupled from the neutron number distribution. In other words, the backward formulation permits us to write an equation for the FPDF without knowledge of the neutron number distribution. The distribution of total fission energy deposition is of tantamount interest as this quantity is directly related to the thermal energy deposited within the system, and therefore allows one to predict the system behavior response due to neutron chain reactions. Once the FPDF is known for a time-interval of interest, the thermal-mechanical energy being deposited is known, one may utilize thermodynamic and power models to allow for the inclusion of time-dependent feedback mechanisms [46] that are commonly a concern in characterizing the overall state, and safety, of a fissile system.

Recently, Saxby et al. demonstrated a labor-intensive methodology for obtaining the full phase-space neutron number PDF in spherical systems [41], the process of which requires solving the survival probability equation as well as an equation for each

neutron number probability, which is unidirectionally coupled to all lower population number solutions. The topic of Chapter 8 seeks to expedite the solution process by treating the neutron population variable as a continuous one, developing a system of nonlinearly coupled Boltzmann Master equations for the neutron number PDF and to then solve said system.

Chapter 2

Modeling Stochastic Neutron Populations in Lumped Systems

In this chapter, we derive equations for determining the neutron number probability distribution function in lumped (no phase-space dependence) systems. There are two primary formulations that are employed in practice, known as the Forward Formulation and the Backward Formulation, both resulting in differential Chapman-Kolmogorov (CK) equations. In the lumped setting, there is no advantage one formulation has over the other and the choice in which to use is merely based on preference. We begin this chapter with a discussion on the basic physical nuclear processes and notation in Sec. 2.1, followed by an exploration between the relationship of the forward and backward formulations in Sec. 2.2. The remainder of the chapter exclusively concerns the forward formulation as a means of garnering analytical equations for the neutron number PDF, but the backward formulation is necessary in later chapters when we expand to phase-space dependence. The chapter concludes with a discussion on the asymptotic limits of the PDFs in Sec. 2.6 followed by a demonstration of obtaining closed-form expressions for the moments of the PDFs in Sec. 2.7.

2.1 Introductory Concepts and Notation

We consider zero-dimensional systems composed of material that free neutrons may interact with which may also contain an intrinsic neutron source. The primary interactions to consider are those that remove neutrons from or introduce neutrons to the system; these mutually exclusive events are the processes known as radiative capture, leakage, induced fission (IF), and spontaneous fission (SF). The system may be characterized by reaction rates, λ_x, that are defined as the probability per neutron per unit time that the particular event x will occur and a source, S, is defined as the probability that a source event may occur per unit time. In a lumped one energy group setting, the reaction rates at a given time, t, are typically calculated using the macroscopic cross section for reaction x, Σ_x, and the neutron velocity, v, as

$$\lambda_x(t) = v\Sigma_x(t), \tag{2.1}$$

where we will use the subscripts $x = \{c, f\}$ for capture and induced fission, and we will be required to consider assumed geometric features of the system to determine the leakage rate, $\lambda_\ell(t)$. More sophisticated lumped reaction rate calculation methods will be discussed in a later chapter of this document when such considerations are relevant. We note that the absorption reaction rate is the sum of the capture and induced fission rates and the total reaction rate is then the absorption added with the leakage rate:

$$\lambda_a(t) = \lambda_c(t) + \lambda_f(t) \tag{2.2a}$$

$$\lambda_t(t) = \lambda_a(t) + \lambda_\ell(t) \tag{2.2b}$$

$$\tau(t) = \frac{1}{\lambda_t(t)}, \tag{2.2c}$$

where we have introduced τ as the neutron lifetime. We may also calculate the intrinsic source for a given system with mass m which may be composed of any number of isotopes that may undergo radioactive decay using the formula

$$S = mN_A \sum_i \frac{p_{sp,i}\lambda_i w_i}{M_i}, \tag{2.3}$$

where N_A is Avogadro's Constant, $p_{sp,i}$ is the probability that a radioactive decay of isotope i is a spontaneous fission event, λ_i is the radioactive decay constant, w_i is i's weight fraction, and M_i is the molar mass.

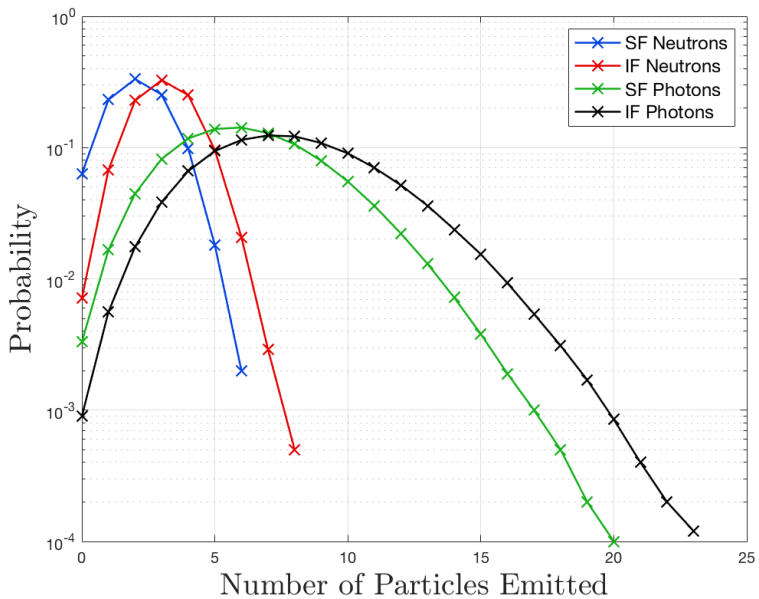

Figure 2.1: Particle multiplicity distributions for a Pu system.

The neutron interactions (and source events) are the principle stochastic elements of a nuclear system insofar that, upon collision with a nucleus, a neutron will initiate a random process with an associated probability. An often underappreciated stochastic feature concerns the random multiplets of particles that emerge from the IF and SF processes. Each of these emission numbers has an associated probability q_ν, defined as the probability that ν neutrons are emitted in a given event, and the distribution is normalized as

$$\sum_{\nu=0}^{\nu_m} q_\nu = 1. \tag{2.4}$$

As an example, Fig. 2.1 shows the neutron and photon multiplicity distributions for IF and SF events for a 20 wt% ^{240}Pu and 80 wt% ^{239}Pu system. We can see that the

number of neutrons emerging from a fission event may range from zero up to some max number, ν_m, typically between 6 and 8.

Given the interaction rates and the multiplicity distributions, we are now ready to apply probability balances to quantify the neutron-multiplying systems we wish to study. In the next section, we introduce the mathematical framework used to derive what are known as Master equations.

2.2 On the Formulation of Master Equations

As we are interested in systems for which the neutron population behaves stochastically, i.e., the mean of the population is not representative of the true state of the population at any given time, we must transition our thinking and formulations from a moment based (mean) setting to that of a probabilistic one where we consider the distribution of discrete states that the neutron population may occupy. We then assume that, for a given state at a given time, the collection of random walks of the particles in a system is Markovian. That is, the individual paths of the particles are uncorrelated and that the current state of the system, and not its past, alone dictates the temporal evolution of the system [1].

We consider the exact neutron population of a system, n, to be a unique state that has a single associated probability of being observed. Defining $P_{n|m}(t_f|t)$ as the probability of being in state n at a time of observation t_f conditioned on the system being in state m at an earlier time t, and assuming that the m connected states are finite and known, this quantity may be determined by the sum of all probabilistic pathways the system may traverse beginning at some time t:

$$P_{n|m}(t_f|t) = \sum_i P_{n|i}(t_f|t')P_{i|m}(t'|t), \tag{2.5}$$

where $t_f > t' > t$. Equation 2.5 may be used to describe the discrete-state continuous-time Markov processes of interest and is known as the Chapman-Kolmogorov (CK)

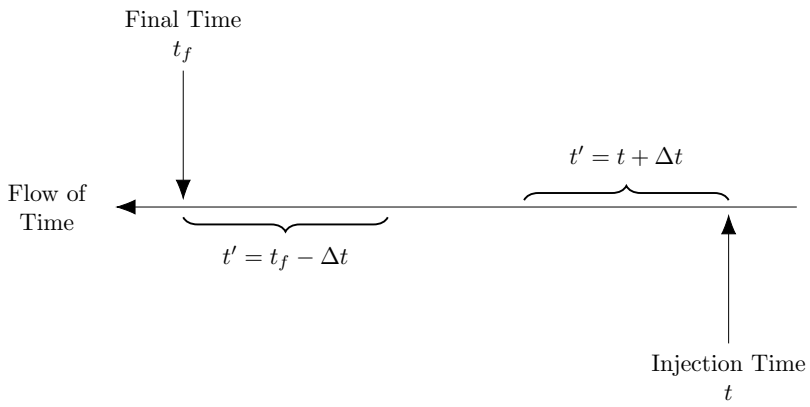

Figure 2.2: Time variables.

equation [2, 5]. As seen in Fig. 2.2, we show time flowing from right to left, and the variable arguments shall be read in the same manner. Equation 2.5 may be restated/interpreted as: in its transition from state m at time t to state n at t_f, the system may go through any number of transitional states, i, at an arbitrary intermediate time t'.

In this chapter, we demonstrate the two methods most often used to obtain the neutron number PDF, namely the Forward Formulation and the Backward Formulation. Equation 2.5 is the starting point for both formulations; where they differ is due to the location within the time interval that the probability balance is conducted over some short time interval Δt. The location may be acquired by translating t' either to the beginning near the injection time, t, or the final time, t_f, defining which formulation is employed:

$$\begin{cases} \text{Forward:} & t' = t_f - \Delta t \\ \text{Backward:} & t' = t + \Delta t. \end{cases}$$

The forward case is a balance in the *last* collision interval leading to t_f while the backward is a balance in the *first* collision interval after t.

To elicit meaningful descriptions of Eq. 2.5, we must recognize that the transitional

probabilities over the time interval Δt, $P_{n|i}(t' + \Delta t|t')$, are the reaction rates:

$$\lambda_{n\leftarrow i}(t')\Delta t = P_{n|i}(t' + \Delta t|t'), \tag{2.6}$$

where we use the notation that the mechanism represented by the reaction rate is directly connected to state n when the system is in state i. It is understood that the reaction rates over a short interval are normalized as $\Delta t \sum_i \lambda_{n\leftarrow i} = 1$. In the limit as $\Delta t \to 0$, the probability of no event occurring is unity, i.e. $\lambda_{n\leftarrow n} = 1$, but the normalization as stated diverges ($1/\Delta t \to \infty$); thus, the no event rate is better expressed as

$$\lambda_{n\leftarrow n}\Delta t = 1 - \sum_{i\neq n} \lambda_{i\leftarrow n}\Delta t. \tag{2.7}$$

Once the balance is performed, we evaluate the limit as $\Delta t \to 0$, resulting in a set of first-order ordinary differential-difference equations which are categorically known to be the differential CK equation [5], which are most commonly referred to as the Forward or Backward Master equation. The name "master equation" was originally coined by Nordsieck, Lamb, and Uhlenbeck [7] in their study of the Furry model of cosmic rain showers. The Master equation is regarded as such because it is indeed the underlying mathematical device used for describing the probabilistic behavior of a system, from which specific properties and characteristics may be derived- thus, the equation is 'ruling' over the subsequent equations. The differential CK equations are obtained from Eq. 2.5 using Eqs. 2.6 and 2.7:

$$\begin{aligned} \text{Forward:} \quad & \frac{\mathrm{d}P_{n|m}(t_f|t)}{\mathrm{d}t_f} = \sum_{i\neq n} \lambda_{n\leftarrow i} P_{i|m}(t_f|t) - P_{n|m}(t_f|t) \sum_{i\neq n} \lambda_{i\leftarrow n} \\ \text{Backward:} \quad & -\frac{\mathrm{d}P_{n|m}(t_f|t)}{\mathrm{d}t} = \sum_{i\neq m} P_{n|i}(t_f|t)\lambda_{i\leftarrow m} - P_{n|m}(t_f|t) \sum_{i\neq m} \lambda_{i\leftarrow m}, \end{aligned} \tag{2.8}$$

where we notice that the operating variable in the forward Master equation is the final time, t_f, while the operating variable in the backward Master equation is the initial time, t [6]. The sign of the time derivatives oppose one another and we integrate in

opposing directions in time; i.e., the forward equation is integrated forward in time and the backward equation is integrated backwards in time- hence the names. The forward and backward Master equations describe the same process and will therefore produce the same result, thus one chooses which to use based on which is easier to solve.

2.3 Formulation of the Forward Master Equation

In applying the Forward Formulation to obtain an equation for the neutron number PDF, we postulate that by inserting an ideal internal detector into the system at some time of observation, t_f, we will be able to detect the exact neutron population upon insertion. Each possible population number, n, that may be observed by the detector occurs with probability $P_{n|m}(t_f|t')$, where each population state n is dependent on the set of states m existing at an earlier time t'. As was stated in the previous section, we simplify the notation $P_{n|m}(t_f|t') \rightarrow P_n(t_f)$, where it is understood that state m is known and defined by the initial condition; the variable m is a *nuisance variable* [8] and we may drop it from the notation. Doing so provides the following CK equation:

$$P_n(t_f) = \lambda_{n\leftarrow n}(t_f)\Delta t P_n(t_f - \Delta t) + \sum_{m_i} \lambda_{n\leftarrow m_i}(t_f)\Delta t P_{m_i}(t_f - \Delta t). \tag{2.9}$$

To obtain a more physically insightful balance of Eq. 2.9, we consider the m_i state-changing events a neutron may undergo according to Fig. 2.3. We account for the possibility that there are already n neutrons in the system at $t_f - \Delta t$ and therefore no event occurs, that a neutron either leaks or is captured, requiring $n+1$ particles at at $t_f - \Delta t$, or that ν neutrons may be emitted in either a source or induced fission event, requiring $n-\nu$ and $n+1-\nu$ neutrons to be present at $t_f - \Delta t$,

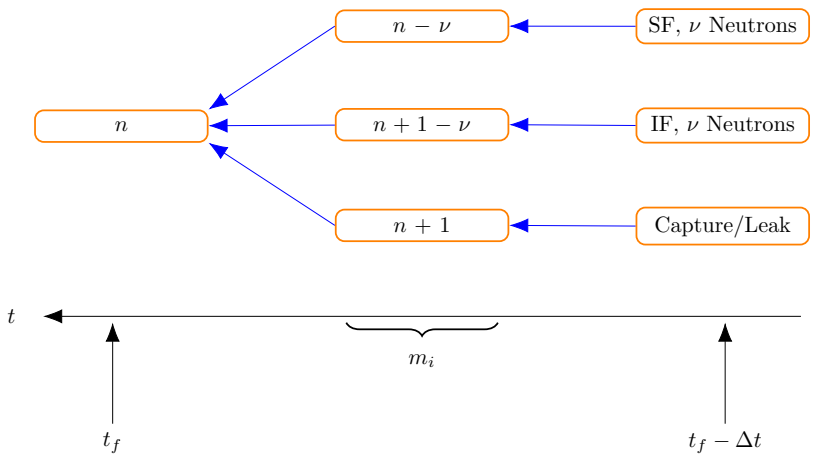

Figure 2.3: Forward formulation time scheme.

respectively. The ensuing CK equation, with the terms in order of introduction, is

$$\begin{aligned} P_n(t_f) = {} & (1 - S\Delta t)(1 - \lambda_t \Delta t)^n P_n(t_f - \Delta t) + (n+1)(\lambda_c + \lambda_\ell)\Delta t P_{n+1}(t_f - \Delta t) \\ & + S\Delta t \sum_{\nu=0}^{\nu_m^S} q_\nu^S P_{n-\nu}(t_f - \Delta t) + \lambda_f \Delta t \sum_{\nu=0}^{\nu_m^f} q_\nu^f (n - \nu + 1) P_{n-\nu+1}(t_f - \Delta t), \end{aligned} \tag{2.10}$$

where $\nu_m^{S/f}$ is the maximum number of neutrons emitted in a source or fission event, and $q_\nu^{S/f}$ is the associated probability that ν neutrons will emerge from said event.

In order to proceed, we must expand the no event transitional probability for neutrons in a Taylor series about $\lambda_t \Delta t = 0$:

$$\begin{aligned} (1 - \lambda_t \Delta t)^n = {} & 1 - n\lambda_t \Delta t + \frac{1}{2} n (n-1) (\lambda_t \Delta t)^2 - \frac{1}{6} n (n-1)(n-2)(\lambda_t \Delta t)^3 + \cdots \\ = {} & 1 - n\lambda_t \Delta t + O\left([\Delta t]^2\right), \end{aligned}$$

allowing us to write the no event probability as

$$\begin{aligned} (1 - S\Delta t)(1 - \lambda_t \Delta t)^n &= (1 - S\Delta t)\left(1 - n\lambda_t \Delta t + O\left([\Delta t]^2\right)\right) \\ &= 1 - (S + n\lambda_t)\Delta t + O\left([\Delta t]^2\right). \end{aligned}$$

Inserting this expression into Eq. 2.10, rearranging, and evaluating the limit as $\Delta t \to 0$, we arrive at an open set of linear ordinary differential-difference equations more often referred to as the differential Chapman-Kolmogorov equation or the forward Master equation:

$$\begin{aligned}\frac{\mathrm{d}P_n(t)}{\mathrm{d}t} = & -\left[S + n\lambda_t\right] P_n(t) + (n+1)\left(\lambda_c + \lambda_\ell\right) P_{n+1}(t) \\ & + S\sum_{\nu=0}^{\nu_m^S} q_\nu^S P_{n-\nu}(t) + \lambda_f \sum_{\nu=0}^{\nu_m^f} q_\nu^f (n-\nu+1) P_{n-\nu+1}(t).\end{aligned} \tag{2.11}$$

Note that we have replaced t_f with t. Assuming the initial state consists of m neutrons within the system at time $t = 0$, the initial condition is

$$P_n(0) = \delta_{n,m}, \tag{2.12}$$

where $\delta_{i,j}$ is the Kronecker delta function. Although m is an arbitrary positive integer, we typically only consider the cases for there being 0 or 1 initial neutrons. In the $m = 0$ case, the number distribution is dictated by the source strength while the $m = 1$ case is used for the determination of a single neutron chain (and the source is then set to $S = 0\ s^{-1}$).

Equation 2.11 is the forward Master equation resembling the general form we established with Eq. 2.8. We will employ several methodologies onto Eq. 2.11 to extract equations we may use to characterize a system of interest; namely the solution $P_n(t)$ and the moments of the probability distribution satisfying the Master equation. The solution to the Master equation 2.11 is intractable due to the set being open as a result of the upward coupling of P_n with P_{n+1} from the loss term (both from capture as well as IF when $\nu = 0$). A numerical solution option is to assume that the distribution decays and that at a sufficiently large population N, the subsequent probability $P_{N+1} \sim 0$ and we may truncate the distribution at order N- closing the system [16]. Analytical solutions require mathematical approximations or restrictions to the physics of the system. We continue the next sections by exploring these two analytical pathways that lead to PDF solutions.

2.3.1 The Probability Generating Function

The solutions to the forward (and backward) Master equation we have introduced is intractable in the form given by Eq. 2.11. It is therefore necessary to employ a transformation onto the Master equations which irresistibly consolidates the infinite number of differential equations into a single equation in the transform function. The transform of choice is the probability generating function (PGF). The PGF is attractive because it is effectively a power series representation of the PDF, which has a well-developed theory established for non-negative coefficients [9].

If we define the PGF for the solution to the forward Master equation as

$$G(z,t) = \sum_{n=0}^{\infty} z^n P_n(t), \tag{2.13}$$

we may multiply Eq. 2.11 by z^n and sum over all n. Performing standard manipulations, we arrive at the corresponding forward PGF equation:

$$\frac{\partial G(z,t)}{\partial t} = g(z,t)\frac{\partial G(z,t)}{\partial z} + S\Big[g_{_S}(z) - 1\Big]G(z,t), \tag{2.14}$$

which has the initial condition: $G(z,0) = z^m$, where m is the initial neutron population. We have defined the coefficient of the $\partial G/\,\partial z$ term as

$$g(z,t) = \Bigg[- \lambda_t z + \lambda_c + \lambda_\ell + \lambda_f g_{_f}(z)\Bigg], \tag{2.15}$$

and $g_x(z)$ is the PGF of the multiplicity distribution of event type x, given by:

$$g_x(z) = \sum_{\nu=0}^{\nu_m^x} z^\nu q_\nu^x. \tag{2.16}$$

Equation 2.14 is a linear PDE of the forward PGF which, under certain conditions, may be solved using the Method of Characteristics. These conditions are discussed in Section 2.4.

2.4 Solutions to the Forward PGF Equation

We seek analytical solutions to the PGF equation resulting from the forward Master equation formulation, Eq. 2.14. In its current general form, Eq. 2.14 does not have a solution in known mathematical functions, but we will steadfastly proceed by recognizing that we may attempt to find solutions using the Method of Characteristics. This is done by comparing Eq. 2.14 with the total derivative of G with respect to time,

$$\frac{\mathrm{d}G}{\mathrm{d}t} = \frac{\partial G}{\partial z}\frac{\mathrm{d}z}{\mathrm{d}t} + \frac{\partial G}{\partial t}. \tag{2.17}$$

By inspection, the system of characteristic equations is:

$$\frac{\mathrm{d}z(t)}{\mathrm{d}t} = -g(z(t)) \tag{2.18a}$$

$$\frac{\mathrm{d}G(z(t),t)}{\mathrm{d}t} = S\Big[g_{_S}\Big(z(t)\Big) - 1\Big]G(z(t),t). \tag{2.18b}$$

Equation 2.18b is an elementary first-order differential equation that is solved by separation of variables followed by integration over the time domain to yield

$$G(z(t),t) = [z(t_o)]^m \exp\left\{S\int_{t_o}^{t}\mathrm{d}t'\Big[g_{_S}\Big(z(t')\Big) - 1\Big]\right\}, \tag{2.19}$$

where we are reminded that $g_{_S}(z(t))$ is an order-ν_m^S polynomial in z. Depending on the form of $z(t)$, obtained by solving Eq. 2.18a, this may prove to be an incalculable integral in and of itself. With that said, we see that Eq. 2.18a takes the integral form:

$$\int_{z(t_o)}^{z(t)}\mathrm{d}z'\frac{1}{g(z')} = \int_{z(t_o)}^{z(t)}\mathrm{d}z'\frac{1}{-\lambda_t z' + \lambda_c + \lambda_\ell + \lambda_f g_{_f}(z')} = -(t - t_o). \tag{2.20}$$

Recalling that $g_f(z(t))$ is an order-ν_m^f polynomial in z, this integral is not solvable for polynomials greater than order 3 [10], prompting us to explore several solution paths in the remainder of this section. There are two ways of solving Eq. 2.14; by means of making a mathematical approximation to the equation itself, known as the Quadratic Approximation, or by restricting the neutron multiplicity, discussed in Sections 2.4.1 and 2.4.2, respectively. Both of these approaches vie to lessen the complexity of Eq. 2.18a by lowering the variable coefficient power to order two.

2.4.1 The Quadratic Approximation

We wish to solve Eq. 2.18a by approximating the form of $g(z(t))$. This is accomplished by expanding g in a Taylor series and retaining only up to the second order terms. This reduces the functional form of g to a quadratic polynomial; for this reason, this process is referred to as the Quadratic Approximation (QA). It was originally performed by Bell in obtaining the neutron number density function for large neutron populations [3] and later employed by Prinja and Souto [11] to extract the discrete number distribution. As this is a replication of previous work, we simply state the relevant equations in moving forward.

By defining the factorial moments of the induced fission multiplicity distribution as

$$\chi_i = \sum_{k=i}^{\nu_m^f} \frac{k!}{(k-i)!} q_k^f, \tag{2.21}$$

it can be shown that g may be approximated as a second-order polynomial function of z:

$$g(z) \approx \frac{1}{\tau}\left[(k-1)(z-1) + p_f \chi_2 \frac{(z-1)^2}{2}\right], \tag{2.22}$$

where $p_f = \lambda_f/\lambda_t$ is the probability of fission, $k = \overline{\nu} p_f$ is the multiplication factor, and $\tau = 1/\lambda_t$ is the neutron lifetime. This is known as the Quadratic Approximation, and it allows us to solve the characteristic equation for $z(t)$. We note that, from the definition of χ_2, we are able to maintain effects of the full multiplicity distribution.

With the QA in-hand, the solution to the approximated form of Eq. 2.18a is

$$z(t) = 1 + \left[\frac{1}{z(t_o)-1} a(t) + b(t)\right]^{-1} \tag{2.23}$$

where we have defined

$$a(t) = \exp\left\{\int_{t_o}^{t} \mathrm{d}t' \alpha(t')\right\} \tag{2.24a}$$

$$b(t) = \int_{t_o}^{t} \mathrm{d}t' \frac{\chi_2'(t')}{2} \exp\left\{ \int_{t'}^{t} \mathrm{d}t'' \alpha(t'') \right\}. \tag{2.24b}$$

along with two well-known variables:

$$\alpha(t) = \frac{k(t) - 1}{\tau(t)}, \tag{2.25}$$

$$\chi_2'(t) = \frac{p_f(t)\chi_2}{\tau(t)}. \tag{2.26}$$

We next insert Eq. 2.23 into the expression for G, Eq. 2.19, in order to solve the PGF equation, Eq. 2.14:

$$G(z(t), t) = z(t_o)^m \exp\left\{ S \int_{t_o}^{t} \mathrm{d}t' \Big[g_S\Big(z(t')\Big) - 1 \Big] \right\}. \tag{2.27}$$

We proceed by addressing the two primary cases that are examined in practice: the case of a single initial neutron without a source present (which we have been referring to as the single chain case), and the case of zero initial neutrons in the presence of a source.

Single Chain Case

For the case of a single initial neutron without a source present, we simply set $S = 0$ s^{-1} and we set $m = 1$ in Eq. 2.27. This tells us that $\mathrm{d}G/\,\mathrm{d}t = 0$, and the PGF is constant along the characteristic curve and is therefore equal to the initial condition, i.e. $G(z(t), t) = G(z(t_o), t_o) = z(t_o)$. Solving Eq. 2.23 for $z(t_o)$ yields

$$G(z(t), t) = 1 + \frac{a(t)}{(z(t) - 1)^{-1} - b(t)}. \tag{2.28}$$

Equation 2.28 is in its simplest of forms, and our next task will be to invert G to determine the single chain neutron number distribution, discussed in Sec. 2.5.

Source Case

The case of a source with no initial neutrons (set $m = 0$ in Eq. 2.27) is more involved than the single chain case due to the retention of the exponential functional form

of G. In reference to Eq. 2.27, we see that the source multiplicity distribution PGF introduces complications due to the ν_m^S-order power of the argument, $z(t')$. For this reason, the integral is not easily computed and we assume the source is singlet emitting, i.e. $q_\nu^S = \delta_{\nu,1}$. After rearranging and further assuming χ_2' is time-independent, we obtain the solution

$$G(z(t),t) = \Big[1 - \Big(z(t) - 1\Big)b(t)\Big]^{-\eta}, \tag{2.29}$$

where we have introduced the parameter, often called Bell's parameter,

$$\eta = \frac{2S}{\chi_2'}. \tag{2.30}$$

Equation 2.29 was obtained for the specific case of a singlet emitting source, where we further assumed the source, S, and χ_2' to be time-independent. We recognize that we did not need to make an assumption on the form of $\alpha(t)$, allowing us to maintain a time-dependence on the system criticality; note that we require χ_2' to be constant and hence the ratio of p_f to τ must be constant (a quantity closely tied to α). Equation 2.29 is in the ideal form to invert G to recover the neutron number distribution in the presence of a source, $P_n(t)$, to be discussed in Sec. 2.5.

2.4.2 Restrictions on the Neutron Multiplicity Distribution (The Generalized Binary Fission Model)

In this section, we explore solutions to the forward PGF equation for which we assume some form the induced fission multiplicity distribution to solve the characteristic equation given by Eq. 2.18a. Solutions have been obtained for the Binary Fission Model [14, 16], which restricts the number of neutrons emitted in a fission event to exactly two, i.e. $q_\nu^f = \delta_{\nu,2}$. In this document, we wish to show a generalization to account for the additional possibility of 0, 1, and 2 particles to be produced in a fission event, and for this reason we refer to this methodology as the Generalized Binary Fission Model (GBFM).

The appeal of having a solution for an exact multiplicity distribution arises in the need to benchmark codes, particularly Monte Carlo codes that we will be developing later in this document. As was discussed in the previous subsection on the Quadratic Approximation, we arrived at solutions to the forward PGF equation by approximating the coefficient containing the nonlinear dependence on z– arising from being operated on by the induced fission multiplicity distribution PGF, $g_f(z)$. The QA then provides an approximate solution to the PGF equation, and if we are attempting to benchmark a MC code for which no approximation in the simulation is translatable, there will be irregularities and disagreements amongst results (specifically for small n and short times). Thus, we require solutions for which the forward PGF equation is solved exactly under an approximation to the physics of the system rather than an approximation to the equation itself.

Proceeding, we assume that any number of neutrons may be emitted from an induced fission event up to 2. Thus, Eq. 2.16 simplifies to $\sum_{\nu=0}^{2} z^{\nu} q_{\nu}^{f}$, and Eq. 2.18a becomes a nonlinear ODE of the Riccati-type with constant coefficients:

$$\frac{\mathrm{d}z}{\mathrm{d}t} = -\left[\lambda_f q_2^f z^2 + (\lambda_f q_1^f - \lambda_t)z + \lambda_c + \lambda_\ell + \lambda_f q_0^f\right]. \tag{2.31}$$

This resultant ODE is separable and we may simply solve the revised version of Eq. 2.20 as it is now an integral of a rational function with a quadratic function in the denominator with the solution:

$$\int_{z(t_o)}^{z(t)} \mathrm{d}z' \frac{1}{Az'^2 + Bz' + C} = \frac{i}{D} \ln\left(\frac{1 - \frac{i}{D}(2Az' + B)}{1 + \frac{i}{D}(2Az' + B)}\right)\Bigg|_{z(t_o)}^{z(t)} = -(t - t_o), \tag{2.32}$$

where i is the unit imaginary number and we have defined the coefficients:

$$A = \lambda_f q_2^f \tag{2.33a}$$

$$B = \lambda_f q_1^f - \lambda_t \tag{2.33b}$$

$$C = \lambda_c + \lambda_\ell + \lambda_f q_0^f \tag{2.33c}$$

$$D = \sqrt{4AC - B^2}. \tag{2.33d}$$

Note that $B \leq 0$. As it is, D in Eq. 2.33d is a complex number residing on the imaginary line (i.e., $\mathrm{Re}(D) = 0$). We then factor i from D such that $D = i\mathcal{D}$, where we have now defined $\mathcal{D}$ as the magnitude of D:

$$\mathcal{D} = \sqrt{|4AC - B^2|} = \sqrt{B^2 - 4AC}. \tag{2.34}$$

Equation 2.32 then becomes

$$\ln\left\{\left(\frac{\mathcal{D} - 2Az(t) - B}{\mathcal{D} + 2Az(t) + B}\right)\left(\frac{\mathcal{D} + 2Az(t_o) + B}{\mathcal{D} - 2Az(t_o) - B}\right)\right\} = -\mathcal{D}(t - t_o), \tag{2.35}$$

and solving for $z(t)$ yields

$$z(t) = \frac{\mathcal{D} - B - (\mathcal{D} + B)\left[\frac{\mathcal{D}-B-2Az(t_o)}{\mathcal{D}+B+2Az(t_o)}\right]\mathrm{e}^{-\mathcal{D}(t-t_o)}}{2A\left(1 + \left[\frac{\mathcal{D}-B-2Az(t_o)}{\mathcal{D}+B+2Az(t_o)}\right]\mathrm{e}^{-\mathcal{D}(t-t_o)}\right)}. \tag{2.36}$$

We will also need an expression for $z(t_o)$, which is easily solved for by rearranging Eq. 2.36. With $z(t)$ and $z(t_o)$, we are now prepared to solve the characteristic equation for G for the cases of a single neutron chain as well as in the presence of a source.

Single Chain Case

The solution for a single neutron fission chain is obtained by setting $m = 1$ and $S = 0$ in Eq. 2.19. As was observed in the previous section on the QA, this shows us that $\mathrm{d}G/\,\mathrm{d}t = 0$ and G is then equal to the initial condition: $G(z(t), t) = G(z(t_o), t_o) = z(t_o)^1$. Thus, we have:

$$G(z(t), t) = z(t_o) = \frac{\mathcal{D} - B - (\mathcal{D} + B)\left[\frac{\mathcal{D}-B-2Az(t)}{\mathcal{D}+B+2Az(t)}\right]\mathrm{e}^{+\mathcal{D}(t-t_o)}}{2A\left(1 + \left[\frac{\mathcal{D}-B-2Az(t)}{\mathcal{D}+B+2Az(t)}\right]\mathrm{e}^{+\mathcal{D}(t-t_o)}\right)}. \tag{2.37}$$

In Sec. 2.5, we will invert this expression to obtain the number distribution for a single chain for which we have restricted there to be 0, 1, or 2 neutrons emitted per induced fission.

Source Case

For the case where there are no initial neutrons but there is a source present within the system, we set $m = 0$ in Eq. 2.19 and we further assume the source produces one and only one particle per event, i.e. $q_\nu^S = \delta_{\nu,1}$; with this, we ultimately find

$$G(z,t) = \left[\frac{2\mathcal{D}}{\mathcal{D}+\mathcal{B}+(\mathcal{D}-\mathcal{B})\mathrm{e}^{-\mathcal{D}\Delta t}+2A(\mathrm{e}^{-\mathcal{D}\Delta t}-1)z}\right]^{\eta} \mathrm{e}^{-S\Delta t\left(1-\frac{\mathcal{B}-\mathcal{D}}{2A}\right)}, \quad (2.38)$$

where $\Delta t = t - t_o$ and we have introduced $\mathcal{B} = |B|$ because $B < 0$. We have also defined the GBFM analog to Bell's parameter:

$$\eta = \frac{S}{A} = \frac{S}{\lambda_f q_2^f}. \quad (2.39)$$

Thus, we have now found a suitable solution from which we may invert to obtain the number distribution in the presence of a source. We next show the process for solving the backward PGF equations.

2.5 Inversion of the Forward Generating Functions

In this section, we show how to invert the expressions for the forward PGFs to obtain the neutron number distribution. We begin by considering the PGFs obtained by application of the Quadratic Approximation for a single chain and a source. We then show the number distributions for the case of restricting the order of the multiplicity distributions for the single chain and source cases.

2.5.1 The Quadratic Approximation PDFs

Single Chain

The PGF solution via the QA for the single chain is given by Eq. 2.28:

$$G(z,t) = 1 + \frac{(z-1)a(t)}{1-(z-1)b(t)} = 1 + \frac{(z-1)a(t)}{1+b(t)}\left[1 - \frac{b(t)}{1+b(t)}z\right]^{-1}. \tag{2.40}$$

Since $0 \leq b/(1+b) \leq 1$ and $0 \leq z \leq 1$, then $0 \leq bz/(1+b) \leq 1$, and we may therefore apply the Binomial Theorem to expand the bracketed term of Eq. 2.40; doing so eventually provides

$$G(z,t) = 1 - \frac{a(t)}{1+b(t)} + \frac{a(t)}{\left[1+b(t)\right]^2}\sum_{n=1}^{\infty}\left[\frac{b(t)}{1+b(t)}\right]^{n-1} z^n. \tag{2.41}$$

Comparing Eq. 2.41 to the original definition of the generating function, $G(z,t) = \sum_{n=0}^{\infty} P_n(t)z^n$, we see that the extinction probability is already isolated and the remainder of the distribution may be inferred accordingly:

$$P_0(t) = 1 - \frac{a(t)}{1+b(t)} \tag{2.42a}$$

$$P_n(t) = \frac{a(t)}{\left[1+b(t)\right]^2}\left[\frac{b(t)}{1+b(t)}\right]^{n-1}, \qquad n = 1,2,3,\ldots. \tag{2.42b}$$

Equations 2.42a and 2.42b constitute the discrete neutron number distribution in the Quadratic Approximation. First obtained by Prinja and Souto [11], this PDF is a natural generalization to Bell's single chain distribution [3].

In the Presence of a Source

We are now interested in inverting the forward PGF solution in the presence of a source, given by Eq. 2.29. The process is wholly the same as for the single chain case, but the resulting distribution is categorically different, as will be seen. Equation 2.29

is already in the ideal format after a simple factorization,

$$G(z,t) = \left[1 - \Big(z-1\Big)b(t)\right]^{-\eta} = \frac{1}{\Big(1+b(t)\Big)^{\eta}}\left[1 - \frac{b(t)}{1+b(t)}z\right]^{-\eta}, \tag{2.43}$$

we may expand the bracketed term into a Taylor series about $z = 0$. In doing so, Eq. 2.43 becomes

$$G(z,t) = \frac{1}{\Big(1+b(t)\Big)^{\eta}} \sum_{n=0}^{\infty} \frac{\eta(\eta+1)\cdots(\eta+n-1)}{m!}\left[\frac{b(t)}{1+b(t)}\right]^{n} z^{n}. \tag{2.44}$$

The rising factorial of η may be written in terms of the Gamma function with the identity $\eta(\eta+1)\cdots(\eta+n-1) = \frac{\Gamma(\eta+n)}{\Gamma(\eta)}$. As before, if we then compare Eq. 2.43 to the definition of the PGF, $G(z,t) = \sum_{n=0}^{\infty} P_n(t) z^n$, we may readily extract the number distribution in the presence of a source:

$$P_n(t) = \frac{1}{\Big(1+b(t)\Big)^{\eta}}\left[\frac{\Gamma(\eta+n)}{n!\,\Gamma(\eta)}\right] \cdot \left[\frac{b(t)}{1+b(t)}\right]^{n}, \qquad n = 0, 1, 2, \ldots. \tag{2.45}$$

Equation 2.45 is the discrete neutron number PDF in the Quadratic Approximation, first obtained by Prinja and Souto [11]. As with the previous section for the single chain distribution, this PDF is a generalization of Bell's distribution in the presence of a source. It will be shown in Sec. 2.6 that Bell's distribution emerges in the asymptotic limit of Eq. 2.45.

2.5.2 PDFs for the Generalized BFM

Single Chain

Following the same procedure as the previous section of rearranging Eq. 2.37 to be expanded with the Binomial Theorem and compared to the definition of G, we may obtain the GBFM number distribution:

$$P_0(t) = \frac{\mathcal{B}-\mathcal{D}}{2A} \cdot \left[\frac{1 - \mathrm{e}^{-\mathcal{D}\Delta t}}{1 - \left(\frac{\mathcal{B}-\mathcal{D}}{\mathcal{B}+\mathcal{D}}\right)\mathrm{e}^{-\mathcal{D}\Delta t}}\right] \tag{2.46a}$$

$$P_n(t) = 4\mathcal{D}^2 \mathrm{e}^{-\mathcal{D}\Delta t} \frac{\left[2A\left(1-\mathrm{e}^{-\mathcal{D}\Delta t}\right)\right]^{n-1}}{\left[\mathcal{B}+\mathcal{D}-(\mathcal{B}-\mathcal{D})\mathrm{e}^{-\mathcal{D}\Delta t}\right]^{n+1}}, \qquad n = 1, 2, 3, \ldots. \tag{2.46b}$$

This distribution is a generalization of the Binary Fission Model distribution presented in [16] and allows for non-singular multiplicity distribution calculations. It differs from Prinja's distribution given by Eq. 2.42 in that it is an exact solution to the PGF PDE for a multiplicity distribution that produces 0, 1, or 2 neutrons per induced fission, while the Prinja Distribution made an approximation to the PGF PDE itself and allows for any multiplicity distribution (encapsulated in the χ_2' parameter). A final note concerns the the coefficient of Eq. 2.46a: $(\mathcal{B}-\mathcal{D})/2A$, we see that when the system is supercritical, $(\mathcal{B}-\mathcal{D})/2A < 1$, and when the system is critical and subcritical, $(\mathcal{B}-\mathcal{D})/2A \equiv 1$. Thus, for a subcritical system, we find $\lim_{t\to\infty} P_0(t) = 1$, while for a supercritical system, $\lim_{t\to\infty} P_0(t) = (\mathcal{B}-\mathcal{D})/2A$. This fact will become useful when we wish to determine the quantity know as the probability of initiation.

In the Presence of a Source

We may invert the PGF for the source case, starting with Eq. 2.38, by again rearranging, Taylor expanding about $z = 0$, and comparing to the definition of G to attain:

$$P_n(t) = (2\mathcal{D})^{\eta} \mathrm{e}^{-S\Delta t\left(1-\frac{\mathcal{B}-\mathcal{D}}{2A}\right)} \left[\frac{\Gamma(\eta+n)}{n!\Gamma(\eta)}\right] \frac{\left[2A\left(1-\mathrm{e}^{-\mathcal{D}\Delta t}\right)\right]^{n}}{\left[\mathcal{B}+\mathcal{D}-(\mathcal{B}-\mathcal{D})\mathrm{e}^{-\mathcal{D}\Delta t}\right]^{\eta+n}}, \tag{2.47}$$

where we recall that, for the GBFM, $\eta = S/\lambda_f q_2^f$, given by Eq. 2.39. Equation 2.47 is a generalization to the source distribution in [16]- where we have allowed for a less stringent induced fission multiplicity distribution. We note that, for a subcritical system $\mathcal{B}-\mathcal{D} = 2A$ and the exponential factor becomes unity and the time-dependence of the distribution behaves according to the remaining decaying exponentials. For a supercritical system, $(\mathcal{B}-\mathcal{D})/2A < 1$, then $1-\frac{\mathcal{B}-\mathcal{D}}{2A} \in [0,1]$, and the exponential factor therefore always decays with the progression of time.

2.6 Asymptotic Limits of the Neutron Number Distribution

In this section, we replicate an exercise performed by Prinja and Souto [11] with the main goal of deriving the well-known Bell distribution [3], which is pivotal in the analysis of systems we will be studying, and as a means of demonstrating its connection to the discrete distributions. This is done by considering asymptotic behavior of the forward discrete distributions for the QA when the neutron population has grown to a point that it may effectively be regarded as a continuum (typically applicable for $n \gtrsim 10$, thus the population is still within a stochastic regime). For a more in-depth demonstration, it is recommended the reader acquire [11].

Single Chain

We note that Eqs. 2.24a and 2.24b can be written in terms of the average of the neutron number, $\overline{n}$ (given by Eq. 2.54a in a later Sec. 2.7), as well as the POI: $a(t) = \overline{n}(t) = \mathrm{e}^{\alpha t}$ and $b(t) = \frac{\overline{n}(t)-1}{P_\infty}$, where we are assuming constant reactivity. The single chain distribution may then be restated as:

$$P_n(t) = P_\infty^2 \frac{\overline{n}(t)}{(\overline{n}(t)-1)^2} \left[\frac{\overline{n}(t)-1}{\overline{n}(t)-(1-P_\infty)}\right]^{n+1}.$$

If we now consider the initial neutron has been propagating for a long time so that $t \gg 1/\alpha$ and $\overline{n}(t) \gg 1$, Prinja and Souto were able to argue that, for large neutron populations, the discrete probability distribution should instead be treated as a continuous probability density function, i.e. $P_n(t) \to P(n,t)\,\mathrm{d}n$. Thus, we may write the single chain number distribution as [11]:

$$P_n(t) \approx (1-P_\infty)\,\delta(n) + \frac{P_\infty^2}{\overline{n}(t)} \exp\left\{-\frac{P_\infty}{\overline{n}(t)} n\right\}, \tag{2.48}$$

where we have included the singular point of the density at $n = 0$, corresponding to the extinction probability, to ensure proper normalization. Equation 2.48 is the result

obtained by Bell [3], but he obtained it by applying an inverse Laplace transform to the solution of the PGF PDE after making the Quadratic Approximation.

In the Presence of a Source

In the presence of a constant randomly emitting source, we note Stirling's Formula for large z arguments of the gamma function: $\Gamma(z+1) \sim \sqrt{2\pi z}\left(\frac{z}{\mathrm{e}}\right)^z$, from which we may write $n! = \Gamma(n+1) \sim \sqrt{2\pi} n^{n+1/2} \exp\{-n\}$. Using this approximation, and appropriate variations of it, in the number distribution in the presence of a source, Eq. 2.45, Prinja and Souto provide [11]:

$$P_n(t) \approx P(n,t)\,\mathrm{d}n = \left(\frac{\eta n}{\overline{n}(t)}\right)^{\eta-1} \frac{\eta}{\overline{n}(t)\Gamma(\eta)} \mathrm{e}^{-\frac{\eta}{\overline{n}(t)}n}\,\mathrm{d}n, \tag{2.49}$$

which is known as Bell's gamma distribution for the neutron number in the presence of a source. The asymptotic analysis was first conducted by Prinja and Souto [11], but Bell obtained his distribution directly from the PGF solution by inverting the PGF using the inverse Laplace transform [3].

2.7 Equations for the Moments

Equations for the moments of the distribution are utilized for a myriad of applications, including, but not limited to: characterizing the number distribution for instances where the QA or GBFM are not applicable; for fitting the distribution to another known distribution based on the calculated moments; for benchmarking codes. For illustrative purposes, we will show the general process for obtaining equations satisfied by the moments of the number distribution under investigation for the forward formulation, but the process is applicable for the backward formulation as well.

To obtain the moments for the neutron number distribution from the forward Master equation, Eq. 2.11, we recognize that the k^{th} derivative of the PGF with

respect to z evaluated at $z = 1$ is the k^{th}-order falling factorial moment of the PDF:

$$\begin{aligned}\left.\frac{\partial^k G(z,t)}{\partial z^k}\right|_{z=1} &= \left.\sum_{n=0}^{\infty} n(n-1)\cdots(n-k+1)z^{n-k}P_n(t)\right|_{z=1} \\ &= \overline{n(n-1)\cdots(n-k+1)}(t). \end{aligned} \tag{2.50}$$

We may then apply Eq. 2.50 to the PGF PDE, Eq. 2.14, and unfold the factorial moment expression to obtain $\overline{n^k}(t)$. The first moment is given by setting $k = 1$, providing a linear first-order ODE:

$$\frac{\mathrm{d}\overline{n}(t)}{\mathrm{d}t} = \alpha\,\overline{n}(t) + S\overline{\nu}_s, \tag{2.51}$$

which is the typical point-reactor kinetic equation without delayed neutrons [3, 11, 46]. In Eq. 2.51, we are using $\alpha = (p_f\overline{\nu}_f - 1)/\tau = (k-1)/\tau$ and we have recognized $\mathrm{d}g_x/\,\mathrm{d}z|_{z=1} = \overline{\nu}_x$ is the average of the multiplicity distribution x, from which we may write the average of the factorial moments as

$$\left.\frac{\mathrm{d}^k g_x(z)}{\mathrm{d}z^k}\right|_{z=1} = \overline{\nu_x(\nu_x-1)\cdots(\nu_x-k+1)} = \overline{(\nu_x)_k}, \tag{2.52}$$

where we are utilizing Pochhammer notation for the falling factorial functions. Equation 2.51 can be solved for using the integrating factor technique:

$$\overline{n}(t) = \overline{n}(0)\mathrm{e}^{\alpha t} + \frac{S\overline{\nu}_s}{\alpha}\left[\mathrm{e}^{\alpha t} - 1\right] \tag{2.53}$$

where we have assumed α and S to be constant in time. For the single chain case, $\overline{n}(0) = 1$ and $S = 0$, while for the source case, $\overline{n}(0) = 0$, thus we have:

$$\text{Single Chain: } \overline{n}(t) = \mathrm{e}^{\alpha t} \tag{2.54a}$$

$$\text{Source: } \qquad \overline{n}(t) = \frac{S\overline{\nu}_s}{\alpha}\left[\mathrm{e}^{\alpha t} - 1\right]. \tag{2.54b}$$

Taking two derivatives with respect to z and evaluating at $z = 1$ yields:

$$\frac{\mathrm{d}\overline{n^2}}{\mathrm{d}t} - 2\alpha\overline{n^2}(t) = \frac{\mathrm{d}\overline{n}}{\mathrm{d}t} + \left[\lambda_f\overline{(\nu_f)_2} - 2\alpha + 2S\overline{\nu}_s\right]\overline{n}(t) + S\overline{(\nu_s)_2}, \tag{2.55}$$

which may be solved via the integrating factor technique to yield:

$$\begin{aligned}\overline{n^2}(t) = &\overline{n^2}(0)\mathrm{e}^{2\alpha t} + \int_0^t \mathrm{d}t' \frac{\mathrm{d}\overline{n}(t')}{\mathrm{d}t'}\mathrm{e}^{-2\alpha(t'-t)} + \frac{S\overline{\nu}_S}{\alpha}\left[\mathrm{e}^{2\alpha t} - 1\right] \\ &+ \left[\lambda_f \overline{(\nu_f)}_2 - 2\alpha + 2S\overline{\nu}_S\right] \int_0^t \mathrm{d}t' \overline{n}(t')\mathrm{e}^{-2\alpha(t'-t)}.\end{aligned} \tag{2.56}$$

This process must be applied as many times as there are desired moments. With some effort, it can be shown that for constant system parameters α and S, the k^{th} moment is:

$$\begin{aligned}\overline{n^k}(t) = \overline{n^k}(0)\mathrm{e}^{k\alpha t} + \frac{S\overline{(\nu_S)}_k}{k\alpha}\left[\mathrm{e}^{k\alpha t} - 1\right] + \sum_{j=1}^{k-1}\Bigg\{ &- s_1(k,j)\int_0^t \mathrm{d}t' \frac{\mathrm{d}\overline{n^j}(t')}{\mathrm{d}t'}\mathrm{e}^{-k\alpha(t'-t)} \\ &+ c_j^{(k)} \int_0^t \mathrm{d}t' \overline{n^j}(t')\mathrm{e}^{-k\alpha(t'-t)}\Bigg\},\end{aligned} \tag{2.57}$$

where the coefficient is defined as:

$$c_j^{(k)} = k s_1(k,j)\alpha + \sum_{i=1}^{k-j} s_1(k-i,j)\left\{\binom{k}{i+1}\overline{(\nu_f)}_{i+1}\lambda_f + \binom{k}{i}\overline{(\nu_S)}_i S\right\}, \tag{2.58}$$

and s_1 is the Signed Stirling Number of the First Kind.

With these moment equations, or any moment equation obtained from an appropriate Master equation, we may benchmark Monte Carlo or deterministic codes. There will be several instances throughout this document where we hinge the accuracy of a result based on its agreement with the moment equations.

Chapter 3

Monte Carlo Methods

In this chapter, we investigate two analog Monte Carlo methods to aid in obtaining stochastically derived information for characterizing nuclear systems– namely the traditional Event-Based Monte Carlo (EBMC) method and a method known as the Stochastic Simulation Algorithm (SSA). Fundamentally, a Monte Carlo method consists of analyzing an aggregate of outcomes of random walks a system may assume in nature. These random walks are simulated by inverting the cumulative distribution functions (CDFs) containing the probability mass functions dictating the behavior of an individual particle (EBMC) or the state transition rate of the system (SSA). In the above, analog refers to the direct simulation of particles by avoiding the use of the particle weight as a variance reduction technique seen in many production codes [36]. It is necessary to avoid such variance reduction techniques as they modify the PDFs for physics interactions to favor events of interest, and by making an assumption on the outcome, or biasing a random walk, of a stochastic system denies true randomness of the simulation at-hand.

Regardless of the MC method employed, the quantities of interest are not dependent on individual outcomes, but instead on the collection of outcomes, and either MC method should provide the same statistical results. For this reason, the

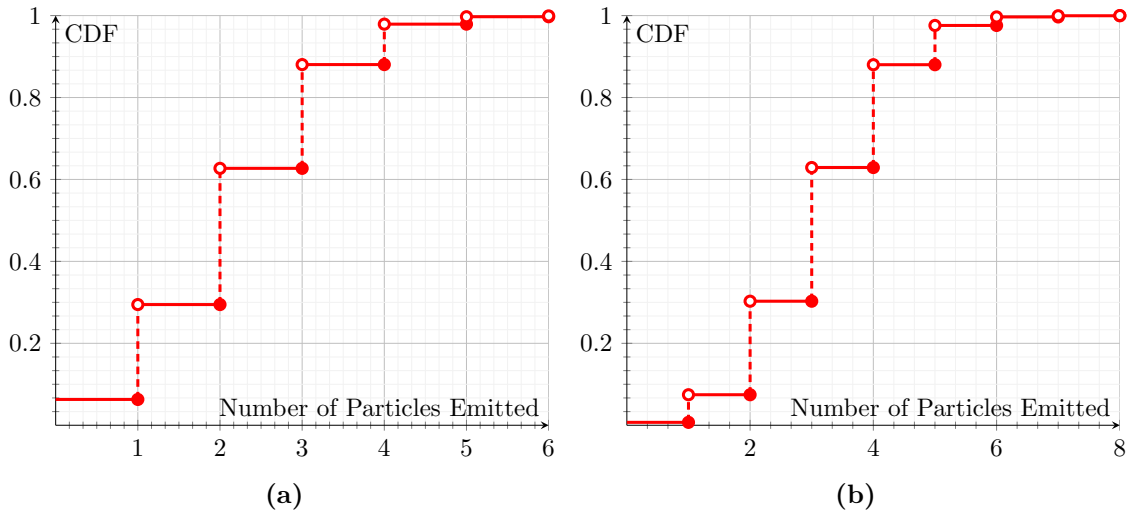

Figure 3.1: Cumulative distribution functions for multiplicity distributions of (a) spontaneous fission and (b) induced fission for the Pu system in Fig. 4.5.

post-processing of the set of simulations should be the same and we therefore discuss the two quantities of interest: calculating the neutron number distribution in Sec. 3.1 and calculating the moments of the distribution in Sec. 3.2. Beforehand, we discuss the cumulative distribution functions we sample from as well as the random number generator used. We then discuss the individual algorithms in Secs. 3.3 and 3.4, corresponding to the EBMC method and SSA, respectively.

Cumulative Distribution Functions and Random Number Generators

Central to the study of the stochasticity of nuclear systems are the random emission of particle multiplets in spontaneous and induced fission events. The CDFs for these particle-multiplying events are shown in Fig. 3.1 for the 20 wt% ^{240}Pu and 80 wt% ^{239}Pu system with multiplicity distributions depicted in Fig. 2.1. If we generate a random number, $\xi \in [0, 1)$, we may then determine the number of particles emitted in a given event depending on where its value lies on the vertical axis, projecting to where that value intercepts the CDF, and the corresponding horizontal axis value

provides the sampled number of particles for that ξ; this is the basis for inverting any and all discrete CDF. For continuous PDFs, one must resort to analytical inversion of the CDF or, if the CDF is noninvertible, some other form of inversion is required, such as rejection sampling. Often when the CDF is analytically represented (i.e., the integral has a solution), the variable we wish to sample may be transcendental in the solution and we must then perform an iteration such as the Newton-Raphson method.

In practice, ξ is truly a *pseudorandom* number pulled from a pseudorandom number generator (PRNG); for the results shown throughout this document, we use the PRNG from FORTRAN90, which uses the `xoshiro256**` PRNG. This generator has a period of $2^{256} - 1$ and, when using multiple threads, up to 2^{128} threads can each generate 2^{128} random numbers before any aliasing occurs [52]. For our purposes, this PRNG is sufficient for providing true Monte Carlo results.

3.1 Calculating the Neutron Number Distribution

As was the focus in Chapter 2, we are primarily concerned with determining the neutron number distribution using Monte Carlo methods. In this section, we describe, in broad terms disregarding mechanics of specific algorithms, how to obtain the probability of there being n neutrons in the system at some final time t_f due to some initial state of the population: $P_n(t_o)$ for $n = 0, 1, 2, \ldots$.

For a given history, or simulation, there will be a single outcome, or state, that the system occupies. The final state of history h will have a corresponding neutron population, n_h, at the final time of observation, t_f; this state may be defined as $\mathbf{X}_h(n_h, t_f)$. The probability of there being n neutrons at the final time, then, is simply the total number of instances that that state occurs divided by the total number of

histories simulated, H, given by

$$P_n(t_f) = \frac{1}{H} \sum_{h|n_h=n} \mathbf{X}_h(n_h, t_f), \tag{3.1}$$

where the above is read as the sum over h conditioned on $n_h = n$, In practice, the summation of Eq. 3.1 is accomplished by populating a histogram for every outcome on-the-fly, preventing the need to store every outcome as an individual value in a computer. Note that Eq. 3.1 assumes the bin width is unity, but if one were to have bin widths greater than one, Δn_i for the i^{th} bin, we would simply perform the division: $P_n(t_f)/\Delta n_i$ for $n \in \Delta n_i$.

3.2 Calculating the Moments

The moments of the neutron number distribution are determined by first partitioning the total number of histories into sets, or batches. For each batch, the desired moments are calculated and saved; the first four moments may be calculated using the "Set of Histories" column of Table 3.1, where h is the number of histories per batch. Once every batch has been simulated and there is a corresponding moment for each batch, we then use the equations in the "Set of Batches" column of Table 3.1 to find the final results, where B is the total number of batches. Typically, a batch may contain 10^3 to 10^6 histories with unique outcomes. Note that the minimal number of batches must be equal to the order of the moments being calculated to avoid singularities; e.g. four batches are required if we wish to calculate the kurtosis.

Once the simulation of all of the batches is concluded, a distribution of the batch moments is obtained and, for increasing B, this distribution is expected to approach the Gaussian distribution in accordance with the Central Limit Theorem for independent identically distributed random variables [51]. The distribution of the batch moments is typically referred to as the Sample Distribution. One may assess the state of the sample distribution for a given moment by calculating the skewness,

Table 3.1: Equations for the moments for an individual batch and for the total set of simulations.

	Set of Histories (j^{th} Batch)	Set of Batches (Sample Moments)
Mean	$\overline{x}_j = \frac{1}{h}\sum_{i=1}^{h} x_i$	$\overline{x} = \frac{1}{B}\sum_{j=1}^{B} \overline{x}_j$
Variance, V	$\frac{1}{h}\sum_{i=1}^{h} (x_i - \overline{x}_j)^2$	$\frac{1}{B-1}\sum_{i=1}^{B} (x_i - \overline{x})^2$
Skewness, γ	$\sqrt{h}\frac{\sum_{i=1}^{h}(x_i-\overline{x}_j)^3}{\left[\sum_{i=1}^{h}(x_i-\overline{x}_j)^2\right]^{3/2}}$	$\frac{B\sqrt{B-1}}{B-2}\frac{\sum_{i=1}^{B}(x_i-\overline{x})^3}{\left[\sum_{i=1}^{B}(x_i-\overline{x})^2\right]^{3/2}}$
Kurtosis, κ	$h\frac{\sum_{i=1}^{h}(x_i-\overline{x}_j)^4}{\left[\sum_{i=1}^{h}(x_i-\overline{x}_j)^2\right]^{2}}$	$\frac{B(B+1)(B-1)}{(B-2)(B-3)}\frac{\sum_{i=1}^{B}(x_i-\overline{x})^4}{\left[\sum_{i=1}^{B}(x_i-\overline{x})^2\right]^{2}}$

γ, and kurtosis, κ, of said moment's sample distribution and, if $\gamma \sim 0$ and $\kappa \sim 3$, the distribution is said to be converged because enough batches have been completed.

An estimate on the error of the reported moments is conducted by calculating the confidence interval of the j^{th} moment, C_j, using the 95% confidence level coefficient of 1.96:

$$C_j = 1.96\frac{\sigma_j}{\sqrt{B}}, \tag{3.2}$$

where σ_j is the standard deviation of the sample distribution of moment j, calculated as $\sigma_j = \sqrt{V_j}$.

3.3 Event-Based Monte Carlo Simulation

Event-Based Monte Carlo lends itself to, perhaps, the most intuitive means of simulating a particle's random walk through a nuclear system. The method, as

implemented in this document, initiates a simulation based on a given initial condition– whether it be a single initial neutron without a source or there are zero initial neutrons with a source present. We then follow the particles throughout the system until the population goes to zero, grows to a preset maximum value, or until the final time is surpassed, from which we catalog all of the desired information and move onto the next history. In this subsection, we show the methodology for lumped systems in Sec. 3.3.1 and we then expand the algorithm to account for spatial and energy dependence in Sec. 3.3.2.

3.3.1 Lumped Simulations

For a lumped system simulation, we are only concerned with the temporal evolution of the neutron population and we disregard spatial effects during the random walk. As shown in Appendix B, one may incorporate spatial effects, such as leakage and inhomogeneities of the material, in the value of the reaction rates. As the main focus of this work is in obtaining the neutron number distribution and its moments, we will describe the algorithm with these quantities in mind, but incorporating other quantities, such as the amount of energy deposited in a fission event, should be straightforward and clear to the reader once the algorithm is divulged. First, we will describe how one may simulate a single chain and we will then show how a source (which should be thought of as producing multiple independent single chains per event) may be incorporated, and we will then show an example pseudocode. We will be referring to a *persistent neutron* as being a neutron that has propagated passed the final time of observation, and therefore exists at t_f. On a final note, we consider monoenergetic neutrons with velocity v and we will discuss inclusion of energy in the next subsection.

For the single chain simulation, we initiate the system clock at t_o and then need to determine or, rather, sample the distance the particle travels, s, to its first collision.

This distance is sampled by constructing the CDF for the probability that a particle will travel a distance s and collide, $F(s)$. The CDF contains the probability mass function that a particle will travel a distance and not collide and then, by traveling an additional distance, will collide. This PDF may be separated into two probabilities: the probability that the particle travels a distance x' and does not collide, given by $\exp\{-\int_0^{x'} \mathrm{d}x''\Sigma_t(x'')\}$, and the probability that the neutron travels a short distance $\Delta x'$ and undergoes a collision, given by $\Delta x'\Sigma_t(x')$. Thus, the probability that a particle travels a distance s and collides is given by the product of the aforementioned probabilities, and taking the limit for $\Delta x' \to 0$ gives:

$$F(s) = \int_0^s \mathrm{d}x'\Sigma_t(x') \exp\left\{-\int_0^{x'} \mathrm{d}x''\Sigma_t(x'')\right\}. \tag{3.3}$$

Noting that $F(s) \in [0,1)$ (in the limit $\lim_{s\to\infty} F(s) \to 1$) we may then obtain a random number, $\xi \in [0,1)$ and set it equal to Eq. 3.3. For spatially constant Σ_t we may evaluate the integral to find

$$\xi = 1 - \mathrm{e}^{-\Sigma_t s}. \tag{3.4}$$

Solving for s, we arrive at the distance to collision sampling formula:

$$s = -\frac{1}{\Sigma_t}\ln(\xi), \tag{3.5}$$

where we made the simplification $\xi \leftarrow 1-\xi$ as both numbers are uniformly distributed between 0 and 1. The system time, t_s, is then updated as $t_s = t_o + s/v$. If $t_s \geq t_f$, the neutron is considered persistent, at which point we bin the particle and cycle through to the next history. If $t_s \ngeq t_f$, the neutron collided before the observation time and we must sample which event occurs. As an aside, an alternative approach to sampling s and then updating t_s would be to use the total reaction rate to directly sample a time interval to collision as $\Delta t = -\ln(\xi)/\lambda_t$, and then $t_s \leftarrow t_s + \Delta t$ would provide the update.

For this exercise, we assume that the neutrons may either be captured or cause fission, thus $\Sigma_t = \Sigma_c + \Sigma_f$, but other collision outcomes are readily implemented. As

we are considering monoenergetic neutrons, we do not account for scattering events because a particle is not removed from the system; in an energy-dependent setting, scattering must be accounted for because we need to account for removal/addition to and from energy groups. In practice, one may sample leakage events as well if a system geometry is assumed and the leakage probability is calculated in a global sense (see Appendix B). Proceeding, the event that occurs may be sampled by obtaining a new ξ and comparing $0 \leq \xi \leq \Sigma_c/\Sigma_t$ for a capture or $\Sigma_c/\Sigma_t \leq \xi \leq 1$ for an induced fission. If it is a capture, the neutron chain perishes and we bin that there are 0 persistent neutrons before cycling histories. If the event is an induced fission, we then sample the induced fission multiplicity distribution CDF, see Fig. 3.1b, to determine the number of particles emerging from the event. It is then necessary to simulate each of these branches, following the same algorithm just discussed for each particle, until the branches die away or the final time is surpassed.

Regarding a source-driven system, we sample the number of source events that have occurred by first sampling a time interval between successive source events (or t_o, the initial time, for the first sample) using the formula

$$\Delta t = -\frac{1}{S} \ln(\xi) \,. \tag{3.6}$$

We then update the pseudo-system time $t_s \leftarrow t_s + \Delta t$ and continue to sample time intervals until we surpass $t_s \geq t_f$, and the number of source events is then the number of time intervals that were sampled before surpassing t_f. The time at which the source events occur are then independently sampled. As we are considering time-independent sources, t_j for source event j is then determined by $t_j = -\ln(\xi)/S$, such that $t_j < t_f$ as it is defined to correspond to a source event within the time interval of the simulation.

A Fortran code has been written to simulate neutron random walks, shown in Fig. 3.2 for a given batch of histories, where we have eliminated numeric-type (e.g., real, integer) designation to declutter the code. The displayed code is written in

```
do i = 1,histories
   persistent_ns = 0
   call INITIAL_CONDITION(SF_events, SF_times, initial_n)
   Events_to_track = SF_events + initial_n
   !Follow initial n (if there is one) and all SF events:
   do j = 1,Events_to_track
      if (j .eq. SF_events + 1) then
         !Tracking the initial n (if there is one):
         ns = 1
      else !SF_events>0 & we are tracking a SF-born n
         !Sample # of ns emitted in the j^th SF event
         call SFMD_SAMPLER(ns)
      end if

      !Follow individual k ns produced in j^th event:
      do k = 1,ns
         !Assign initial time or emission time:
         if (j .eq. SF_events + 1) then
            !We are simulating the initial n (last)
            t = t_o
         else
            t = SF_times(j)
         end if
         call random_number(xi)
         s = -log(xi)/XS_a
         t = t + s/vel
         !Check for persistence passed tf
         if (t .gt. tf) then
            call BIN_POP(persistent_ns)
            cycle
         end if
         !Sample outcome:
         call random_number(xi)
         if (xi .le. micro_xs_c/micro_xs_a) then
            !Captured:
            cycle
         else
            !Induced Fission:
            call FISSION(t, persistent_ns)
         end if
      end do !Individual particle loop
   end do !Event track loop
end do !history loop
```

Figure 3.2: Essence of an Event Based MC Algorithm (for a single batch).

a general sense to allow for simulations of single chains, source-driven systems, or the combination of both. The simulation is commenced by determining the initial population of the system as well as sampling the number of source events and their corresponding source times (if applicable). From this, we engage a nested loop that will simulate each event throughout the time interval given the time the event occurred. If the event being simulated is a source event, we sample from the multiplicity CDF which then prompts a nested loop that then individually simulates each particle. It is here that we perform the random sampling which was just discussed in the previous paragraphs. By sampling a distance to collision, updating the time, checking if $t_s \geq t_f$ (if true, call on `BIN_POP`, which simply adds `persistent_ns = persistent_ns + 1`), and then determining the interaction that takes place, we capture the essence of an event based MC algorithm.

Of utmost interest to the study of neutron-multiplying systems is contained with the `FISSION` subroutine, and an example code is displayed in Appendix D. Following the progeny of a fission event may become quite an involved process when successive fissions may be induced by any number of neutrons. The example code shows how we implemented a systematic methodology for saving the current generation and previous generation of particles and follow each particle in the current generation either to its demise, the final time is surpassed, or another fission is induced. If another fission is induced, we sample the multiplicity of particles and bank them in the next generation to be simulated once the current generation has finished. For supercritical systems, a chain may diverge and as the criticality increases the number of diverging chains will follow suit. There then must be a mechanism built into the code to abandon the `FISSION` subroutine if it is clear that the chain will continue to grow without bound. For marginally supercritical systems, the time it takes for certain chains to reach such a level makes the analog MC method wholly inefficient as the chains will persist for long times. It has been proposed by Méchitoua that the

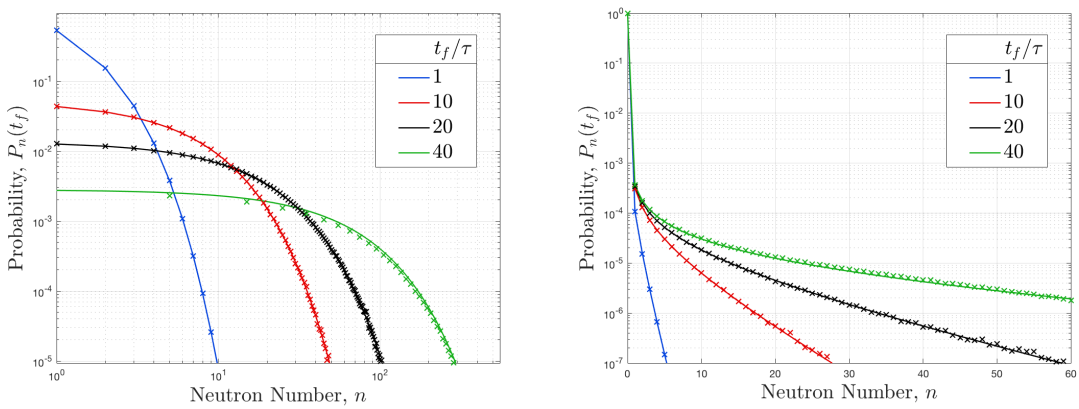

Figure 3.3: Comparison of MC (x) and analytical (-) GBFM number distributions for a supercritical system for (a) single chains and (b) in the presence of a weak source.

population cutoff, C, should follow the formula [33]:

$$C = \frac{10}{k-1} \tag{3.7}$$

for $k > 1$. That is, as $k \to 1$, the likelihood of a single chain to diverge is less certain and one must simulate to longer chain lengths to guarantee divergence. As has been observed in practice by Gregson [34], one may set C to 10^6 for $k = 1.00001$, which may be regarded as the transition from a strongly stochastic to a weakly stochastic population regime. For this reason, in any MC result we show, we set the divergence cutoff to 10^6.

Figure 3.3 demonstrates a supercritical system with $k = 1.0500$ and a neutron lifetime of $\tau = 1.4689\ ns$ using an IF multiplicity distribution of $\langle q_0^f, q_1^f, q_2^f \rangle = \langle 0.1, 0.35, 0.55 \rangle$ (giving $\overline{\nu} = 1.45$), corresponding to the Generalized BFM. Figure 3.3a shows the single chain number distribution of Eq. 2.46 compared with the MC simulation results. For the $t_f/\tau = 40$ case, the code switched to bin widths of $\Delta n = 5$ due to the increasing persistence of the particles. As expected, the later we observe the system, the higher likelihood we will see larger particle populations. Figure 3.3b

shows the number distribution in the presence of a source of strength $S = 10^5\ 1/s$ and $\eta = 3.6881 \cdot 10^{-4}$ compared with Eq. 2.47.

3.3.2 Incorporation of Space and Energy

In this section, we present the equations necessary to adapt an EBMC algorithm to account for space and energy dependence. The primary motivation for doing so is to contrast the other MC method, the Stochastic Simulation Algorithm, discussed later in this chapter. For detailed discussions and results, we refer the reader to [16].

Spatial Dependence

In this section, we consider spatial dependence in one-dimensional slab geometry and then show how to simulate one-dimensional spherical systems. The process of source time emission is the same as in the previous and now we assume the source is evenly distributed in space and we can sample a SF event location x by generating a random number $\xi \in [0, 1)$ using the equation

$$x = (x_R - x_L)\xi + x_L \tag{3.8}$$

where x_L and x_R are the left and right boundary coordinates of the slab. From this source event, we sample the cosine of the angle of emission relative to the x-axis, μ such that $\mu \in [-1, 1]$, by assuming isotropic emission and, upon generating a new random number, we have

$$\mu = 2\xi - 1. \tag{3.9}$$

Now that we have a position of emission and a direction of travel, we must determine the distance travelled to the next collision site, s, using Eq. 3.5. The updated position within the slab, x', relative to the x-axis is then calculated as

$$x' = x + s\mu, \tag{3.10}$$

and the updated time t_s is $t_s = t + s/v$. We must now concern ourselves with four possible scenarios before we proceed:

1. $t_s > t_f$, $x' \in [x_L, x_R]$: n^0 collision site is within the system and the n^0 is still in transit at t_f , bin as persistent n^0 and move onto the next particle.

2. $t_s < t_f$, $x' \notin [x_L, x_R]$: n^0 collision site is out of the system and the n^0 arrives at site before t_f , bin as either left- or right-leaked n^0 and move onto the next particle.

3. $t_s > t_f$, $x' \notin [x_L, x_R]$: n^0 has either leaked or persisted, we must determine the distance to the boundary and the time to get to the boundary and compare to the final time. Discussed below.

4. $t_s < t_f$, $x' \in [x_L, x_R]$: n^0 collision site is within the system

Concerning item 3, the collision site is out of the system and the time to get there is greater than the final time. To determine if the neutron is classified as persistent or leaked, we calculate the distance to the boundary, s_b, as

$$s_b = \begin{cases} s - \frac{x - x_R}{\mu} & \text{for } \mu > 0 \\ s - \frac{x - x_L}{\mu} & \text{for } \mu < 0. \end{cases} \tag{3.11}$$

Recall x is the original location of the neutron, not the collision site. We then determine the time to get to the boundary, t_b, as being

$$t_b = t + \frac{s_b}{v}, \tag{3.12}$$

where t is, again, the time that the neutron was at the original site. We can then determine whether the neutron was in the system at the final time, if $t_b > t_f$ (the time to get to the boundary was greater than the final time), or if it had leaked, $t_b < t_f$. Concerning item 4, we must then proceed to sample from the discrete CDF of the cross-sections and carry out the event that occurs.

We now consider the algorithm for a spherical system. We maintain the assumptions that source emission as well as scattering events are isotropic and that the source is evenly distributed in space. In order to sample locations of spontaneous fission events within the sphere, the spatial probability density function at a radial position, $f(r)$, must depend on the mass associated with that position. The mass of a sphere is proportional to the volume V and and incremental mass is proportional to the volume of an incremental shell, $\mathrm{d}V$, thus the appropriate spatial probability distribution is [51]:

$$f(r)\,\mathrm{d}r = \frac{\mathrm{d}V}{V} = \frac{3r^2}{R^3}\,\mathrm{d}r, \tag{3.13}$$

and the CDF, $F(r)$, for which to sample a radial position of emission is then

$$F(r) = \xi = \int_0^r \mathrm{d}r' f(r') \quad \rightarrow \quad r = \sqrt[3]{\xi} R \tag{3.14}$$

where R is the radius of the system, $r \leq R$. Once the radial position is known, we sample an angle of emission, assumed to be isotropic, and use Eq. 3.9. Note that $\mu \in [-1, 1]$ is now the cosine of the angle made between the radial coordinate vector and the direction of neutron travel. Next, the distance to collision is sampled using Eq. 3.5 and the new radial position r' is updated using

$$r' = \sqrt{r^2 + s^2 + 2rs\mu}. \tag{3.15}$$

We use the same enumerated steps as stated above, where the distance to the boundary may be calculated as:

$$s_b = \sqrt{R^2 - r^2(1 - \mu^2)} - r\mu. \tag{3.16}$$

If the neutron number distribution for the single chain in a spatial setting is to be determined, one must consider a single injection location site for all batches to be performed. This opposes the above random sampling of source emission locations discussed above and introduces greater inefficiencies to the analog EBMC algorithm.

Regarding the resultant number distribution, this will provide the probability of having n particles in the system due to the introduction of a neutron at the given point at the earlier time. This is equivalent to the solution of the Pál-Bell equation, to be discussed in Chapter 5.

Energy Dependence

We next discuss the incorporation of multigroup energy binning of the neutrons, following the work in [16] whose goal was to benchmark LANL's deterministic neutron transport code PARTISN [35]. Extending the MC to account for multigroup neutrons is accomplished by converting the cross-sections, multiplicity distributions, and sources into arrays (with max dimension equal to the number of energy groups) that are then used to sample a neutron's energy or, more specifically, which energy bin the neutron is in. As an example, if a neutron appears as a result of a spontaneous fission, the discrete CDF of the group-dependent source strengths are sampled to determine the energy, whereas a neutron born from an induced fission will have its energy sampled from the χ-spectrum. The data is extracted from a PARTISN output file and this allows one to construct the necessary CDFs for energy bin sampling as a means of replicating the exact same system that the multigroup adjoint deterministic transport code is solving.

Perhaps the most important difference between the monoenergetic and the multigroup calculations is found in the scattering interactions. As it turns out, PARTISN has absorption-emission events, such as $(n, 2n)$, embedded in the scattering matrix produced in the output file when NDI is used to generate the data. Thus, it has proven necessary to include these events in the simulation process by calculating an effective $\overline{\nu}_{s,g}$ for scattering events as a function of the incident neutron energy and sampling the number of neutrons created in every scatter event. This sampling is done by selecting a random number ξ and comparing it to the difference $d = \overline{\nu}_{s,g} - \lfloor \overline{\nu}_{s,g} \rfloor$, so that if $\xi \leq d$, the number of neutrons born in the scatter event is $\lceil \overline{\nu}_{s,g} \rceil$, and if

$\xi > d$, the number of neutrons born in the scatter event is $\lfloor \overline{\nu}_{s,g} \rfloor$. Note that the notation $\lfloor x \rfloor$ and $\lceil x \rceil$ are the floor and the ceiling functions of x, respectively. It would be ideal to sample the number of neutrons created in an (n, xn) reaction from a multiplicity distribution, just as with any other stochastic neutron source, rather than sampling only two possible outcomes about the average number emitted per scatter event.

3.4 The Stochastic Simulation Algorithm

The Stochastic Simulation Algorithm (SSA) was developed by Gillespie for the study of the dynamics of chemical reactions [37], although the fundamentals had been known since the 1940s and 1950s with work done by Bartlett [38]. The SSA samples time intervals between interactions and the resultant outcomes based on the reaction rates of the particle populations. The sum of the population reaction rates is the state transition rate CDF, which is simply obtained from the coefficients of the forward Master equation. In that sense, the SSA is effectively a direct simulation of the forward Master equation [39].

In traditional event based MC simulations, one simulates a single particle and samples distance and time intervals dependent on the cross-sections of the system the neutron is traversing. In the event of secondary particle production, one must save location and time of birth, and simulate those particles as well. In the SSA approach, we instead propagate the population state of the system and sample time intervals between events that transition the system to a new population state. The appeal of the SSA is that we do not need to allocate computer memory for all secondary particles and the associated phase-space coordinates but, rather, simply update the state of the system based off of those particles produced.

In proceeding, we consider a system composed of J regions, each with a neutron population, n_j. We allow for a neutron source in any region, S_j, to be defined as

the probability of a source emission per unit time and we recall the probability of a neutron interacting per unit time in region j is $\lambda_{y,j}$, where $y = \{c, f, \ell\}$ for capture, induced fission, and leakage, respectively. The probability that, upon leaking from region j, a neutron's trajectory coincides with region k is symbolized as $p_{j\to k}$ and is referred to as the transfer probability, and its complement, the non-transfer probability is $p_{j\to\infty} = 1 - \sum_k p_{j\to k}$. We consider the determination of the reaction rates in Appendix B and transfer probabilities later in Sec. 4.2.

We define the state the system occupies at a time t as $\mathbf{X}(\vec{n}, t)$, where

$$\vec{n} = \langle n_1, n_2, \ldots, n_J \rangle^T \tag{3.17}$$

is the vector composed of the region-specific particle populations. We may then write an expression defining the total probability per unit time that an event will occur within the system that will cause a departure from state $\mathbf{X}$, which we will henceforth call the state transition probability rate, $\mu(\mathbf{X})$. The transition probability rate is simply the sum of the individual event probability rates. Thus, if the probability of event i in region j is $e_{i,j}$, the transition probability rate is

$$\mu(\mathbf{X}) = \sum_{j=1}^{J} \sum_{i} e_{i,j},$$

and as we are considering source events and events in which the neutron population is altered upon interacting with the material, our transition probability per unit time is

$$\mu(\mathbf{X}) = \sum_{j=1}^{J} \left\{ S_j + n_j \lambda_{t,j} \right\}, \tag{3.18}$$

where the total state transfer rate for region j is $\lambda_{t,j} = \lambda_{c,j} + \lambda_{f,j} + \lambda_{\ell,j}$.

In order to simulate our collection of regions and the particles interacting within them, we employ the SSA. The rates may be time-dependent, but for introductory purposes of the algorithm we reserve time-dependent rates until Sec. 4.4. It is vital to make clear that the rates are an input into the SSA and are assumed known. The SSA does not permit the determination of the rates, but is rather a means of ascertaining

the time-evolution of the system, dependent on the rates and the imposed initial state. The general computer algorithm is outlined as follows:

1. Form a list of all rates in the system, i.e., calculate $\lambda_{y,j}$ and S_j.
2. Initialize the system at time $t = 0$ with a predetermined initial neutron population state, $\mathbf{X}(\vec{n}, 0)$.
3. Calculate the cumulative function, $\mu(\mathbf{X}(\vec{n}, t))$.
4. Obtain a uniform random number $\xi \in [0, 1]$.
5. Determine the event to carry out, i, in region j by finding the i, j for which

   $$e_{i-1,j} \ < \ \xi\mu \ < \ e_{i,j}$$

   Carry out event i, finding new population: $\vec{n} \rightarrow \vec{n}'$.
6. Obtain another uniform random number $\xi \in [0, 1]$
7. Update the time with

   $$t' \ = \ t \ + \ \Delta t$$

   where

   $$\Delta t \ = \ -\frac{1}{\mu} \ln(\xi)$$

8. Update new state: $\mathbf{X}(\vec{n}, t) \rightarrow \mathbf{X}(\vec{n}', t')$
9. Either go to step 3 if $t < t_f$ or terminate the simulation if $t \geq t_f$.

By design, steps 5 and 7 are interchangeable as they are independent of each other. The events to consider in step 5 are outlined in Table 3.2. Also, note that as the

population and/or source strength increases, so does μ, causing the time intervals between events to decrease. If the population becomes too large, the sampled Δt may become unmanageably minute that the SSA may be effectively forced into an infinite loop calculation.

Table 3.2: SSA events that may occur in a given region, j.

Event, $e_{l,j}$	Probability per unit time	Effect	
		n_j	n_k
Source Emission	$S_j q_\nu^{S_j}$	$+\nu$	
Capture	$n_j \lambda_{c,j}$	-1	
Induced Fission	$n_j \lambda_{f,j} q_\nu^{f_j}$	$+(\nu$-1)	
Leakage & no Transfer	$n_j \lambda_{\ell,j} p_{j\to\infty}$	-1	
Leakage & Transfer from $j \to k$	$n_j \lambda_{\ell,j} p_{j\to k}$	-1	+1

In the code-implementation of the SSA, we apply a nested approach to avoid calculating all of the individual probabilities associated with the events in Table 3.2 unless deemed necessary [56]. As an example, suppose we have two regions with sources S_1 and S_2 and total transition rates $\lambda_{t,1}$ and $\lambda_{t,2}$. We call the probability per unit time that a source event occurred $P_S = S_1 + S_2$ and the probability per unit time that a neutron interaction occurred $P_N = n_1\lambda_{t,1} + n_2\lambda_{t,2}$, where $\mu = P_S + P_N$. If we then compare a random number ξ to determine which is satisfied: $0 \leq \xi \leq P_S/\mu$ or $P_S/\mu < \xi \leq 1$, we may then determine that it was either a source event or a neutron interaction in either region 1 or 2.

If a source event occurs in region 1, the criteria (with a different ξ) $0 \leq \xi \leq S_1/P_S$ is satisfied, otherwise $S_1/P_S < \xi \leq 1$ is true and the source event occurs in region 2. Once the region is known, we then sample the number of neutrons emitted in the event using the appropriate CDF of the source multiplicity distribution and update $n_j \to n_j + \nu$.

If a neutron induced event occurs, we first decide which region the event occurred in by checking which criteria is satisfied: $0 \leq \xi \leq \lambda_{t,1}/P_N$ or $\lambda_{t,1}/P_N < \xi \leq 1$ for

region 1 or region 2, respectively. From there, the event that occurs is determined by scanning $0 \leq \xi \leq \lambda_{c,j}/\lambda_{t,j}$ for capture; $\lambda_{c,j}/\lambda_{t,j} < \xi \leq (\lambda_{c,j} + \lambda_{f,j})/\lambda_{t,j}$ for an induced fission; or $(\lambda_{c,j} + \lambda_{f,j})/\lambda_{t,j} < \xi \leq 1$ for a leakage event. For a capture event, simply update the population as $n_j \to n_j - 1$; for an induced fission, we sample from $q_\nu^{f_j}$ to find ν neutrons emitted, and update the population as $n_j \to n_j + \nu - 1$; and for leakage, we say $n_j \to n_j - 1$, and if there is a successful transfer to region k, we update $n_k \to n_k + 1$. Our system is now in state $\mathbf{X}'$, and we then update $\mu(\mathbf{X}')$ using the updated populations to once again repeat the process until either the populations go extinct or the final time is surpassed.

3.5 Number Distribution Parameter Fitting

The discrete neutron number distribution, for single chains and in the presence of a source, were first derived by Prinja and Souto [11] using the Quadratic Approximation of the PGF PDE discussed in Sec. 2.5.1. They then showed the equivalence of their distributions to Bell's original 1963 work when certain conditions on the neutron population and system time are met [11, 12], discussed in Sec. 2.6. We consider the essence of their findings below and we then discuss the importance of these asymptotic distributions in the characterization of fissile multiplying systems and how we may apply this information to quantifying the status of the neutron population in coupled regions using the SSA.

We only consider systems with sources for which the system reactivity is constant. For long times periods since the initial time such that $t \gg 1/\alpha$, we may assume that the neutron population has grown so that probabilities away from $n = 1$ have developed to non-negligible values. This implies that the average of the population, $\overline{n}(t)$, has departed from the low population domain. Under similar arguments outlined by Prinja and Souto, one may find the Bell distribution for a system with a singlet

emitting source to be a limiting case of Eq. 2.45 to be

$$P(n,t) = \left[\frac{\eta n}{\overline{n}(t)}\right]^{\eta-1} \frac{\eta}{\Gamma(\eta)\overline{n}(t)} \exp\left\{-\frac{\eta}{\overline{n}(t)} n\right\}. \tag{3.19}$$

With this, we wish to determine if the systems composed of coupled regions are behaving like this asymptotic distribution at a given time. In particular, we are interested in establishing whether or not the PDF of an individual region, or the composite PDF for the collection of regions, in the presence of a source will behave as the gamma distribution given by Eq. 3.19. As an example, we show the behavior of the Bell distribution compared with the Prinja-Souto distribution for sub- and supercritical systems in Figs. 3.4 with $\eta = 9.7351 \cdot 10^{-4}$. For Fig. 3.4a, a subcritical system with $k = 0.8788$, we see that both distributions asymptotically converge by 100 lifetimes, but they do not converge onto one another. Thus, the distributions for subcritical systems do not share an asymptotic form. However, the supercritical system of Fig. 3.4b, with $k = 1.0035$, shows that the discrete and continuous distributions do indeed converge to a common form.

Given an SSA simulation (or any MC simulation) resulting in the successful, statistically converged, calculation of the PDFs of each region, $P_{n,j}(t_f)$, given by Eq. 3.1, as well as the first two moments according to the batching method in Table 3.1, we wish to determine if any of these PDFs are gamma-like. This can be done by comparing Eq. 3.19 to the general form of a gamma distribution:

$$f(n|\alpha,\beta) = \frac{\beta^\alpha}{\Gamma(\alpha)} n^{\alpha-1} \exp\{-\beta n\}, \tag{3.20}$$

where we see that $\alpha = \eta$ is the shape parameter and $\beta = \eta/\overline{n}(t_f)$ is the scale parameter. The mean, $\mu_{\Gamma}(t_f)$, and variance, $V_{\Gamma}(t_f)$, of the gamma distribution are given by

$$\mu_{\Gamma}(t_f) = \frac{\alpha}{\beta} = \overline{n}(t_f) \tag{3.21a}$$

$$V_{\Gamma}(t_f) = \frac{\alpha}{\beta^2} = \frac{[\overline{n}(t_f)]^2}{\eta}. \tag{3.21b}$$

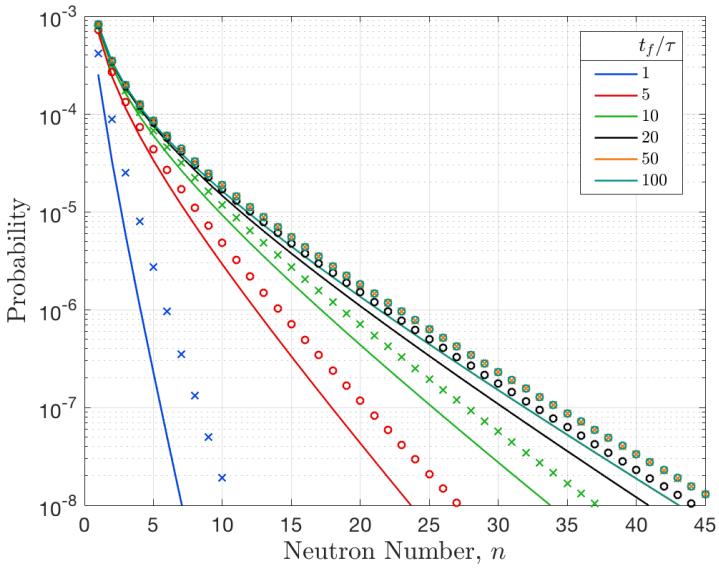

(a)

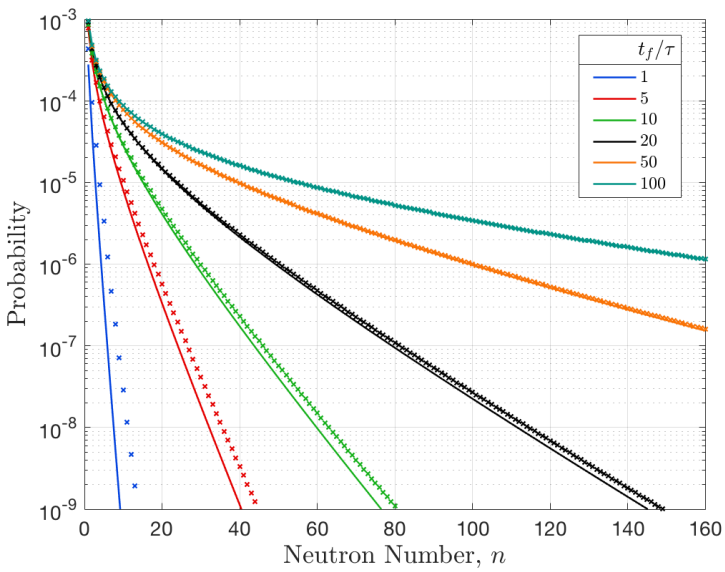

(b)

Figure 3.4: Comparison of the Bell and Prinja-Souto distributions for (a) a subcritical system and (b) a supercritical system. Solid lines are the Bell distribution and the discrete points, x and ∘, are the Prinja-Souto distribution.

If we then set the moments as determined from the SSA to the quantities above, we may then compare the SSA PDF to the gamma distribution with the moments derived from the SSA simulation to aid in the determination of whether or not the SSA PDF is indeed gamma-like. Thus, if $\mu_{SSA}(t_f)$ is the average obtained through SSA and $V_{SSA}(t_f)$ is likewise the variance, we set $\mu_{SSA}(t_f) = \mu_\Gamma(t_f)$ and $V_{SSA}(t_f) = V_\Gamma(t_f)$ to find the appropriate $\overline{n}(t_f)$ and η to insert into Eq. 3.19:

$$\overline{n}(t_f) = \mu_{SSA} \tag{3.22a}$$

$$\eta = \frac{\mu_{SSA}^2}{V_{SSA}}. \tag{3.22b}$$

As a preliminary assessment, we may evaluate the fitted PDF, $P_\Gamma(n, t_f)$, at the same n values corresponding to the SSA PDFs and calculate the error at the i^{th} point of $n = n_i$ as

$$\epsilon_i = \left| 1 - \frac{P_{n_i,SSA}(t_f)}{P_\Gamma(n_i, t_f)} \right|, \tag{3.23}$$

and if the maximum error is less than some prescribed tolerance, ε, we may say that the SSA PDF has evolved into a gamma distribution. One must be wary when evaluating the fitted distribution for values of n near zero when $\eta < 1$, as this causes a singularity in the first coefficient of Eq. 3.19 for $n \to 0$. It is recommended that, when determining the error for such fitted distributions, to begin the error calculation at a mesh point away from the $n = 0$ point; we have seen that starting the error at the next mesh point of $n = 1$ is sufficient to avoiding any unrealistic and insurmountable errors that would prevent one from recognizing the SSA PDF to be that of a gamma PDF.

On a final note, the Central Limit Theorem tells us that the gamma distribution of shape parameter α will converge to the normal distribution for large α [62] (application of Slutsky's Theorem which shows that the moment generating function of the gamma distribution converges to that of the normal distribution). This knowledge will prove beneficial when we happen upon number distributions with large mean and

small standard deviation relative to the mean. For such systems, the calculation of the gamma function will become difficult, and effectively impossible for arguments $\eta > 171.62$ (Eq. 3.22b), i.e., $\Gamma(\eta > 171.62) \geq 1.7 \cdot 10^{308}$– the largest number conventional computation can handle. For this reason, we check for arguments $\eta > 170$ and use a normal distribution with mean μ and standard deviation σ to estimate the convergence of our SSA PDFs to a known distribution:

$$f\left(n|\mu,\sigma^2\right) = \frac{1}{\sqrt{2\pi\sigma^2}} \exp\left\{-\frac{(n-\mu)^2}{2\sigma^2}\right\}. \tag{3.24}$$

Thus, we may simply set $\mu = \mu_{_{SSA}}$ and $\sigma^2 = V_{_{SSA}}$ in the above equation and perform the necessary error computation to assess convergence to a gamma/Gaussian distribution. As expressed previously in Sec. 3.2, we also know that a normal distribution has a skew value $\gamma = 0$ and kurtosis $\kappa = 3$; then if the respective moments of the SSA PDF are near these values, we may further conjecture on the certainty of the convergence to a normal distribution.

In the results section of Chapter 4, we will assess whether or not a system will be properly represented by the gamma distribution for a given final time and, when placed within the proximity of another neutron-multiplying system, under what conditions will a system that would not reach a gamma distribution approach one.

3.6 Comparison of the EBMC and the SSA

In this section, we explore the efficiency of the two Monte Carlo methods we have explored in this chapter and whether one outperforms another for a range of criticality values. We perform this analysis on lumped systems with monoenergetic neutrons and we only consider single neutron chain simulations to remove the stochasticity of times of source events. Following the same reasoning, we also reduce the induced fission neutron multiplicity to produce 2 particles per event, i.e., $q_\nu^f = \delta_{\nu,2}$, reducing

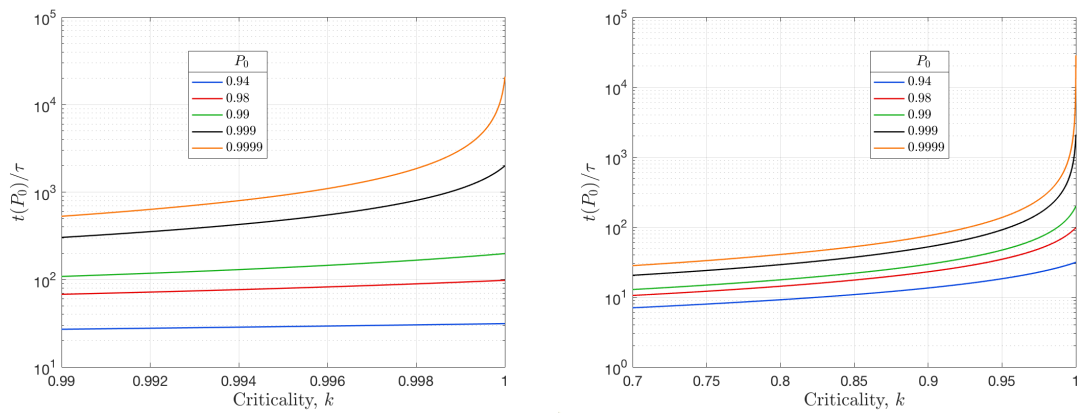

Figure 3.5: Lifetime-normalized time at which there is a certain probability that a single neutron chain will have gone extinct for the BFM for (a) very near critical and (b) over a greater k domain.

the GBFM equations of Sec. 2.5.2 to the BFM equations of [16]:

$$P_0(t) = \frac{\lambda_c \left(1 - \mathrm{e}^{\alpha t}\right)}{\lambda_c - \lambda_f \mathrm{e}^{\alpha t}} \tag{3.25a}$$

$$P_n(t) = \alpha^2 \mathrm{e}^{\alpha t} \left[\lambda_f \left(1 - \mathrm{e}^{\alpha t}\right)\right]^{n-1} \left[\lambda_c - \lambda_f \mathrm{e}^{\alpha t}\right]^{-(n+1)} \qquad n = 1, 2, \ldots \tag{3.25b}$$

Before showing results, we present a set of metrics for choosing an appropriate final time and population limit as a means of reducing unnecessary computation time but to allow for the codes to simulate the majority of the fission chains we initiate. Finally, we remove all neutron number PDF and moment calculation capabilities from the codes so as to eliminate any unnecessary time taken to work with said arrays for what are effectively auxiliary capabilities not inherent in the algorithms.

For subcritical systems, we determine the final time to run a system to by inverting the extinction probability, Eq. 3.25a, and setting $P_0(t)$ to some value near unity, giving the expression:

$$t(P_0) = \frac{1}{\alpha} \ln\left(\frac{1 - P_0}{1 - \frac{\lambda_f}{\lambda_c} P_0}\right), \tag{3.26}$$

where we recall that $\alpha = (k-1)/\tau$. We show the time to a certain probability of extinction of a single chain in Fig. 3.5 for the BFM for varying system criticality normalized by the neutron lifetime at that criticality. As the system approaches exactly critical, the time that the fission chain will propagate increases and, for near certain extinction ($P_0 = 0.9999$), we must effectively simulate $\sim 30,000$ generations of particles before the chain most certainly perishes. If we do not go above $k = 0.995$, we may keep the final time below $10^3\tau$.

Concerning supercritical regimes, we will use Eq. 3.7 to determine at what population, C, to terminate a simulation dependent on the criticality; we will round C to the next largest integer (i.e., $C = \lceil C \rceil$). This presents challenges in the fission subroutine for the EBMC due to the need to bank the times of fission events of the progeny. As stated earlier, the fission subroutine has been written to allow for dynamic allocation of the "time bank" arrays, but in this study, we remove this capability and preallocate the bank arrays to be the size of C, removing a potential slow-down of the EBMC code. For consistency, we embed this cutoff feature in the single chain SSA code as well.

If we wish to simulate the majority of the supercritical chains to an assured diverged population level, we must devise a means of determining how long it must take for a chain to have grown to C or greater. We accomplish this by first defining $Q_N(t)$, the probability that the neutron population has grown to N or greater. Noting the normalization: $1 = P_0(t) + \sum_{n=1}^{C-1} P_n(t) + \sum_{n=C}^{\infty} P_n(t)$, we may write:

$$Q_C(t) = \sum_{n=C}^{\infty} P_n(t) = 1 - P_0(t) - \sum_{n=1}^{C-1} P_n(t). \tag{3.27}$$

In the limit of $t \to \infty$, we know for supercritical systems that the only two non-zero probabilities of the number distribution are $P_0(\infty)$ and $P_\infty(\infty) = P_\infty$, or commonly referred to as the probability of initiation or POI [11]; then $Q_C(\infty) = P_\infty$. From this, if we are able to predict the time at which a system has converged to the POI within a given percentage, we may determine an appropriate cutoff time for the efficiency

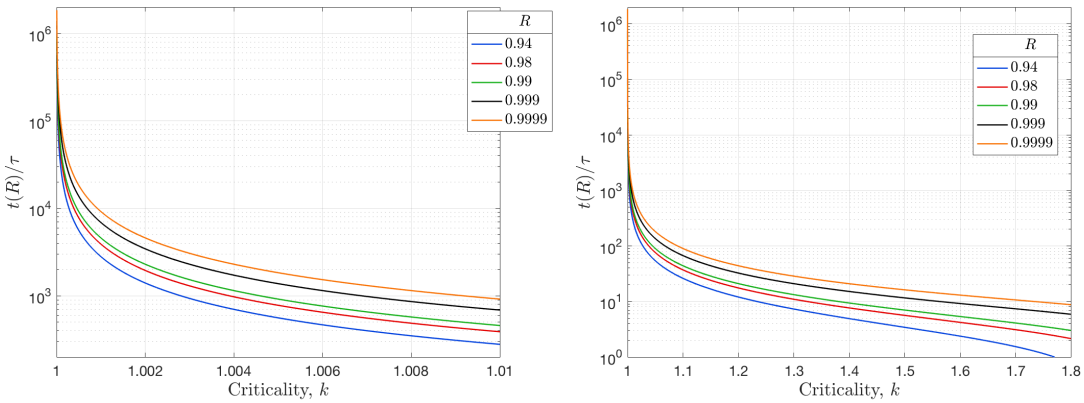

Figure 3.6: Lifetime-normalized time at which there is a certain probability that a single neutron chain will have diverged for the BFM for (a) very near critical and (b) a larger breadth of k values.

simulations. Noting that the survival probability of a single chain, $P_S(t)$, converges to the POI, P_∞, we then define the ratio of the POI to the survival probability as

$$R(t) = \frac{P_\infty}{P_S(t)}, \tag{3.28}$$

where $R(t) \in [P_\infty, 1]$ and $P_\infty = 1 - \frac{\lambda_c}{\lambda_f}$ for the BFM. By setting R to a desired convergence threshold, we may once again solve the BFM distribution equations for t to find:

$$t(R) = \frac{1}{\alpha} \ln\left(\frac{\lambda_c}{\lambda_f} \cdot \frac{1}{1-R}\right). \tag{3.29}$$

Figure 3.6 shows the lifetime-normalized solution to Eq. 3.29 for a range of super-critical values. If we examine the $R = 0.9999$ line in Fig. 3.6a, we see that for the system to have effectively converged to the POI (at a finite time), we need to run the simulation to at least $10^3\tau$ for $k = 1.01$; we will avoid $k < 1.01$ for this reason. As we approach critical, we need to run the simulation to over $10^6\tau$ or more to converge to the POI. Keeping Eqs. 3.26 and 3.29 in mind, we are now prepared to assess the EBMC and the SSA for all interesting criticality values.

Using FORTRAN90's intrinsic CPU timing function, `cpu_time`, we determine the average time, $\bar{t}$, to perform $H = 10^4$ histories by running H histories 10^3 times and taking the average time to complete the set. Each simulation is initiated with a random seed derived from random data retrieved from the operating system [52]. Table 3.3 shows the cutoff criteria used in the EBMC and the SSA simulations along with the average time to complete H histories. Taking the ratio of the two times, we see in the final column of Table 3.3 that the SSA tends to outperform the EBMC quite substantially, especially in the subcritical regime. Interestingly, the ratio between the times for the supercritical tests appear to be constant around 3. One possible slow down of the EBMC code may reside in the preallocation of the arrays and the continual sorting through those arrays to retrieve the times that fission events occurred. This is entirely circumvented in the SSA as a single integer number, the instantaneous population, is required to propagate the algorithm. As this was written as a test of the utmost minimal capabilities of the codes, it is no surprise that the SSA tends to outperform the EBMC for the range of parameters specified herein.

Table 3.3: Performance of the EBMC and the SSA.

k	C	t_f/τ	$\bar{t}$ for $H = 10^4$, $[sec]$		$\bar{t}_{\mathrm{EBMC}}/\bar{t}_{\mathrm{SSA}}$
			EBMC	SSA	
0.70	150	30	0.21112	0.0048777	43.2827
0.75	150	35	0.24877	0.0058497	42.5270
0.80	150	40	0.29824	0.0071449	41.7417
0.85	150	50	0.37193	0.0094989	39.1551
0.90	150	80	0.46364	0.014117	32.8427
0.95	150	110	0.57968	0.028111	20.6211
0.98	200	300	1.18472	0.069667	17.0055
0.99	300	500	2.3024	0.13847	16.6274
1.01	$1,000$	$1,000$	7.67601	2.59001	2.9637
1.02	500	400	3.70768	1.33885	2.7693
1.05	200	200	1.34369	0.507638	2.6469
1.10	100	100	0.675714	0.247192	2.7336
1.15	66	60	0.442542	0.148314	2.9838
1.20	50	45	0.331859	0.107099	3.0986
1.25	40	35	0.266438	0.0834514	3.1927
1.30	34	30	0.218202	0.0666220	3.2752

Chapter 4

Coupling Effects of Communicable Assemblies

In this chapter, we consider the effects on the neutron number distribution when multiplying assemblies are placed within close proximity. In particular, we vie to understand source driven lumped systems where we allow for energy-dependence on the neutron number and we also incorporate the possibility of leakage events. We employ methods discussed in the previous chapters to better understand such arrangements. We develop Master equations and moment equations for code benchmarking purposes in Sec. 4.1, followed by a discussion on two possible methods for calculating the probabilities of leaking and transferring from one lumped assembly to another in Sec. 4.2. In Sec. 4.3, we utilize the efficient Stochastic Simulation Algorithm (SSA) to simulate two regions and to garner an intuition of the PDFs, and the chapter is concluded by demonstrating results for time-dependent reactivity insertions in Sec. 4.4.

4.1 Master and Moment Equations

In this section, we derive the forward Master equations and, subsequently, equations for the moments of the particle population distributions of interest. We begin by considering the general case of an arbitrary number of regions and monoenergetic neutrons in Sec. 4.1.1, each with a neutron population and we then allow for two energy groups in the next section, Sec. 4.1.2.

4.1.1 Multiple Regions with Monoenergetic Neutrons

Consider a collection of J lumped regions, with the j^{th} region being characterized by neutron interaction rates for capture, fission, and leakage, as well as containing an intrinsic constant randomly emitting source, S_j. We state the forward Master equation whose solution is the probability that at some time t there are n_1 neutrons in region 1, n_2 neutrons in region 2, and so on to n_J neutrons in region J- defined by $P_{\vec{n}}(t)$, where $\vec{n} = \langle n_1, n_2, \ldots, n_J \rangle^\top$:

$$\begin{aligned}\frac{\mathrm{d}P_{\vec{n}}(t)}{\mathrm{d}t} + \sum_{j=1}^{J} \left[S_j + n_j\lambda_{t,j}\right] P_{\vec{n}}(t) = \sum_{j=1}^{J} \Bigg\{ & S_j \sum_{\nu=0}^{\nu_m^{S_j}} q_\nu^{S_j} P_{\vec{n}-\nu\vec{\delta}_j}(t) + \lambda_{c,j}(n_j+1)P_{\vec{n}+\vec{\delta}_j}(t) \\ & + \lambda_{\ell,j}(n_j+1)\left[p_{j\to\infty}P_{\vec{n}+\vec{\delta}_j}(t) + \sum_{\substack{k=1\\k\neq j}}^{J} p_{j\to k}P_{\vec{n}+\vec{\delta}_j-\vec{\delta}_k}(t)\right] \\ & + \lambda_{f_j}\sum_{\nu=0}^{\nu_m^{f_j}} q_\nu^{f_j}(n_j-\nu+1)P_{\vec{n}+(1-\nu)\vec{\delta}_j}(t)\Bigg\},\end{aligned} \tag{4.1}$$

where $\vec{\delta}_j$ is a J-length column vector whose only non-zero entry is in position j and is equal to one. The initial condition of Eq. 4.1 is

$$P_{\vec{n}}(t=0) = \prod_{j=1}^{J} \delta_{n_j,N_j}, \tag{4.2}$$

where N_j is the initial particle population in region j.

In proceeding, we obtain ODEs for the moments of the distribution, which can be solved analytically for simple region configurations or numerically in practice. To obtain closed-form equations for the moments (and ideally the PDF as well), we employ the probability generating function (PGF) to transform the Master equation into a PDE:

$$G(\vec{x},t) = \sum_{n_1=0}^{\infty} \cdots \sum_{n_J=0}^{\infty} \prod_{j'=1}^{J} x_{j'}^{n_{j'}} P_{\vec{n}}(t), \tag{4.3}$$

where $\vec{x}$ is a J-length column vector whose j^{th} entry, $x_j \in [0,1]$, is the PGF variable for region j. Applying Eq. 4.3 to Eq. 4.1, we obtain the following PDE:

$$\frac{\partial G}{\partial t} = \sum_{j=1}^{J} \Bigg\{ \Bigg[-\lambda_{t,j} x_j + \lambda_{c,j} + \lambda_{\ell,j} \Bigg(p_{j\to\infty} + \sum_{\substack{j'=1 \\ j'\neq j}}^{J} p_{j\to j'} x_{j'} \Bigg) + \lambda_{f,j} h_f(x_j) \Bigg] \frac{\partial G}{\partial x_j} + S_j \Big(h_S(x_j) - 1 \Big) G(\vec{x},t) \Bigg\}, \tag{4.4}$$

with the initial condition,

$$G(\vec{x}, t=0) = \prod_{j=1}^{J} x_j^{N_j}. \tag{4.5}$$

The generating functions for the multiplicity distributions once again appear naturally and are defined for region i and fission type $y = \{S, f\}$, for spontaneous and induced fission, as

$$h_y(x_i) = \sum_{\nu=0}^{\nu_m^{y_i}} x_i^{\nu} q_{\nu}^{y_i}. \tag{4.6}$$

We now utilize the methodology outlined in Sec. 2.7 to obtain the moments of the PDF directly from Eq. 4.4. In doing so, we arrive at a coupled system of linear ODEs for the first moment of region j:

$$\frac{\mathrm{d}\overline{n}_j(t)}{\mathrm{d}t} = \alpha_j \overline{n}_j(t) + S_j \overline{\nu}_{S,j} + \sum_{\substack{j'=1 \\ j'\neq j}} \lambda_{\ell,j'} p_{j'\to j} \overline{n}_{j'}(t), \tag{4.7}$$

where $\alpha_j = \overline{\nu}_{f,j}\lambda_{f,j} - \lambda_{t,j}$. The initial condition of Eq. 4.7 is $\overline{n}_j(0) = N_j$- the initial number of particles in region j. The moments of the neutron multiplicity distributions, $\overline{(\nu_{y_j})}_m$ (using Pochhammer notation found in Appendix A), appear in the moment equations from taking the necessary m derivatives of Eq. 4.6 and evaluating at $x_i = 1$. Equation 4.7 constitute a set of linear coupled ODEs that can be solved with relative ease using standard time-stepping methods. The size of the system for the first moments is J, but the size of the system of equations drastically grows when we wish to calculate higher order moments.

The second moment for region j are obtained by taking the second order derivative of Eq. 4.4 with respect to x_j, evaluating at $\vec{x} = \vec{1}$, and unfolding the factorial moments to obtain:

$$\begin{aligned}\frac{\mathrm{d}\overline{n_j^2}(t)}{\mathrm{d}t} - 2\alpha_j\overline{n_j^2}(t) = \frac{\mathrm{d}\overline{n}_j(t)}{\mathrm{d}t} + \left[\lambda_{f,j}\overline{(\nu_{f,j})}_2 + 2S_j\overline{\nu}_{S_j} - 2\alpha_j\right]\overline{n}_j(t) + S_j\overline{(\nu_{S_j})}_2 \\ + 2\sum_{\substack{j'=1\\ j'\neq j}}^{J}\lambda_{\ell,j'}p_{j'\to j}\overline{n_j n_{j'}}(t),\end{aligned} \tag{4.8a}$$

$$\begin{aligned}\frac{\mathrm{d}\overline{n_j n_k}(t)}{\mathrm{d}t} - (\alpha_j + \alpha_k)\,\overline{n_j n_k}(t) = \lambda_{\ell,j}p_{j\to k}\left(\overline{n_j^2}(t) - \overline{n}_j(t)\right) + \lambda_{\ell,k}p_{k\to j}\left(\overline{n_k^2}(t) - \overline{n}_k(t)\right) \\ + \sum_{\substack{i=1\\ i\neq j,k}}\lambda_{\ell,i}\left[p_{i\to j}\overline{n_i n_k}(t) + p_{i\to k}\overline{n_i n_j}(t)\right] \\ + S_j\overline{\nu}_{S,j}\overline{n}_k(t) + S_k\overline{\nu}_{S,k}\overline{n}_j(t).\end{aligned} \tag{4.8b}$$

The size of the system of equations given by Eqs. 4.7, 4.8 is $2J + \binom{J}{2}$, where $\binom{J}{2}$ is the binomial coefficient. The initial conditions are simply the products of the initial populations, i.e., $\overline{n_j^2}(0) = N_j^2$ and $\overline{n_j n_k}(0) = N_j N_k$. We will use these moment equations, as well as those in the next subsection, to benchmark new features that are implemented in the SSA code. Numerical methods used for solving these equations are discussed in the results section of this chapter, Sec. 4.3.

4.1.2 Multiple Regions with Multigroup Neutrons

We now allow for neutrons to have an energy dependence to which these neutrons may be characterized as either fast or thermal. We denote the fast group as $g = 1$ and thermal neutrons are then in group 2, $g = 2$. If a superscript is used in the following formulations, it denotes the region that quantity is representing. Per usual, we construct a probability balance for all mutually exclusive events that will alter the neutron population and bring the system to state $\mathbf{n}$, where $\mathbf{n}$ is a $2 \times J$ matrix whose $(g, j)^{th}$ position is $n_{g,j}$– the neutron population for energy group g and region j. In developing the forward Master equation, we assume that only thermal neutrons induce fission, only fast neutrons are born from both induced fission and spontaneous fission events, and thermal neutrons do not up-scatter. From these assumptions, the forward Master equation is

$$\begin{aligned}\frac{\mathrm{d}P_{\mathbf{n}}(t)}{\mathrm{d}t} + \sum_{j=1}^{J}\left\{S_1^j + \sum_{g=1}^{2} n_{g,j}\lambda_{t,g}^j\right\}P_{\mathbf{n}}(t) = \sum_{j=1}^{J}\Bigg\{&(n_{1,j}+1)\lambda_{s,1\to 2}^j P_{\mathbf{n}+\boldsymbol{\delta}_{1,j}-\boldsymbol{\delta}_{2,j}}(t) \\ &+ S_1^j \sum_{\nu=0}^{\nu_m^{S,j}} q_\nu^{S,j} P_{\mathbf{n}-\nu\boldsymbol{\delta}_{1,j}}(t) + (n_{2,j}+1)\lambda_{f,2}^j \sum_{\nu=0}^{\nu_m^{f,j}} q_\nu^{f,j} P_{\mathbf{n}+\boldsymbol{\delta}_{2,j}-\nu\boldsymbol{\delta}_{1,j}}(t) \\ &+ \sum_{g=1}^{2}(n_{g,j}+1)\left[\lambda_{c,g}^j P_{\mathbf{n}+\boldsymbol{\delta}_{g,j}}(t) + \lambda_{\ell,g}^j\left(p_{j\to\infty}P_{\mathbf{n}+\boldsymbol{\delta}_{g,j}}(t) + \sum_{\substack{k=1\\k\neq j}}^{J} p_{j\to k}P_{\mathbf{n}+\boldsymbol{\delta}_{g,j}-\boldsymbol{\delta}_{g,k}}(t)\right)\right]\Bigg\}\end{aligned} \tag{4.9}$$

with the initial condition

$$P_{\mathbf{n}}(t=0) = \prod_{j=1}^{J}\prod_{g=1}^{2}\delta_{n_{g,j},N_{g,j}}. \tag{4.10}$$

We note that $\boldsymbol{\delta}_{g,j}$ is a $2 \times J$ zero-matrix whose only nonzero element is located at (g, j) and is equal to unity.

We wish to derive the equations for the moments of this joint distribution and we thus introduce the PGF:

$$G(\mathbf{x}, t) = \sum_{j=1}^{J}\sum_{g=1}^{2}\sum_{n_{g,j}=0}^{\infty}\prod_{j'=1}^{J}\prod_{g'=1}^{2} x_{g',j'}^{n_{g',j'}} P_{\mathbf{n}}(t), \tag{4.11}$$

from which a PDE is obtained:

$$\frac{\partial G(\mathbf{x},t)}{\partial t} = \sum_{j=1}^{J}\Bigg[S_1^j\Big[h_{S,1}^j(x_{1,j})-1\Big]G(\mathbf{x},t) + \lambda_{s,_{1\to 2}}^j x_{2,j}\frac{\partial G}{\partial x_{1,j}} + \lambda_{f,2}^j h_{f,2}^j(x_{1,j})\frac{\partial G}{\partial x_{2,j}} + \sum_{g=1}^{2}\left(-\lambda_{t,g}^j x_{g,j} + \lambda_{c,g}^j + \lambda_{\ell,g}^j\left\{p_{j\to\infty} + \sum_{\substack{k=1\\k\neq j}} p_{j\to k}x_{g,k}\right\}\right)\frac{\partial G}{\partial x_{g,j}}\Bigg] \tag{4.12}$$

with the initial condition

$$G(\mathbf{x},0) = \prod_{j=1}^{J}\prod_{g=1}^{2} x_{g,j}^{n_{g,j}}. \tag{4.13}$$

Here, the generating function for the multiplicity distribution for fission process ζ is defined as:

$$h_{\zeta,g}^j(x_{i,k}) = \sum_{\nu=0}^{\nu_{m,g}^{\zeta,j}} q_{\nu,g}^{\zeta,j}\cdot x_{i,k}^{\nu}. \tag{4.14}$$

Using similar identities as the previous section, we obtain equations for the moments by taking the desired order of derivatives with respect to the variable that corresponds to the moment we seek and then evaluating at $\mathbf{x}=\mathbf{1}$. In doing so, ODEs for the first moments are:

$$\frac{\mathrm{d}\overline{n}_{1,j}(t)}{\mathrm{d}t} = -\lambda_{t,1}^j\overline{n}_{1,j}(t) + \overline{\nu}_{f,2}^j\lambda_{f,2}^j\overline{n}_{2,j}(t) + \overline{\nu}_{S,1}^j S_1^j + \sum_{\substack{k=1\\k\neq j}}^{J}\lambda_{\ell,1}^k p_{k\to j}\overline{n}_{1,k}(t) \tag{4.15a}$$

$$\frac{\mathrm{d}\overline{n}_{2,j}(t)}{\mathrm{d}t} = -\lambda_{t,2}^j\overline{n}_{2,j}(t) + \lambda_{s,_{1\to 2}}^j\overline{n}_{1,j}(t) + \sum_{\substack{k=1\\k\neq j}}^{J}\lambda_{\ell,2}^k p_{k\to j}\overline{n}_{2,k}(t), \tag{4.15b}$$

where we emphasize the j superscripts denote the region which the property is to be evaluated and is not a power. The initial condtions are simply the initial populations for each group and region, i.e., $\overline{n}_{g,j}(0) = N_{g,j}$.

For the second moments, we find:

$$\frac{\mathrm{d}\overline{n_{1,j}^2}(t)}{\mathrm{d}t} + 2\lambda_{t,1}^j\overline{n_{1,j}^2}(t) = \frac{\mathrm{d}\overline{n}_{1,j}}{\mathrm{d}t} + 2\left(\lambda_{t,1}^j + \overline{\nu}_{S,1}^j S_1^j\right)\overline{n}_{1,j}(t) + 2\overline{\nu}_{f,2}^j\lambda_{f,2}^j\overline{n_{1,j}n_{2,j}}(t) + \overline{(\nu_{f,2}^j)_2}\lambda_{f,2}^j\overline{n}_{2,j}(t) + \overline{(\nu_{S,1}^j)_2}S_1^j + 2\sum_{\substack{k=1\\k\neq j}}^{J}\lambda_{\ell,1}^k p_{k\to j}\overline{n_{1,j}n_{1,k}}(t)$$

$$\tag{4.16a}$$

$$\begin{aligned}\frac{\mathrm{d}\overline{n_{2,j}^2}(t)}{\mathrm{d}t} + 2\lambda_{t,2}^j\overline{n_{2,j}^2}(t) =& \frac{\mathrm{d}\overline{n}_{2,j}}{\mathrm{d}t} + 2\lambda_{t,2}^j\overline{n}_{2,j}(t) + 2\lambda_{s,1\to 2}^j\overline{n_{1,j}n_{2,j}}(t) \\ &+ 2\sum_{\substack{k=1\\k\neq j}}^{J}\lambda_{\ell,2}^k p_{k\to j}\overline{n_{2,j}n_{2,k}}(t)\end{aligned} \tag{4.16b}$$

where the initial conditions are $\overline{n_{g,j}^2}(0) = N_{g,j}^2$. We see that we now require equations for the correlated moments, and we now show the set of correlated moment equations for the case where $J = 2$:

$$\begin{aligned}\frac{\mathrm{d}\overline{n_{1,j}n_{2,j}}}{\mathrm{d}t} + (\lambda_{t,1}^j + \lambda_{t,2}^j)\overline{n_{1,j}n_{2,j}} =& \ \lambda_{s,1\to 2}^j\left(\overline{n_{1,j}^2} - \overline{n}_{1,j}\right) + \overline{\nu}\lambda_{f,2}^j\left(\overline{n_{2,j}^2} - \overline{n}_{2,j}\right) + \overline{\nu}S_1^j\overline{n}_{2,j} \\ &+ \sum_{\substack{k=1\\k\neq j}}^{J} p_{k\to j}\left(\lambda_{\ell,1}^k\overline{n_{1,k}n_{2,j}} + \lambda_{\ell,2}^k\overline{n_{1,j}n_{2,k}}\right)\end{aligned} \tag{4.17a}$$

$$\begin{aligned}\frac{\mathrm{d}\overline{n_{1,1}n_{1,2}}}{\mathrm{d}t} + (\lambda_{t,1}^1 + \lambda_{t,1}^2)\overline{n_{1,1}n_{1,2}} =& \ \overline{\nu}\lambda_{f,2}^1\overline{n_{1,2}n_{2,1}} + \overline{\nu}\lambda_{f,2}^2\overline{n_{1,1}n_{2,2}} + \overline{\nu}S_1^1\overline{n}_{1,2} + \overline{\nu}S_1^2\overline{n}_{1,1} \\ &+ \lambda_{\ell,1}^1 p_{1\to 2}\left(\overline{n_{1,1}^2} - \overline{n}_{1,1}\right) + \lambda_{\ell,1}^2 p_{2\to 1}\left(\overline{n_{1,2}^2} - \overline{n}_{1,2}\right)\end{aligned} \tag{4.17b}$$

$$\begin{aligned}\frac{\mathrm{d}\overline{n_{2,1}n_{2,2}}}{\mathrm{d}t} + (\lambda_{t,2}^1 + \lambda_{t,2}^2)\overline{n_{2,1}n_{2,2}} =& \ \lambda_{s,1\to 2}^1\overline{n_{1,1}n_{2,2}} + \lambda_{s,1\to 2}^2\overline{n_{1,2}n_{2,1}} \\ &+ \lambda_{\ell,2}^1 p_{1\to 2}\left(\overline{n_{2,1}^2} - \overline{n}_{2,1}\right) + \lambda_{\ell,2}^2 p_{2\to 1}\left(\overline{n_{2,2}^2} - \overline{n}_{2,2}\right)\end{aligned} \tag{4.17c}$$

$$\begin{aligned}\frac{\mathrm{d}\overline{n_{g,1}n_{h,2}}}{\mathrm{d}t} + (\lambda_{t,g}^1 + \lambda_{t,h}^2)\overline{n_{g,1}n_{h,2}} =& \ \overline{\nu}\lambda_{f,2}^g\overline{n_{2,1}n_{2,2}} + \overline{\nu}S_1^g\overline{n}_{2,h} + \lambda_{s,1\to 2}^h\overline{n_{1,1}n_{1,2}} \\ &+ \lambda_{\ell,h}^1 p_{1\to 2}\overline{n_{1,1}n_{2,1}} + \lambda_{\ell,g}^2 p_{2\to 1}\overline{n_{1,2}n_{2,2}}\end{aligned} \tag{4.17d}$$

where it is understood that $\overline{\nu}S_g^j = \overline{\nu}_{S,g}^j S_g^j$, and $\overline{\nu}\lambda_{f,g}^j = \overline{\nu}_{f,g}^j\lambda_{f,g}^j$. For the case of 2 coupled regions, we will need to solve a system of 14 ODEs in order to determine the means and variances of the 4 respective neutron number PDFs.

The reaction rates will be calculated using the methodology outlined in Appendix B. We need to consider specific geometric arrangements of and between the regions

to determine the leakage and transfer probabilities. In the next section, we explore two methods to calculate the transfer probabilities– the effective communication mechanism between the regions in the system.

4.2 Calculation of the Transfer Probabilities

There are several methods for calculating the probability that a neutron, upon leaking, will transfer from one region to another. The two methods we consider in this section are by means of the view factor method as well as random point sampling on a spherical surface coupled with trajectory sampling. The view factor method appears to have the computational advantage when considering approximations of the integrals involved, and will prove beneficial in verification of the SSA code. The point sampling method is more computationally expensive as it requires several random number samplings per leakage as well as for sampling the particle trajectory, but it has the advantage of adhering to a purely Monte Carlo sampling scheme. The point sampling method may be necessary in an experimental validation situation as there are no approximations required. An alternative method to couple to the point sampling method would be to sample a solid angle of emission from the surface and to the solve the equations describing the quadric surface intersection curves to determine if the particle transfers successfully [61]; such a method may be deemed competitive, but is currently out of the scope of this study.

4.2.1 The View Factor Method

The view factor method essentially provides an expression for the fraction one surface 'sees' of another surface, and can be treated as the probability that radiation that is emanating from a surface will then collide with another surface. Unfortunately, there are no closed form analytical expressions for the view factors of two spheres near each

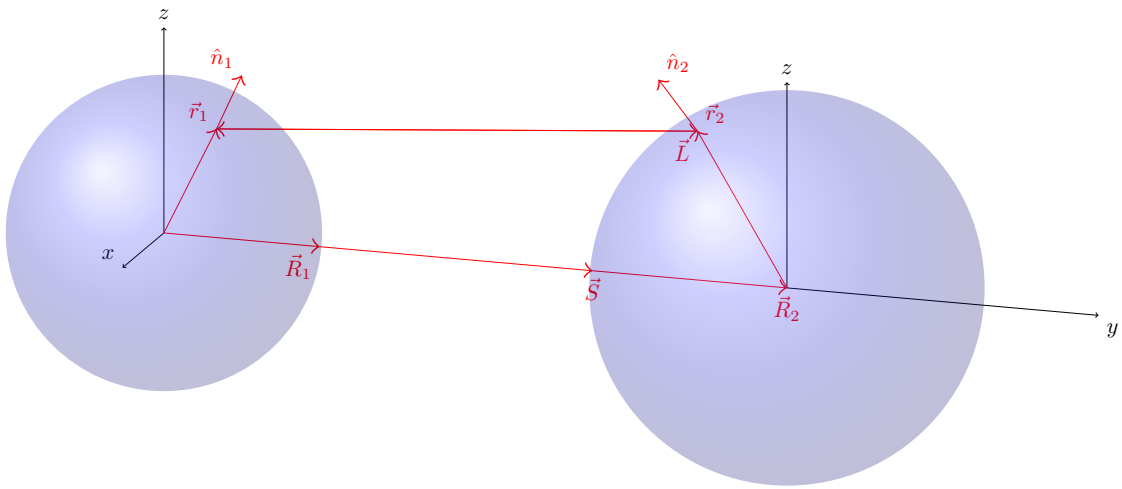

Figure 4.1: Variables involved in the view factor method.

other, but there are some appropriate approximations that we consider. The view factor for one general surface, A_1, to another general surface, A_2, is defined as [58]

$$F_{1\to 2} = \frac{1}{A_1} \oiint_{\partial V_1} \mathrm{d}A_1 \oiint_{\partial V_2} \mathrm{d}A_2 \frac{\cos(\zeta_1)\cos(\zeta_2)}{\pi L^2}, \tag{4.18}$$

where L is the length of a line connecting both surfaces and ζ_1 and ζ_2 are the angles between L and the respective surface normal. From the configuration seen in Fig. 4.1, we may define the surface unit vector for region j as

$$\vec{\hat{n}}_j = \langle \cos(\theta_j),\, \sin(\theta_j)\cos(\phi_j),\, \sin(\theta_j)\cos(\phi_j) \rangle\,, \tag{4.19}$$

and the radial vector anchored at the center of the sphere is defined as

$$\vec{r}_j = R_j \vec{\hat{n}}_j. \tag{4.20}$$

From Fig. 4.1, we see that $\vec{R}_1 = \langle 0,\, R_1,\, 0 \rangle$, $\vec{R}_2 = \langle 0,\, R_2,\, 0 \rangle$, and $\vec{S} = \langle 0,\, S,\, 0 \rangle$, which allows us to define

$$\vec{L} = \vec{r}_1 - \vec{R}_1 - \vec{S} - \vec{R}_2 - \vec{r}_2. \tag{4.21}$$

The cosine of the angles between the surface normal and $\vec{L}$ may be determined using the relationship

$$\cos(\zeta_j) = \frac{\hat{n}_j \cdot \vec{L}}{|\hat{n}_j||\vec{L}|}. \tag{4.22}$$

At this point, we may insert all the relevant equations into Eq. 4.18 and as can be seen, the expression balloons into an incalculable integral, even for this simple geometric setup. One option is to numerically compute this integral [59]. The other option is to approximate the radiating sphere as a point source with a modification that takes into account some of the spatial effects, allowing for the integrand of the double area integral to be separable [60]. This results in a closed-form expression of the view factor with a maximum 5.8% error, occurring in the extreme situation where the radii are equal and the spheres are touching (S=0). The view factor is

$$F_{1\to 2} = \left(\frac{\mathcal{Q}}{\mathcal{R}}\right)^2 \left\{1 - \sqrt{1 - \left(\frac{\mathcal{R}}{\mathcal{Q}}\right)^2}\right\} \left\{1 - \sqrt{1 - \left(\frac{1}{\mathcal{Q}}\right)^2}\right\}, \tag{4.23}$$

where $\mathcal{R} = R_1/R_2$, $\mathcal{S} = S/R_2$, and $\mathcal{Q} = \mathcal{R} + \mathcal{S} + 1$. By the Reciprocity Theorem, if we know the view factor of one surface to another, then the view factor in the opposite direction is related to the ratio of the areas, i.e. $F_{2\to 1} = (A_1/A_2) \cdot F_{1\to 2}$; this gives us the view factor for the other region to the first:

$$F_{2\to 1} = \mathcal{R}^2 F_{1\to 2}. \tag{4.24}$$

Thus, if we consider a system of just two spherical regions, our transfer probabilities are given by

$$\begin{aligned} p_{1\to 2} &= F_{1\to 2} & p_{1\to\infty} &= 1 - F_{1\to 2} \\ p_{2\to 1} &= \mathcal{R}^2 F_{1\to 2} & p_{2\to\infty} &= 1 - \mathcal{R}^2 F_{1\to 2}. \end{aligned} \tag{4.25}$$

Upon leaking from region j, one may sample a neutron transfer to the other system by using a random number ξ. If $0 \leq \xi \leq p_{j\to k}$, then the neutron transfers to region k, and if $p_{j\to k} < \xi \leq 1$, then the neutron drifts into the cosmos. Once this

outcome is known, the populations are updated accordingly and we continue the algorithm outlined in Section 3.4.

This method is attractive because the calculation of the view factors is done once before the SSA commences, and only one random number is needed per leakage to determine whether a transfer is successful or not. Another advantage is the readiness of the transfer probabilities to be placed into benchmarking equations, which is addressed later in this document. On the other hand, for validation purposes, this sampling scheme may prove to be too inaccurate, forcing us to consider a purely Monte Carlo sampling scheme, which we refer to as the Sphere Point Picking Method, described below.

4.2.2 The Sphere Point Picking Method

The sphere point picking method is a drastically more involved process than the previously discussed view factor method, albeit purely Monte Carlo and potentially more accurate given appropriately converged statistics. The method consists of picking a random location on the surface of the leaked-from sphere along with a random direction. Once the leakage point and trajectory are known, we simply check to see if the neutron will then collide with the other system- updating the populations accordingly.

The location of leakage is chosen by sampling a polar angle and azimuthal angle, ϕ and θ, respectively, which map to an (x, y, z) location on the surface- initially a unit sphere centered at the origin. Picking a direction of ejection is similarly done by mapping a random set of polar and azimuthal angles to an *elevated* location near the leakage point. The steps to do so involve first selecting the ϕ' and θ' from the positive four octants of the unit sphere centered at the origin. We then translate the coordinates to the north pole (i.e., simply add 1 to the z' coordinate), and we then rotate these coordinates about the unit sphere to appropriately align with the

leakage point. We then scale these now-rotated coordinates to match with the true size of the sphere the neutron is exiting from, and we then translate the coordinates to the proper location of that sphere. Given these two points (leakage point and the elevated point corresponding to the direction of ejection), we devise a parameterized line and compare whether or not this line intersects the surface of the other system.

Once a neutron exits the system, a location on the spherical surface may be sampled by obtaining two random numbers, ξ_ϕ and ξ_θ, to calculate the polar angle, ϕ, and azimuthal angle, θ. The Formulae to do so are

$$\phi = \cos^{-1}(1 - 2\xi_\phi) \tag{4.26a}$$

$$\theta = 2\pi\xi_\theta. \tag{4.26b}$$

To perform the aforementioned steps as clearly as possible, we first consider selecting points on a unit sphere centered at the origin. Equations 4.26a and 4.26b map to the following leakage coordinates on that surface:

$$x_\ell = \sin(\phi)\cos(\theta) \tag{4.27a}$$

$$y_\ell = \sin(\phi)\sin(\theta) \tag{4.27b}$$

$$z_\ell = \cos(\phi). \tag{4.27c}$$

With these coordinates on the surface of the unit sphere, we use two more random numbers to pick the unique direction the neutron is traveling when ejected from the system. The range of the polar angles relative to the (radially parallel) surface normal at (x_ℓ, y_ℓ, z_ℓ) is now restricted to $\phi' \in [0, \pi/2]$. This is because the $\phi' \in (\pi/2, \pi]$ would correspond to a reentrant neutron, which is precluded by virtue that we are simulating a leakage event. The range of the azimuthal angles remains $\theta' \in [0, 2\pi]$.

The sampling equations and the coordinate mapping are thusly

$$\phi' = \cos^{-1}(\xi_{\phi'}) \tag{4.28a}$$

$$\theta' = 2\pi\xi_{\theta'} \tag{4.28b}$$

$$x' = \sin(\phi')\cos(\theta') \tag{4.28c}$$

$$y' = \sin(\phi')\sin(\theta') \tag{4.28d}$$

$$z' = 1 + \cos(\phi'), \tag{4.28e}$$

where we have translated the coordinates to the north pole of the unit system. The north pole vector, $\hat{N} = \langle 0, 0, 1\rangle$, the ejection direction vector, $\hat{d} = \langle x', y', z' - 1\rangle$, and the vector pointing to the coordinate defining the direction of leakage, $\vec{N}_d = \hat{N} + \hat{d}$ must now be rotated about an axis to align with the leakage location, defined by $\hat{\ell} = \langle x_\ell, y_\ell, z_\ell\rangle$. Specifically, the north pole needs to be rotated *onto* the leakage point by the angle separating them, ϕ, and the other two vectors will follow suit.

Recognizing that we know that ϕ is the angle between $\hat{N}$ and $\hat{\ell}$, we may construct a rotation matrix that we can then use to rotate $\vec{N}_d$ to find $\vec{\ell}_d$ as well as $\hat{d}_\ell = \vec{\ell}_d - \hat{\ell}$ for the unit system as seen in Fig. 4.2. The axis of rotation is the vector that is normal to both $\hat{N}$ and $\hat{\ell}$, and is given by

$$\vec{V} = \hat{N} \times \hat{\ell}. \tag{4.29}$$

The rotation matrix, $\mathcal{R}$, to rotate $\hat{N}$ onto $\hat{\ell}$ is given by

$$\mathcal{R} = \mathbf{I} + [\vec{V}]_\times + [\vec{V}]_\times^2 \frac{1 - \cos(\phi)}{\sin^2(\phi)}, \tag{4.30}$$

where $\mathbf{I}$ is the identity matrix and $[\vec{V}]_\times$ denotes the skew-symmetric cross-product matrix of $\vec{V} = \langle V_x, V_y, V_z\rangle$:

$$[\vec{V}]_\times \equiv \begin{bmatrix} 0 & -V_z & V_y \\ V_z & 0 & -V_x \\ -V_y & V_x & 0 \end{bmatrix}.$$

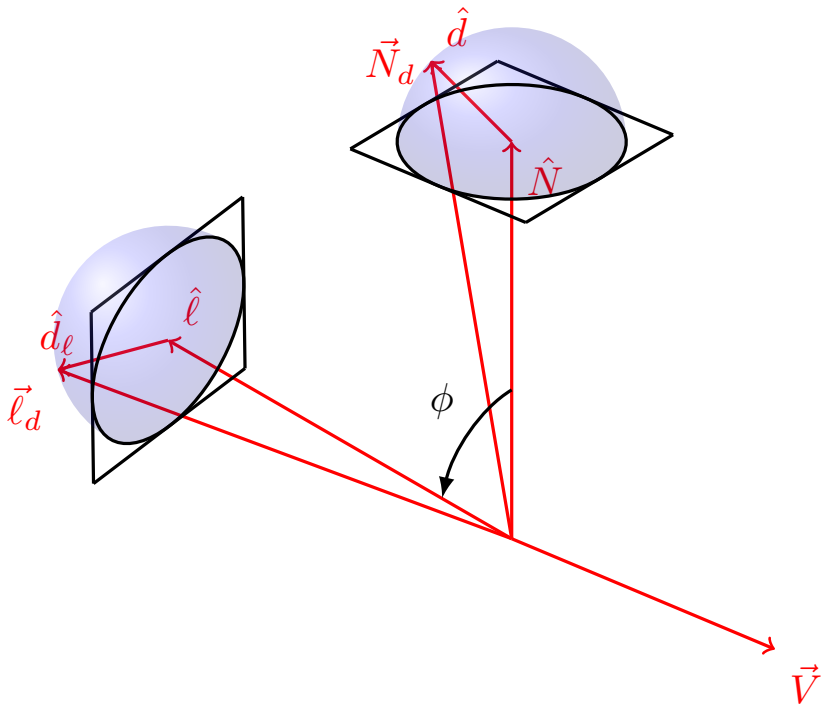

Figure 4.2: An example of rotating the north pole coordinates to the leakage point. (Not drawn to scale)

We should recover $\hat{\ell}$ from the operation: $\mathcal{R}\hat{N}$, where $\hat{N}$ is explicitly a column vector. We may then find the rotated ejection direction vector as:

$$\vec{\ell}_d = \mathcal{R}\vec{N}_d, \tag{4.31}$$

to then find the unit vector defining the particle direction: $\hat{d}_\ell = \vec{\ell}_d - \vec{\ell}$. We simultaneously scale $\hat{\ell} \to \vec{\ell}$ and $\vec{\ell}_d$ to the true system size and location in space of region j using the formulae:

$$\vec{\ell} = \vec{C}_j + R_j\hat{\ell} \tag{4.32a}$$

$$\vec{\ell}_d = \vec{C}_j + R_j\vec{\ell}_d \tag{4.32b}$$

$$\vec{d}_\ell = \vec{\ell}_d - \vec{\ell}. \tag{4.32c}$$

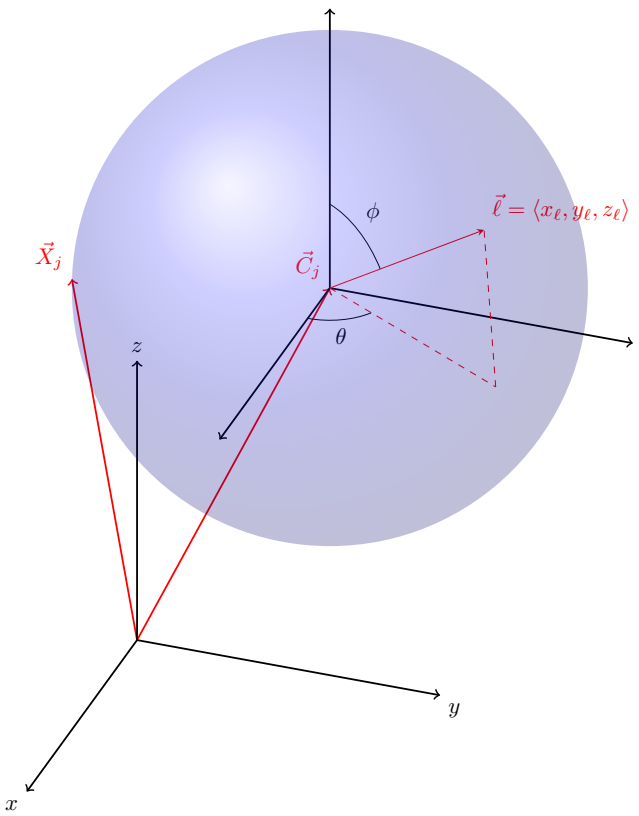

Figure 4.3: Variables involved in parameterizing the leaked neutron trajectory vector.

It is clear that the magnitude of $\vec{d}_\ell$ is equal to R_j, so to recover a unit vector for the direction, we find $\hat{d}_\ell = \vec{d}_\ell / R_j$.

Using the two terminal points of these two vectors, $\vec{\ell}$ and $\vec{\ell}_d$, we may now extend a line following the neutron trajectory to determine if it coincides with another system, say the k^{th} one with center $\vec{C}_k$ and radius R_k. If we define $\vec{P}_\ell$ as the vector connecting the leakage point with the origin, the parameterized trajectory line, $\vec{L}(t)$, is

$$\vec{L}(t) = \vec{P}_\ell + t\hat{d}_\ell. \tag{4.33}$$

If $\vec{X}_k$ is the collection of points defining the surface of region k, the equation for the

target sphere is given by

$$\begin{aligned} R_k^2 &= \left|\left|\vec{X}_k - \vec{C}_k\right|\right|^2 \\ &= \left(\vec{X}_k - \vec{C}_k\right) \cdot \left(\vec{X}_k - \vec{C}_k\right), \end{aligned} \tag{4.34}$$

and at the collection of points where $\vec{L}(t)$ intersects the surface, we have an equation that is quadratic in t:

$$\begin{aligned} 0 &= \left(\vec{L}(t) - \vec{C}_k\right) \cdot \left(\vec{L}(t) - \vec{C}_k\right), \\ &= \left(\hat{d}_\ell \cdot \hat{d}_\ell\right) t^2 + 2\hat{d}_\ell \cdot \left(\vec{P}_\ell - \vec{C}_k\right) t + \left(\vec{P}_\ell - \vec{C}_k\right) \cdot \left(\vec{P}_\ell - \vec{C}_k\right) - R_k^2, \end{aligned} \tag{4.35}$$

which we may solve for t using the quadratic formula:

$$t = -\hat{d}_\ell \cdot \left(\vec{P}_\ell - \vec{C}_k\right) \pm \sqrt{\left(\hat{d}_\ell \cdot \left(\vec{P}_\ell - \vec{C}_k\right)\right)^2 - \left|\left|\vec{P}_\ell - \vec{C}_k\right|\right|^2 + R_k^2} \tag{4.36}$$

where we have used $\hat{d}_\ell \cdot \hat{d}_\ell = ||\vec{d}_\ell||^2 = 1$. We may determine if the neutron collides with system k by considering cases of the discriminant of Eq. 4.36, $D = \left(\hat{d}_\ell \cdot \left(\vec{P}_\ell - \vec{C}_k\right)\right)^2 - \left(\left|\left|\vec{P}_\ell - \vec{C}_k\right|\right|^2 - R_k^2\right)$. If $D < 0$, the solutions are complex and the neutron does not collide with the other system. If $D \geq 0$, the solutions are real and we have potential intersection of the trajectory with the other system. If the solutions are both negative, $t_1, t_2 < 0$, then the neutron is traveling in the opposite direction from region k and it is that neutrons "past" trajectory that would have collided with the other region. Finally, if both solutions are real and positive, $t_1, t_2 > 0$, the neutron does indeed collide with region k.

The transfer probability of a leaked neutron going from region $j \to k$ may then be calculated by running H leakage simulations, determining if that leaked neutron coincides with the other region, binning success of transfer such that the total number of successful transfers is Y, and dividing by H to find:

$$p_{j \to k} = \frac{Y}{H}. \tag{4.37}$$

Calculating the reverse requires performing the H simulations on the surface of the opposite system, thus it is necessary to perform $2H$ simulations to attain the

aggregate transfer probabilities. Alternately, one may simply perform the sphere point picking method during the MC simulation for every instance of a leakage event.

As has been shown, this process is far more expensive than the view factor method. It has the advantage of being a purely stochastic method that should give more accurate results than the view factor method, particularly for systems that are close in size and proximity. As was emphasized before, the authors believe that the view factor method should be used for verification of Monte Carlo codes with analytical and numerical solutions. The sphere point picking method appears more suitable for validation of the SSA with that of potential experimental results.

4.2.3 Comparison of the Two Methods

As mentioned earlier, the View Factor approximation provides acceptable transfer probabilities for systems that are reasonably distanced from each other. The previous analysis hedged the numerical solution of the double area integral with the approximate view factor expression; we now compare the approximate expression to the purely Monte Carlo Sphere Point Picking (coupled with trajectory picking) Method. For reference, Fig. 4.4 gives the transfer probabilities, as calculated by the MC Sphere Point Picking Method, from one sphere to another as a function of the ratio of the radii, $\mathcal{R} = R_1/R_2$, for several separation distances, S.

Assuming that the MC provides the true result within statistical noise, Fig. 4.5 then demonstrates the relative error between the transfer probabilities. We have also assumed that region 1 is the approximate point source in the View Factor calculations. The sphere point picking results are obtained by simulating 10^7 leakage events for each sphere at distances of $S = 0.05\ cm$ through $S = 1.00\ cm$ and the 51 evenly spaced $\mathcal{R}$ values ranging from $[10^{-3}, 1]$. As the distance between spheres increases, the MC noise does as well because the transfer probabilities decrease, necessitating an increase in the number of realizations required to ascertain an accurate transfer

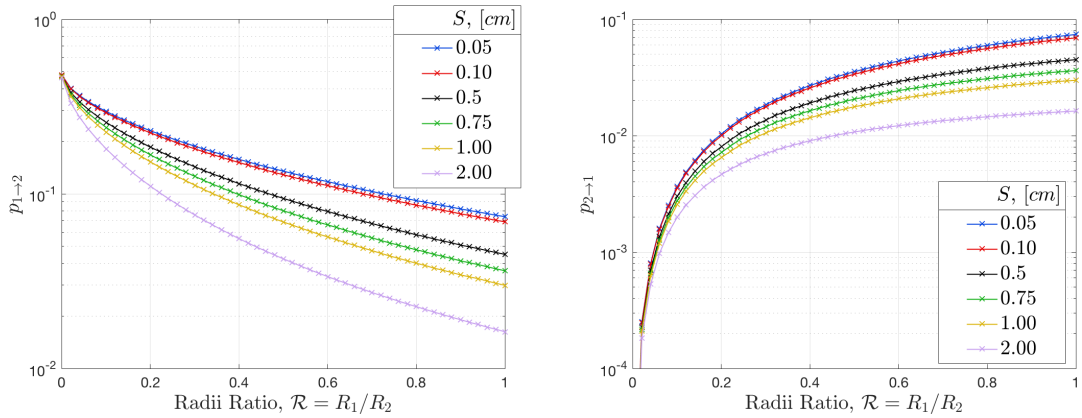

(a) **(b)**

Figure 4.4: Transfer probabilities for two spheres of varying radii and separation distances as calculated by the MC Sphere Point Picking Method.

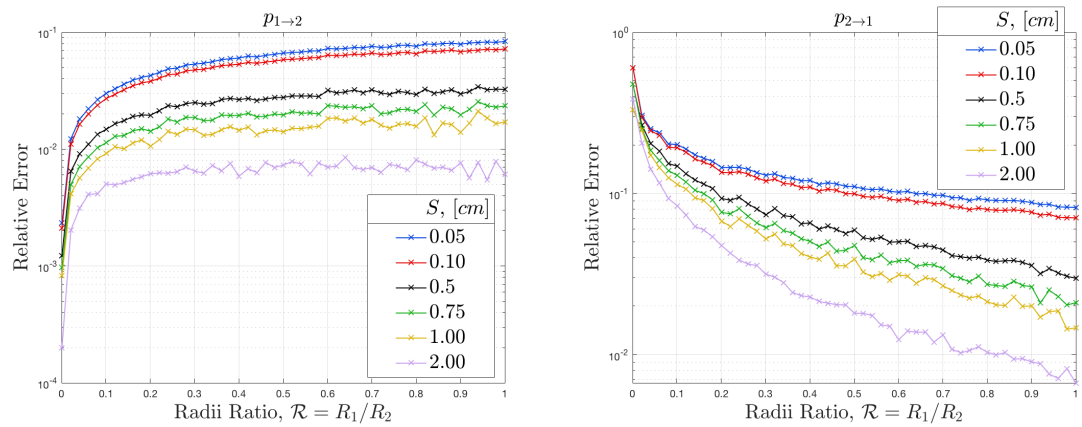

(a) **(b)**

Figure 4.5: Relative error between the View Factor approximation with the MC Sphere Point picking method for (a) $p_{1\to2}$ and (b) $p_{2\to1}$.

probability. Thus, for the $S = 2$ *cm* case, we ran 10^8 leakage events per data point.

Figure 4.5a shows the error in the view factor transfer probability going from sphere 1 to 2, and we see that the error is entirely below the 1% threshold for $S = 2$ *cm*. The reverse transfer is seen in Fig. 4.5b, where we see that if we are transferring from a larger system to a smaller one at close distances, the view factor approximation

is inaccurate at a max error percentage of $\sim 6\%$, in-line with observations in [60], and it is therefore advised to avoid the approximation if the systems are in close proximity of each other.

4.3 Analysis of Coupled Regions

4.3.1 Two Regions with Monoenergetic Neutrons

We now consider a system consisting of two spherical regions composed of pure ^{235}U metal with radii R_1 and R_2 and a number density of $N = 5.0884 \cdot 10^{-2}\ (b \cdot cm)^{-1}$. We choose region 1 to have a center located at the origin such that $\vec{C}_1 = \langle 0, 0, 0 \rangle$, while the second region has a center located a distance $L = R_1 + \mathcal{L} + R_2$ along the y-axis ($\mathcal{L}$ is the shortest distance between the two surfaces), giving $\vec{C}_2 = \langle 0, L, 0 \rangle$. For problems that we consider a single initiating neutron with no source in either region, we assume that the initiating neutron appears in region 1 at $t = 0$. For problems that sources are considered, we need not differentiate systems based on neutron population as the initial condition is nonunique: $P_{\vec{n}}(0) = \delta_{n_1,0}\delta_{n_2,0}$. Further, we assume that the reaction rates are time-independent; this should be an appropriate assumption if, say, region 2 were very slowly brought closer to region 1 from $\vec{C}_2 \sim \vec{\infty}$ until its final location at $\vec{C}_2$.

To begin our analysis of coupled regions, we consider monoenergetic *fast* neutrons where both systems are identical in composition but differ in size such that $R_1 = 5.9$ cm and $R_2 = 5.0$ cm and we use the spatially constant data in Table 4.1a for both regions. Values for the cross sections were calculated from `JENDL`-4.0 at 300 K. We obtain the reaction rates and neutron lifetime for each system by solving the forward k-eigenvalue transport equation in one-dimensional spherical geometry in vacuum,

$$\left[\frac{\mu}{r^2}\frac{\partial}{\partial r}\left(r^2\right) + \frac{1}{r}\frac{\partial}{\partial \mu}\left[\left(1-\mu^2\right)\right] + \Sigma_{t,j}\right]\psi(r,\mu) = \frac{1}{2}\left[\Sigma_{s,j} + \frac{1}{k}\overline{\nu}_j\Sigma_{f,j}\right]\phi(r), \quad (4.38)$$

Table 4.1: Data used for the two sphere system.

(a)

Energy $[eV]$	σ_f $[b]$	σ_c $[b]$	σ_s $[b]$	v $\left[\frac{cm}{s}\right]$
$14 \cdot 10^6$	2.053	$889.7 \cdot 10^{-6}$	2.839	$5.175 \cdot 10^9$
0.0253	585.1	98.71	15.12	$2.200 \cdot 10^5$

(b) $\sigma_{s,g\to g'}$, $[b]$.

g \ g'	1	2
1	1.5376	1.3014
2	0.0	15.12

Table 4.2: Calculated reaction rates for a purely fast system.

Region	$k_{eff,j}$	τ_j $[s]$	$\lambda_{f,j}$ $[1/s]$	$\lambda_{c,j}$ $[1/s]$	$\lambda_{\ell,j}$ $[1/s]$
1	1.0035	$7.741 \cdot 10^{-10}$	$5.406 \cdot 10^8$	$2.343 \cdot 10^5$	$7.509 \cdot 10^8$
2	0.8788	$6.584 \cdot 10^{-10}$	$5.406 \cdot 10^8$	$2.343 \cdot 10^5$	$9.779 \cdot 10^8$

along with its adjoint counterpart. In Eq. 4.38, r is the radial coordinate and μ is the direction cosine with respect to r. We numerically solve Eq. 4.38 using a standard discrete ordinates in angle, diamond difference in space discretization with source- and power-iteration to obtain the k-eigenvalue and the fundamental mode [51]. Once we have the forward and adjoint solutions, $\psi(r,\mu)$ and $\psi^\dagger(r,\mu)$, we may then obtain the neutron lifetime, τ_j, and the reaction rates for event y, $\lambda_{y,j}$, (to be more precise, they are the probability per neutron per unit time that event y will occur) given by Eqs. B.6 and B.11, respectively. These quantities are summarized in Table 4.2, where we note that the algorithm we have outlined is only concerned with reactions that alter the neutron population, thus the out-scattering reaction rate for monoenergetic neutrons is zero and therefore not reported.

We are now prepared to demonstrate the SSA for the two-region system, and we initially benchmark the SSA code against the numerical solutions of the moment

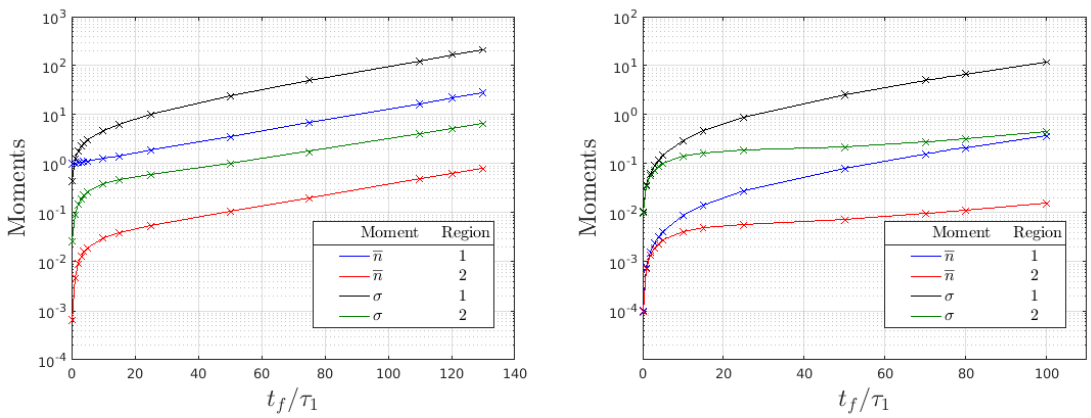

Figure 4.6: Comparison of the SSA (x) moments with the numerical solution (-) of the moment ODEs derived from the forward Master equation for (a) the single chain and (b) with a source.

equations defined by Eqs. 4.7 and 4.8. The system of ODEs are solved by a modified divided difference form of the Adams PECE Formulae and local extrapolation, adjusting the order and step size to control the local error per unit step [63].

By setting the distance between the sphere surfaces to $\mathcal{L} = 5.0\ cm$, we use the view factor method to define the transfer probabilities which, for the aforementioned system configuration, Eq. 4.25 gives $p_{1\to 2} = 1.2376 \cdot 10^{-2}$, $p_{1\to\infty} = 0.98762$, $p_{2\to 1} = 8.8879 \cdot 10^{-3}$, and $p_{2\to\infty} = 0.99111$. In Fig. 4.6, we compare the numerical solution of Eqs. 4.7 and 4.8 with the results from the SSA for (a) a single neutron chain with the initial populations being $N_1 = 1$ and $N_2 = 0$, and (b) for the case where both regions have sources of $S = 10^6\ 1/s$ and the initial condition being $N_1 = N_2 = 0$. The SSA results were obtained by setting the final time to some scaled value of the neutron lifetime in region 1 and running 10^3 batches each with 10^5 histories, amounting to 10^8 total simulations, resulting in highly converged confidence intervals. We see excellent agreement between the solution methods out to many lifetimes.

A means of assessing the accuracy of the SSA results is to analyze the form of

Table 4.3: Skew, γ, and Kurtosis, κ, of the sample distributions of the mean and variance of the neutron population in both regions.

t_f/τ_1	$\gamma_{\overline{n}_1}$	$\kappa_{\overline{n}_1}$	$\gamma_{\overline{n}_2}$	$\kappa_{\overline{n}_2}$
1	$8.59 \cdot 10^{-2}$	2.85	$6.85 \cdot 10^{-3}$	2.94
10	$7.48 \cdot 10^{-2}$	3.08	0.18	2.80
50	$7.31 \cdot 10^{-2}$	2.86	$-1.89 \cdot 10^{-2}$	2.92
100	0.13	2.89	0.17	2.93
150	$-6.72 \cdot 10^{-3}$	2.74	$1.03 \cdot 10^{-2}$	2.82
t_f/τ_1	γ_{V_1}	κ_{V_1}	γ_{V_2}	κ_{V_2}
1	$4.78 \cdot 10^{-2}$	2.93	0.39	3.44
10	$7.70 \cdot 10^{-2}$	2.85	0.34	3.27
50	0.11	2.66	0.13	2.93
100	$1.70 \cdot 10^{-2}$	2.86	0.18	3.28
150	$3.41 \cdot 10^{-2}$	2.86	$9.48 \cdot 10^{-2}$	3.04

the sample distribution, i.e., the batch results distribution. It is known that the distributions of the batch moments will asymptotically approach a normal distribution for increasing batches of histories, where these histories represent outcomes produced by independent and identically distributed random variables. If we then compare the moments of the SSA sample distribution for a given moment of the neutron population, we may determine if the batch results are truly normally distributed. This is most easily done by considering the skewness and kurtosis of the distribution being analyzed, and it is expected that these moments should be near zero and three, respectively. We see in Table 4.3 that the third and fourth moments of the first and second moment distributions of the neutron population have approached these expected values, indicating that the batch distributions are characteristic of the normal distribution.

Next, we consider the neutron number PDFs for this coupled region configuration. We are primarily concerned with the effects the coupling will have in bringing long-time behavior closer to the initial time. In particular, we wish to determine whether or

not the neutron number distribution will approach Bell's distribution in source-present systems earlier in time than if those systems were completely isolated. Considering the case when there is a source present, we may determine if a system in isolation has achieved the Bell distribution by comparing Eq. 2.45 with Eq. 3.19. If we select a tolerance of deviation, ε, in comparing two corresponding n values between the true discrete distribution (Prinja-Souto) and the asymptotic distribution (Bell), we may confidently say that the distributions have converged if the maximum relative error is less than ε:

$$\varepsilon \leq \max_i \left| 1 - \frac{P(n_i, t_f)}{P_{n_i}(t_f)} \right|, \tag{4.39}$$

where $i = 1, 2, \ldots, I$. Equation 4.39 implies we must truncate the error calculation at some n_I, which must be sufficiently large that when we obtain the PDF from the SSA algorithm, the PDF tails will have an expected exponential extrapolatory behavior that may be inferred from the general trend regardless of statistical noise. For each isolated region, the error is shown in Fig. 4.7 where each region has a source of $S = 10^6$ $1/s$; relevant data are shown in Table 4.4. Note that these error profiles also correspond to the distributions displayed in Fig. 3.4 of Sec. 3.5. Note that $\eta < 1$, thus the source is considered weak and the number distributions will be monotonically decreasing and the neutron population is therefore stochastic [11]. We see from the plots that the error is always highest at the tail of the distribution, and thus convergence is dictated by the choice in n_I for a set ε. For this analysis, we choose $n_I = 100$ and $\varepsilon = 10^{-2}$, meaning we consider the asymptotic form to be achieved when $P_{100}(t_f)$ is within 1% of $P(100, t_f)$. From Fig. 4.7a, we see that this criteria is satisfied in Region 1 around $t_f = t_{a,1} = 77\tau_1$, where $t_{a,j}$ is the time to converge to the asymptotic form. The behavior depicted in Fig. 4.7b for the isolated second region is quite different; it is clear that the error between the two distributions itself approaches a constant profile over time, indicating that the discrete distribution does indeed converge to a distribution of a particular shape, but that distribution is not of the gamma-type. In other words, the true distribution in Region 2 will never

Table 4.4: Neutron source data.

Region	Volume $[cm^3]$	S_j $[1/s]$	S_j/V_j $[1/(cm^3 \cdot s)]$	η_j	$t_{a,j}/\tau_1$
1	860.3	10^6	$1,162.4$	$9.7351 \cdot 10^{-4}$	76.961
2	523.6	10^6	$1,909.6$	$9.7351 \cdot 10^{-4}$	∞

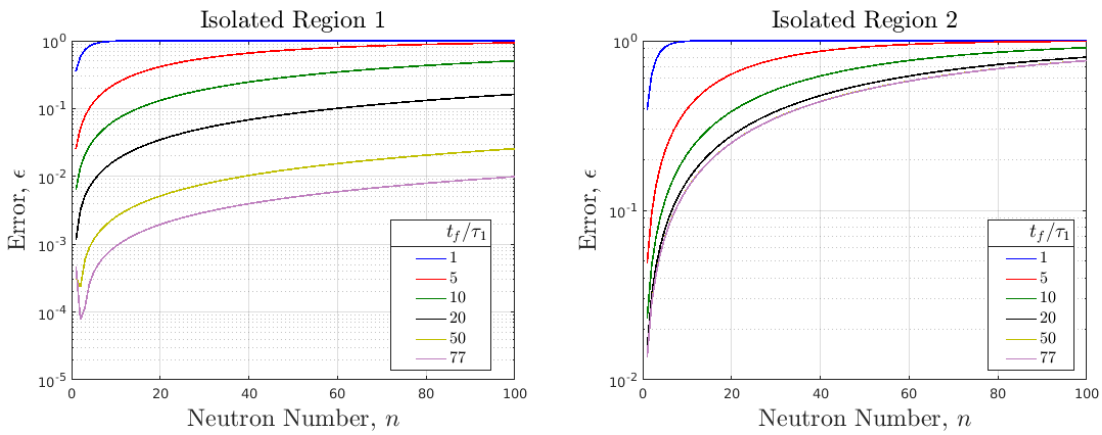

(a) **(b)**

Figure 4.7: Error between the discrete PDF and the asymptotic PDF for the neutron number in (a) Region 1 and (b) Region 2 if both were isolated.

converge to the Bell distribution and thus $t_{a,2}/\tau_1 = \infty$.

Figure 4.8 shows the comparison between the actual neutron number PDF as calculated by SSA as well as the gamma distribution that was produced by fitting the first two SSA moments for two regions that are 5.0 *cm* apart. The presented results were obtained by running $5 \cdot 10^3$ batches and 10^7 histories per batch to resolve the tails of the PDFs as much as possible for the error calculations. We see that the larger system, region 1 in Fig. 4.8a, visually agrees very well with the fitted gamma as early as 5 lifetimes- a significant reduction from the ~ 77 lifetime limit we would observe in isolation. Region 2 in Fig. 4.8b shows a similar approach to agreement and certainly agrees by 100 lifetimes. For a more rigorous comparison, Figs. 4.9a and 4.9b show that the relative error between the SSA and fitted gamma distributions do indeed reside below 1% for $n = 100$ at $t_f = 50\tau_1$ for region 1 (possibly even $t_f = 20\tau_1$

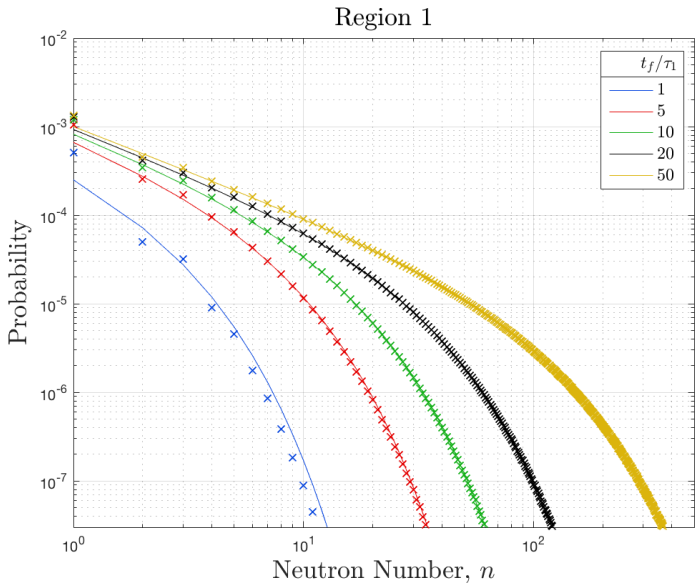

(a)

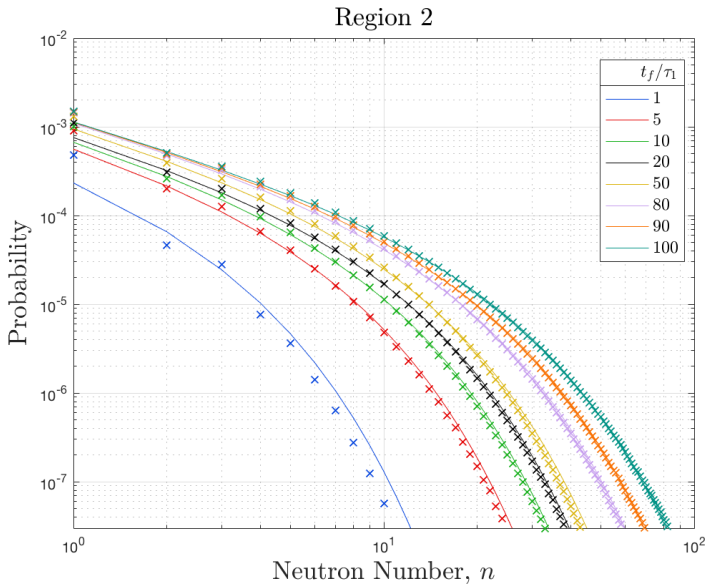

(b)

Figure 4.8: Comparison of the neutron number PDFs as calculated by SSA (x) and the gamma distribution fit (-) for (a) region 1, (b) region 2.

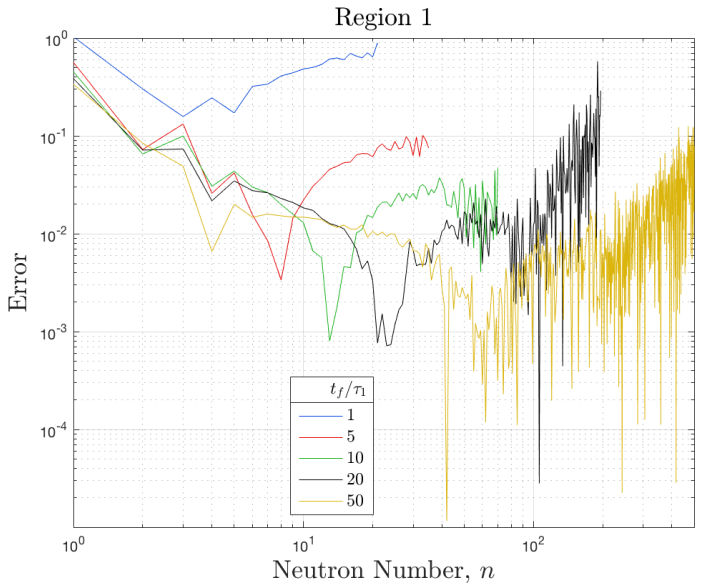

(a)

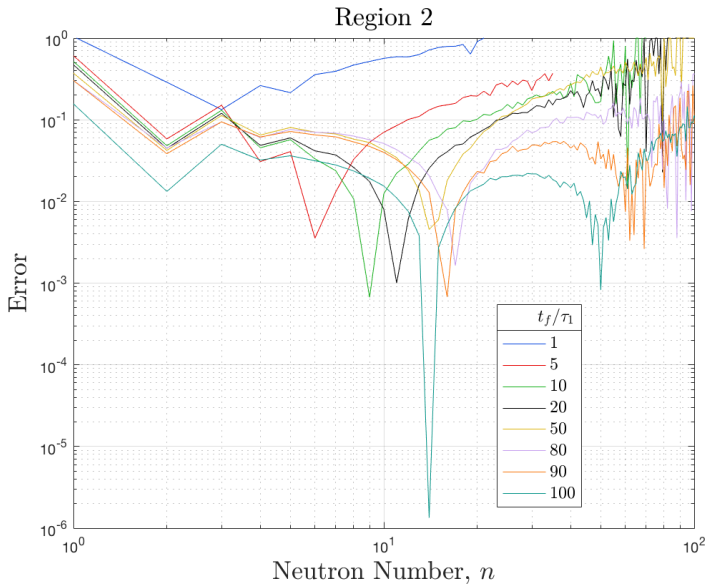

(b)

Figure 4.9: Per Fig. 4.8, but for the relative error between the SSA and gamma fit for (a) region 1 and (b) region 2.

if the SSA noise were to be reduced) and $t_f = 100\tau_1$ for region 2. Clearly, the inherent Monte Carlo noise begins to dominate the error calculation and the decreasing trend in the error is reversed. For region 2 depicted in Fig. 4.8b, we see the higher n probabilities converge to the fitted gamma distribution by $t_f \approx 100\tau_1$, showing that the addition of the other region (equivalent to adding multiplying mass or a source to a single system) will help to drive the other region to achieve a gamma distribution. As an aside, it is clear that the probabilities for $n = 1$ do not agree for any time, but this is of no concern as we are interested in the large n probabilities for which Bell originally gleaned his distributions.

4.3.2 Two Regions with Two Energy Groups

For two regions with two energy groups, we first benchmark our code by simplifying the physical model to be simulated, in-line with the assumptions made in deriving the moment equations in Sec. 4.1.2. The key assumptions made were that only thermal neutrons induce fission, only fast neutrons are born from both induced fission and spontaneous fission events, and that thermal neutrons do not up-scatter. The reaction rates must now be partitioned into appropriate energy groups and calculated following the form of Eq. B.12 in Appendix B, and the total reaction rate for group g is:

$$\lambda_{t,g} = \lambda_{f,g} + \lambda_{c,g} + \lambda_{\ell,g} + \sum_{g' \neq g} \lambda_{s,g \to g'}, \tag{4.40}$$

for which we do not include the self-scattering reaction rates as those events do not alter the population state of the system. The neutron lifetime for a given group is then calculated with the inclusion of the out-scatter reaction rates. In the ensuing analysis, we benchmark the SSA code using the data in Table 4.1a, with the stipulation that we set $\sigma^j_{f,1} = 0$ b, and we use the scattering matrix displayed in Table 4.1b as well as the relevant multiplicity data is Table 4.5.

Table 4.5: Multiplicity distributions.

	$\overline{\nu}$	$\overline{\nu^2}$	q_ν							
			0	1	2	3	4	5	6	7
g_1, IF	4.472	21.39	0.0	0.009	0.022	0.179	0.310	0.310	0.112	0.060
g_2, IF	2.476	7.382	0.0222	0.200	0.306	0.307	0.136	0.035	0.004	0.0
SF	2.154	5.945	0.0638	0.2316	0.3325	0.2533	0.0987	0.0181	0.0020	0.0

Figure 4.10 shows the mean and variance as calculated by the numerically solved system of coupled ODEs defined by Eqs. 4.15 through 4.17 and compared to the SSA solution for the cases of the initiating neutron being fast in Fig. 4.10a, the initiating neutron being thermal in Fig. 4.10b, and 4.10c shows the moments when there are no initial neutrons and there is a fast singlet emitting source in each region equivalent to the sources in Table 4.4. In every case, both systems are highly subcritical with $k_{eff,1} = 0.579$ and $k_{eff,2} = 0.500$, with lifetimes given by $\tau_1^1 = 0.48\ ns$, $\tau_2^1 = 4.0\ ms$, $\tau_1^2 = 0.38\ ns$, $\tau_2^2 = 4.0\ ms$. The moments, however, appear to reach a steady state distribution. This behavior is understood when we note that the thermal neutron lifetime is about seven orders of magnitude longer than the fast neutron lifetime, and there simply has not been enough time for the system to respond to the thermal neutron interactions. In Fig. 4.11, we show that by observing the system at final times on the scale of the thermal neutron lifetime in region 1, τ_2^1, the means for the non-source systems do indeed decrease globally, as expected.

For a more realistic set of simulations, we next consider two regions where fast neutrons may cause fission. Group-dependent reaction rates are displayed in Table 4.6, where we altered the system sizes to radii of $R_1 = 2.484\ cm$ and $R_2 = 2.122\ cm$ such that the effective multiplication factors are the same as before; as expected, the critical mass decreases substantially when induced fission from fast and thermal neutrons is accounted for (compared to the $R_1 = 5.9\ cm$ from the previous section).

Now by spatially coupling the two regions and separating them by 5.0 cm, we demonstrate the convergence of the energy-dependent neutron number PDFs for fast

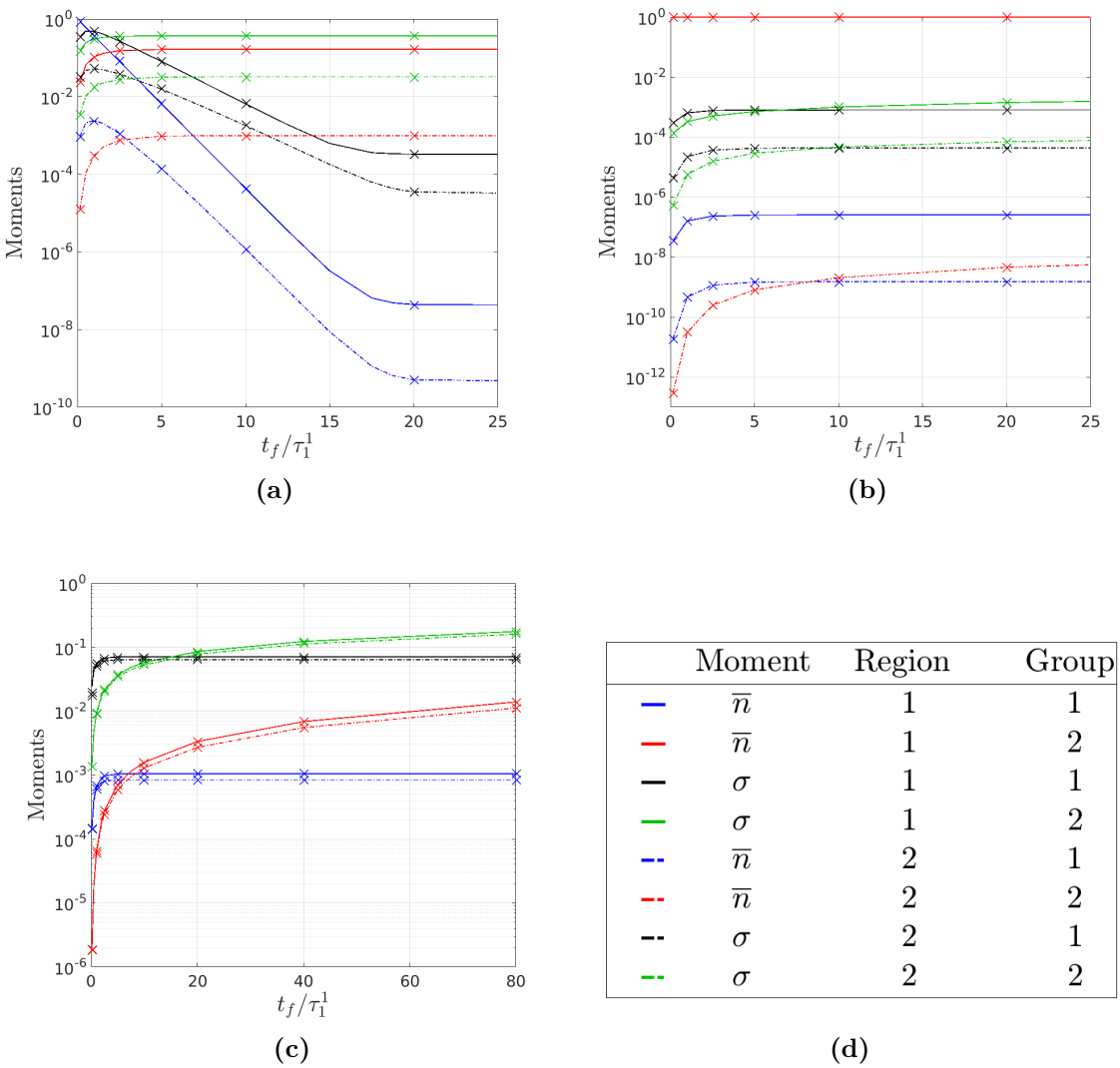

Figure 4.10: Moments for two groups and two regions for (a) an initiating fast neutron, (b) an initiating thermal neutron, and (c) when there are fast neutron sources present in each region. (d) is the shared legend for each plot, and the (x) markations denote SSA results.

neutron source driven systems in Fig. 4.12. As was observed in the previous section, the timescales worth considering are on the order of the thermal neutron lifetime (for region 1). We see that the stochastic fast neutron sources give rise to deterministic thermal neutron distributions within 5 thermal neutron lifetimes. The fast neutron

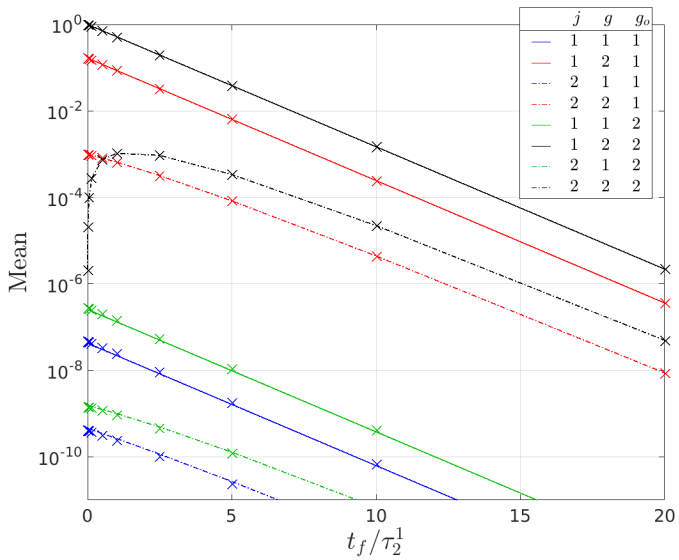

Figure 4.11: Behavior of the means for final times on the order of the thermal neutron lifetime, τ_2^1. Here, g_o is the energy group of the initial neutron and $j_o = 1$ for all cases. (x) signifies a SSA calculation.

PDFs remain stochastic, at least in this example, due to the fact that all fast neutrons that are born from fast fission, thermal fission, and source events will quickly vanish by reacting with the medium or leaking. The large number of fast neutrons that are down-scattering to the thermal regime accumulate in population because the thermal neutrons are so much slower-moving, easily observed in the reaction rate values of Table 4.6a. We also observe the thermal neutron PDFs in Fig. 4.12b are not quite in agreement with a gamma distribution fit (dotted lines) obtained from the SSA moments. We show how the SSA thermal PDFs are essentially bounded by a gamma distribution and a Gaussian distribution at an early time corresponding to $t_f = 0.5\tau_2^1$, and by $t_f = 5\tau_2^1$, the SSA PDF is in agreement with a fitted Gaussian distribution.

Table 4.6: Calculated reaction rates for a fast and thermal system. All reaction rates have units of inverse seconds: $[1/s]$.

(a)

Region j	Group g	$k_{eff,j}$	τ_g^j	$\lambda_{f,g}^j$	$\lambda_{c,g}^j$	$\lambda_{\ell,g}^j$
1	1	1.0035	0.1753 ns	$5.406 \cdot 10^8$	$2.343 \cdot 10^5$	$4.820 \cdot 10^9$
1	2	-	3.982 ms	214.4	36.16	0.5889
2	1	0.8788	0.1445 ns	$5.406 \cdot 10^8$	$2.343 \cdot 10^5$	$6.039 \cdot 10^9$
2	2	-	3.980 ms	214.4	36.16	0.7268

(b) Scattering reaction rates

$\lambda_{s,g\to g'}^1$			$\lambda_{s,g\to g'}^2$		
g \ g'	1	2	g \ g'	1	2
1	$4.049 \cdot 10^8$	$3.427 \cdot 10^8$	1	$4.049 \cdot 10^8$	$3.427 \cdot 10^8$
2	0.0	5.5395	2	0.0	5.5395

4.4 Time-Dependent Reactivity Insertions

4.4.1 Sampling Formulae

In this section, we derive Formulae for sampling time intervals to the next event in systems with time-dependent reactivites. As it turns out, we may invert the state transition CDF for an arbitrary order polynomial and we therefore write the reactivity for region j as

$$\rho_j(t) = \rho_j(0) + \sum_{m=1}^{M} a_{j,m} t^m, \tag{4.41}$$

where $\rho_j = \rho_j(0)$ is the initial value of the reactivity in region j and $a_{j,m}$ are known coefficients. Allowing for multigroup energy dependence with a total of G energy groups, we may define the neutron population in region j and energy group g to be $n_{g,j}$. We will also define S_g^j to be the probability per unit time that a source event occurs in region j, producing a neutron in energy group g, and $\Lambda_g^j = \tau_g^j / k_j$ is the mean generation time for neutrons in g, j. Noting that $\lambda_{t,g}^j = 1/\tau_g^j$ and $k_j = 1/(1-\rho_j)$, we

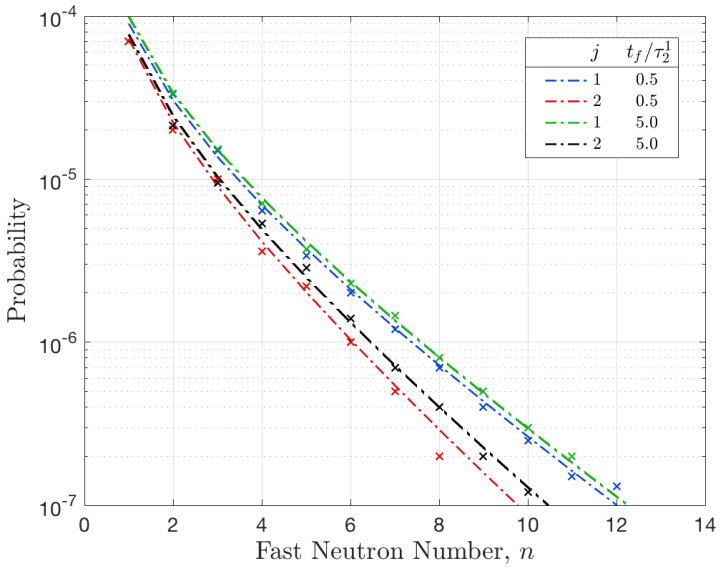

(a)

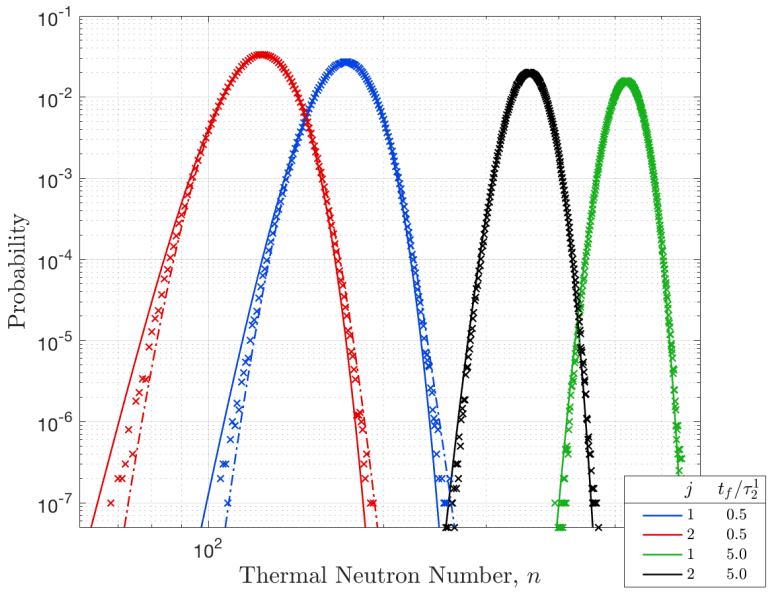

(b)

Figure 4.12: Neutron number PDFs in a two-region assembly at different times for (a) fast neutrons and (b) thermal neutrons. The xs are SSA results, solid lines are Gaussian fits, and dotted lines are Gamma fits.

may rewrite μ of Eq. 3.18 in terms of the time-dependent region-collective reactivity:

$$\mu(\mathbf{X},t) = \sum_{j=1}^{J}\sum_{g=1}^{G}\left\{S_g^j + \left[\frac{1-\rho_j(t)}{\Lambda_g^j}\right] n_{g,j}\right\}. \tag{4.42}$$

The cumulative distribution function of the transition probability per unit time is

$$F(t) = \int_0^t \mathrm{d}t'\mu(\mathbf{X},t')\exp\left\{-\int_0^{t'}\mathrm{d}t''\mu(\mathbf{X},t'')\right\}. \tag{4.43}$$

In general, an integral with an integrand of this form (i.e., $y(x)\exp(\int^x y(x')\,\mathrm{d}x')$) can be solved regardless of the functional form of the kernel, in this case $\mu(\mathbf{X},t)$. If we make the substitution $y(t') = \int_0^{t'}\mathrm{d}t''\mu(\mathbf{X},t'')$, then $\mathrm{d}y = \mu(\mathbf{X},t')\,\mathrm{d}t'$ and the CDF becomes

$$\begin{aligned} F(t) &= \int_0^{y(t)}\mathrm{d}y'\exp\{-y'\} \\ &= 1-\exp\left\{-\int_0^t \mathrm{d}t'\mu(\mathbf{X},t')\right\}. \end{aligned} \tag{4.44}$$

Computing the integral of the transition probability per unit time is a straightforward integration of a sum of polynomial terms:

$$\begin{aligned} \int_0^t \mathrm{d}t'\mu(\mathbf{X},t') = \sum_{j=1}^{J}\sum_{g=1}^{G}\Bigg\{ &\left[S_g^j + \left(\frac{1-\rho_j(0)}{\Lambda_g^j}\right) n_{g,j}\right] t \\ &- \frac{n_{g,j}}{\Lambda_g^j}\sum_{m=1}^{M}\frac{a_{j,m}}{m+1}t^{m+1}\Bigg\}. \end{aligned} \tag{4.45}$$

Upon inserting Eq. 4.45 into Eq. 4.44, we may implicitly invert the CDF by setting $F(t) = \xi$ to arrive at an $(M+1)$-order polynomial in t:

$$\sum_{m=1}^{M} A_m t^{m+1} + Bt + C = 0, \tag{4.46}$$

with the coefficients defined as

$$\begin{aligned} A_m &= \frac{1}{m+1}\sum_{j=1}^{J} a_{j,m}\sum_{g=1}^{G}\frac{n_{g,j}}{\Lambda_g^j} \\ B &= -\sum_{g=1}^{G}\sum_{j=1}^{J}\left[S_g^j + \left(\frac{1-\rho_j(0)}{\Lambda_g^j}\right) n_{g,j}\right] \\ C &= -\ln\xi. \end{aligned}$$

The time of the next event, t, is determined by finding the principle root of Eq. 4.46 for a sampled ξ.

For demonstrative purposes, we limit the reactivity for all J regions to a linear functional form by setting $M = 1$. Recognizing that the extrema of a line occur at the endpoints, we define the maximum or minimum value of the reactivity at the completion time of the insertion, t_{in}, to be $\rho_j(t_{in}) = \rho_{j,m}$. From this, the coefficients become $a_{j,1} = \Delta\rho_j/t_{in}$ and the ramp reactivity is:

$$\rho_j(t) = \rho_j(0) + \Delta\rho_j \frac{t}{t_{in}}\,, \tag{4.47}$$

where $\Delta\rho_j = \rho_{j,m} - \rho_j(0)$. From this, Eq. 4.46 reduces to a quadratic polynomial with the roots

$$t = -\frac{B}{2A_1} \pm \frac{1}{2A_1}\sqrt{B^2 - 4A_1C}. \tag{4.48}$$

As we are interested in the response of one region due to the change in another, we further reduce the time-dependence of the reactivity to be in a single region, say region ℓ, thus $a_{j,1} = \Delta\rho_j\delta_{j,\ell}/t_{in}$. The coefficients B and C do not change while A_1 changes accordingly:

$$A_1 = \frac{\Delta\rho_\ell}{2t_{in}} \sum_g \frac{n_{g,\ell}}{\Lambda_g^\ell} = \frac{1}{2t_{in}} \sum_g \left(\lambda_{t,g}^\ell(0) - \lambda_{t,g}^\ell(t_{in})\right) n_{g,\ell} \tag{4.49a}$$

$$B = -\sum_g \sum_j \left[S_g^j + \lambda_{t,g}^j(0) n_{g,j}\right] \tag{4.49b}$$

$$C = -\ln(\xi) \tag{4.49c}$$

where we have further rewritten A and B in terms of the total time-dependent reaction rates.

Results pertaining to systems with time dependent reactivity are shown in Sec. 4.4.2 for a system composed of two regions ($J = 2$). In particular, we will study the effects of the neutron number distributions when one of the regions has a ramp reactivity insertion and the other has static reactivity.

Table 4.7: Coefficients of polynomial fits (see Eq. 4.50) for $t_{in} = 0.5\tau_2^1(0)$.

	c_4	c_3	c_2	c_1	c_0
$k_{eff,1}$	0	$4.48774 \cdot 10^6$	$-5,369.43$	76.7274	0.498436
ϱ	$2.77831 \cdot 10^{10}$	$-1.17728 \cdot 10^8$	$4.42826 \cdot 10^5$	$1,054.81$	9.02805
$\lambda_{f,1}^1$	$6.63819 \cdot 10^{12}$	$-3.23238 \cdot 10^{10}$	$8.98483 \cdot 10^7$	53156.0	374.621
$\lambda_{f,2}^1$	$3.59697 \cdot 10^{12}$	$-1.75182 \cdot 10^{10}$	$4.86670 \cdot 10^7$	$28,589.0$	200.835
$\lambda_{c,1}^1$	$2.87676 \cdot 10^9$	$-1.40080 \cdot 10^7$	$38,937.2$	23.0360	0.162348
$\lambda_{c,2}^1$	$6.06832 \cdot 10^{11}$	$-2.95544 \cdot 10^9$	$8.21042 \cdot 10^6$	$4,823.15$	33.8821
$\lambda_{\ell,1}^1$	$2.47391 \cdot 10^{12}$	$-3.62303 \cdot 10^9$	$6.55149 \cdot 10^7$	$4.19049 \cdot 10^5$	$3,717.77$
$\lambda_{\ell,2}^1$	$1.97452 \cdot 10^9$	$-3.72182 \cdot 10^6$	$48,856.6$	293.322	2.73307
$\lambda_{s,1\to2}^1$	$4.20796 \cdot 10^{12}$	$-2.04901 \cdot 10^{10}$	$5.69550 \cdot 10^7$	$33,695.7$	237.472

4.4.2 SSA Results

We choose to alter the material density of region 1 in order to achieve a reactivity that varies linearly in time while keeping the radius and cross-sections constant and all properties of region 2 constant. If the initial reactivity is $\rho_1(0) = \rho_{o,1} = -1.0$, and the final reactivity (at the end of the insertion at t_{in}) is $\rho_1(t_{in}) = \rho_{m,1} = 0.\overline{0909}$; the criticality then varies from $k_{eff,1}(0) = 0.50$ to $k_{eff,1}(t_{in}) = 1.10$. We also choose to vary region 1 properties over time intervals relative to the initial thermal neutron lifetime in region 1, $\tau_2^1(0) = 8.7299\ ms$, as this is the longest lifetime in the system. As a reminder, the criticality of region 2 is $k_{eff,2} = 0.8788$ which corresponds to a constant reactivity of $\rho_2 = -0.1379$.

Given the linear reactivity profile for region 1 stated by Eq. 4.47, (i.e., $\rho_1(t) = \rho_1(0) + \Delta\rho\, t/t_{in}$), we determined the system density required to achieve the criticality and corresponding reactivity profile. For the previously used microscopic cross-sections, the initial density must be $\varrho(0) = 9.02221825\ g/cm^3$ and the final density must be $\varrho(t_{in}) = 22.21289\ g/cm^3$. Solving the k-eigenvalue neutron transport equation

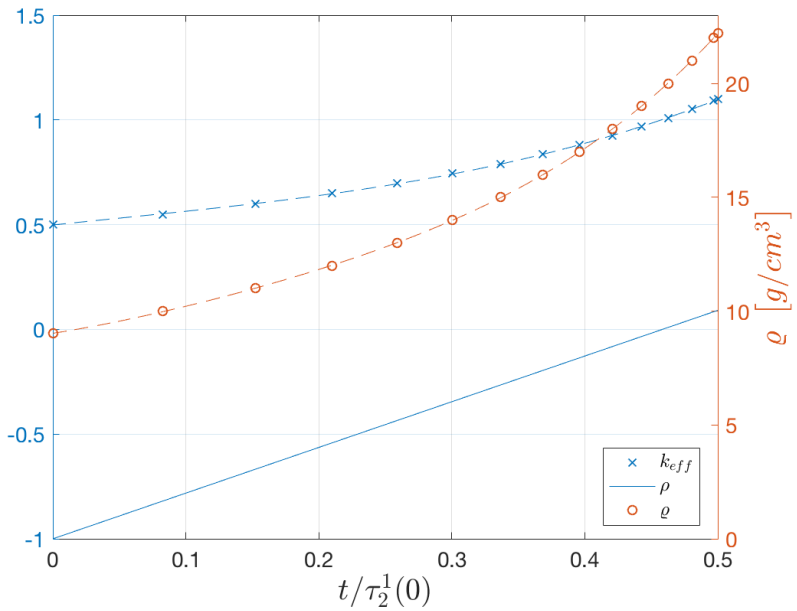

Figure 4.13: Time dependent region 1 density, multiplication factor, and reactivity data (∘ and x points) compared with polynomial fits (dashed lines) used in SSA code.

for every integer value of density between these two values gives an array of 15 $k_{eff,1}$ values. For a given $k_{eff,1}$, we calculate the reactivity with $\rho_1(k_{eff,1}) = 1 - 1/k_{eff,1}$, and we then determine the corresponding time using $t = t_{in}[\rho_1(k_{eff,1}) - \rho_1(t=0)]/\Delta\rho$. From this, we then perform a least-squares fit to the data points using MATLAB's polyfit function. Figure 4.13 shows the data values (∘ and x markations) and the fourth-order polynomial fit lines for k_{eff} and ϱ out to a $t_{in} = 0.5\tau_2^1(0)$. Table 4.7 presents the coefficients for the polynomial fits of the functional form:

$$f(t) = c_4 t^4 + c_3 t^3 + c_2 t^2 + c_1 t + c_0, \tag{4.50}$$

that we will then use to update our reaction rates and other values in the SSA code for time interval sampling. Note that, if t_{in} is altered for a given $\Delta\rho$, one must refit the polynomials. For the sake of reproducibility of the upcoming examples, we provide coefficient tables in Appendix C for two other t_{in} values.

By now altering the final time of the reactivity insertion, t_{in}, we may effectively

alter the severity of the insertion; in the extreme case where $t_{in} \to 0$ (while holding $\Delta\rho$ constant), the region would experience a discontinuous, or jump, insertion. We will refer to a faster, more stark, insertion as a more *severe* insertion. Figure 4.14 shows the reactivity profile from Fig. 4.13 along with two additional, more severe, profiles that we will investigate. We note that the system remains subcritical for $\sim 90\%$ of any of the given reactivity insertion time intervals, but will be supercritical for the remainder of the simulations.

Figure 4.15a shows the fast neutron population PDFs at the end of the respective insertions, depicted in Fig. 4.14, for region 1; we do not show the fast PDFs for region 2 as the means are so low and seem to be constant values of $\overline{n}_{1,2}(0.01\tau_2^1(0)) \approx 1.87 \cdot 10^{-4}$, $\overline{n}_{1,2}(0.1\tau_2^1(0)) \approx 1.30 \cdot 10^{-4}$, and $\overline{n}_{1,2}(0.5\tau_2^1(0)) \approx 1.50 \cdot 10^{-4}$. Figure 4.15b shows the thermal neutron number PDFs for both regions at the end of the respective reactivity insertions. As was shown in Sec. 4.3, we compare the SSA (true) results with a gamma distribution and Gaussian distribution by matching the moments (see Sec. 3.5 for details on fitting), where it is clear that the SSA result is always

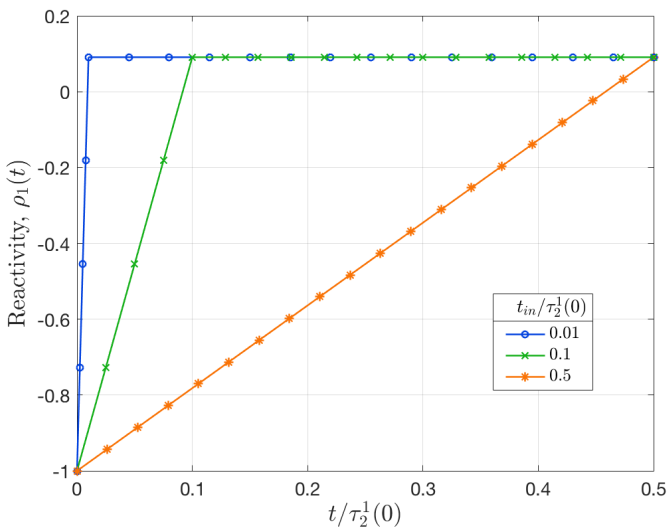

Figure 4.14: Reactivity insertion profiles of differing severity.

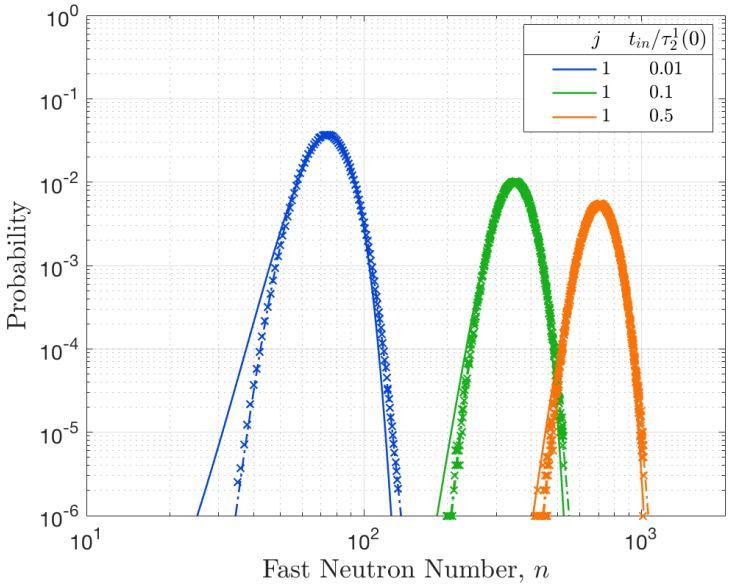

(a)

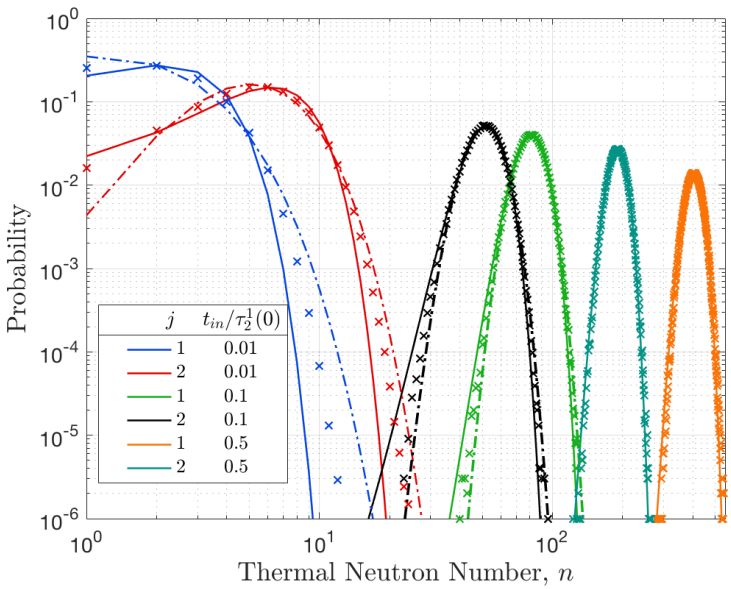

(b)

Figure 4.15: Neutron population PDFs at the end of several reactivity insertions in region 1 for (a) fast neutrons and (b) thermal neutrons. xs are SSA results, solid lines are Gaussian fits, and dotted lines are Gamma fits.

bounded by the fitted distributions. Interestingly, the region 1 fast neutron PDFs agree perfectly with the fitted gamma distribution (the x's lie atop the dotted gamma fit line), while the thermal neutron PDFs converge to the Gaussian fitted line (for which the gamma has converged to as well due to smaller variances), even though the populations are smaller than their fast counterparts. We note that at the earlier time of $t_{in} = 0.01\tau_2^1(0)$, although region 1 is the region experiencing the reactivity insertion, it is region 2 that has a larger thermal neutron population average. This is most likely due to the increase in the neutrons leaking, specifically fast neutrons, from region 1 which then transfer the the other region.

We now complete the simulations by running past the insertion times to a communal final time of $t_f = 0.5\tau_2^1(0)$, in reference to the region 1 reactivity profiles of Fig. 4.14. In the SSA code, once the system time surpasses the prescribed t_{in}, the reaction rates are held constant at their max values occurring at the end of the insertion. This is accomplished by simply checking whether the system time is less than or greater than t_{in}, and if it is greater than, simply setting $t = t_{in}$ in Eq. 4.50. Illustrated in Fig. 4.16 are the corresponding energy-dependent neutron number distributions for fast neutrons in Fig. 4.16a and thermal neutrons in Fig. 4.16b. Again, we do not display the fast PDFs of region 2 as the average number of particles is so low due to either down-scatter to the thermal range or leakage from the system and the relative standard deviation is much larger than the average. As expected, the PDFs of the more severe reactivity insertions have much larger population averages. This can be explained by considering the extreme case of $t_{in} = 0.01\tau_2^1(0)$ (the blue and red lines), where the system is only abruptly subcritical and is then highly supercritical for $\sim 99\%$ of the simulation- it is also for this reason that the statistics are not as converged as the other distributions because of the larger number of divergent chains (which corresponds to sampled $\Delta t \to 0$). We are able to discern that the fast distributions are still atop the gamma fit (more so than on the Gaussian) while the thermal distributions for the longer times appear to agree with the gamma

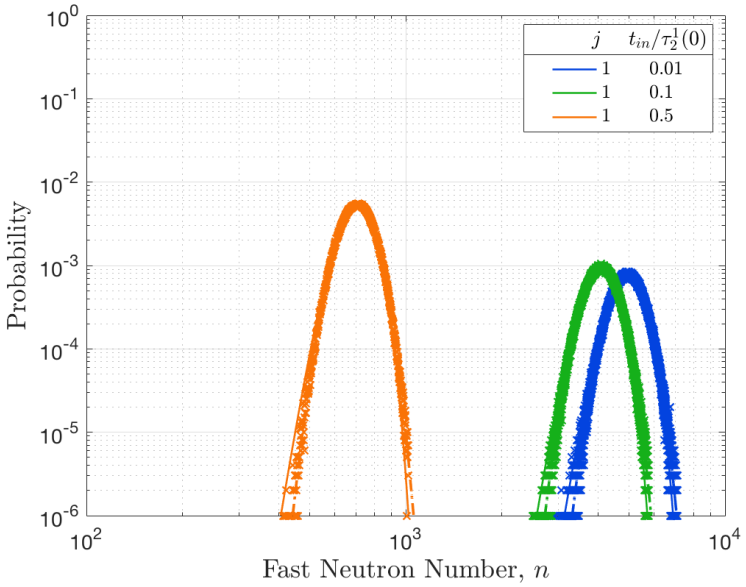

(a)

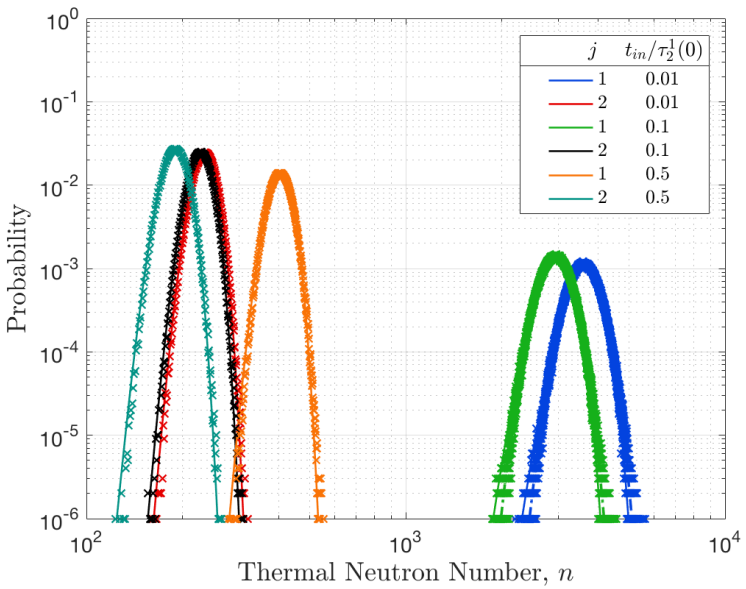

(b)

Figure 4.16: Per Fig. 4.15, to later times. xs are SSA results, solid lines are Gaussian fits, and dotted lines are Gamma fits.

fits as well. This suggests that once a distribution's standard deviation relative to the mean has decreased enough, it will agree more closely with a gamma distribution, even when the fitted gamma distribution has not converged to its asymptotic Gaussian shape.

Chapter 5

Modeling Stochastic Neutron Populations in Unlumped Systems

In this chapter, we derive the well known Pál-Bell Equation following the process outlined by Bell [18], which was first published by Pál in 1958 [19, 20] in Hungarian. Their formulations result in an integral Chapman-Kolmogorov equation where the only difference is that Bell used a probability generating function to transform the Master equation while Pál preferred to use the moment generating function. Later, Lewins demonstrated a more direct methodology for obtaining the differential form of the Pál-Bell Equation [21]. We demonstrate the essence of Bell's formulation in Sec. 5.1 and we then derive the principle equations of interest in Sec. 5.2 that we will then numerically investigate in Chapter 6. The primary motivation for this chapter is to (1) inform the reader of the space of applications that the Backward Formulation proves superior to the Forward Formulation of Ch. 2 (an unlumped forward formulation was founded by Stacey [22]) and (2) to provide the framework and logic used in obtaining Backward Master equations in the ensuing chapters.

5.1 Derivation of the Pál-Bell Equation

The probability of there being a specific number of neutrons within an unlumped system of volume V and convex surface ∂V is of interest in this section. Historically, the Backward Formulation has proven advantageous in deriving an equation for $P_n(\mathcal{R}, t_f|\vec{r}, \hat{\Omega}, t)$: the probability of there being n neutrons in $\mathcal{R}$ at a final time, t_f, due to the introduction of a single neutron at the point $\vec{r}$ traveling in the direction $\hat{\Omega}$ at an earlier time t. Here, $\mathcal{R}$ is some element of $(\vec{r}, \hat{\Omega})$-space. Clearly, this is the number distribution for a single neutron chain and we will address the number distribution in the presence of a source subsequently. Without loss of generality, we assume that the neutrons are monoenergetic with velocity v, emerge from scattering events isotropically, and we neglect delayed neutron precursors.

In words, P_n may be calculated as the probability that the initiating neutron has a first collision at some point multiplied by the probability that the particles emerging from the collision then lead to n neutrons, added to the probability that the initiating neutron does not have a collision and the subsequent events then lead to n neutrons in $\mathcal{R}$ at t_f. Thus, by noting that the probability that the initiating neutron collides in a short distance $\mathrm{d}s$ is $\Sigma_t(\vec{r} + s\hat{\Omega}, t + s/v)\,\mathrm{d}s$ and the probability that the neutron will not collide after traveling a distance s as $\exp\left\{-\int_0^s \mathrm{d}s'\Sigma_t(\vec{r} + s'\hat{\Omega}, t + s'/v)\right\}$. Then the probability the neutron will collide in $\left[\vec{r} + s\hat{\Omega}, \vec{r} + (s + \mathrm{d}s)\,\hat{\Omega}\right]$ is

$$\Sigma_t\left(\vec{r} + s\hat{\Omega}, t + \frac{s}{v}\right) \exp\left\{-\int_0^s \mathrm{d}s'\Sigma_t\left(\vec{r} + s'\hat{\Omega}, t + \frac{s'}{v}\right)\right\} \mathrm{d}s.$$

From this first collision, i neutrons emerging with probability $c_i(\vec{r} + s\hat{\Omega}, t + s/v)$ then must lead to n neutrons in $\mathcal{R}$ at t_f. If $i = 0$, then the chain perishes and we are guaranteed to have $n = 0$ neutrons in $\mathcal{R}$ at t_f. If $i = 1$, this one neutron will then lead to n neutrons provided that $s/v < t_f - t$ (the initiating neutron collided before the final time). If $i = 2$, one neutron will lead to m neutrons and the second will lead to $n - m$ neutrons, and so on. Introducing the notation: $\ell(s_b, s_t)$ as taking on the

value of the lesser between s_b, the distance to the boundary, and $s_t = v(t_f - t)$, the distance the neutron will travel if unimpeded, we may write the probability balance as:

$$\begin{aligned} P_n\left(\mathcal{R}, t_f | \vec{r}, \hat{\Omega}, t\right) = & \int_0^{\ell(s_b,s_t)} \mathrm{d}s \Sigma_t\left(\vec{r} + s\hat{\Omega}, t + \frac{s}{v}\right) \mathrm{e}^{-\int_0^s \mathrm{d}s' \Sigma_t\left(\vec{r}+s'\hat{\Omega}, t+\frac{s'}{v}\right)} \Bigg[\\ & + \sum_{\nu=0}^{\nu_m^f} c_\nu\left(\vec{r} + s\hat{\Omega}, t + \frac{s}{v}\right) \sum_{n_1+\cdots+n_\nu=n} \prod_{k=1}^{\nu} \int_{4\pi} \frac{\mathrm{d}\Omega_k}{4\pi} P_{n_k}\left(\mathcal{R}, t_f | \vec{r} + s\hat{\Omega}, \hat{\Omega}_k, t + \frac{s}{v}\right) \Bigg] \\ & + \sum_{j=1}^{3} A_j, \end{aligned} \tag{5.1}$$

where we recognize that the combinatorial sum and product of the $\nu = 0$ term are unity when $n = 0$ and zero otherwise (i.e., $c_0\delta_{n,0}$). The A_j terms are:

$$A_1 = \delta_{n,0} A_1' = \delta_{n,0} \mathbb{H}\left(s_t - s_b\right) \exp\left\{-\int_0^{s_b} \mathrm{d}s' \Sigma_t\left(\vec{r} + s'\hat{\Omega}, t + \frac{s'}{v}\right)\right\} \tag{5.2a}$$

$$A_2 = \delta_{n,0} A_2' = \delta_{n,0} \mathbb{H}\left(s_b - s_t\right)\Big|_{(\vec{r}+s_t\hat{\Omega},\hat{\Omega})\notin\mathcal{R}} \exp\left\{-\int_0^{s_t} \mathrm{d}s' \Sigma_t\left(\vec{r} + s'\hat{\Omega}, t + \frac{s'}{v}\right)\right\} \tag{5.2b}$$

$$A_3 = \delta_{n,1} A_3' = \delta_{n,1} \mathbb{H}\left(s_b - s_t\right)\Big|_{(\vec{r}+s_t\hat{\Omega},\hat{\Omega})\in\mathcal{R}} \exp\left\{-\int_0^{s_t} \mathrm{d}s' \Sigma_t\left(\vec{r} + s'\hat{\Omega}, t + \frac{s'}{v}\right)\right\} \tag{5.2c}$$

where $\mathbb{H}$ is the Heaviside function. A_1 is the probability that the initial neutron streamed out of the system, A_2 is the probability that the neutron has not collided but it is not in $\mathcal{R}$, and A_3 is the probability that the neutron has not collided but it is in $\mathcal{R}$. The terminal condition for the single chain is

$$\lim_{t_f \leftarrow t} P_n(\mathcal{R}, t_f | \vec{r}, \hat{\Omega}, t) = \begin{cases} \delta_{n,1} & \text{if } \left(\vec{r}, \hat{\Omega}\right) \in \mathcal{R} \\ \delta_{n,0} & \text{if } \left(\vec{r}, \hat{\Omega}\right) \notin \mathcal{R} \end{cases} \tag{5.3}$$

and the boundary condition is

$$P_n\left(\mathcal{R}, t_f | \vec{r}, \hat{\Omega}, t\right) = \delta_{n,0} \quad \text{for } \vec{r} \in \partial V, \text{ and } \hat{n}_b \cdot \hat{\Omega} > 0, \tag{5.4}$$

where $\hat{n}_b$ is the surface unit normal vector. Equation 5.3 can be easily verified by taking the limit of $t_f \leftarrow t$, in which case $s_t \rightarrow 0$, causing the foremost integral of Eq. 5.1 to vanish because $\ell(s_b, s_t) = s_t = 0$. In the limit, A_1 will also vanish due to the argument of $\mathbb{H}$ being negative, while $A_2 = \delta_{n,0}$ or 0 and $A_3 = \delta_{n,1}$ or 0 depending on whether or not $(\vec{r}, \hat{\Omega}) \in \mathcal{R}$, respectively.

Equation 5.1 is in the integral form of the Chapman-Kolmogorov equation for the neutron number distribution; it is an open set of coupled equations and we must resort to the probability generating function (PGF) to transform the set of equations into a single equation. The PGF in the unlumped backward formulation is defined as

$$G\left(z, \mathcal{R}, t_f | \vec{r}, \hat{\Omega}, t\right) = \sum_{n=0}^{\infty} z^n P_n\left(\mathcal{R}, t_f | \vec{r}, \hat{\Omega}, t\right), \tag{5.5}$$

where we will suppress the $\mathcal{R}$ and t_f dependence for clarity in the ensuing equations. By multiplying Eq. 5.1 by z^n and summing over all n, we find an equation for G:

$$G\left(z|\vec{r}, \hat{\Omega}, t\right) = \int_0^{\ell(s_b,s_t)} \mathrm{d}s \Sigma_t\left(\vec{r} + s\hat{\Omega}, t + \frac{s}{v}\right) \mathrm{e}^{-\int_0^s \mathrm{d}s' \Sigma_t\left(\vec{r}+s'\hat{\Omega}, t+\frac{s'}{v}\right)} \Bigg[\sum_{\nu=0}^{\nu_m^f} c_\nu\left(\vec{r} + s\hat{\Omega}, t + \frac{s}{v}\right) \left\{G_o\left(z|\vec{r} + s\hat{\Omega}, t + \frac{s}{v}\right)\right\}^\nu \Bigg] + A_1' + A_2' + zA_3'. \tag{5.6}$$

Here, we have defined the angle-integrated PGF:

$$G_o(z|\vec{r}, t) = \int_{4\pi} \frac{\mathrm{d}\Omega'}{4\pi} G\left(z|\vec{r}, \hat{\Omega}', t\right). \tag{5.7}$$

If we now evaluate Eq. 5.6 at a short distance away from the original injection coordinates, δs, such that the LHS becomes $G(z|\vec{r} + \delta s\hat{\Omega}, \hat{\Omega}, t + \delta s/v)$, the only difference in the corresponding equation and Eq. 5.6 is the value of the lower integral limits change from 0 to δs. By then subtracting the two equations, we find:

$$G\left(z|\vec{r} + \delta s\hat{\Omega}, \hat{\Omega}, t + \frac{\delta s}{v}\right) - G\left(z|\vec{r}, \hat{\Omega}, t\right) = \mathcal{B}(z|\delta s, \vec{r}, \hat{\Omega}, t) - \mathcal{B}(z|0, \vec{r}, \hat{\Omega}, t) + \Delta A' \tag{5.8}$$

where we have defined

$$\mathcal{B}(z|a,\vec{r},\hat{\Omega},t) = \int_a^\ell \mathrm{d}s\mathcal{F}\left(z|\vec{r}+s\hat{\Omega},t+\frac{s}{v}\right)\exp\left\{-\int_a^s \mathrm{d}s'\Sigma_t\left(\vec{r}+s'\hat{\Omega},t+\frac{s'}{v}\right)\right\} \tag{5.9a}$$

$$\mathcal{F}(z|\vec{r},t) = \Sigma_t(\vec{r},t)\sum_{\nu=0}^{\nu_m^f} c_\nu(\vec{r},t)\left[G_o(z|\vec{r},t)\right]^\nu \tag{5.9b}$$

$$\Delta A' = A_1'(\delta s) - A_1'(0) + A_2'(\delta s) - A_2'(0) + zA_3'(\delta s) - zA_3'(0), \tag{5.9c}$$

where the value in the parentheses of Eq. 5.9c are the lower limits of the integrals in Eq. 5.2. By now dividing Eq. 5.8 by δs and taking the limit as $\delta s \to 0$, the LHS becomes the total derivative of G with respect to s, which simplifies to

$$\frac{\mathrm{d}G(z|\vec{r},\hat{\Omega},t)}{\mathrm{d}s} = \frac{\partial G}{\partial t}\frac{\mathrm{d}t}{\mathrm{d}s} + \frac{\partial G}{\partial \vec{r}}\cdot\frac{\mathrm{d}\vec{r}}{\mathrm{d}s},$$

where $\mathrm{d}\hat{\Omega}/\,\mathrm{d}s = 0$ because $\hat{\Omega}$ is not a function of space. By definition, the gradient of G is $\vec{\nabla}G = \partial G/\,\partial\vec{r}$. Also, the time derivative of space is the definition of velocity: $\mathrm{d}s/\,\mathrm{d}t = v$, and noting that $\vec{r} = s\hat{\Omega}$, we have $\mathrm{d}\vec{r}/\,\mathrm{d}s = \hat{\Omega}$. From these, the limiting LHS of Eq. 5.8 is

$$\frac{\mathrm{d}G(z|\vec{r},\hat{\Omega},t)}{\mathrm{d}s} = \frac{1}{v}\frac{\partial G}{\partial t} + \hat{\Omega}\cdot\vec{\nabla}G. \tag{5.10}$$

Now by dividing the RHS of Eq. 5.8 by δs and evaluating the limit $\delta s \to 0$, we see that the $\lim_{\delta s\to 0}\Delta A'/\delta s$ and $\lim_{\delta s\to 0}(\mathcal{B}(\delta s) - \mathcal{B}(0))/\delta s$ are indeterminate $(0/0)$. Applying L'Hôpital's Rule, we find that we must evaluate $\lim_{\delta s\to 0}\partial(A_1'(\delta s) + A_2'(\delta s) + zA_3'(\delta s))/\,\partial\delta s$ and $\lim_{\delta s\to 0}\partial\mathcal{B}(\delta s)/\,\partial\delta s$. These derivatives may be evaluated by following the Leibniz Integral Rule (see Eq. A.8) in concert with the chain rule:

$$\frac{\partial[A_1'(\delta s) + A_2'(\delta s) + zA_3'(\delta s)]}{\partial\delta s} = \Sigma_t\left(\vec{r}+\delta s\hat{\Omega},t+\frac{\delta s}{v}\right)\left[A_1'(\delta s) + A_2'(\delta s) + zA_3'(\delta s)\right]$$

and

$$\frac{\partial\mathcal{B}(\delta s)}{\partial\delta s} = -\mathcal{F}\left(z|\vec{r}+\delta s\hat{\Omega},t+\frac{\delta s}{v}\right) + \Sigma_t\left(\vec{r}+\delta s\hat{\Omega},t+\frac{\delta s}{v}\right)\times$$
$$\times\int_{\delta s}^\ell \mathrm{d}s\mathcal{F}\left(z|\vec{r}+s\hat{\Omega},t+\frac{s}{v}\right)\exp\left\{-\int_{\delta s}^s \mathrm{d}s'\Sigma_t\left(\vec{r}+s'\hat{\Omega},t+\frac{s'}{v}\right)\right\}.$$

Evaluating the limit, the RHS of Eq. 5.8 (divided by δs) is therefore

$$\begin{aligned}\lim_{\delta s\to 0}\text{RHS} &= -\mathcal{F}\left(z|\vec{r},t\right)+\Sigma_t\left(\vec{r},t\right)\Bigg\{\int_0^{\ell}\mathrm{d}s\mathcal{F}\left(z|\vec{r}+s\hat{\Omega},t+\frac{s}{v}\right)\mathrm{e}^{-\int_0^s \mathrm{d}s'\Sigma_t\left(\vec{r}+s'\hat{\Omega},t+\frac{s'}{v}\right)}\\ &\qquad +A_1'(0)+A_2'(0)+zA_3'(0)\Bigg\}\\ &= -\mathcal{F}\left(z|\vec{r},t\right)+\Sigma_t\left(\vec{r},t\right)G\left(z|\vec{r},\hat{\Omega},t\right).\end{aligned} \tag{5.11}$$

Combining Eqs. 5.10 and 5.11, we arrive at the Pál-Bell equation for the PGF of the neutron number distribution for a single chain:

$$\begin{aligned}\frac{1}{v}\frac{\partial G}{\partial t}+\hat{\Omega}\cdot\vec{\nabla}G\left(z|\vec{r},\hat{\Omega},t\right) &= \Sigma_t\left(\vec{r},t\right)G\left(z|\vec{r},\hat{\Omega},t\right)\\ &\quad -\Sigma_t\left(\vec{r},t\right)\sum_{\nu=0}^{\nu_m^f}c_\nu\left(\vec{r},t\right)\left[\int_{4\pi}\frac{\mathrm{d}\Omega'}{4\pi}G\left(z|\vec{r},\hat{\Omega}',t\right)\right]^{\nu}\end{aligned} \tag{5.12}$$

with terminal conditions given by

$$\lim_{t_f\leftarrow t}G\left(z,\mathcal{R},t_f|\vec{r},\hat{\Omega},t\right)=\begin{cases}z & \text{if } \left(\vec{r},\hat{\Omega}\right)\in\mathcal{R}\\ 1 & \text{if } \left(\vec{r},\hat{\Omega}\right)\notin\mathcal{R}\end{cases} \tag{5.13}$$

and the boundary condition is

$$G\left(z,\mathcal{R},t_f|\vec{r},\hat{\Omega},t\right)=1 \quad \text{for } \vec{r}\in\partial V, \text{ and } \hat{n}_b\cdot\hat{\Omega}>0, \tag{5.14}$$

Equation 5.12 is a nonlinear transport-like equation whose operational variables are the injection neutron's phase-space coordinates. As is customary, we may put Eq. 5.12 into a more suitable form by introducing the complementary PGF:

$$\mathcal{G}\left(z,\mathcal{R},t_f|\vec{r},\hat{\Omega},t\right)=1-G\left(z,\mathcal{R},t_f|\vec{r},\hat{\Omega},t\right). \tag{5.15}$$

Solving Eq. 5.15 for G and inserting into Eq. 5.12, we find:

$$\begin{aligned}-\frac{1}{v}\frac{\partial\mathcal{G}}{\partial t}-\hat{\Omega}\cdot\vec{\nabla}\mathcal{G}\left(z|\vec{r},\hat{\Omega},t\right) &= \Sigma_t\left(\vec{r},t\right)\left[1-\mathcal{G}\left(z|\vec{r},\hat{\Omega},t\right)\right]\\ &\quad -\Sigma_t\left(\vec{r},t\right)\sum_{\nu=0}^{\nu_m^f}c_\nu\left(\vec{r},t\right)\left[1-\int_{4\pi}\frac{\mathrm{d}\Omega'}{4\pi}\mathcal{G}\left(z|\vec{r},\hat{\Omega}',t\right)\right]^{\nu}.\end{aligned} \tag{5.16}$$

Expanding the nonlinear terms using the Binomial Theorem, we have

$$\begin{aligned}-\frac{1}{v}\frac{\partial \mathcal{G}}{\partial t}-\hat{\Omega}\cdot\vec{\nabla}\mathcal{G}\left(z|\vec{r},\hat{\Omega},t\right)&=\Sigma_t\left(\vec{r},t\right)\left[1-\mathcal{G}\left(z|\vec{r},\hat{\Omega},t\right)\right]\\&\quad-\Sigma_t\left(\vec{r},t\right)\sum_{\nu=0}^{\nu_m^f}\frac{(-1)^\nu}{\nu!}\left[\mathcal{G}_o(z|\vec{r},t)\right]^\nu\sum_{k=\nu}^{\nu_m^f}\frac{j!}{(j-\nu)!}c_j\left(\vec{r},t\right),\end{aligned}\tag{5.17}$$

where $\mathcal{G}_o(z|\vec{r},t)=\int_{4\pi}\mathrm{d}\Omega'\mathcal{G}(z|\vec{r},\hat{\Omega}',t)/4\pi$. Recognizing now that c_j, the probability of j neutrons emerging from a collision, may be written in terms of the macroscopic cross sections as:

$$c_0=\frac{\Sigma_c}{\Sigma_t}+q_0^f\frac{\Sigma_f}{\Sigma_t}\tag{5.18a}$$

$$c_1=\frac{\Sigma_s}{\Sigma_t}+q_1^f\frac{\Sigma_f}{\Sigma_t}\tag{5.18b}$$

$$c_j=q_j^f\frac{\Sigma_f}{\Sigma_t}\qquad j\geq 2,\tag{5.18c}$$

we may rearrange the RHS to ultimately find

$$\begin{aligned}\left[-\frac{1}{v}\frac{\partial}{\partial t}-\hat{\Omega}\cdot\vec{\nabla}+\Sigma_t\left(\vec{r},t\right)\right]\mathcal{G}\left(z|\vec{r},\hat{\Omega},t\right)&=\left[\Sigma_s\left(\vec{r},t\right)+\overline{\nu}\Sigma_f\left(\vec{r},t\right)\right]\int_{4\pi}\frac{\mathrm{d}\Omega'}{4\pi}\mathcal{G}\left(z|\vec{r},\hat{\Omega}',t\right)\\&\quad-\Sigma_f\left(\vec{r},t\right)\sum_{\nu=2}^{\nu_m^f}\frac{(-1)^\nu\chi_\nu(\vec{r})}{\nu!}\left[\int_{4\pi}\frac{\mathrm{d}\Omega'}{4\pi}\mathcal{G}(z|\vec{r},\hat{\Omega}',t)\right]^\nu,\end{aligned}\tag{5.19}$$

where the space-dependent case of Eq. 2.21 is

$$\chi_\nu(\vec{r})=\sum_{j=\nu}^{\nu_m^f}\frac{j!}{(j-\nu)!}q_j^f\left(\vec{r}\right).\tag{5.20}$$

Finally, the terminal conditions are

$$\lim_{t_f\leftarrow t}\mathcal{G}\left(z,\mathcal{R},t_f|\vec{r},\hat{\Omega},t\right)=\begin{cases}1-z & \text{if } \left(\vec{r},\hat{\Omega}\right)\in\mathcal{R}\\ 0 & \text{if } \left(\vec{r},\hat{\Omega}\right)\notin\mathcal{R}\end{cases}\tag{5.21}$$

and the boundary condition is

$$\mathcal{G}\left(z,\mathcal{R},t_f|\vec{r},\hat{\Omega},t\right)=0\quad\text{for } \vec{r}\in\partial V,\text{ and } \hat{n}_b\cdot\hat{\Omega}>0.\tag{5.22}$$

To complete this section, we now consider the neutron number distribution in the presence of an isotropically emitting source of strength $\mathcal{S}(\vec{r},t) = \omega(\vec{r})S(t)\ s^{-1}cm^{-3}$, where $\omega(\vec{r})$ is normalized such that $\int_V \mathrm{d}\vec{r}\omega(\vec{r}) = 1$. The probability of there being n neutrons within the system at time t_f due to the "turning on" of the source at some earlier time $t_o \leq t_f$ is $\Theta_n(t_f|t_o)$. There is no particle streaming requirement as there are no initial neutrons within the system.

A probability balance in the first collision interval proceeding the introduction time $t_o + \Delta t_o$ may be conducted. The probability of a source event occurring somewhere in the system in the first collision interval is $\Delta t_o \int_V \mathrm{d}\vec{r}\mathcal{S}(\vec{r},t_o)$. The probability that no source event occurs must then be multiplied by the probability that subsequent source events occur in the time interval $[t_o + \Delta t_o, t_f]$ resulting in n neutrons at t_f, $\Theta_n(t_f|t_o + \Delta t_o)$. Also, if a source event occurs in the first collision interval, emitting a multiplicity of ν neutrons with probability q_ν^S, each of these branches may propagate to produce $n_1, n_2, \ldots, n_\nu$ neutrons and subsequent source events in the time interval $[t_o + \Delta t_o, t_f]$ must then produce m_ν neutrons such that $n_1 + \cdots + n_\nu + m_\nu = n$. The probability balance is

$$\begin{aligned}\Theta_n(t_f|t_o) = \Theta_n(t_f|t_o + \Delta t_o)&\left(1 - \Delta t_o \int_V \mathrm{d}\vec{r}\mathcal{S}(\vec{r},t_o)\right) \\ &+ \Delta t_o \sum_{\nu=1}^{\nu_m^S} \sum_{n_1+\ldots+n_\nu+m_\nu=n} \Theta_{m_\nu}(t_f|t_o + \Delta t_o)\times \\ &\left\{\int_V \mathrm{d}\vec{r}q_\nu^S(\vec{r})\mathcal{S}(\vec{r},t_o)\prod_{\nu'=1}^{\nu}\int_{4\pi}\frac{\mathrm{d}\Omega_{\nu'}}{4\pi}P_{n_{\nu'}}\left(\mathcal{R},t_f|\vec{r},\hat{\Omega}_{\nu'},t_o+\Delta t_o\right)\right\}.\end{aligned} \tag{5.23}$$

By subtracting $\Theta_n(t_f|t_o + \Delta t_o)$, dividing by Δt_o and taking the limit $\Delta t_o \to 0$, we obtain the backward Master equation for a system with a spatially distributed isotropically emitting neutron source:

$$\begin{aligned}-\frac{\partial\Theta_n(t_f|t_o)}{\partial t_o} = \ &-S(t_o)\Theta_n(t_f|t_o) + S(t_o)\sum_{\nu=1}^{\nu_m^S}\sum_{n_1+\ldots+n_\nu+m_\nu=n}\Theta_{m_\nu}(t_f|t_o)\times \\ &\left\{\int_V \mathrm{d}\vec{r}q_\nu^S(\vec{r})\omega(\vec{r})\prod_{\nu'=1}^{\nu}\int_{4\pi}\frac{\mathrm{d}\Omega_{\nu'}}{4\pi}P_{n_{\nu'}}\left(\mathcal{R},t_f|\vec{r},\hat{\Omega}_{\nu'},t_o\right)\right\},\end{aligned} \tag{5.24}$$

with final condition:

$$\lim_{t_f \leftarrow t_o} \Theta_n(t_f|t_o) = \delta_{n,0}. \tag{5.25}$$

Equation 5.24 is linearly coupled in the number distribution in the presence of a source and is nonlinearly dependent on the number distribution for a single chain. By now applying the PGF for the source,

$$H(z, t_f|t_o) = \sum_{n=0}^{\infty} z^n \Theta_n(t_f|t_o), \tag{5.26}$$

the Master equation given by Eq. 5.24 reduces to:

$$\frac{\partial H}{\partial t_o} = S(t_o)\left\{1 - \sum_{\nu=1}^{\nu_m^S} \int_V \mathrm{d}\vec{r} q_\nu^S(\vec{r})\omega(\vec{r})\left[\int_{4\pi} \frac{\mathrm{d}\Omega}{4\pi} G\left(z, \mathcal{R}, t_f|\vec{r}, \hat{\Omega}, t_o\right)\right]^\nu\right\} H(z, t_f|t_o), \tag{5.27}$$

with final condition:

$$\lim_{t_f \leftarrow t_o} H(z, t_f|t_o) = 1. \tag{5.28}$$

Finally, by rewriting the single chain PGF as $G = 1 - \mathcal{G}$, we can expand the bracketed term with the Binomial Theorem to simplify Eq. 7.18:

$$\frac{\partial H}{\partial t_o} = -S(t_o)\left\{\sum_{\nu=1}^{\nu_m^S} \frac{(-1)^\nu}{\nu!} \int_V \mathrm{d}\vec{r} \chi_\nu^S(\vec{r})\omega(\vec{r})\left[\int_{4\pi} \frac{\mathrm{d}\Omega}{4\pi} \mathcal{G}\left(z, \mathcal{R}, t_f|\vec{r}, \hat{\Omega}, t_o\right)\right]^\nu\right\} H(z, t_f|t_o) \tag{5.29}$$

subject to the final condition given by Eq. 7.19, where the spatially dependent factorial moments of the source multiplicity distribution is defined as

$$\chi_\nu^S(\vec{r}) = \sum_{j=\nu}^{\nu_m^f} \frac{j!}{(j-\nu)!} q_j^S(\vec{r}). \tag{5.30}$$

5.2 Equations for Quantities of Interest

The value of expressing the Master equation in terms of the generating function is that closed equations for the desired probabilities can be readily obtained. For instance, setting $z = 0$ in Eq. 5.5 immediately gives:

$$G\left(z=0,\mathcal{R},t_f|\vec{r},\hat{\Omega},t\right) \equiv P_0\left(\mathcal{R},t_f|\vec{r},\hat{\Omega},t\right), \tag{5.31}$$

which is the probability of extinction of the neutron chain, i.e, the probability that no neutrons from a chain initiated by the original neutron survive to time t_f in $\mathcal{R}$. Similarly, it's complement, obtained by setting $z = 0$ in Eq. 5.15, is just the probability of survival:

$$P_S\left(\mathcal{R},t_f|\vec{r},\hat{\Omega},t\right) = 1 - P_0\left(\mathcal{R},t_f|\vec{r},\hat{\Omega},t\right) \equiv \mathcal{G}\left(z=0,\mathcal{R},t_f|\vec{r},\hat{\Omega},t\right), \tag{5.32}$$

i.e., the probability that the chain has not become extinct at time t_f. The time-asymptotic limit of the probability of survival, also known as the probability of initiation or POI, is of particular interest as it gives the probability that a neutron chain will grow without bound in a supercritical medium [11, 13]. This is given by:

$$P_\infty\left(\mathcal{R},t_f|\vec{r},\hat{\Omega}\right) = \lim_{t\to-\infty} P_S\left(\mathcal{R},t_f|\vec{r},\hat{\Omega},t\right). \tag{5.33}$$

Noting that the variable z does not appear explicitly in the equation for the generating function, but does so in the terminal condition, setting $z = 0$ does not alter the form of the equation and hence closed equations for the probabilities of interest are easily obtained. Thus the survival probability satisfies:

$$\left[-\frac{1}{v}\frac{\partial}{\partial t} + T^\dagger\right] P_S\left(\mathcal{R},t_f|\vec{r},\hat{\Omega},t\right) = \left[S^\dagger + F^\dagger - N\right] P_S\left(\mathcal{R},t_f|\vec{r},\hat{\Omega}',t\right), \tag{5.34}$$

with the final condition:

$$P_S\left(\mathcal{R},t_f|\vec{r},\hat{\Omega},t_f\right) = \begin{cases} 1 & \text{if } \left(\vec{r},\hat{\Omega}\right) \in \mathcal{R} \\ 0 & \text{if } \left(\vec{r},\hat{\Omega}\right) \notin \mathcal{R}, \end{cases} \tag{5.35}$$

and boundary condition:

$$P_S\left(\mathcal{R}, t_f|\vec{r}, \hat{\Omega}, t\right) = 0, \quad \vec{r} \in \partial V, \quad \hat{n}_b \cdot \hat{\Omega} > 0. \tag{5.36}$$

the various operators in the above equation are defined as:

$$T^\dagger \equiv -\hat{\Omega} \cdot \vec{\nabla} + \Sigma_t\left(\vec{r}, t\right), \tag{5.37a}$$

$$S^\dagger \equiv \int_{4\pi} \frac{\mathrm{d}\Omega'}{4\pi} \Sigma_s\left(\vec{r}, \hat{\Omega} \cdot \hat{\Omega}', t\right), \tag{5.37b}$$

$$F^\dagger \equiv \overline{\nu}\Sigma_f\left(\vec{r}, t\right) \int_{4\pi} \frac{\mathrm{d}\Omega'}{4\pi}, \tag{5.37c}$$

$$N \equiv \Sigma_f\left(\vec{r}, t\right) \sum_{\nu=2}^{\nu_m^f} \frac{(-1)^\nu \chi_\nu\left(\vec{r}\right)}{\nu!} \left[\int_{4\pi} \frac{\mathrm{d}\Omega'}{4\pi}\right]^\nu, \tag{5.37d}$$

where we have relaxed the isotropic scattering condition from the previous section.

Setting the time derivative to zero in Eq. 5.40 gives the corresponding equation for the chain divergence probability or POI:

$$T^\dagger P_\infty(\mathcal{R}|\vec{r}, \hat{\Omega}) = \Big[S^\dagger + F^\dagger - N\Big] P_\infty(\mathcal{R}|\vec{r}, \hat{\Omega}'). \tag{5.38}$$

with boundary condition given by Eq. 5.36. Once again, Eqs. 5.40 and 5.38 are time-dependent and steady state nonlinear adjoint transport equations and amenable to numerical solution by standard phase-space discretization schemes adapted to account for the nonlinear terms. It is known that the only solution to the POI equation in subcritical and critical systems is zero, but the POI may take on non-zero values for supercritical systems [32, 1]. Finally, although not of interest in this investigation, setting $z = 0$ in successively higher orders of derivatives of G and its defining equation yields the individual neutron number probabilities P_n of successively higher orders [41].

On a final note concerning sources, the extinction probability in the presence of a source, $\Theta_0(t_f|t_o) = H(z = 0, t_f|t_o)$, satisfies [18, 41]:

$$-\frac{\partial \Theta_0(t_f|t_o)}{\partial t_o} = S(t_o) \left\{ \sum_{\nu=1}^{\nu_m^S} \frac{(-1)^\nu}{\nu!} \int_V \mathrm{d}\vec{r} \chi_\nu^S(\vec{r}) \omega(\vec{r}) \left[\int_{4\pi} \frac{\mathrm{d}\Omega}{4\pi} P_S(\vec{r}, \hat{\Omega}, t_o)\right]^\nu \right\} \Theta_0(t_f|t_o),$$

Table 5.1: Source terms for the moments of the neutron number distribution.

k	$\mathcal{S}_k(\vec{r},t;\overline{n},\ldots,\overline{n^{k-1}})$
1	0
2	$2\Lambda_2\langle\overline{n}\rangle^2$
3	$6\langle\overline{n}\rangle\left[\Lambda_2\left\langle\overline{n^2}\right\rangle+\Lambda_3\langle\overline{n}\rangle^2\right]$
4	$6\Lambda_2\left\langle\overline{n^2}\right\rangle^2+\langle\overline{n}\rangle\left[8\Lambda_2\left\langle\overline{n^3}\right\rangle+36\Lambda_3\left\langle\overline{n^2}\right\rangle\langle\overline{n}\rangle+24\Lambda_4\langle\overline{n}\rangle^3\right]$

(5.39)

with final condition $\lim_{t_f\leftarrow t_o}\Theta_0(t_f|t_o)=1$. Thus, once the single chain survival probability has been obtained, the survival probability when a random intrinsic source exists is directly obtained by solving the linear ODE given in Eq. 5.39 as $\Theta_S=1-\Theta_0$.

Finally, the moments of the neutron number distribution may be determined using a methodology outlined in [43]. The equation for the k^{th} moment, $\overline{n^k}(\mathcal{R},t_f|\vec{r},\hat{\Omega},t)$, is calculated as:

$$\left[-\frac{1}{v}\frac{\partial}{\partial t}+T^\dagger\right]\overline{n^k}\left(\mathcal{R},t_f|\vec{r},\hat{\Omega},t\right)=\left[S^\dagger+F^\dagger\right]\overline{n^k}\left(\mathcal{R},t_f|\vec{r},\hat{\Omega}',t\right)+\mathcal{S}_k\left(\vec{r},t;\overline{n},\ldots,\overline{n^{k-1}}\right), \tag{5.40}$$

with the final condition: $\lim_{t_f\leftarrow t}\overline{n^k}\left(\mathcal{R},t_f|\vec{r},\hat{\Omega},t\right)=1$ for $\left(\vec{r},\hat{\Omega}\right)\in\mathcal{R}$ and 0 otherwise, and boundary condition $\overline{n^k}\left(\mathcal{R},t_f|\vec{r},\hat{\Omega},t\right)=0$, for $\vec{r}\in\partial V$, and $\hat{n}_b\cdot\hat{\Omega}>0$. The inhomogeneous source term for the k^{th} moment, $\mathcal{S}_k$, is a function of all lower order moments and is therefore assumed to be known. The first four source terms are shown in Table 5.1, where we have introduced the coefficient:

$$\Lambda_i(\vec{r},t)=\Sigma_f(\vec{r},t)\sum_{j=i}^{\nu_m^f}\binom{j}{i}q_j^f, \tag{5.41}$$

and we note that the notation $\langle \cdot \rangle$ refers to integrating over all angles (and χ spectrum-weighted energy when applicable). Thus, the moment equations must be solved in an ascending order starting with the first moment.

Chapter 6

Solution Methods for the Survival Probability Equation

In this chapter, we describe two methods for solving Eq. 5.40 and its steady state version Eq. 5.38. One is a type of nonlinear eigenvalue method, originally devised and demonstrated by Bell and Lee [26] for the POI and subsequently extended by Baker [28] to the time dependent case. This method, known as the λ-Acceleration Method (λAM), is unconditionally stable and while the algorithm has been described in the literature we reproduce it here so as to provide a contrast with the second, very different method based on a k-eigenmode expansion [64].

To solve Eq. 5.40 "directly" by Picard Iteration, or commonly referred to as Fixed-Point Iteration, we simply follow the algorithmic procedure of the common Source Iteration method [51]. This is done by performing standard adjoint reversals in time and direction, and for a given time-step we "lag" the scattering and fission source that now includes the nonlinear terms by one iteration and solve for the angular-dependent survival probability for the next iteration. The source terms are then updated with this new value for P_S, and the process is iterated until a convergence criteria is met and advanced to the next time step.

Employing the discrete ordinates in angle, diamond difference in space, and Crank-Nicholson in time discretizations, the Picard iteration proves efficient for highly supercritical systems, when $k \geq 1.1$. However, under these conditions the time variation is exceedingly rapid, as the survival probability converges to the POI at a faster rate, and requires smaller time steps to adequately resolve the solution. For near-critical systems, $k \sim 1$, the time dependent solution takes longer to converge to the POI as neutron chains can survive very long times before one diverges. In other words, a neutron must be injected farther into the past in a nearly critical system for its progeny to grow without bound. We conclude that the Picard iteration is not an efficient algorithm for computation of the survival and divergence probabilities.

6.1 A Nonlinear Scaling Method

We describe the λAM implementation for the static case, i.e., for the POI which satisfies:

$$T^{\dagger} P_{\infty}(\vec{r}, \hat{\Omega}) = \left[S^{\dagger} + F^{\dagger} - N \right] P_{\infty}(\vec{r}, \hat{\Omega}'), \tag{6.1}$$

where the operators, $T^{\dagger}$, $S^{\dagger}$, $F^{\dagger}$, and N are defined by Eq. 8.64. The time dependent case is a straightforward generalization of the static case and is described in [28]. The λAM solution proceeds by first solving the linear adjoint k-eigenvalue equation:

$$T^{\dagger} P_{\infty}(\vec{r}, \hat{\Omega}) = \left[S^{\dagger} + \frac{1}{k^{\dagger}} F^{\dagger} \right] P_{\infty}(\vec{r}, \hat{\Omega}'), \tag{6.2}$$

and using this solution as an initial guess to the nonlinear equation. Next, we integrate Eqs. 6.1 and 6.2 over the phase space, subtract the two, and then scale $P_{\infty,o} = \int_{4\pi} \frac{d\Omega}{4\pi} P_{\infty}$ by some factor λ, from which we obtain an order $J-1$ polynomial equation for λ:

$$\sum_{j=2}^{J} \frac{(-1)^j}{j!} \lambda^{j-1} \int_V \mathrm{d}\vec{r} \Sigma_f \chi_j P_{\infty,o}^j = \left(1 - \frac{1}{k^{\dagger}} \right) \int_V \mathrm{d}\vec{r} \vec{\nu} \Sigma_f P_{\infty,o}, \tag{6.3}$$

where J is the maximum number of neutrons emitted in an induced fission. Taking the largest root of Eq. 6.3, the scaling factor is then used to estimate the scatter term and scaled fission source term of Eq. 6.1,

$$\mathcal{Q}^{(n)}(\vec{r}) = S^{\dagger} P_{\infty}^{(n)}(\vec{r}, \hat{\Omega}') + \left[F^{\dagger} - N\right] \lambda^{(n)} P_{\infty}^{(n)}(\vec{r}, \hat{\Omega}')$$

where the superscript (n) denotes the n^{th} iteration. Once $\mathcal{Q}^{(0)}$ is known, we proceed by performing a classical source iteration [51] until $F^{\dagger} P_{\infty}^{(n+1)} / F^{\dagger} P_{\infty}^{(n)} \to 1$. Upon convergence, the scaling factor, $\lambda^{(n+1)}$, is then updated by solving for λ in the polynomial:

$$\sum_{j=2}^{J} \frac{(-1)^j}{j!} \left[\lambda^{(n+1)}\right]^{j-1} \int_V \mathrm{d}\vec{r} \chi_j \Sigma_f \left[P_{\infty,o}^{(n+1)}\right]^j = \int_V \mathrm{d}\vec{r} \left\{ F^{\dagger} P_{\infty}^{(n+1)} - \left[F^{\dagger} - N\right] P_{\infty}^{(n)} \right\}; \tag{6.4}$$

from which, we again use the greatest upper bound root of Eq. 6.4 to scale our fission source term for the next λ-iteration. This process is continued until λ converges to 1. In the time dependent case, the λ scaling is applied at each time step and the lagged source terms supplemented with the solution from the previous time step [28].

For numerical illustration, the subvolume $\mathcal{R}$ is taken to be the domain $V \times S^2$, i.e., we compute the divergence and survival probabilities over the entire system volume. Although the cross sections are permitted to be piecewise constant in space, they are assumed to be time independent, in which case the solution depends on the time variables only through the time difference $\tau = t_f - t$. It is then convenient for numerical purposes to transform to this forward time variable and, without risk of confusion, we further restore the time variable back from τ to t. Introducing the change $\partial/\partial t \to -\partial/\partial t$ in Eq. 5.40 gives for one-dimensional slab geometry with

isotropic scattering:

$$\left[\frac{1}{v}\frac{\partial}{\partial t} - \mu\frac{\partial}{\partial z} + \Sigma_t(z)\right] P_S(z,\mu,t) = \left[\Sigma_s(z) + \overline{\nu}\Sigma_f(z)\right] \int_{-1}^{1} \frac{\mathrm{d}\mu'}{2} P_S(z,\mu',t) - \Sigma_f(z) \sum_{j=2}^{J} \frac{(-1)^j}{j!} \chi_j(z) \left[\int_{-1}^{1} \frac{\mathrm{d}\mu'}{2} P_S(z,\mu',t)\right]^j, \tag{6.5}$$

with the now initial condition, as opposed to terminal or final condition, given by:

$$P_S(z,\mu,0) = 1, \tag{6.6}$$

and boundary conditions:

$$P_S(z_L,\mu,t) = 0, \mu < 0, \qquad P_S(z_R,\mu,t) = 0, \mu > 0, \tag{6.7}$$

where z_L and z_R are the left and right boundary coordinates.

In the next section, we use the λAM method to assess the accuracy and computational performance of the eigenfunction expansion method. In all calculations requiring the numerical solution of the steady state nonlinear transport equation (the POI equation) as well as the computation of the eigenspectrum of the linear transport equation, we use diamond-difference discretization in space and discrete ordinates in angle, and the nonlinear terms are evaluated at the cell centers. For the λAM, a standard semi-implicit backward-Euler time discretization [35] is used for the solution of the survival probability equation while the time dependent mode amplitude equations are solved in MATLAB using the `ode15s` stiff ODE solver. Unless otherwise stated, all numerical results for the probabilities were obtained with 300 spatial cells, S_{16} discrete ordinates angular discretization, and a time-step width of $\Delta t = 10^{-3} t_f$.

To ensure the correctness of the implementation of the λAM method, we first benchmark this method using the Method of Manufactured Solutions (MMS), which apparently has not been done before.

Table 6.1: Static system iterations required to converge to the POI.

k	Picard	λAM		
		Initial Guess	Total Inner	Outer
1.1	604	67	664	25
1.05	1,098	64	654	24
1.01	4,779	61	629	22
1.001	38,262	59	588	17

6.1.1 Viability of the λAM for Marginally Supercritical Systems

In this section, we demonstrate the advantage of the λAM for near-critical static systems in a one-dimensional sphere composed of ^{235}U metal. The fundamental mode is scaled by altering the system radius and Table 6.1 shows the computational cost in the limit $k \to 1^+$ for both the Picard Iteration Method and the λAM. Solutions to the POI as calculated by the Picard Method have convergence criteria of 10^{-9} for the max error in the shape of the solution and the λAM has convergence criteria of 10^{-9} for the fundamental mode (initial guess via the Power Method), the shape of the POI for successive inner iterations, and the convergence of λ onto unity.

Regarding the Picard scheme, a dramatic increase in the number of iterations required to converge occurs in the approach to exactly critical; this is due to the decrease in the solution's magnitude toward zero (but greater than zero) and the flattening of the gradient which causes the calculation of the relative error between iterations to increase. The λAM appears consistent, and in fact reduces in the total number of iterations for the calculation, proving a clear advantage to it's utility in any criticality regime. For this reason, we choose to use the λAM code to benchmark the EEM results. This harkens one to question the accuracy of the solutions produced by the λAM code, and we next show results of the verification of this code using the Method of Manufactured Solutions.

6.1.2 Verification of the Nonlinear Scaling Method

The MMS method consists of assuming a convenient closed form solution for the survival probability, called the manufactured solution, and defining the residual obtained by substituting this analytical solution in the equation for the survival probability as a source. If the survival probability equation is then numerically solved with this source and initial and boundary conditions chosen to be consistent with the manufactured solution, the solution will represent a numerical approximation to the manufactured solution [53, 54]. This approach therefore enables the accuracy and order of convergence of the discretized problem to be established for the original nonlinear equation without having to rely on analytical benchmark solutions that inevitably require oversimplifying the original problem.

Following standard practice, the manufactured solution is constructed as a convenient product of 1D factors:

$$\hat{P}_S(z,\mu,t) = Af(z)g(\mu)h(t), \tag{6.8}$$

where the coefficient A is arbitrary and is chosen here by fixing the global maximum of the survival probability $\hat{P}_m$. We further impose the normalization $\int_{-1}^{1} \mathrm{d}\mu g(\mu) = 1$. Substituting the manufactured solution Eq. 6.8 into Eq. 6.5 readily yields the manufactured source:

$$\begin{aligned}\frac{1}{A}Q(z,\mu,t) = {} & fg\,\frac{1}{v}\frac{\mathrm{d}h}{\mathrm{d}t} - \mu gh\frac{\mathrm{d}f}{\mathrm{d}z} + \Sigma_t fgh - \left(\Sigma_s + \overline{\nu}\Sigma_f\right)\frac{fh}{2} \\ & + \Sigma_f \sum_{j=2}^{J} \frac{(-1)^j \chi_j A^{j-1}}{j!}\left[\frac{fh}{2}\right]^j .\end{aligned} \tag{6.9}$$

Several examples of the separable factors that define the manufactured solution are shown in Table 6.2, which provide relatively simple initial and boundary conditions. We set $z_L = 0\ cm$, $z_R = 1\ cm$, choose the number of cells, n_I, to be equal to the number of time steps, n_t, and we select an S_N order $N = 2n_I = 2n_t$. We further restrict time variation to $t \leq 1$. The error between the manufactured solution and the

Table 6.2: MMS test functions.

Case	$f(z)$	$g(\mu)$	$h(t)$
1	1	$\frac{1}{2}$	1
2	$1 - z/z_R$	$\frac{1}{2}$	1
3	$1 - z/z_R$	$\frac{1}{4} + \frac{3}{2}\mu + \frac{3}{4}\mu^2$	1
4	$1 - z/z_R$	$\frac{1}{2}$	e^{-t}
5	$z(z_R - z)$	$\frac{1}{4} + \frac{3}{2}\mu + \frac{3}{4}\mu^2$	e^{-t}
6	$\frac{z}{z_R}e^{-z/z_R}$	$\frac{3}{2}\mu^2$	$1 - e^{-t}$
7	1	$\frac{1}{2}$	$1 - t$
8	$\begin{cases} 1, & z < z_I, \\ 1 - \frac{z}{z_R}, & z_I < r < z_R \end{cases}$	$\frac{1}{2}$	1

numerical result, $P_S(z_i, \mu_m, t_j)$, is calculated using the following L_2 error norm [55]:

$$\epsilon(n_I, N, n_t) = \sqrt{\sum_{j=1}^{n_t}\sum_{i=1}^{n_I}\sum_{m=1}^{N}\left(\hat{P}_S(z_i, \mu_m, t_j) - P_S(z_i, \mu_m, t_j)\right)^2 w_m \Delta z_i \Delta t_j}, \quad (6.10)$$

where w_m is the Gauss-Legendre quadrature weight, Δz_i is the width of cell i with z_i the midpoint, and Δt_j is the width of the j^{th} time-step.

Figure 6.1 shows the error between various manufactured solutions given in Table 6.2 and the numerical solution. For Case 1, the constant solution is obtained practically exactly to machine precision, regardless of the level of mesh refinement. But it is also evident from the error plot that the chosen discretizations are able to resolve practically exactly the manufactured solutions that display constant or linear spatial and temporal variation and quadratic angular variation, as in Cases 2, 3 and 7. This indicates that the numerical scheme is second-order in space and time. When the spatial or time variation of the manufactured solution is nonlinear, as in Cases 4 - 6, the error is larger and decays linearly with increasing numbers of cells, i.e., the overall scheme is first order. For the two-region slab in Case 8 with constant material properties and the interface in the center, $z_I = 0.5\ cm$, the manufactured solution is

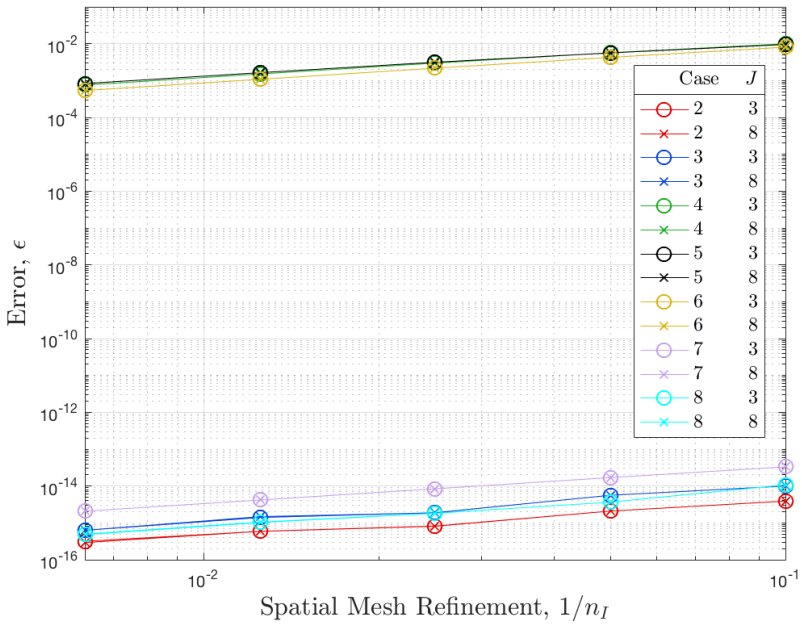

Figure 6.1: MMS error for several test problems.

again highly resolved, indicating that the treatment of the material interface does not introduce additional errors for a continuous solution. Finally, it is seen that the order of the nonlinearity J has no effect on the convergence order for all manufactured solutions. These results show that the λAM code converges to the manufactured solution and provides verification of the code.

6.2 The Eigenfunction Expansion Method

We now describe an indirect but physically appealing method for the solution of Eq. 5.40. It is known that for marginally supercritical media the space-angle shape of the POI is well approximated by the fundamental mode [18], which reduces the computation of the survival probability to a point kinetic equation for the time amplitude and for the divergence probability to a nonlinear algebraic equation. Here

we generalize this concept by representing the survival probability as an expansion in terms of higher eigenfunctions of the adjoint transport operator to extend the validity of this approach to more strongly supercritical media. This work extends to the transport formulation from our previous application of the eigenmode expansion method in the diffusion approximation [49, 50].

Proceeding, we express $P_S(\mathcal{R}, t_f|\vec{r}, \hat{\Omega}, t)$ as:

$$P_S\left(\mathcal{R}, t_f|\vec{r}, \hat{\Omega}, t\right) = \sum_{m=1}^{\infty} \mathcal{T}_m\left(t_f|t\right) \Psi_m^{\dagger}\left(\mathcal{R}|\vec{r}, \hat{\Omega}\right), \tag{6.11}$$

where $\Psi_m^{\dagger}\left(\mathcal{R}|\vec{r}, \hat{\Omega}\right)$ represents the m^{th} adjoint eigenfunction and $\mathcal{T}_m\left(t_f|t\right)$ is the associated time-dependent coefficient or mode amplitude. The adjoint eigenfunctions are the nontrivial solutions of the linear homogeneous adjoint transport equation:

$$\left[T^{\dagger} - S^{\dagger}\right] \Psi_m^{\dagger} = \frac{1}{k_m^{\dagger}} F^{\dagger} \Psi_m^{\dagger}, \tag{6.12}$$

where $k_m^{\dagger}$ are the corresponding eigenvalues, which are the same as the forward eigenvalues, that is $k_m^{\dagger} = k_m$, therefore we will use k_m for the remainder of the chapter. Now inserting the expansion Eq. 6.11 into Eq. 5.40 and noting Eq. 6.12 gives after some algebra:

$$\sum_{m=1}^{\infty} \left\{ -\Psi_m^{\dagger} \frac{1}{v} \frac{\mathrm{d}\mathcal{T}_m}{\mathrm{d}t} + \mathcal{T}_m \left(1 - \frac{1}{k_m}\right) F^{\dagger} \Psi_m^{\dagger} \right\} = -N \left(\sum_{m=1}^{\infty} \mathcal{T}_m \Psi_m^{\dagger} \right). \tag{6.13}$$

The spectrum of k-eigenfunctions, $\mathbf{\Psi}^{\dagger}$ and corresponding reciprocal k-eigenvalues, $\boldsymbol{\lambda}$, is obtained by discretizing the adjoint neutron transport equation using N discrete ordinates and I spatial cells, then solving the system of $I\,N$ equations in the form of a generalized eigenvalue problem:

$$\left[\mathbf{T}^{\dagger} - \mathbf{S}^{\dagger}\right] \mathbf{\Psi}^{\dagger} = \mathbf{F}^{\dagger} \mathbf{\Psi}^{\dagger} \boldsymbol{\lambda}, \tag{6.14}$$

where $[\mathbf{T}^{\dagger} - \mathbf{S}^{\dagger}]$ and $\mathbf{F}^{\dagger}$ are square matrices of order $I\,N \times I\,N$, $\boldsymbol{\lambda}$ is a diagonal matrix of generalized eigenvalues and $\mathbf{\Psi}^{\dagger}$ is a full matrix whose columns are the

corresponding right eigenvectors. The eigenspectrum is obtained by solving Eq. 6.14, and the m^{th} k-eigenvalue is determined by reciprocating the (m,m) position of $\boldsymbol{\lambda}$ as $k_m = 1/\boldsymbol{\lambda}(m,m)$.

The forward and adjoint eigenfunctions satisfy the bi-orthogonality condition:

$$\left\langle \Psi_m, F^\dagger \Psi^\dagger_{m'} \right\rangle = \left\langle \Psi^\dagger_m, F \Psi_{m'} \right\rangle = \gamma_m \delta_{m,m'}, \tag{6.15}$$

where the inner product $\langle \cdot \rangle$ denotes integration over the spatial and angular domain and γ_m is the normalization coefficient. Operating on Eq. 6.13 with $F^\dagger$ and taking the inner product over the forward eigenfunctions $\Psi_{m'}$ then yields the following set of coupled nonlinear ordinary differential equations for the time-dependent mode amplitudes:

$$\begin{aligned} -\gamma_m \frac{1}{v}\frac{\mathrm{d}\mathcal{T}_m}{\mathrm{d}t} = &\sum_{m'=1}^{M} \mathcal{T}_{m'} \left[1 - \frac{1}{k_{m'}}\right] \int_V \mathrm{d}\vec{r} \left[\overline{\nu}\Sigma_f\right]^2 \Phi_m \Phi^\dagger_{m'} \\ &- \sum_{j=2}^{J} \frac{(-1)^j}{j!} \int_V \mathrm{d}\vec{r}\, \overline{\nu}[\Sigma_f]^2 \chi_j \Phi_m \left[\sum_{m'=1}^{M} \mathcal{T}_{m'} \Phi^\dagger_{m'}\right]^j, \end{aligned} \tag{6.16}$$

where $\Phi^\dagger_m(\vec{r}) = \int_{4\pi} \mathrm{d}\Omega' \Psi^\dagger_m(\vec{r}, \hat{\Omega}')/4\pi$ and the expansion is truncated at order M and expanded via the Multinomial Theorem. The terminal condition and normalization factor are given by:

$$\begin{aligned} \mathcal{T}_m(t_f|t_f) &= \frac{1}{\gamma_m} \int_V \mathrm{d}\vec{r}\, \overline{\nu}\Sigma_f(\vec{r}) \Phi_m(\vec{r}), \\ \gamma_m &= \int_V \mathrm{d}\vec{r}\, \overline{\nu}\Sigma_f(\vec{r}) \Phi_m(\vec{r}) \Phi^\dagger_m(\vec{r}). \end{aligned} \tag{6.17}$$

Once the mode amplitudes have been computed by numerically solving the above M nonlinear differential equations, the space, angle and time-dependent survival probability can be reconstructed by truncating the expansion in Eq. 6.11 at order M.

In the next section we present and contrast numerical results from both methods of solution for the survival probability and POI.

6.3 Eigenfunction Expansion Method Results

We now consider the Eigenfunction Expansion Method (EEM) for solving the neutron chain survival probability equation in one-dimensional slab geometry. We obtain the space-angle adjoint eigenspectrum by solving Eq. 6.14 with the QZ algorithm, and the coupled temporal coefficient ODEs, Eq. 6.16, are solved using MATLAB's built-in stiff ODE solver, `ode15s`.

6.3.1 Obtaining the Eigenspectrum

The eigenspectrum is computed by solving the linear forward and adjoint k-eigenvalue slab-geometry transport equations as generalized eigenvalue problems. Additionally, we take advantage of the fact that the one-speed forward and adjoint scalar eigenfunctions are identical, as shown in Fig. 6.2a for an 8 cm Pu slab flanked by two 2.5 cm graphite slabs in vacuum, where the vertical lines indicate material interfaces. Plutonium neutron multiplicity data for induced and spontaneous fission events is taken from [48], pertaining to a system composed of 80 wt% ^{239}Pu and 20 wt% ^{240}Pu, replicated in Table 6.3 for convenience. Figure 6.2b shows the k-eigenvalue spectra for this slab system for two different fundamental mode values ($k_1 = 1.0025$ and $k_1 = 1.5019$), which have the same eigenvector spectrum for a given geometry, for which we see a sharp reduction in the magnitude of first few eigenvalues for increasing m followed by a slower decay of the spectrum. The fact that the eigenvectors are identical for different eigenvalue spectra is due to our choice in artificially altering $\overline{\nu}$ values without changing the multiplicity distribution. Thus, only $F^\dagger$ changes and to rebalance Eq. 6.12, only the $1/k$ factor changes to compensate for the change in $\overline{\nu}$. This would not be true if we altered the fission cross section as $T^\dagger$ (and N) would also change and recalculating the eigenspectrum would become necessary.

We note that the eigenvectors with even-valued indices of the displayed spectrum correspond to odd functions with respect to z and will therefore not contribute to

Table 6.3: Neutron multiplicity data.

k	0	1	2	3	4	5	6	7	8
q_k^f	0.0071	0.0674	0.2283	0.3263	0.251	0.0958	0.0208	0.0029	0.0004
q_k^S	0.0638	0.2316	0.3325	0.2533	0.0987	0.0181	0.0020	-	-

the solution of the system of ODEs defined by Eq. 6.16 because their final conditions will be zero, i.e., because

$$\int_{z_L}^{z_R} \mathrm{d}z\overline{\nu}(z)\Sigma_f(z)\Phi_{2m}^{\dagger}(z) = 0,$$

where $m = 1, 2, \ldots$, then $\mathcal{T}_{2m}(t_f|0) = 0$ and these amplitudes will remain null for all time. Thus, in the ensuing results, we only use the odd-value index eigenvectors and corresponding eigenvalues. In general, this is not the case and only occurs here because the slab system is symmetric - we simply exploit this symmetry to demonstrate the EEM without loss of generality of the behavior of the resultant survival probability distributions.

The convergence of the eigenvalue spectrum with spatial mesh refinement is shown in Figure 6.3, which gives the relative error of the k-spectrum for a system very near critical, $k = 1.0025$, and a highly supercritical system, $k = 1.5019$, respectively, for which the reference converged spectrum contains 300 cells (100 cells per region) for either system. If we choose the maximum deviation from the $I = 300$ spectrum to be no more than 4%, we may safely use up to 9 modes with 120 cells (40 cells per region) for any practical range of criticality we may be interested in. Similar results hold true for the convergence on the angular eigenvector spectrum, where the integral global balance of the neutron transport equation was compared. For the remainder of the paper, we will use the spectrum with $I = 300$ cells to minimize spatial error in calculating the projection integrals.

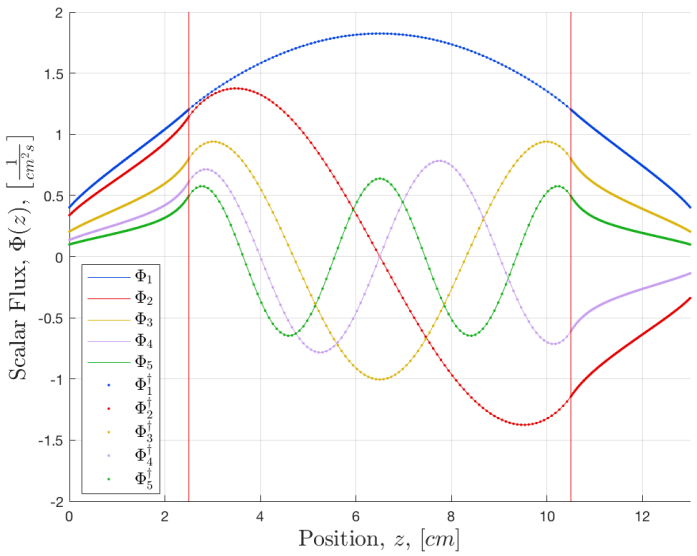

(a)

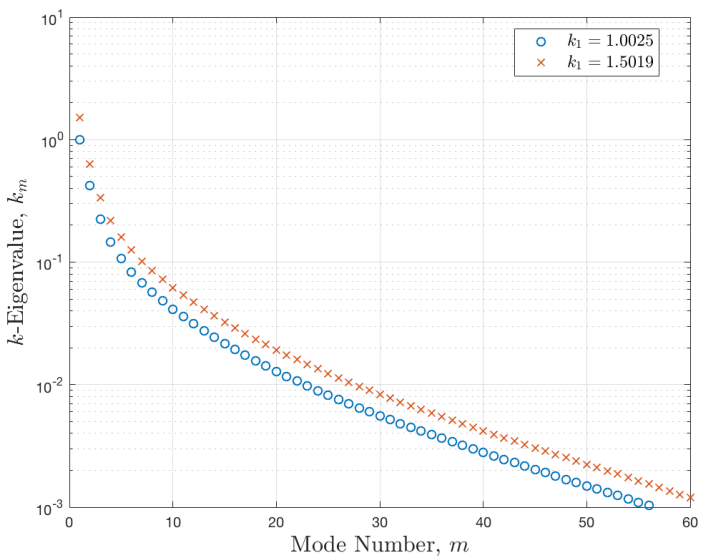

(b)

Figure 6.2: For a three-region slab: (a) the forward and adjoint scalar flux spectrum and (b) the k-eigenvalue spectrum.

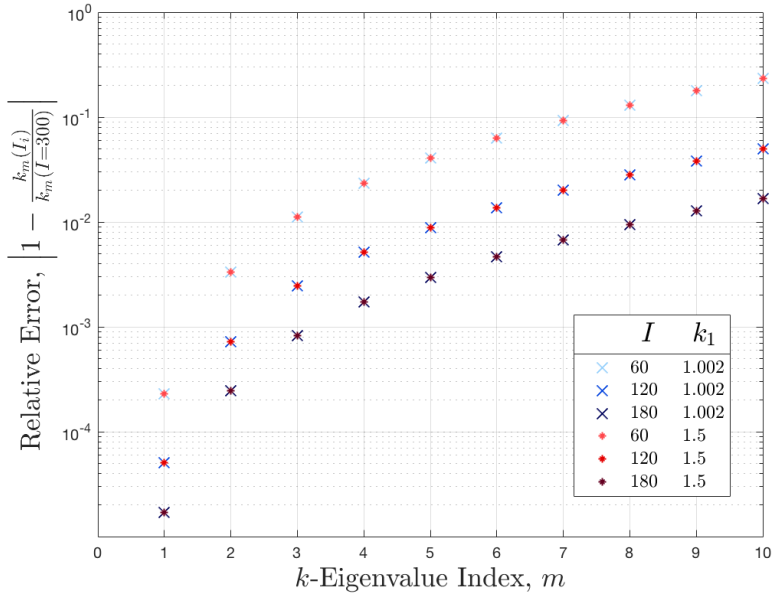

Figure 6.3: Relative error of the eigenvalue spectrum for differing I as compared to spectrum values calculated for $I = 300$.

6.3.2 Single Chain Survival and Divergence Probabilities

Figure 6.4a shows the absolute value of the relative error spatial profiles for the scalar POI as calculated by the benchmark λAM and the EEM for the near-critical and highly supercritical three-region system with eigenspectrum depicted in Figs. 6.2a and 6.2b. It is observed that, for a fixed modal expansion order M and system criticality k_1, the nonlinearity order J has the same error profile indicating that the EEM provides consistent results for differing J when compared to the λAM; this shows that the modal truncation order and the nonlinearity order are not correlated, so we may parametrically analyze the effects on the solution of one quantity without considering a change in the other quantity. Figures 6.4b and 6.4c show the right-half of the inner multiplying region ($6.5\ cm \leq z \leq 10.5\ cm$) for the $k_1 = 1.0025$ and 1.5019, respectively, to allow for better examination of the details of the error profiles. Another observation in Fig. 6.4 concerns the error profiles within the center of the

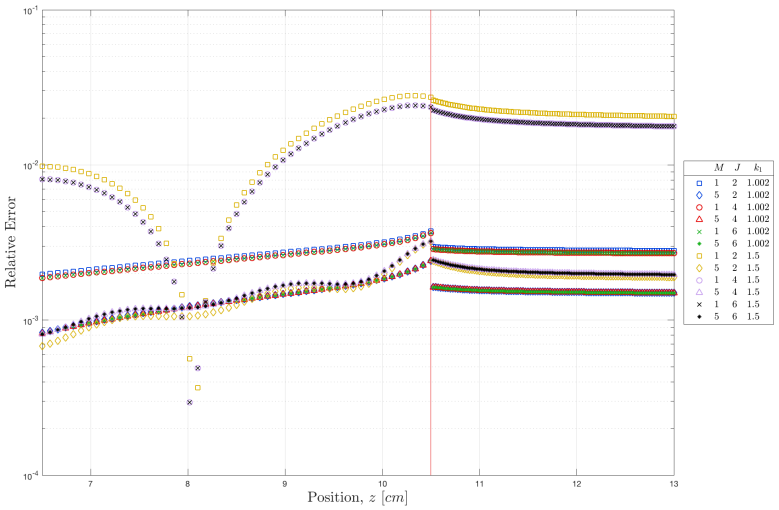

(a)

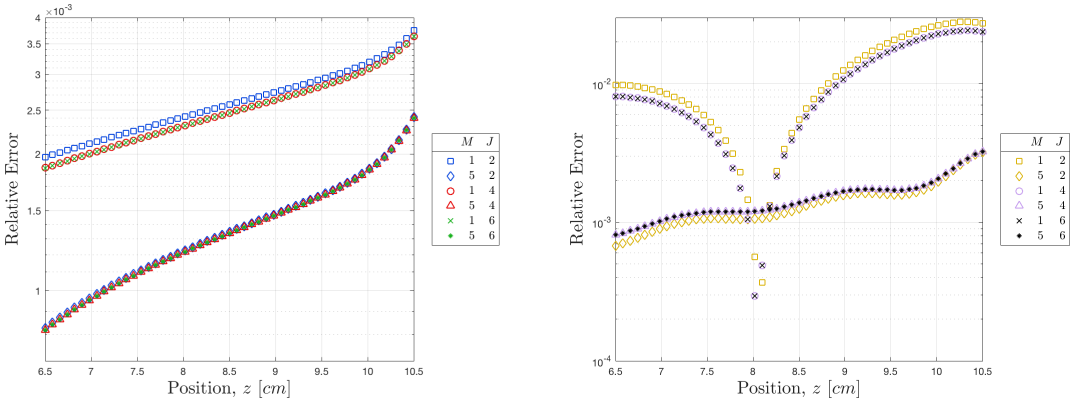

(b) **(c)**

Figure 6.4: Relative error of the scalar POI, $P_{\infty,o}(z)$, as calculated by the λAM and the EEM for (a) the right-half of the three-region $Pu-C$ slab system along with detailed comparisons within the multiplying regions for (b) $k_1 = 1.0025$ and (c) $k_1 = 1.5019$.

system as a function of criticality. We see in Fig. 6.4c, for the $k_1 = 1.5$ case, the error in the center drastically decreases by an order of magnitude when going from $M = 1$ to $M = 5$, but for the $k_1 = 1.0025$ case in Fig. 6.4b, the magnitude of the error in

the center for the $M = 1$ and $M = 5$ cases is only about halved. This phenomena is due to the fact that for increasing supercriticality, i.e. increasing multiplication, the branches of a chain reaction resulting from the propagation of the initial neutron's progeny have a greater effect, and a more accurate representation of the nonlinear terms (by increasing M) is necessary; conversely, for near-critical systems, where the multiplication between successive generations is not as great, the essence of the solution is sufficiently represented due to the fundamental mode and the nonlinear terms are merely supplemental. A final note concerning Fig. 6.4c concerns the relative error around $z = 8\ cm$ for the $M = 1$, $k = 1.5$ case, where all J values show it. This dip is indicative of a crossing-over of the EEM solution with the λAM solution. The dip shows how the fundamental mode 'hugs' the λAM solution, but the fundamental mode is not appropriate for higher k-systems. This is evident in the $k = 1.002$ case, where the error is lower. Alternatively, one may utilize the α eigenspectrum to represent the exponential time-dependent behavior of the neutron flux [29]. The α eigenspectrum is obtained from the linear neutron transport operator with inclusion of a time-component [30], and result in an imaginary eigenvalue spectrum (except the fundamental mode remains on the real line) [31]. This then requires one to solve two amplitude equations for non-fundamental amplitudes, which is acceptable for systems that require only a few modes to resolve.

Figure 6.5 shows the spatial profiles of the scalar POI for differing M and J for systems with fundamental modes of $k_1 = 1.0025$ in (6.5a), $k_1 = 1.1567$ in (6.5b), and $k_1 = 1.5019$ in (6.5c). The system criticality was altered by scaling $\overline{\nu}$ in order to hold the system dimensions constant. For the near-critical system depicted in Fig. 6.5a, there is almost no visual difference in the profiles, regardless of the modal truncation and the nonlinearity order; this is expected for such a system for the reasons described regarding the error profiles in Fig. 6.4, where the fundamental mode dominates. Fig. 6.5b shows an appreciable separation between the $J = 2$ lines and the higher nonlinear lines, where the $J = 4$ and $J = 6$ lines lie atop one another. Thus, for such

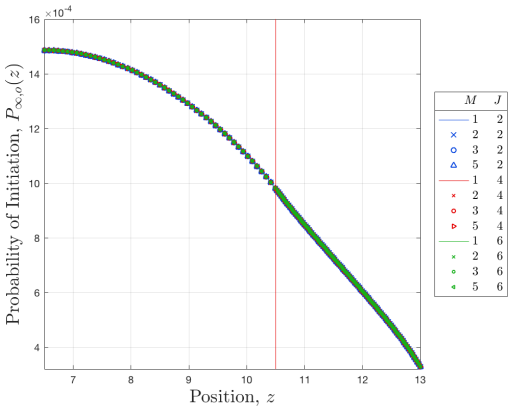

(a)

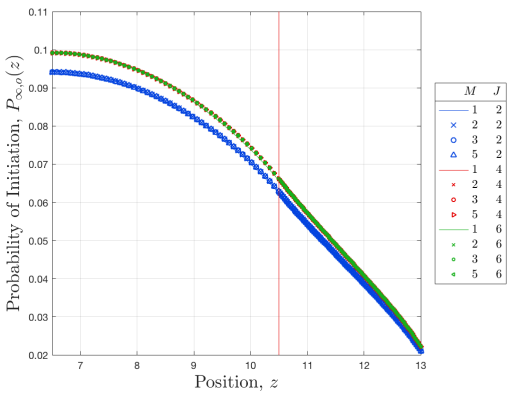

(b)

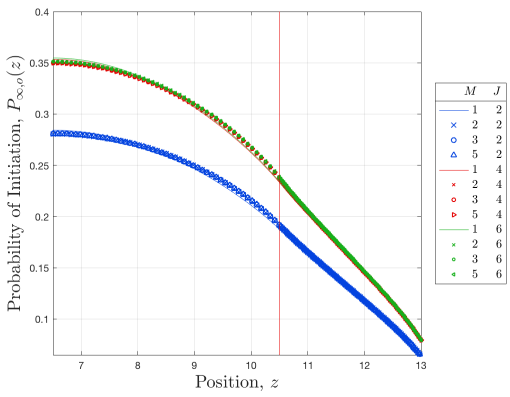

(c)

Figure 6.5: Scalar POI profiles for systems with fundamental modes of (a) $k = 1.0025$, (b) $k = 1.1567$, and (c) $k = 1.5019$, for differing M and J.

a system with increasing supercriticality, the nonlinear terms begin to become more relevant and a second-order or quadratic representation of the branching terms is insufficient. Also, we observe less of an appreciable separation between the differing M lines for a given J, but when we compare this phenomena between Fig. 6.5b and Fig. 6.5c, the relative separation between modal truncation becomes a visually noticeable feature in the $J = 6$ distribution for the $k = 1.5$ case. In the following figures, we analyze this highly supercritical system in depth to determine the number

of modes and degree of nonlinearity that must be retained in extreme cases.

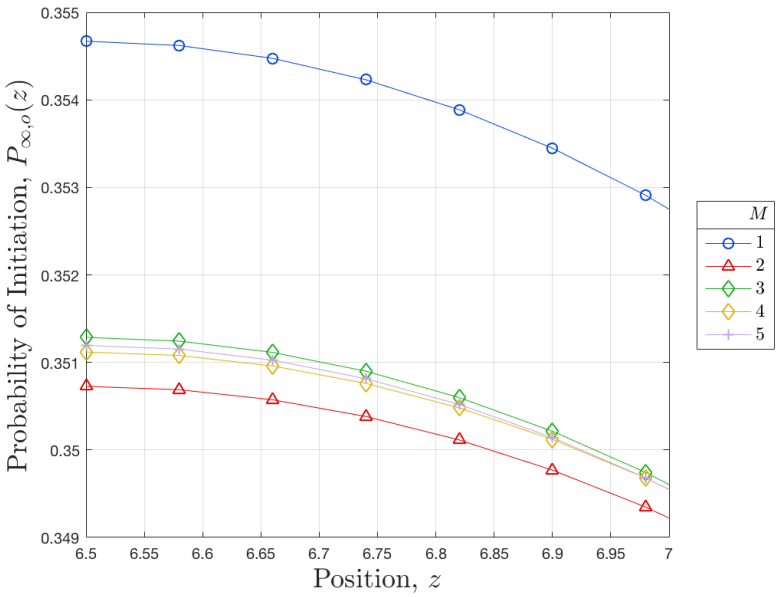

Figure 6.6: Convergence of the modes.

Figures 6.6 and 6.7 illustrates the convergence onto the true solution for varying mode truncation and nonlinearity order, respectively, for the $k_1 = 1.50$ three-region slab system. In Fig. 6.6, we hold $J = 6$ and vary M from 1 to 5 to demonstrate the convergence of the solution. It can be seen that odd M values overestimate while even M values underestimate, and if we consider $M = 5$ to be sufficiently converged, the $M = 3$ line tends toward this value. This suggests that for the most extreme case of this study, only three modes are required to represent the solution, and the distribution produced for the $M = 3$ case will give a conservative over-estimate of the solution. Considering Fig. 6.7, where we now hold $M = 3$ constant and vary J from 2 to 6, we see that the $J = 2$ and 3 lines make large jumps toward the $J = 6$ solution, and the $J = 5$ line is indiscernible from the $J = 6$ line, suggesting that a nonlinearity order of 5 is sufficient for such a calculation.

If we now vary the fundamental mode and observe the solution in the center

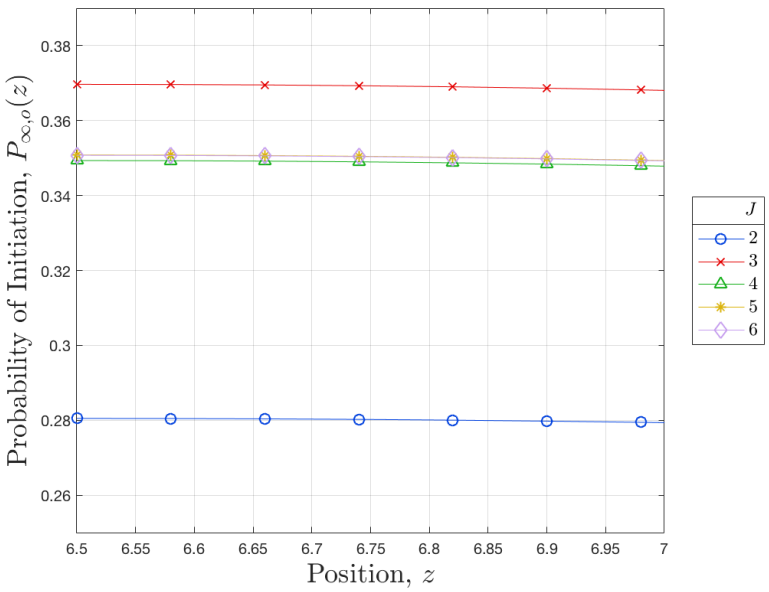

Figure 6.7: Convergence of the nonlinear terms.

of the slab ($z = 6.5\ cm$) as a function of the neutron lifetime, $\tau = 1/v\Sigma_a$, in the multiplying Pu region, it is seen in Fig. 6.8 that the approach to the POI is more abrupt for systems with higher multiplication, i.e., one may introduce a neutron into the system at times closer to the present to achieve a self-sustaining chain reaction and that associated probability tends to increase for increasing system criticality. If we concern ourselves with the number of modes required to sufficiently represent the scalar survival probability during the time-dependent regimes depicted in Fig. 6.8, for the $k_1 = 1.15$ case, we see the POI is not achieved until $\tau = 20$. Figure 6.9 depicts the spatial distribution for differing values of τ to demonstrate the necessity for increasing mode order for shorter time intervals for the $k_1 = 1.15$ system. It can be seen that for the very early introduction times shown in Fig. 6.9a, for which the scalar survival probability is relatively flat across the system, as many as 10 modes are required to roughly capture this level behavior. As the injection time occurs farther into the past, the scalar survival probability approaches the shape of the POI,

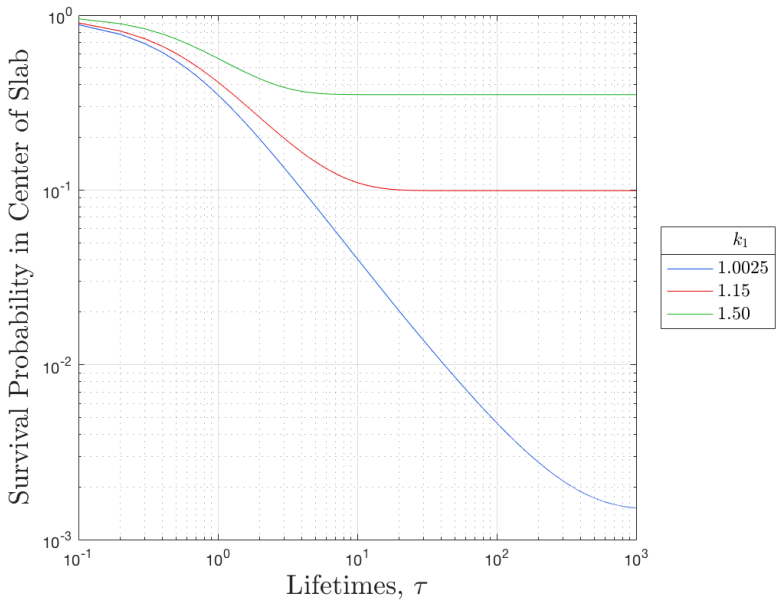

Figure 6.8: Transition of the survival probability to the POI for differing fundamental eigenvalues.

the temporal coefficients of the higher oscillatory modes decrease in magnitude, and within $\tau = 1$ in Fig. 6.9b, the maximum number of modes needed is $M = 2$ to 3.

Finally, Fig. 6.10 shows the the survival probability as a function of both spatial location and angular orientation of the initial neutron at one lifetime (6.10a) and 100 lifetimes (6.10b). The results correspond to $k_1 = 1.15$ with $M = 3$ and $J = 5$ (providing sufficient problem resolution, as seen in Figs. 6.6 and 6.7). Figure 6.8 shows that for $k_1 = 1.15$ the scalar survival probability is varying rapidly with time after 1 lifetime while it has converged to the POI well before 100 lifetimes. Although the magnitude of the angle-dependent survival probability decreases over time from a maximum of ~ 0.2 down to ~ 0.05, the overall spatial and angular shape of the solution is observed to remain unaltered. The space-angle symmetry of the solution is a direct consequence of the symmetry of the problem geometry, with the probability being zero for the neutron located at either free surface and directed along outward

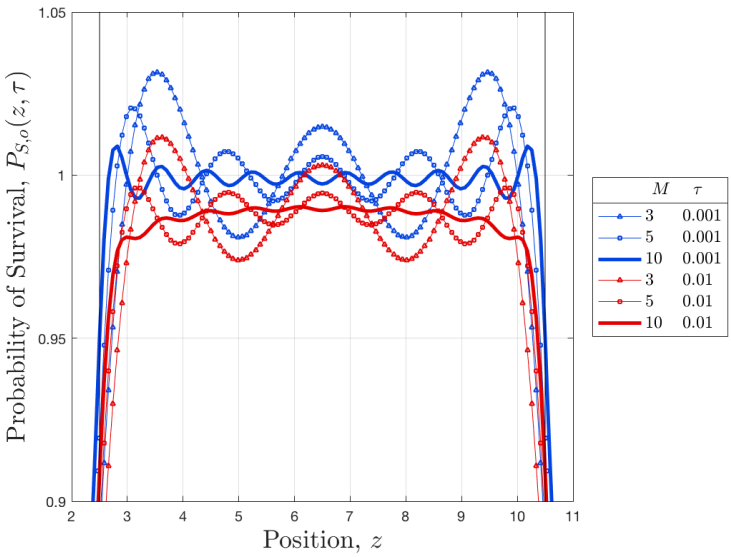

(a)

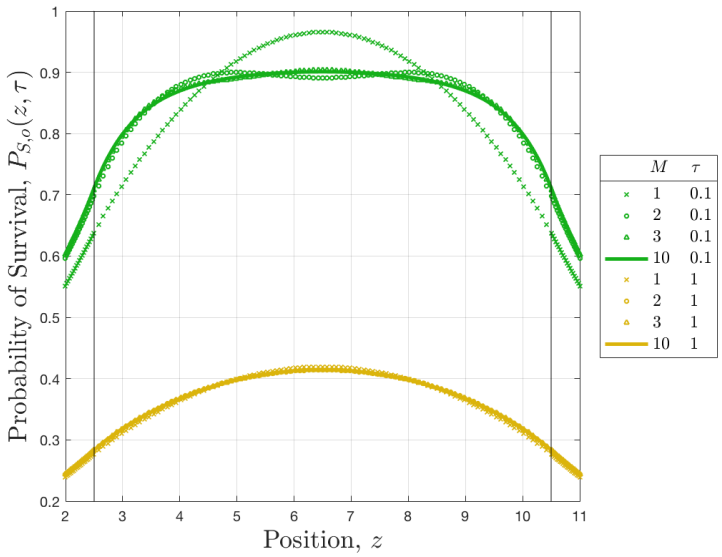

(b)

Figure 6.9: Modal convergence of the modes for early τ values of (a) $\tau = 0.001$ and 0.01 as well as (b) $\tau = 0.1$ and 1.

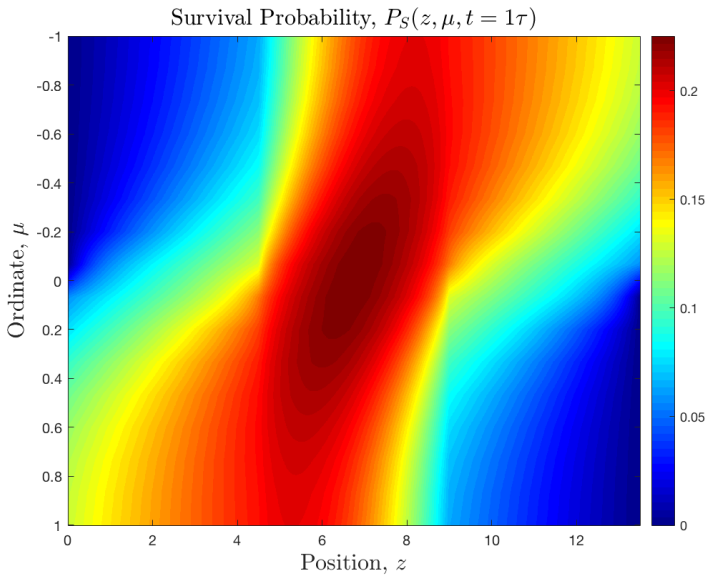

(a)

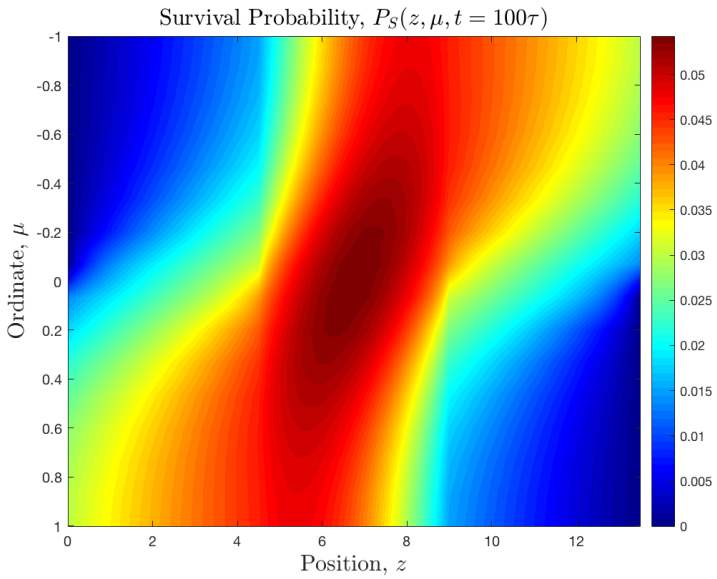

(b)

Figure 6.10: Angle-dependent survival probability after (a) 1τ, and (b) 100τ.

directions.

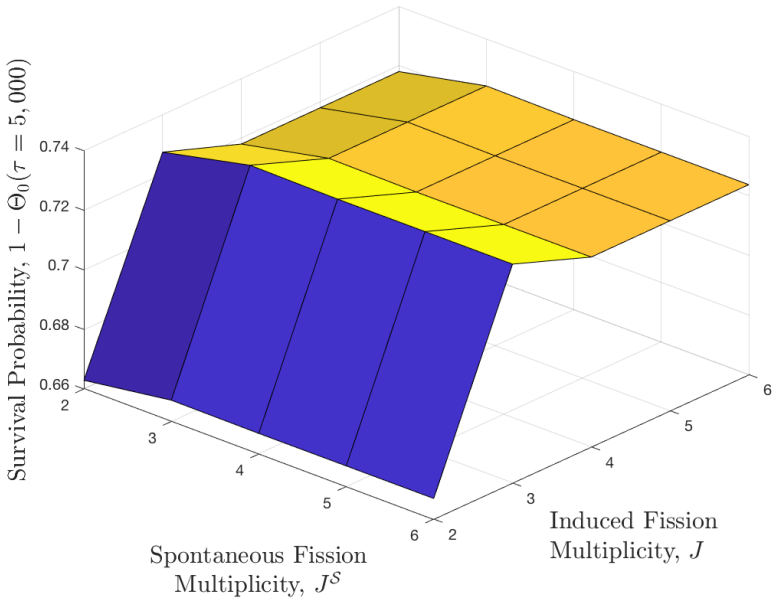

Figure 6.11: Surface plot of $\Theta_0(\tau = 5,000)$ for differing J and $J^{\mathcal{S}}$.

6.3.3 Randomly Emitting Source Results

We now consider solutions of Eq. 5.39, the neutron extinction probability in the presence of a random neutron source $\Theta_0(\tau)$, and it's complement, $1 - \Theta_0(\tau)$, for the $k_1 = 1.5$ three-region system with a constant source with magnitude $S = 2.78 \cdot 10^5$ n^0/s within the multiplying region. Then $\omega(z) = 1/(z_{I_2} - z_{I_1})$, where z_{I_1}, z_{I_2} are the first and second interface locations, respectively. Figure 6.11 shows the survival probability in the presence of a source at $5,000$ lifetimes for several combinations of nonlinearity orders corresponding to the induced fission multiplicity, J, and the source multiplicity, $J^{\mathcal{S}}$. We see the expected behavior in the solution due to increasing J, where the solution appears converged at $J = 4$, but the solution converges for a source multiplicity order of $J^{\mathcal{S}} = 3$. Finally, Fig. 6.12 shows the probability of survival for differing source strengths given by $S = 2.78 \cdot 10^x$ n^0/s where the exponent x is varied, for the $k_1 = 1.15$ system with $J = 5$ and $J^{\mathcal{S}} = 3$. As expected, the survival

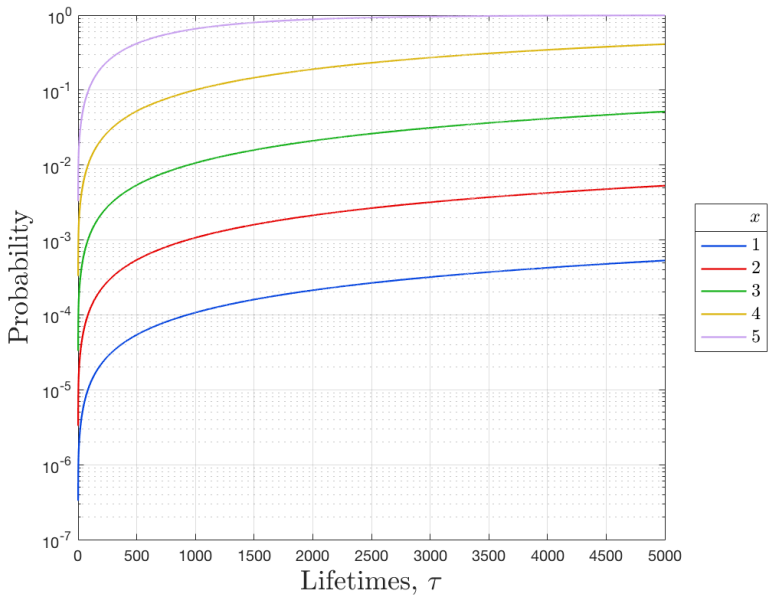

Figure 6.12: Survival probability in the presence of neutron sources of varying strength.

probability increases more rapidly with increasing source strength.

6.3.4 Numerical Performance

We now contrast the relative numerical performance of the iterative and reduced order methods described in the previous sections. Recall, the first requires repeated solution of a linear transport equation with a root finding step at each iteration while the second requires computation of the adjoint eigenspectrum up to a certain order followed by the solution of coupled first order nonlinear ODEs in time. Costs were estimated of the major parts of the computation associated with each method but only the total time of computation is contrasted. The run times reported below are averages of 50 identical calculations performed on a MacBook Pro with a 3 GHz Intel Core i7 processor using two 8 GB 1600 MHz DDR3 cores. All computations were done in MATLAB.

As the numerical results for the eigenfunction expansion method clearly demonstrate, retaining between one and three modes in the expansion yields sufficiently accurate divergence and survival (for times beyond a fraction of a neutron lifetime) probabilities. The cost of generating the spectrum can therefore be substantially reduced by employing a method that can compute modes successively, starting with the fundamental, instead of all possible modes corresponding to the dimension of the discretized problem. To this end, the Wielandt Deflation Method is a particularly efficient technique for isolating the first few eigenvalues of the generalized eigenvalue problem given by:

$$\mathbf{B}^{\dagger}\boldsymbol{\Psi}^{\dagger} = \boldsymbol{k}\boldsymbol{\Psi}^{\dagger}, \tag{6.18}$$

where $\mathbf{B}^{\dagger} = [\mathbf{T}^{\dagger} - \mathbf{S}^{\dagger}]^{-1}\mathbf{F}^{\dagger}$ and $\boldsymbol{k}$ is a diagonal matrix composed of the k-eigenvalues. The eigenspectrum is obtained by first computing the largest eigenvalue and associated eigenvector (the fundamental mode) of Eq. 6.18 using the standard Power Method and then deflating the matrix to make the second eigenvalue the dominant eigenvalue, and so on with the third and higher eigenvalues.

For the three-region symmetric slab problem considered above, with 300 spatial cells, discrete ordinate order 16, and a critical eigenvalue $k_1 = 1.15$, the cost of the eigenfunction expansion method consists of: setting up the $[\mathbf{T}^{\dagger} - \mathbf{S}^{\dagger}]$ and $\mathbf{F}^{\dagger}$ matrices, the calculation of $\mathbf{B}^{\dagger}$, the deflation calculation for the required number of eigenpairs, and the calculation of the coupled nonlinear time-coefficient ODEs defined by Eq. 6.16. The matrices $[\mathbf{T}^{\dagger} - \mathbf{S}^{\dagger}]$ and $\mathbf{F}^{\dagger}$ are $4,800 \times 4,800$ and together take an average of 13.24 *sec* to build while $\mathbf{B}^{\dagger}$ takes an average time of 4.17 *sec* to calculate. Table 6.4 shows the average computation time for the indicated number of eigenvalues via Wielandt deflation, where the absolute error tolerance applied during the Power method is set to 10^{-9} (convergence is measured in terms of the maximum norm of the difference between successive terms in the eigenvector sequence).

Table 6.5 shows the average computation times for the single-chain survival

Table 6.4: Wielandt Deflation Method computation times.

Modal Truncation Order, M	1	2	3	4	5	6	7	8	9
Eigenspectrum Computation Time [*sec*]	0.226	1.08	1.94	3.11	4.27	5.49	6.94	8.42	10.08

Table 6.5: ODE system average computation time [*sec*].

J \ M	1	2	3	4	5
2	0.55	1.22	1.97	2.83	4.04
3	0.58	1.24	2.31	3.73	6.59
4	0.68	1.43	3.01	5.80	11.78
5	0.62	1.59	3.88	8.92	21.99

probability, using MATLAB's built-in ODE solver `ode15s`, for the given number of modes, M, and varying orders of nonlinearity, J, to a final time of 100τ with 10^3 time-steps. As explained before, only the odd-indexed eigenvectors are needed for the symmetric problem geometry considered here. Thus, when calculating the set of M nonlinear coupled ODEs, the $2M-1$ largest eigenpairs are needed.

For the calculation of the survival probability using the λAM method [28], we use a convergence tolerance of 10^{-9} on the inner iterations and 10^{-5} on the outer "λ" iterations per time step for the same space, angle, and time refinement as the EEM calculations for the three-slab problem. Table 6.6 shows the average inner iteration computation times and the average total computation times for varying orders of nonlinearity. As expected, there is a slight increase in the average overall computation time for increasing J, simply because an increase in J requires an increase in the number of calculations performed per iteration and time-step. Interestingly, the inner iteration times seem to oscillate in a similar manner as the P_S distribution magnitudes do for increasing J (see Fig. 6.7). This may be due to the magnitude of the solution

Table 6.6: λAM average computation times.

J	2	3	4	5	6
Total Inner IterationTime [*sec*]	65.59	54.94	58.01	56.51	56.56
Total Time [*sec*]	171.87	175.59	178.51	180.51	183.31

for increasing J as an input to the inner iteration scheme- for a smaller magnitude solution like $J = 2$, the source iteration will take longer to converge than a larger magnitude solution like $J = 3$.

Contrasting the computational costs of the two methods, we see that for $J = 5$ and $M = 5$ (requiring the calculation of the 9 largest eigenpairs), the EEM takes an average of 49.5 *sec* while the λAM takes an average of 180.5 *sec*– about 3.6 times slower than the EEM for the particular problem considered here. If only two modes are retained in the eigenfunction expansion, which in the previous sections was shown to give the probabilities with excellent accuracy, the timing-cost of the calculation drops by another factor of two. More efficient numerical tools (including accelerating inner iterations in the λAM method with, e.g., diffusion synthetic acceleration) and using a more advanced programming language such as C++ will undoubtedly yield computational speedups for both methods, but sufficient numerical evidence has been provided to demonstrate the efficacy of the k-eigenmode expansion method for computing both the divergence and survival probabilities in a supercritical medium.

Finally, we have implemented the k-eigenmode expansion method for a homogeneous sphere and observed similar numerical performance as for the planar geometry case. The standard sphere-to-plane transformation was used to map the planar modes to spherical modes but otherwise the same software was used to compute the probabilities in spherical geometry. For nonhomogeneous spheres this simple mapping does not hold but the experience with the approach thus far suggests efficiency and accuracy of the eigenmode expansion method is unlikely to suffer when applied to

nonhomogeneous media in curvilinear geometries, provided the correct eigenspectrum is used.

Chapter 7

The Cumulative Fission Energy Deposition Distribution

The emphasis of much of the work to date has been on the neutron number distribution; however, a complete description of certain phenomena of interest also requires a knowledge of the amount of energy deposited in fissions due to the kinetic energy of the fission fragments liberated during fission events. The energy released in fission reactions is partitioned between kinetic energy of the fission fragments and the energy of particles released in fission. This energy partitioning further depends on the masses of the fission fragments and the multiplicities of the emitted particles and is therefore itself a stochastic quantity. It follows that the deposited fission energy distribution cannot be inferred directly from the distribution of neutron numbers or indeed from the distribution of fission numbers. In general, it must be obtained from an independent formulation that accounts for both the random occurrence of fission events and the random distribution of deposited energy in each fission. In this chapter, we demonstrate the application of the backward Master equation formulation in obtaining the distribution for the cumulative fission energy deposited within a system due to single neutron chains as well as in the presence of a randomly emitting

neutron source.

The energy deposited in any fission event is a random function and we define $W_\nu(\phi, \vec{r})\,\mathrm{d}\phi$ as the joint probability that ν neutrons are emitted in a fission event and an amount of fission energy in the range $(\phi, \phi + \mathrm{d}\phi)$ is deposited at the location $\vec{r}$. For the sake of generality, the fission energy deposited is allowed to be correlated with the number of neutrons liberated in any fission event. If $q_\nu^f(\vec{r})$, $\nu = 0, 1, \cdots \nu_m^f$, is the fission neutron multiplicity, we can write:

$$W_\nu(\phi, \vec{r})\,\mathrm{d}\phi = q_\nu^f(\vec{r})\,W(\phi|\nu, \vec{r})\,\mathrm{d}\phi \tag{7.1}$$

where $W(\phi|\nu, \vec{r})$ is the energy deposition distribution conditioned on ν neutrons having been emitted in the fission event. These distributions have the following normalizations:

$$\sum_{\nu=0}^{\nu_m^f} \int_0^\infty \mathrm{d}\phi\, W_\nu(\phi, \vec{r}) = 1, \tag{7.2a}$$

$$\int_0^\infty \mathrm{d}\phi\, W_\nu(\phi, \vec{r}) = q_\nu^f(\vec{r}), \tag{7.2b}$$

$$\sum_{\nu=0}^{\nu_m^f} W_\nu(\phi, \vec{r}) = W(\phi, \vec{r}), \tag{7.2c}$$

$$\sum_{\nu=0}^{\nu_m^f} q_\nu^f(\vec{r}) = 1, \tag{7.2d}$$

$$\int_0^\infty \mathrm{d}\phi\, W(\phi, \vec{r}) = 1, \tag{7.2e}$$

where $W(\phi, \vec{r})$ is the deposited energy distribution in a fission event regardless of the number of neutrons emitted. If the neutron number and deposited energy are uncorrelated, Eq. 7.1 reduces to:

$$W_\nu(\phi, \vec{r})\,\mathrm{d}\phi = q_\nu^f(\vec{r})\,W(\phi, \vec{r})\,\mathrm{d}\phi. \tag{7.3}$$

Finally, for later convenience, we introduce the multi-index notation:

$$\vec{\alpha}_k = \{\alpha_1, \alpha_2, \ldots, \alpha_k\}, \quad |\vec{\alpha}_k| = \alpha_1 + \alpha_2 + \cdots + \alpha_k, \tag{7.4}$$

where α will subsequently denote the energy deposition variable, ϕ.

7.1 Master Equations for Unlumped Systems

In this section, we formulate backward Master equations satisfied by probability density function for the total energy deposited in a system due to single neutron chains and in the presence of sources. In either case, the Master equations have strong similarities to the analogous neutron number equations of Chapters 5 and 6, but with the inclusion of the elemental stochasticity of the random amount of energy deposited due to random induced fission and spontaneous fission events. We will often refer to the cumulative fission energy deposition PDF simply as the FPDF for brevity, where the context for single chains and sources will be clear.

7.1.1 Single Chain

Following the integral backward Master equation formulation given by Bell [18] and further detailed in Chapter 5, we may write an equation for $P(\phi, \mathcal{R}, t_f|\vec{r}, \hat{\Omega}, t)$: the probability of a total of ϕ energy being deposited in $\mathcal{R}$ at a final time, t_f, due to the appearance of a single neutron at $\vec{r}$ moving in direction $\hat{\Omega}$ at an earlier time $t < t_f$. We introduce the notation $p_x(\vec{r}, t) = \Sigma_x/\Sigma_t$ for $x = \{c, s, f\}$ being the probability of event x occurring due to a collision at $\vec{r}, t$ with normalization $p_c + p_s + p_f = 1$.

Given a collision resulting in capture with probability $p_c(\vec{r}, t)$, the chain deceases and there must then be no energy deposited due to fission. In the event of a scatter event after traveling a distance s, the initial neutron will emerge with a new direction, $\hat{\Omega}'$, and we must then consider the probability $P(\phi, \mathcal{R}, t_f|\vec{r} + s\hat{\Omega}, \hat{\Omega}', t + s/v)$ for $\forall\, \hat{\Omega}'$. After traveling a distance s and inducing a fission resulting in the deposition of $\phi' \in [0, \phi_u]$ energy, where ϕ_u is the maximum fission energy deposited per fission, predicated on the emission of ν neutrons has probability $W_\nu(\phi', \vec{r} + s\hat{\Omega})$, we then need to account for the probability of the resultant ν branches each depositing $\phi_1, \phi_2, \ldots, \phi_\nu$ energies conditioned on $\phi_1 + \cdots \phi_\nu + \phi' = \phi$. With these probabilities in mind and recalling that s_b is the distance to the system boundary from the point $\vec{r}$ in direction

$\hat{\Omega}$, $s_t = v(t_f - t)$ is the distance the neutron will travel unimpeded, and $\ell(s_b, s_t)$ takes on the lesser of the two arguments, the integral Chapman-Kolmogorov equation of interest is:

$$\begin{aligned} P\left(\phi, \mathcal{R}, t_f | \vec{r}, \hat{\Omega}, t\right) = \int_0^{\ell(s_b,s_t)} \mathrm{d}s \Sigma_t \left(\vec{r} + s\hat{\Omega}, t + \frac{s}{v}\right) \mathrm{e}^{-\int_0^s \mathrm{d}s' \Sigma_t \left(\vec{r} + s'\hat{\Omega}, t + \frac{s'}{v}\right)} \Bigg[\\ p_c\left(\vec{r} + s\hat{\Omega}, t + \frac{s}{v}\right) \delta(\phi) \\ + p_s\left(\vec{r} + s\hat{\Omega}, t + \frac{s}{v}\right) \int_{4\pi} \frac{\mathrm{d}\Omega'}{4\pi} P\left(\phi, \mathcal{R}, t_f | \vec{r} + s\hat{\Omega}, \hat{\Omega}', t + \frac{s}{v}\right) \\ + p_f\left(\vec{r} + s\hat{\Omega}, t + \frac{s}{v}\right) \Bigg\{ W_0(\phi, \vec{r} + s\hat{\Omega}) \mathbb{H}(\phi_u - \phi) + \sum_{\nu=1}^{\nu_m^f} \int_0^{\ell(\phi_u,\phi)} \mathrm{d}\phi' W_\nu(\phi', \vec{r} + s\hat{\Omega}) \Bigg[\\ \int_{|\vec{\phi}_\nu| = \phi - \phi'} \mathrm{d}^\nu \phi \prod_{k=1}^{\nu} \int_{4\pi} \frac{\mathrm{d}\Omega'}{4\pi} P\left(\phi_k, \mathcal{R}, t_f | \vec{r} + s\hat{\Omega}, \hat{\Omega}', t + \frac{s}{v}\right) \Bigg] \Bigg\} \Bigg] + \sum_{j=1}^{3} A_j, \end{aligned} \tag{7.5}$$

where $\mathbb{H}$ is the Heaviside function and $|\vec{\phi}_\nu| = \sum_{i=1}^{\nu} \phi_i$ is the combination of energy deposited by each of the ν branches of the first fission event that satisfies the condition $\phi - \phi' = |\vec{\phi}_\nu|$. The A_j terms are:

$$A_1 = \delta(\phi) A_1' = \delta(\phi) \mathbb{H}\left(s_t - s_b\right) \exp\left\{ - \int_0^{s_b} \mathrm{d}s' \Sigma_t \left(\vec{r} + s'\hat{\Omega}, t + \frac{s'}{v}\right) \right\} \tag{7.6a}$$

$$A_2 = \delta(\phi) A_2' = \delta(\phi) \mathbb{H}\left(s_b - s_t\right) \Big|_{(\vec{r} + s_t\hat{\Omega}, \hat{\Omega}) \notin \mathcal{R}} \exp\left\{ - \int_0^{s_t} \mathrm{d}s' \Sigma_t \left(\vec{r} + s'\hat{\Omega}, t + \frac{s'}{v}\right) \right\} \tag{7.6b}$$

$$A_3 = \delta(\phi) A_3' = \delta(\phi) \mathbb{H}\left(s_b - s_t\right) \Big|_{(\vec{r} + s_t\hat{\Omega}, \hat{\Omega}) \in \mathcal{R}} \exp\left\{ - \int_0^{s_t} \mathrm{d}s' \Sigma_t \left(\vec{r} + s'\hat{\Omega}, t + \frac{s'}{v}\right) \right\}, \tag{7.6c}$$

where A_1 is the probability that the initial neutron streamed out of the system, A_2 is the probability that the neutron has not collided but it is not in $\mathcal{R}$, and A_3 is the

probability that the neutron has not collided but it is in $\mathcal{R}$. The terminal condition for the single chain is

$$\lim_{t_f \leftarrow t} P\left(\phi, \mathcal{R}, t_f | \vec{r}, \hat{\Omega}, t\right) = \delta(\phi)\, \mathcal{I}_{\mathcal{R}}\left(\vec{r}, \hat{\Omega}\right) \tag{7.7}$$

and the boundary condition is

$$P\left(\phi, \mathcal{R}, t_f | \vec{r}, \hat{\Omega}, t\right) = \delta(\phi) \quad \text{for } \vec{r} \in \partial V, \text{ and } \hat{n}_b \cdot \hat{\Omega} > 0, \tag{7.8}$$

where $\mathcal{I}_{\mathcal{R}}(\vec{r}, \hat{\Omega})$ is the indicator function that is unity for $(\vec{r}, \hat{\Omega}) \in \mathcal{R}$ and zero otherwise and $\hat{n}_b$ is the surface unit normal vector. Equation 7.7 can be easily verified by taking the limit of $t_f \leftarrow t$, in which case $s_t \rightarrow 0$, causing the foremost integral of Eq. 7.5 to vanish because $\ell(s_b, s_t) = s_t = 0$. In the limit, A_1 will also vanish due to the argument of $\mathbb{H}$ being negative, while $A_2 = \delta(\phi)$ or 0 and $A_3 = \delta(\phi)$ or 0 depending on whether or not $(\vec{r}, \hat{\Omega}) \in \mathcal{R}$, respectively.

Further analysis of the problem is facilitated by transforming the equation for the PDF to one for the moment generating function (MGF), defined as:

$$G(\lambda, \mathcal{R}, t_f | \vec{r}, \hat{\Omega}, t) = \int_0^\infty \mathrm{d}\phi\, \mathrm{e}^{-\lambda\phi}\, P(\phi, \mathcal{R}, t_f | \vec{r}, \hat{\Omega}, t), \tag{7.9}$$

which is equivocally the Laplace transform with respect to the deposited energy variable. From the normalization of the FPDF we have $G(\lambda = 0, \mathcal{R}, t_f | \vec{r}, \hat{\Omega}, t) = 1$. Laplace transforming Eq. 7.5 then yields

$$\begin{aligned} G\left(\lambda, \mathcal{R}, t_f | \vec{r}, \hat{\Omega}, t\right) = \int_0^{\ell(s_b, s_t)} \mathrm{d}s \Sigma_t \left(\vec{r} + s\hat{\Omega}, t + \frac{s}{v}\right) \mathrm{e}^{-\int_0^s \mathrm{d}s' \Sigma_t \left(\vec{r} + s'\hat{\Omega}, t + \frac{s'}{v}\right)} \Bigg[\\ p_c\left(\vec{r} + s\hat{\Omega}, t + \frac{s}{v}\right) + p_s\left(\vec{r} + s\hat{\Omega}, t + \frac{s}{v}\right) \int_{4\pi} \frac{\mathrm{d}\Omega'}{4\pi} G\left(\lambda, \mathcal{R}, t_f | \vec{r} + s\hat{\Omega}, \hat{\Omega}', t + \frac{s}{v}\right) \\ + p_f\left(\vec{r} + s\hat{\Omega}, t + \frac{s}{v}\right) \sum_{\nu=0}^{\nu_m^f} \overline{W}_\nu\left(\lambda, \vec{r} + s\hat{\Omega}\right) \left[\int_{4\pi} \frac{\mathrm{d}\Omega'}{4\pi} G(\lambda, \mathcal{R}, t_f | \vec{r}, \hat{\Omega}', t)\right]^\nu \Bigg] + \sum_{j=1}^{3} A'_j, \end{aligned} \tag{7.10}$$

where the Laplace transform for the fission energy deposition distribution is

$$\overline{W}_\nu(\lambda, \vec{r}) = \int_0^\infty \mathrm{d}\phi\, \mathrm{e}^{-\lambda\phi} W_\nu(\phi, \vec{r}). \tag{7.11}$$

Next, by evaluating Eq. 7.10 at a short distance away from the original injection location, δs, the only difference between such an equation and Eq. 7.10 will be the lower limits of the distance traveled integrals will change from 0 to δs. Following the manipulations from Chapter 5, we obtain a nonlinear inhomogeneous adjoint transport equation:

$$\begin{aligned}\left[-\frac{1}{v}\frac{\partial}{\partial t}-\hat{\Omega}\cdot\vec{\nabla}+\Sigma_t\left(\vec{r},t\right)\right]G\Big(\lambda,\mathcal{R},t_f|\vec{r},\hat{\Omega},t\Big)&=\Sigma_c\left(\vec{r},t\right)\\&+\Sigma_s\left(\vec{r},t\right)\int_{4\pi}\frac{\mathrm{d}\Omega'}{4\pi}G\left(\lambda,\mathcal{R},t_f|\vec{r},\hat{\Omega}',t\Big)\right.\\&+\Sigma_f\left(\vec{r},t\right)\sum_{\nu=0}^{\nu_m^f}\overline{W}_\nu(\lambda,\vec{r}\,)\left[\int_{4\pi}\frac{\mathrm{d}\Omega'}{4\pi}G\left(\lambda,\mathcal{R},t_f|\vec{r},\hat{\Omega}',t\Big)\right.\right]^\nu\end{aligned}\tag{7.12}$$

with the terminal and boundary conditions:

$$\lim_{t_f\leftarrow t}G\left(\lambda,\mathcal{R},t_f|\vec{r},\hat{\Omega},t\Big)=\mathcal{I}_{\mathcal{R}}\left(\vec{r},\hat{\Omega}\right),\tag{7.13a}$$

$$G\left(\lambda,\mathcal{R},t_f|\vec{r},\hat{\Omega},t\Big)=1,\quad\vec{r}\in\partial V,\,\hat{n}_b\cdot\hat{\Omega}>0.\tag{7.13b}$$

In the event that the deposited energy distribution in a single fission event is independent of the neutron multiplicity we have $\overline{W}_\nu(\lambda,\vec{r}\,)=q_\nu^f(\vec{r}\,)\,\overline{W}(\lambda,\vec{r}\,)$. In the next section, the backward Master equation for the FPDF in the presence of a source is derived.

7.1.2 With a Random Source

Consider a system with no initial neutrons with an intrinsic isotropically-emitting neutron source of strength $\mathcal{S}(\vec{r},t_o)=\omega(\vec{r})S(t_o)$, where $\omega(\vec{r}\,)$ is normalized such that $\int_V\mathrm{d}\vec{r}\omega(\vec{r}\,)=1$. The probability of a total of ϕ energy being deposited within the system at time t_f due to the "turning on" of the source at some earlier time $t_o\leq t_f$ is $Q(\phi,t_f|t_o)$. There is no particle streaming requirement as there are no initial neutrons within the system.

A probability balance in the first time interval proceeding the introduction time $t_o + \Delta t_o$ may be conducted. The probability of a source event occurring somewhere in the system in the first collision interval is $\Delta t_o \int_V \mathrm{d}\vec{r}\mathcal{S}(\vec{r}, t_o) = \Delta t_o S(t_o)$. The probability that no source event occurs, $(1 - \Delta t_o S(t_o))$, must then be multiplied by the probability that subsequent source events occur in the time interval $[t_o + \Delta t_o, t_f]$ resulting in ϕ energy being deposited at t_f, $Q(\phi, t_f | t_o + \Delta t_o)$. Alternatively, a source event does occur in the first interval at point $\vec{r}$, depositing ϕ' energy conditioned on the emission of ν neutrons with probability $W_\nu^S(\phi', \vec{r})$. In the remaining time interval, $[t_o + \Delta t_o, t_f]$, each of the ν branches will propagate and deposit $\phi_1, \phi_2, \ldots, \phi_\nu$ energies with probabilities $P(\phi_k, \cdots)$ and subsequent source events must then deposit $\phi_{\nu+1}$ energy such that $|\vec{\phi}_{\nu+1}| = \sum_{i=1}^{\nu+1} \phi_i = \phi - \phi'$ is satisfied. The probability balance is therefore

$$\begin{aligned} Q(\phi, t_f | t_o) = & \left(1 - \Delta t_o \int_V \mathrm{d}\vec{r}\mathcal{S}(\vec{r}, t_o)\right) Q(\phi, t_f | t_o + \Delta t_o) \\ & + \Delta t_o \sum_{\nu=0}^{\nu_m^S} \int_V \mathrm{d}\vec{r}\mathcal{S}(\vec{r}, t_o) \int_0^{\ell(\phi_u, \phi)} \mathrm{d}\phi' W_\nu^S(\phi', \vec{r}) \int\limits_{\left|\vec{\phi}_{\nu+1}\right| = \phi - \phi'} \mathrm{d}^{\nu+1}\phi \Bigg\{ \\ & Q(\phi_{\nu+1}, t_f | t_o + \Delta t_o) \prod_{k=1}^{\nu} \int_{4\pi} \frac{\mathrm{d}\Omega'}{4\pi} P\left(\phi_k, \mathcal{R}, t_f | \vec{r}, \hat{\Omega}', t_o + \Delta t_o\right) \Bigg\}. \end{aligned} \tag{7.14}$$

Rearranging Eq. 7.14 and taking the limit $\Delta t_o \to 0$, we obtain the backward Master equation for a system with a spatially distributed isotropically emitting neutron source:

$$\begin{aligned} -\frac{\partial Q(\phi, t_f | t_o)}{\partial t_o} = & -S(t_o) Q(\phi, t_f | t_o) + S(t_o) \sum_{\nu=0}^{\nu_m^S} \int_V \mathrm{d}\vec{r}\omega(\vec{r}) \int_0^{\ell(\phi_u, \phi)} \mathrm{d}\phi' W_\nu^S(\phi', \vec{r}) \Bigg\{ \\ & \int\limits_{\left|\vec{\phi}_{\nu+1}\right| = \phi - \phi'} \mathrm{d}^{\nu+1}\phi\, Q(\phi_{\nu+1}, t_f | t_o) \prod_{k=1}^{\nu} \int_{4\pi} \frac{\mathrm{d}\Omega'}{4\pi} P\left(\phi_k, \mathcal{R}, t_f | \vec{r}, \hat{\Omega}', t_o\right) \Bigg\}, \end{aligned} \tag{7.15}$$

with final condition:

$$\lim_{t_f \leftarrow t_o} Q(\phi, t_f|t_o) = \delta(\phi). \tag{7.16}$$

Equation 7.15 is linearly coupled in the number distribution in the presence of a source and is nonlinearly dependent on the number distribution for a single chain. By now applying the MGF for the source,

$$H(\lambda, t_f|t_o) = \int_0^\infty \mathrm{d}\phi\, \mathrm{e}^{-\lambda\phi} Q(\phi, t_f|t_o), \tag{7.17}$$

the Master equation given by Eq. 7.15 is transformed accordingly

$$\frac{\partial H}{\partial t_o} = S(t_o)\left\{1 - \sum_{\nu=0}^{\nu_m^S} \int_V \mathrm{d}\vec{r}\omega(\vec{r})\overline{W_\nu^S}(\lambda, \vec{r}) \left[\int_{4\pi} \frac{\mathrm{d}\Omega}{4\pi} G\left(\lambda, \mathcal{R}, t_f|\vec{r}, \hat{\Omega}, t_o\right)\right]^\nu\right\} H(\lambda, t_f|t_o) \tag{7.18}$$

with final condition:

$$\lim_{t_f \leftarrow t_o} H(\lambda, t_f|t_o) = 1. \tag{7.19}$$

Note that $\overline{W_\nu^S}$ is defined by Eq. 7.11, where we simply replace W_ν with W_ν^S. We can easily solve Eq. 7.18 to yield

$$H(\lambda, t_f|t_o) = \exp\left\{\int_{t_f}^{t_o} \mathrm{d}t_o S(t_o)\left[1 - \sum_{\nu=0}^{\nu_m^S} \int_V \mathrm{d}\vec{r}\omega(\vec{r})\overline{W_\nu^S}(\lambda, \vec{r}\,)\left[G_o\left(\lambda, \mathcal{R}, t_f|\vec{r}, t_o\right)\right]^\nu\right]\right\} \tag{7.20}$$

where $G_o = \int_{4\pi} \mathrm{d}\Omega G(\hat{\Omega})/4\pi$. Next, we derive equations for the moments of the respective FPDFs.

7.1.3 Moment Equations

While the Master equation or the equation for the MGF are complex and difficult to analyze without approximation, the statistical moments of the FPDF satisfy standard

linear transport equations that can be solved using standard numerical techniques. These moments are related to the MGF through the following readily verified identity:

$$\left.\frac{\partial^k G(\lambda,\mathcal{R},t_f|\vec{r},\hat{\Omega},t)}{\partial\lambda^k}\right|_{\lambda=0} = (-1)^k \int_0^\infty \mathrm{d}\phi\, \phi^k \mathrm{e}^{-\lambda\phi} P(\phi,\mathcal{R},t_f|\vec{r},\hat{\Omega},t)\Big|_{\lambda=0} \equiv (-1)^k\, \overline{\phi^k}(\mathcal{R},t_f|\vec{r},\hat{\Omega},t), \tag{7.21}$$

and similarly for H to find the k^{th} FPDF moment due to a source: $\overline{\phi_S^k}(t_f|t_o)$. Applying Eq. 7.21 to the single chain MGF equation, Eq. 7.12, yields

$$\begin{aligned}\Big[-\frac{1}{v}\frac{\partial}{\partial t} - \hat{\Omega}\cdot\vec{\nabla} + \Sigma_t\Big]\overline{\phi^k}(\mathcal{R},t_f|\vec{r},\hat{\Omega},t) &= \Sigma_s \int_{4\pi}\frac{\mathrm{d}\Omega'}{4\pi}\,\overline{\phi^k}(\mathcal{R},t_f|\vec{r},\hat{\Omega}',t) \\ &+ \overline{\nu}\Sigma_f \int_{4\pi}\frac{\mathrm{d}\Omega'}{4\pi}\,\overline{\phi^k}(\mathcal{R},t|\vec{r},\hat{\Omega}',t) + \mathcal{S}_k\left(\vec{r},t;\,\overline{\phi},\ldots,\overline{\phi^{k-1}}\right),\end{aligned} \tag{7.22}$$

with:

$$\lim_{t_f\leftarrow t}\overline{\phi^k}(\mathcal{R},t_f|\vec{r},\hat{\Omega},t) = 0, \tag{7.23a}$$

$$\overline{\phi^k}(\mathcal{R},t_f|\vec{r},\hat{\Omega},t) = 0, \quad \vec{r}\in\partial V,\ \hat{n}_b\cdot\hat{\Omega} > 0. \tag{7.23b}$$

In the above, $\mathcal{S}_k(\cdots)$ is an inhomogeneous source term in the k^{th} moment equation that depends only on the lower moments and hence considered known. When the coupling between the amount of energy deposited in a single fission and the number of fission neutrons emitted can be ignored so that Eq. 7.3 holds, the inhomogeneous terms for varying $k = 1$ are given in Table 7.1. Note $\langle\cdot\rangle$ indicates integration over angle (as well as energy if there were an energy dependence) and $\overline{E_f^k}$ is the k^{th} moment of the fission energy deposition distribution:

$$\overline{E_f^k}(\vec{r}) = \left.\frac{\partial^k \overline{W}(\lambda,\vec{r})}{\partial\lambda^k}\right|_{\lambda=0}, \tag{7.24}$$

where we specify that we have assumed Eq. 7.3 holds and we note that $\overline{E_f^1} = E_f$. From the source terms, it is clear that we must solve the system of transport equations in ascending k up to the desired order. We observe that the moment equations are

Table 7.1: Inhomogeneous source terms for the single chain moment equations of the FPDF.

k	$\mathcal{S}_k(\vec{r},t;\overline{\phi},\ldots,\overline{\phi^{k-1}})$
1	$\Sigma_f(\vec{r},t)E_f$
2	$\Sigma_f(\vec{r},t)\left[\overline{E_f^2}+2\overline{\nu}E_f\left\langle\overline{\phi}\right\rangle+\overline{(\nu)}_2\left\langle\overline{\phi}\right\rangle^2\right]$
3	$\Sigma_f(\vec{r},t)\left[\overline{E_f^3}+3\overline{\nu}\left(\left\langle\overline{\phi^2}\right\rangle E_f+\left\langle\overline{\phi}\right\rangle\overline{E_f^2}\right)+3\overline{(\nu)}_2\left(\left\langle\overline{\phi}\right\rangle^2E_f+\left\langle\overline{\phi}\right\rangle\left\langle\overline{\phi^2}\right\rangle\right)+\overline{(\nu)}_3\left\langle\overline{\phi}\right\rangle^3\right]$
4	$\Sigma_f(\vec{r},t)\Bigg[\overline{E_f^4}+4\overline{\nu}\left(\left\langle\overline{\phi^3}\right\rangle E_f+\frac{3}{2}\left\langle\overline{\phi^2}\right\rangle\overline{E_f^2}+\left\langle\overline{\phi}\right\rangle\overline{E_f^3}\right)$ $+4\overline{(\nu)}_2\left(3\left\langle\overline{\phi}\right\rangle\left\langle\overline{\phi^2}\right\rangle E_f+\frac{3}{2}\left\langle\overline{\phi}\right\rangle^2\overline{E_f^2}+\frac{3}{4}\left\langle\overline{\phi^2}\right\rangle^2+\left\langle\overline{\phi}\right\rangle\left\langle\overline{\phi^3}\right\rangle\right)$ $+4\overline{(\nu)}_3\left(\left\langle\overline{\phi}\right\rangle^3E_f+\frac{3}{2}\left\langle\overline{\phi}\right\rangle^2\left\langle\overline{\phi^2}\right\rangle\right)+\overline{(\nu)}_4\left\langle\overline{\phi}\right\rangle^4\Bigg]$

simply time-dependent, inhomogeneous, linear adjoint transport equations that can be numerically solved using standard discretization methods, as is shown in the next section.

In the presence of a constant randomly *singlet-emitting* neutron source, the corresponding MGF equation, Eq. 7.18, simplifies to:

$$-\frac{\partial H(\lambda,t_f|t)}{\partial t}=-SH+SH\int_V \mathrm{d}\vec{r}\omega(\vec{r})\overline{W}_S(\lambda,\vec{r})G_o(\lambda,\mathcal{R},t_f|\vec{r},t), \tag{7.25}$$

with final condition $\lim_{t_f\leftarrow t}H(\lambda,t_f|t)=1$ and $G_o=\int_{4\pi}\mathrm{d}\Omega G(\hat{\Omega})/4\pi$. Applying the moment identity, the moments of the FPDF in the presence of a source, $\overline{\phi_S^n}(t_f|t)$ may be determined:

$$-\frac{\partial\overline{\phi_S^k}(t_f|t_o)}{\partial t_o}=S\mathcal{Q}_k\left(t_f|t_o,\overline{\phi}_S,\ldots,\overline{\phi_S^{k-1}},\overline{\phi},\ldots,\overline{\phi^k}\right), \tag{7.26}$$

with the terminal conditions being $\overline{\phi_S^k}(t_f|t_f)=0$ and $\mathcal{Q}_k$ are inhomogeneous source terms that are functions of all lower order $\overline{\phi}_S$ moments and all single chain moments up to order k. These source terms are defined for the first four moments in Table 7.2.

Table 7.2: Inhomogeneous source terms for the moment equations of the FPDF in the presence of a source.

k	$\mathcal{Q}_k(t_f\|t_o,\overline{\phi}_S,\ldots,\overline{\phi_S^{k-1}},\overline{\phi},\ldots,\overline{\phi^k})$
1	$\left\langle \omega(\vec{r}),\overline{\phi}(\mathcal{R},t_f\|\vec{r},t_o)+\overline{E}_S(\vec{r})\right\rangle$
2	$\left\langle \omega(\vec{r}),\overline{E_S^2}+2\overline{E}_S\left(\overline{\phi}+\overline{\phi}_S\right)+\overline{\phi^2}+2\overline{\phi}\,\overline{\phi}_S\right\rangle$
3	$\left\langle \omega(\vec{r}),\overline{E_S^3}+3\overline{E_S^2}\left(\overline{\phi}+\overline{\phi}_S\right)+3\overline{E}_S\left(\overline{\phi^2}+2\overline{\phi}\,\overline{\phi}_S+\overline{\phi_S^2}\right)\right.$ $\left.+\,\overline{\phi^3}+3\overline{\phi^2}\,\overline{\phi}_S+3\overline{\phi}\,\overline{\phi_S^2}\right\rangle$
4	$\left\langle \omega(\vec{r}),\overline{E_S^4}+4\overline{E_S^3}\left(\overline{\phi}+\overline{\phi}_S\right)+6\overline{E_S^2}\left(\overline{\phi^2}+2\overline{\phi}\,\overline{\phi}_S+\overline{\phi_S^2}\right)\right.$ $+\,4\overline{E}_S\left(\overline{\phi^3}+3\overline{\phi^2}\,\overline{\phi}_S+3\overline{\phi}\,\overline{\phi_S^2}+\overline{\phi_S^3}\right)$ $\left.+\,\overline{\phi^4}+4\overline{\phi^3}\,\overline{\phi}_S+6\overline{\phi^2}\,\overline{\phi_S^2}+4\overline{\phi}\,\overline{\phi_S^3}\right\rangle$

This elementary ODE has the solution:

$$\overline{\phi_S^k}(t_f|t_o)=\int_{t_o}^{t_f}\mathrm{d}t'S(t')\mathcal{Q}_k\left(t_f|t',\overline{\phi}_S,\ldots,\overline{\phi_S^{k-1}},\overline{\phi},\ldots,\overline{\phi^k}\right). \tag{7.27}$$

We make a few precautionary notes regarding Table 7.2: $\langle\cdot,\cdot\rangle$ is the inner product over the entire spatial domain of interest; $\overline{\phi^k}$ for the single chain is pre-angle-integrated; $\overline{\phi_S^k}$ are not themselves functions of space and the spatial integrals do not operate on those terms. Finally, we note that the subscript S for $\overline{E_S^k}$ denotes the k^{th} moment of the source fission energy deposition distribution which, in general, differs from the induced fission deposition distribution but is appropriately defined by Eq. 7.24 using $\overline{W}_S$.

A final note concerns the moments of the fission energy deposition spectrum, $\overline{E_f^n}$ and $\overline{E_S^n}$. To obtain explicit expressions for the moments from the distributions we have considered in this document, we may insert the desired $W(\phi)$ into

$$\overline{W}(\lambda)=\int_0^\infty \mathrm{d}\phi\,\mathrm{e}^{-\lambda\phi}W(\phi),$$

Table 7.3: Moments of $W(\phi)$ for different types of distributions. Note that c_n of the truncated Gaussian distribution is given by Eq. 7.28.

Distribution	$\overline{E_f^n}$
Gamma	$2^{-n}(n+1)!E_f^n$
Beta	$\phi_u^n \frac{B(n+\alpha,\beta)}{B(\alpha,\beta)}$
Truncated Gaussian	$c_n \left\{ \sqrt{2}\frac{\overline{\phi}_p}{\sigma_p}\Gamma\left(\frac{n+2}{2}\right) {}_1F_1\left(\frac{1-n}{2};\frac{3}{2};-\frac{\overline{\phi}_p^2}{2\sigma_p^2}\right) + \Gamma\left(\frac{n+1}{2}\right) {}_1F_1\left(-\frac{n}{2};\frac{1}{2};-\frac{\overline{\phi}_p^2}{2\sigma_p^2}\right) \right\}$

take n successive derivatives with respect to λ and evaluate at $\lambda = 0$. Expressions for $\overline{E_f^n}$ are displayed in Table 7.3 for several distributions that we will investigate in greater depth later in this chapter (for details on notation, the reader is referred to Sec. 7.4). Note that we have defined the truncated Gaussian coefficient to be

$$c_n = \frac{2^{\frac{n}{2}-1}\sigma_p^n}{\sqrt{\pi}\left(\Omega(a) - \Omega(b)\right)}, \tag{7.28}$$

and ${}_1F_1(\cdots)$ is Kummer's confluent hypergeometric function (also referred to as the confluent hypergeometric function of the first kind).

7.2 Numerical Results for the Moments

We consider monoenergetic neutrons in a one-dimensional sphere in vacuum, and we wish to determine the moments of the FPDF by means of the deterministic method as well as Monte Carlo simulation. We describe the solution process for both methods and show that they agree with one another in Sec. 7.2.1 and then show deterministically-derived results for the moments in multi-layered spheres in Sec. 7.2.2 and the effects of differing the fission energy deposition distribution, $W(\phi)$, on the moments in Sec. 7.2.3.

7.2.1 Benchmarking with EBMC

In this section, we demonstrate the efficacy of the deterministic solution process by benchmarking it with EBMC strictly for single neutron chains. For the deterministic approach, we must solve the linear inhomogeneous one-dimensional spherical geometry transport equations; for the k^{th} moment of the single chain FPDF, we have

$$\begin{aligned}\left[-\frac{1}{v}\frac{\partial}{\partial t}-\frac{\mu}{r^2}\frac{\partial}{\partial r}\left(r^2\right)-\frac{1}{r}\frac{\partial}{\partial \mu}\left[\left(1-\mu^2\right)\right]+\Sigma_t(r)\right]\overline{\phi^k}(\mathcal{R},t_f|r,\mu,t)= \\ +\frac{1}{2}\left[\Sigma_s(r)+\overline{\nu}\Sigma_f(r)\right]\int_{-1}^{1}\mathrm{d}\mu'\overline{\phi^k}(\mathcal{R},t_f|r,\mu',t) \\ +\mathcal{S}_k(r,t;\overline{\phi},\ldots,\overline{\phi^{k-1}}),\end{aligned} \tag{7.29}$$

where r is the radial coordinate and μ is the direction cosine with respect to r. We have assumed neutrons isotropically scatter and the $\mathcal{S}_k$ source terms are found in Table 7.1. We numerically solve Eq. 7.29 using a standard discrete ordinates in angle, diamond difference in space discretization with source-iteration convergence to then advance the solution using the Crank-Nicolson time-stepping method [35, 51].

In order to simulate such systems with the Event-Based Monte Carlo method, patently, we must initiate our MC simulations at the discrete mesh point values for r and μ that the deterministic numerical transport solution resides upon. If we call the i^{th} spatial point r_i and the n^{th} ordinate μ_n, then we may designate a specific injection location, $r_{i,o}$, as well as an injection direction, $\mu_{n,o}$, at the initiating time, t_o. With these initial phase space coordinates, we then perform random walks to attain the moments using the batching statistics method, discussed in Sec. 3.2, to find $\overline{\phi^k}_{MC}(\mathcal{R},t_f|r_{i,o},\mu_{n,o},t_o)$. If we wish to compare with the scalar (angle-integrated) deterministic solution, we then run the MC code for each $\mu_{n,o}$ at the given $r_{i,o}$ for as many batches and histories per batch that are required to attain statistically quiet results. Clearly, if we wish to have a one-to-one comparison, the MC method is far more computationally expensive, and will require a *minimum* number of calculations of $C_{min}=2BHIN$, where B and H are the number of batches and histories per

Table 7.4: Fast neutron data used for a ^{239}Pu system.

$N\ \left[\frac{1}{b \cdot cm}\right]$	$\sigma_c\ [\mu b]$	$\sigma_s\ [b]$	$\sigma_f\ [b]$	$v \cdot 10^{-9}\ \left[\frac{cm}{s}\right]$
0.04998	847.4	2.944	2.334	5.1753

batch, respectively, and I and N are the number of spatial cells and ordinates used in the deterministic solution process. The coefficient of 2 comes from the initial neutron distance to collision calculation, $r' = \Sigma_t^{-1} \ln(\xi)$, where ξ is a random number, and then updating the new radial position, $r'' = \sqrt{(r_{i,o})^2 + (r')^2 + 2r_{i,o}r'\mu_{n,o}}$, which can then be used to determine if the neutron is still in the system. Alternatively, one could calculate the updated system time, $t_s = s_o + r'/v$, to determine if the collision occurred before or after the final time; regardless, the other calculation will have to be made if the particle did not leak or stream too long, but this is not the case in every simulation. The angle integrations are performed using Gauss-Legendre quadrature to find:

$$\overline{\phi^k}_{MC}(\mathcal{R}, t|r_{i,o}, t_o) = \sum_{n=1}^{N} w_n \overline{\phi^k}_{MC}(\mathcal{R}, t|r_{i,o}, \mu_{n,o}, t_o), \tag{7.30}$$

where w_n are the quadrature weights.

We show a comparison between the Monte Carlo and deterministic solution methods for a single initiating neutron in Fig. 7.1, where we have also solved the neutron population moment equations, found in [43] and Sec. 5.2, for contrast. The system depicted is a 3.9339 cm ball of ^{239}Pu ran to $t_f = \tau = 1.6558\ ns$ using the one-group 14 MeV neutron data in Table 7.4, calculated from `JENDL`-4.0 at 300 K. We have set $W(\phi)$ to a gamma distribution with $E_f = 180\ MeV$, and the higher order moments, $\overline{E_f^n}$, in the inhomogenous source terms may be determined by the formulae in Table 7.3. The determinstic solution is obtained for an S_8-order discrete ordinates discretization with 50 mesh points and 100 time steps. As we described

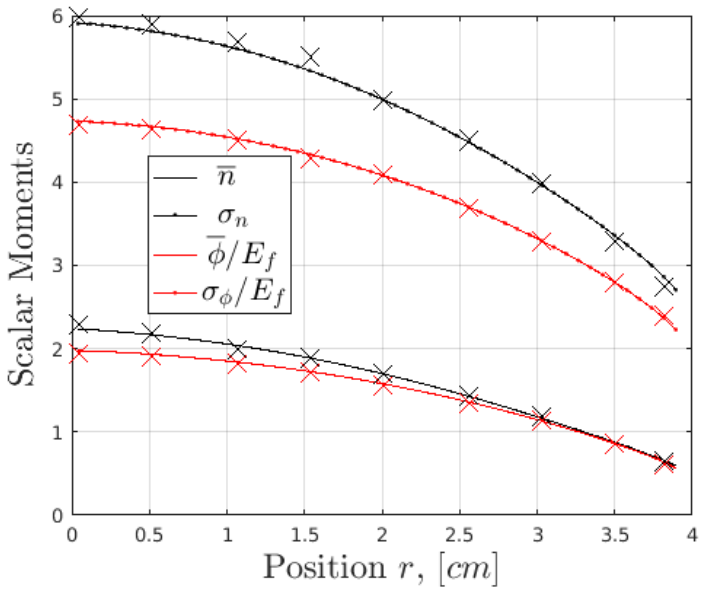

Figure 7.1: Comparison of Monte Carlo (x) and deterministic (-) solutions for the moments of the neutron population and FPDF for a single initiating neutron in a symmetric sphere.

earlier, we obtain the MC results by initiating at the radial mesh points and along the trajectories corresponding to the S_8 ordinates to then apply Eq. 7.30 to find the reported values in Fig. 7.1. Each of the 8 initiation trajectories at each of the 9 radial points was simulated with 200 batches, each with 10^4 histories, amounting to a total of $2 \cdot 10^6$ per ordinate per mesh point. In total, we simulated $1.44 \cdot 10^8$ histories to arrive at the few points shown in Fig. 7.1. Overall, we see excellent agreement between the two methods, providing us with confidence in moving forward to using the superior deterministic method to analyze more complicated systems over greater time intervals.

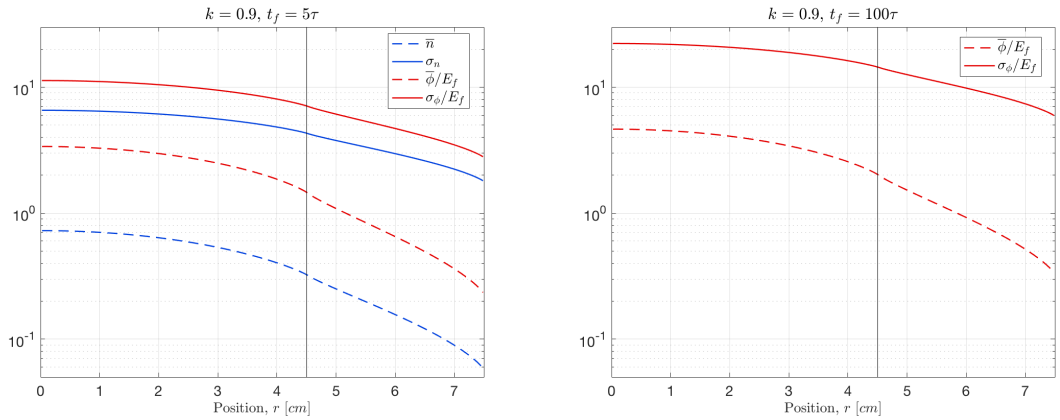

(a) **(b)**

Figure 7.2: Moments of the single chain FPDF in a subcritical system for (a) $t_f = 5\tau$ and (b) $t_f = 100\tau$.

7.2.2 Multi-Layered Spheres

We now consider a ^{235}U ball encased in a graphite shell and solve Eq.7.29 for the first two moments ($n = 1,\ 2$) in spherically symmetric geometry. We used 100 spatial cells per region, S_{80} discrete ordinates, and a time-step width of $\Delta t = 0.05$, which provides adequately resolved numerical solutions. The fission energy deposition distribution is that of a gamma function, and the respective moments, $\overline{E_f^n}$, may be found in Table 7.3 corresponding to the source terms of Table 7.1. The average energy emitted in a single fission is set to $E_f = 180\ MeV$. The neutron number moments are also calculated and the respective inhomogeneous source terms are found in Table 5.1. The spatial profile (recall, in the backward approach, the radial location refers to the point of injection of the initial neutron) of the mean and standard deviation of the deposited energy and the neutron number for a single initiating neutron without a source are shown in Figs. 7.2, 7.3, and 7.4 at 5 and 100 neutron lifetimes for different k-eigenvalues.

For the subcritical system of $k = 0.9$ in Fig. 7.2a, after 5 lifetimes we see that the average neutron population has begun to decline with a large standard deviation.

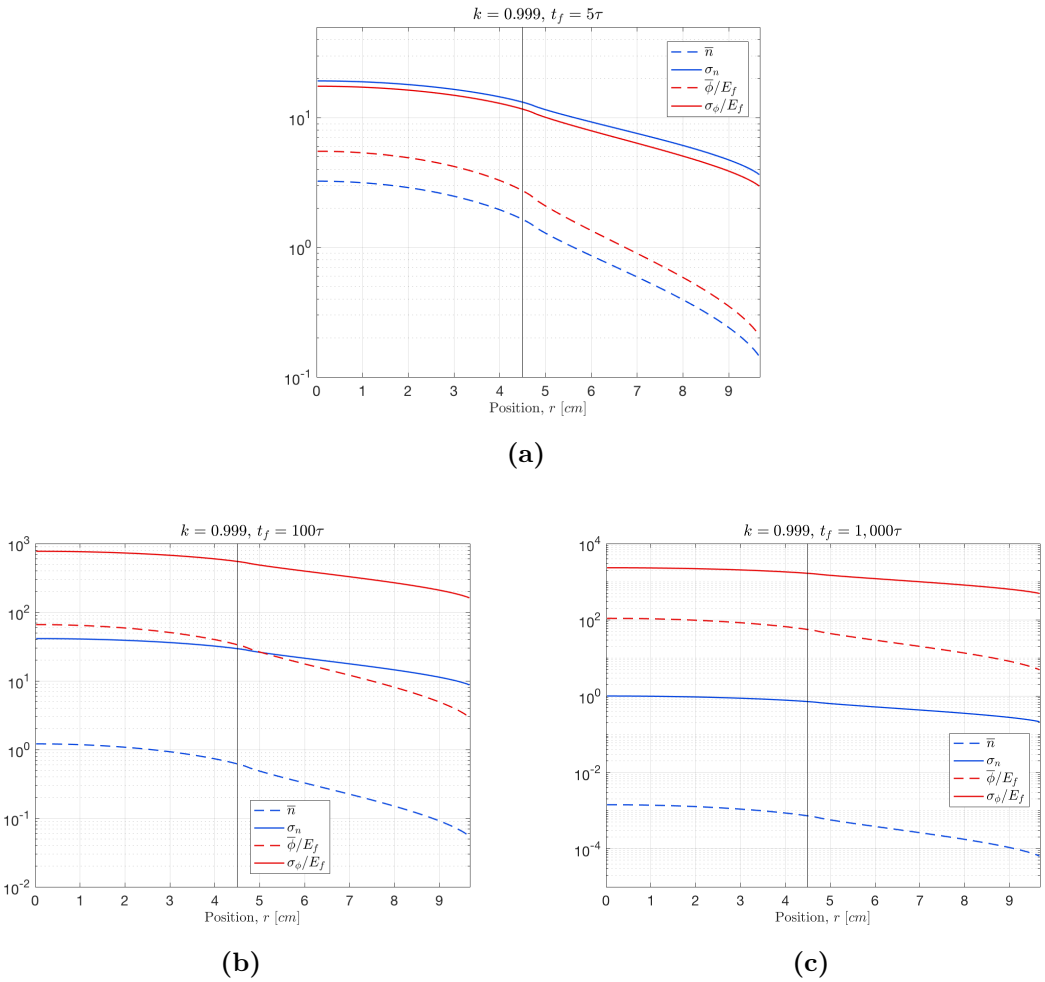

Figure 7.3: Moments of the single chain FPDF in a near critical system for (a) $t_f = 5\tau$, (b) $t_f = 100\tau$, and (c) $t_f = 1,000\tau$.

The total amount of fission energy deposited in the system is maximum when the injected neutron is in the center of the sphere with a value of $\overline{\phi} \approx 3.4E_f$. If we then observe the system at 100 lifetimes after injection, the average neutron population has decreased to below $\overline{n} \approx 10^{-10}$ with the standard deviation of $\sigma_n \approx 10^{-4}$ and thus not shown in Fig. 7.2b; the average total energy deposited increases to $\overline{\phi} \approx 4.6E_f$. For this type of reflected system, as a fission chain extinguishes, on average it will deposit a maximum of around $5E_f$. It is expected that as the system approaches

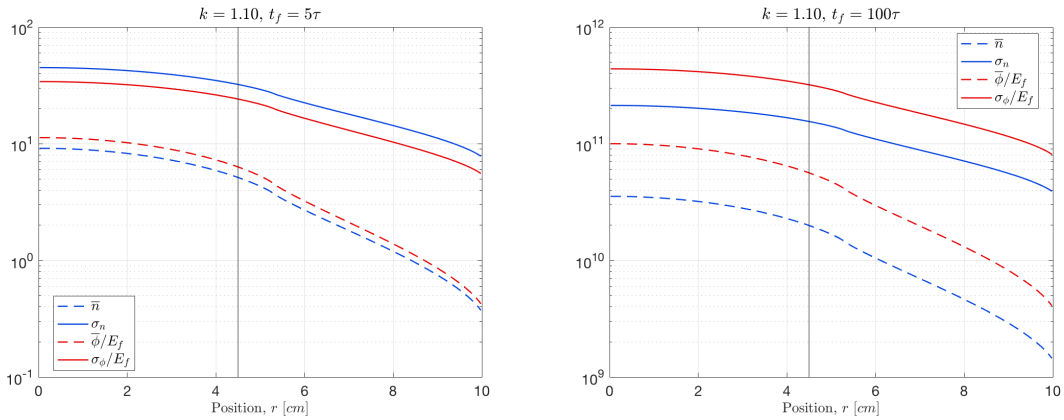

(a) **(b)**

Figure 7.4: Moments of the single chain FPDF in a supercritical system for (a) $t_f = 5\tau$ and (b) $t_f = 100\tau$.

critical from below, the fission chains will propagate for more generations (i.e., cause more fissions) before dying away and the deposited fission energy will dramatically increase as well– we consider this next.

For the near-critical system of $k = 0.999$ depicted in Fig. 7.3, we see that the neutron average grows and eventually drops off for injection locations near the center of the system. This is due to the system being so near critical that a given chain may propagate for long time periods before eventually dying off, strengthened by the possibility that some of the progeny may reflect back into the system if leaked into the moderating graphite shell. It can be seen in Fig. 7.3c that $\overline{n}$ eventually decreases by $t_f = 1,000\tau$, but the total amount of energy deposited within the system continues to grow to $\overline{\phi} \approx 100 E_f$ for a neutron injected in the center. This is an important feature for near-critical systems that one must consider; that is, as a system approaches critical, the fission chains will persist for longer time periods and, although it is certain that those chains will eventually decay away, the amount of energy deposited in the system will continue to accumulate.

We show a supercritical case in Fig. 7.4, for which the neutron average, and

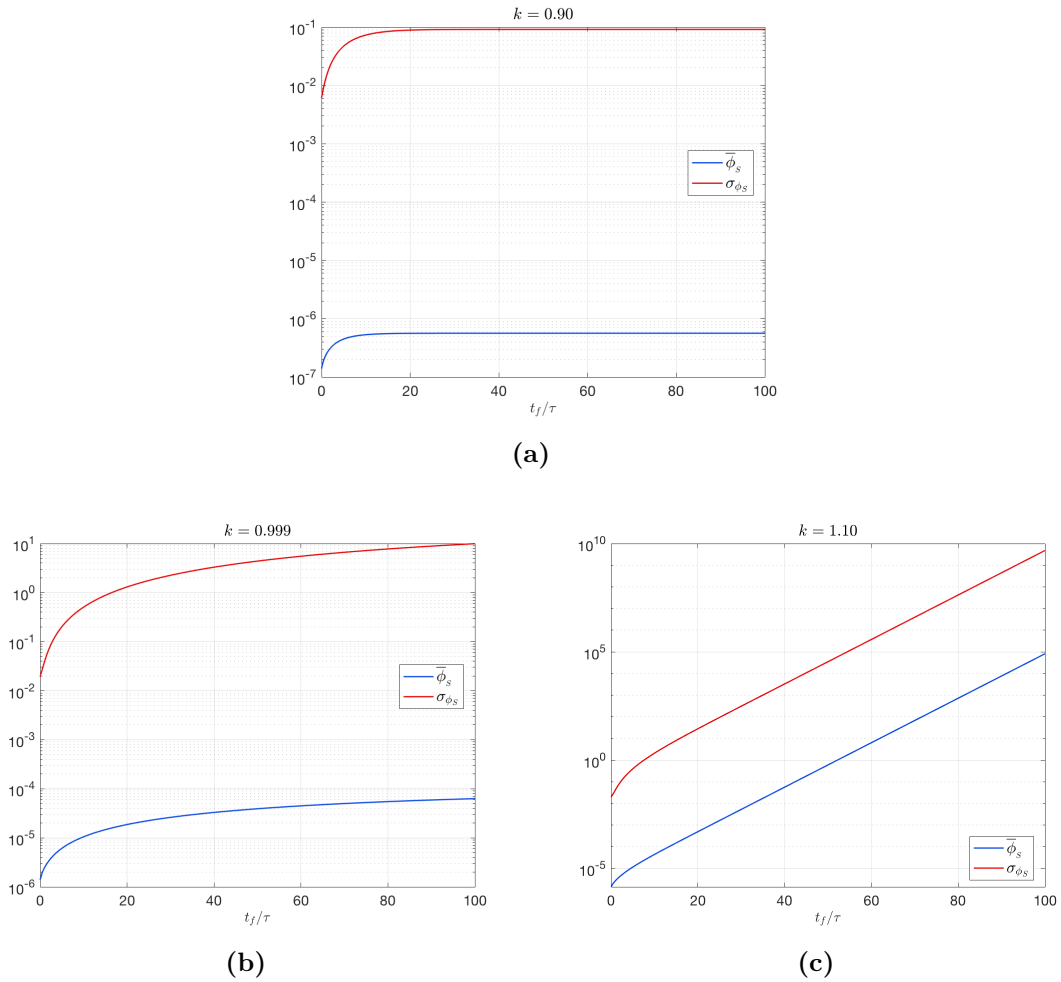

Figure 7.5: Moments of the source FPDF for (a) $k = 0.90$, (b) $k = 0.999$, and (c) $k = 1.10$.

consequently the average cumulative energy deposited, grows without bound. This is obviously expected, but there is a subtlety which is not illustrated here. For any given chain that is initiated in a supercritical system, it will diverge and grow without bound with a probability given by the POI (see Ch. 6). Alternatively, the chain will grow but eventually die off with probability $1 - P_\infty$. Thus, what cannot be captured with these moment figures, is the difference in the averages between those chains that die away, depositing a finite amount of energy, and those chains which diverge,

depositing an infinite amount of energy. We will then need to explore the actual distributions to garner an understanding of this behavior outside of our intuition, which will be done in Secs. 7.3 through7.6.

By now incorporating a constant randomly emitting uniformly distributed source into the inner region, $\mathcal{S}(r) = \omega(r)S$, we may determine the FPDF in the presence of a source. For a uniformly distributed source in the inner uranium region of radius R_i and volume $V_i = \frac{4\pi}{3}R_i^3$, the normalized spatial distribution function is $\omega(r) = 1/V_i$ for $r \in [0, R_i]$ and $\omega(r) = 0$ for $r > R_i$; we also set $S = 1.0\ s^{-1}$. Thus, the FPDF moments in the presence of a source may be calculated using Eq. 7.27. Figure 7.5 shows the first four moments for the systems of varying criticality where we set $W_S(\phi)$ to be a gamma distribution identical to the induced fission $W(\phi)$. As the formulation calls on the cumulative energy that has been deposited, the moments will continue to rise regardless of the system criticality because source events will continue to occur. As this is a very weak source, the average time between events is long, and we see that the subcritical system of Fig. 7.5a appears to reach a steady-state, but if we observe the system much later in time, the amount of energy deposited will eventually grow to infinity. The growth in the moments is more apparent in the near critical system of Fig. 7.5b, and we see the moments growing by 10 orders of magnitude in the first 100 lifetimes of the supercritical system in FIg. 7.5c. If the source strength is a multiple of the original source strength, we may simply scale the solution without returning to the transport code (one will need to recalculate the higher order moment integrals for the source FPDF moments).

7.2.3 Differing $W(\phi)$

In this section, we compare the moment distributions for the systems from the previous section, but for different fission energy deposition distributions, $W(\phi)$. In the previous section, we set $W(\phi)$ to that of a gamma distribution with an average energy deposition

Table 7.5: Calculated moments for different $W(\phi)$.

	E_f $[MeV]$	$\overline{E_f^2}$ $[MeV^2]$	$\overline{E_f^3}$ $[MeV^3]$	$\overline{E_f^4}$ $[MeV^4]$
Gamma	180	48,600	$1.7496 \cdot 10^7$	$7.8732 \cdot 10^9$
Truncated Gaussian	180	48,600	$1.9746 \cdot 10^7$	$8.3971 \cdot 10^9$

per fission of $E_f = 180\ MeV$ and $\overline{E_f^2} = 48,600\ MEV^2$ and $\phi \in [0, \infty]$. We now change $W(\phi)$ to a truncated Gaussian distribution with $\phi \in [0, 558]\ MEV$ and enforce the first two moments of this distribution to be equal to the $E_f = 180\ MeV$ and $\overline{E_f^2} = 48,600\ MEV^2$. Doing so means that the first two moments of the FPDF will be identical for either $W(\phi)$ due to the inhomogeneous source terms being identical, but the higher order moments are expected to differ. Once the transport sweeps are complete, the skew and kurtosis are calculated using the formulae:

$$\gamma(\mathcal{R}, t_f|r, t) = \frac{\overline{\phi^3} - 3\overline{\phi}\sigma_\phi^2 - \overline{\phi}^3}{\sigma_\phi^3} \tag{7.31a}$$

$$\kappa(\mathcal{R}, t_f|r, t) = \frac{\overline{\phi^4} - 4\overline{\phi}\overline{\phi^3} + 6\overline{\phi}^2\overline{\phi^2} - 3\overline{\phi}^4}{\sigma_\phi^4}, \tag{7.31b}$$

where each term is individually angle-integrated. The calculated moments of $W(\phi)$ for the two distributions we consider are found in Table 7.5.

Figure 7.6 shows the skew, γ, and kurtosis, κ, of the single chain FPDF for the different critical systems at the different times of observation. It can be seen that the moments seem not to visually change between the Gamma distribution and the truncated Gaussian for all criticality values and final times displayed. In reference to Table 7.1 containing the inhomogeneous source terms, this lack of difference in the results for differing $W(\phi)$ for the third and fourth moments becomes clear when we see that $\overline{E_f^3}$ and $\overline{E_f^4}$ appear as standalone terms when they first appear and these values are the same magnitude as the other terms in the source expression. Thus,

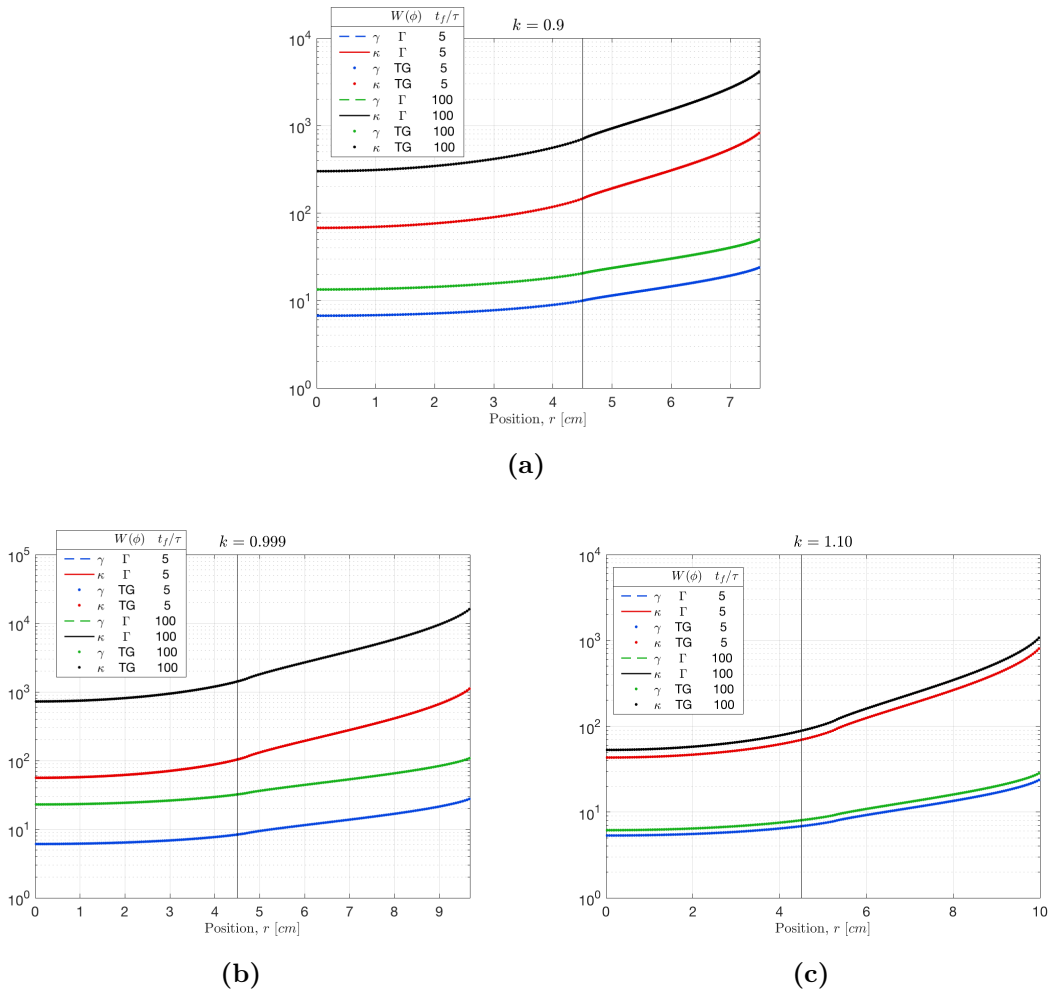

Figure 7.6: Moments of the single chain FPDF at different times for (a) $k = 0.90$, (b) $k = 0.999$, and (c) $k = 1.10$.

one will not see an appreciable difference in the moments of the distribution until the first and second moments of W are also notably different. We will analyze this concept on the actual FPDF distributions at the end of Sec. 7.4.5.

We next consider the moments of the FPDF in the presence of a constant randomly emitting uniformly distributed source. The source is the same as the previous section, such that $S = 1.0\ s^{-1}$ and $\omega(r) = 1/V_i = \frac{3}{4\pi} R_i^{-3}$ for $r \in [0, R_i]$ and 0 otherwise. As for the single chain calculations, we enforce the first two moments of the fission energy

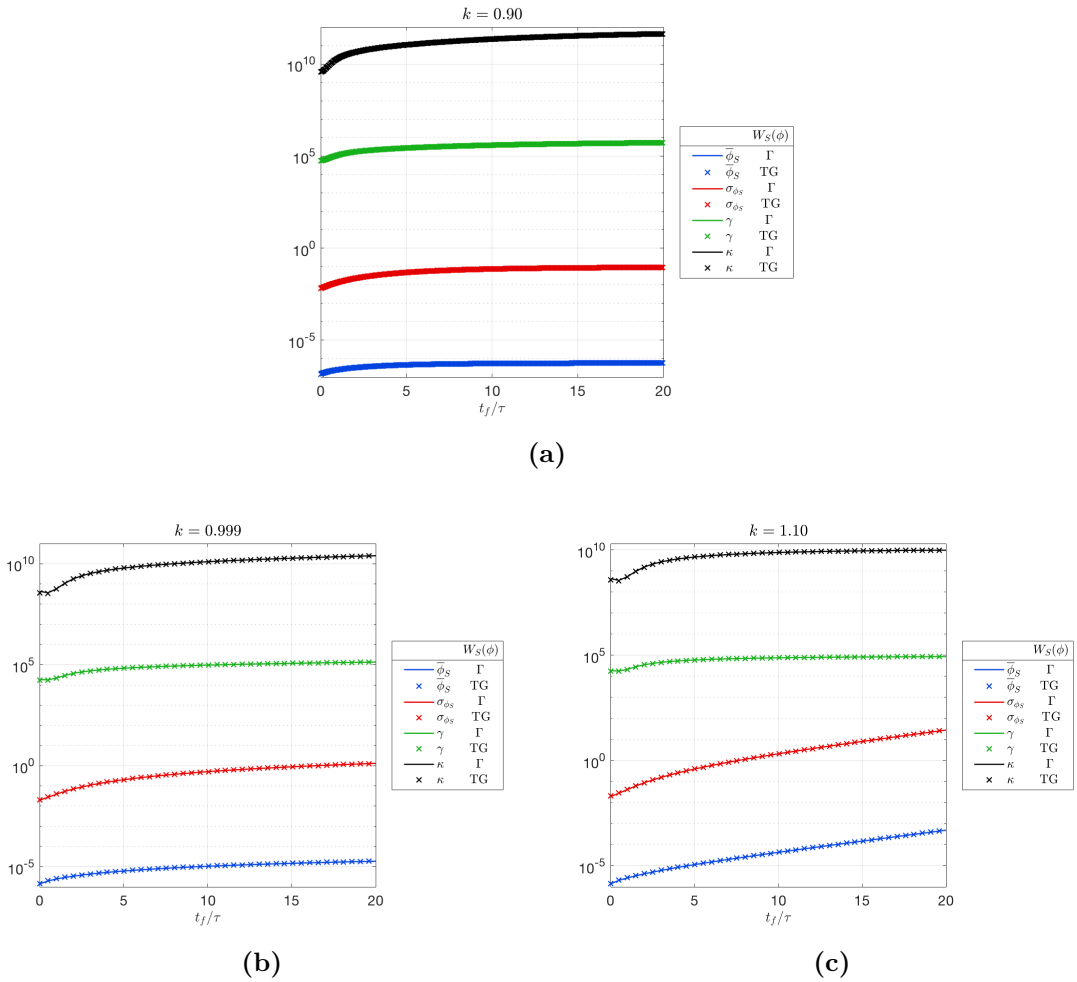

Figure 7.7: Moments of the source FPDF for different $W_S(\phi)$ at different times for (a) $k = 0.90$, (b) $k = 0.999$, and (c) $k = 1.10$.

deposition distributions to be equal regardless of the event type (induced fission or spontaneous fission). We wish to determine whether the moments of the source FPDF will differ if $W_S(\phi)$ is different. As was just demonstrated, the single chain results are practically equivalent for this system, so we will keep $W(\phi)$ as a gamma distribution and compare the source FPDFs for $W_S(\phi)$ being a gamma distribution and a truncated Gaussian distribution. As can be seen in Fig. 7.7, there are no visual differences between the moments for any critical regime. The distributions do

indeed slightly differ, but not enough to be seen in the plots. These results come as no surprise because the first two moments of the distribution are equal for all fission energy deposition distributions in these calculations.

7.3 Lumped Model Description

Reducing our consideration to a lumped model setting permits a more detailed, focused study of the unique attributes of the FPDF. In particular, we wish to examine the actual distribution to better understand the effects of differing $W(\phi)$ for both single chains and sources. In this section, we present the backward Master equations and the low-order moment equations for the single chain and source cases in Sec. 7.3.1, followed by a discussion on an analytical solution obtained using the Binary Fission Model in Sec. 7.3.2. We will then focus our study on the FPDF for lumped systems in the next section, Sec. 7.4 primarily using an event-based Monte Carlo code.

In the ensuing analysis, when numerical results for the FPDF are displayed, we have set the energy cutoff in the Monte Carlo simulations to be 10^5 MeV unless otherwise stated. This was an arbitrary choice, but proves to be an appropriate domain for capturing the majority of the problems analyzed.

7.3.1 Master and Moment Equations

We define $P(\phi, t_f|t)\,\mathrm{d}\phi$ as the probability of there being a cumulative amount of energy deposited within the system in the range $(\phi, \phi + \mathrm{d}\phi)$ at a final time t_f due to the appearance of a single neutron at an earlier time t. Following standard backward formulation practices and considering the physics of the previous section, the FPDF

for a single neutron chain is:

$$-\frac{\partial P(\phi,t_f|t)}{\partial t} = -\lambda_t P(\phi,t_f|t) + \lambda_c\delta(\phi) + \lambda_f q_0^f W(\phi|0)\mathbb{H}(\phi_u-\phi) + \lambda_f\sum_{\nu=1}^{\nu_m^f} q_\nu^f \int_0^{\ell(\phi,\phi_u)} \mathrm{d}\phi' W(\phi'|\nu) \int\limits_{|\vec{\phi}_\nu|=\phi-\phi'} \mathrm{d}^\nu\phi \prod_{k=1}^{\nu} P(\phi_k,t_f|t), \tag{7.32}$$

with final condition given by $\lim_{t_f\leftarrow t} P(\phi,t_f|t) = \delta(\phi)$. It is understood that the ν-fold integrals are computed over the ranges that satisfy the condition: $\left|\vec{\phi}_\nu\right| = \phi_1+\cdots+\phi_\nu = \phi-\phi'$, given by Eq. 7.4.

The appropriate moment generating function transform is defined as:

$$G(\lambda,t_f|t) = \int_0^\infty \mathrm{d}\phi\, \mathrm{e}^{-\lambda\phi} P(\phi,t_f|t), \tag{7.33}$$

which ultimately provides a nonlinear PDE:

$$-\frac{\partial G(\lambda,t_f|t)}{\partial t} + \lambda_t\, G(\lambda,t_f|t) = \lambda_c + \lambda_f \sum_{\nu=0}^{\nu_m^f} q_\nu^f\, \overline{W}(\lambda|\nu)\left[G(\lambda,t_f|t)\right]^\nu, \tag{7.34}$$

with final condition given by the limit: $\lim_{t_f\leftarrow t} G(\lambda,t_f|t) = 1$. We note that we may write Eq. 7.34 in terms of the factorial moments of the fission energy deposition distribution by introducing the modified transform:

$$\mathcal{G}(\lambda,t_f|t) = 1 - G(\lambda,t_f|t). \tag{7.35}$$

Introducing Eq. 7.35 into Eq. 7.34, we derive an equation for $\mathcal{G}$:

$$\frac{\partial \mathcal{G}(\lambda,t_f|t)}{\partial t} = \lambda_t\, \mathcal{G}(\lambda,t_f|t) + \lambda_f\left[-1 + \sum_{\nu=0}^{\nu_m^f} \frac{(-1)^\nu}{\nu!}\chi_\nu(\lambda)\left[\mathcal{G}(\lambda,t_f|t)\right]^\nu\right], \tag{7.36}$$

with final condition $\lim_{t_f\leftarrow t}\mathcal{G}(\lambda,t_f|t) = 0$ and we have defined the factorial moments of the fission energy deposition distribution:

$$\chi_\nu(\lambda) = \sum_{i=\nu}^{\nu_m^f} \frac{i!}{(i-\nu)!} q_i^f \overline{W}(\lambda|i). \tag{7.37}$$

In practice, we may truncate the sum in Eq. 7.36 to obtain a Quadratic Approximation form of the FPDF. In Sec. 7.3.2, we will obtain an analytical solution of the single chain equation for a binary fission model of the induced fission multiplicity distribution and compare the distribution to event-based Monte Carlo simulation results.

Next, we define the probability of a cumulative amount of energy being deposited in the range $(\phi, \phi + \mathrm{d}\phi)$ at a final time, t_f, due to the introduction of a source of strength S at time t_o as $Q(\phi, t_f|t_o)$. Once again following standard procedure, we then obtain the lumped backward Master equation for the cumulative energy deposition distribution due to a constant randomly emitting neutron source and the resultant fission chains:

$$-\frac{\partial Q(\phi, t_f|t_o)}{\partial t_o} = -SQ(\phi,t_f|t_o) + S\sum_{\nu=0}^{\nu_m^S} q_\nu^S \int_0^{\ell(\phi,\phi_u^S)} \mathrm{d}\phi' W_S(\phi'|\nu) \Bigg\{ \int\limits_{\left|\vec{\phi}_{\nu+1}\right|=\phi-\phi'} \mathrm{d}^{\nu+1}\phi\, Q(\phi_{\nu+1}, t_f|t_o) \prod_{k=1}^{\nu} P(\phi_k, t_f|t_o) \Bigg\} \tag{7.38}$$

with final condition $\lim_{t_f \leftarrow t_o} Q(\phi, t_f|t_o) = \delta(\phi)$. Provided the Laplace transform of the energy deposition variable,

$$H(\lambda, t_f|t_o) = \int_0^\infty \mathrm{d}\phi\, \mathrm{e}^{-\lambda\phi} Q(\phi, t_f|t_o), \tag{7.39}$$

we may transform Eq. 7.38 to find

$$-\frac{\partial H(\lambda, t_f|t_o)}{\partial t_o} = S\left[-1 + \sum_{\nu=0}^{\nu_m^S} q_\nu^S \overline{W}_S(\lambda|\nu)\Big[G(\lambda, t_f|t_o)\Big]^\nu\right] H(\lambda, t_f|t_o) \tag{7.40}$$

with final condition $\lim_{t_f \leftarrow t_o} H(\lambda, t_f|t_o) = 1$. Finally, Eq. 7.40 may be solved via separation of variables and integrating backwards in time yields

$$H(\lambda, t_f|t_o) = \exp\left\{-\int_{t_f}^{t_o} \mathrm{d}t' S\left[-1 + \sum_{\nu=0}^{\nu_m^S} q_\nu^S \overline{W}_S(\lambda|\nu)\Big[G(\lambda, t_f|t')\Big]^\nu\right]\right\}. \tag{7.41}$$

By defining the factorial moments of the energy deposition distribution for source events as

$$\chi_\nu^S(\lambda) = \sum_{i=\nu}^{\nu_m^S} \frac{i!}{(i-\nu)!} q_i^S \overline{W}_S(\lambda|i), \tag{7.42}$$

and inserting $G = 1 - \mathcal{G}$ into Eq. 7.41, expanding the $[1-\mathcal{G}]^\nu$ via the Binomial Theorem, we find:

$$H(\lambda, t_f|t_o) = \exp\left\{-\int_{t_f}^{t_o} \mathrm{d}t' S\left[-1 + \sum_{\nu=0}^{\nu_m^S} \frac{(-1)^\nu}{\nu!}\chi_\nu^S(\lambda)\left[\mathcal{G}(\lambda, t_f|t')\right]^\nu\right]\right\}. \quad (7.43)$$

Finally, if we consider singlet-emitting sources, such that $q_\nu^S = \delta_{\nu,1}$, then $\chi_0^S(\lambda) = \overline{W}_S(\lambda|1)$, $\chi_1^S(\lambda) = \overline{W}_S(\lambda|1)$, and $\chi_\nu^S(\lambda) = 0$ for $\nu \geq 2$. The solution for singlet-emitting sources is then

$$\begin{aligned} H(\lambda, t_f|t_o) &= \exp\left\{-\int_{t_f}^{t_o} \mathrm{d}t' S\Big[-1 + \overline{W}_S(\lambda|1)\Big(1 - \mathcal{G}(\lambda, t_f|t')\Big)\Big]\right\} \\ &= \exp\left\{-\int_{t_f}^{t_o} \mathrm{d}t' S\Big[-1 + \overline{W}_S(\lambda|1) G(\lambda, t_f|t')\Big]\right\}. \end{aligned} \quad (7.44)$$

An equation for the k^{th} moment of the single chain FPDF in a lumped setting, $\overline{\phi^k}(t_f|t)$, may be obtained by taking k successive derivatives of the generating function and evaluating at $\lambda = 0$, i.e.,

$$\left.\frac{\partial^k G(\lambda, t_f|t)}{\partial \lambda^k}\right|_{\lambda=0} = (-1)^k \overline{\phi^k}(t_f|t). \quad (7.45)$$

Applying the identity Eq. 7.45 to the Master equation satisfied by $G(\lambda, t_f|t)$, Eq. 7.34, provides:

$$-\frac{1}{v}\frac{\partial \overline{\phi^k}(t_f|t)}{\partial t} - \frac{\alpha}{v}\overline{\phi^k}(t_f|t) = \mathcal{S}_k\left(t_f|t; \overline{\phi}, \ldots, \overline{\phi^{k-1}}\right), \quad (7.46)$$

where $\alpha = (k-1)/\tau$ and we have assumed that the coupling between the amount of energy deposited in a single fission and the number of neutrons emitted can be ignored, such that $\overline{W}_\nu(\lambda) = q_\nu^f \overline{W}(\lambda)$. The right-hand side of Eq. 7.46 can be found in Table 7.1, where one must remove spatial dependence and angular integrals from the terms. The source moment equations are functionally the same as Eq. 7.26, where once again the inhomogeneous source terms must have spatial and angular dependence removed accordingly.

7.3.2 Analytical Solution via the Binary Fission Model

Equation 7.34 is solvable in closed form for a binary fission model, i.e., exactly two neutrons are emitted in each fission, so that $W_\nu(\phi) = \delta_{\nu,2}\, W(\phi)$. The time dependent solution for the generating function, however, cannot be inverted to yield an expression with explicit terms, but the solution in steady state, corresponding to the initial neutron being introduced into the assembly in the infinite past, provides a closed form and very insightful solution for the deposited energy distribution. There are two solutions for the generating function for the binary fission model and the physically correct solution is given by:

$$G(\lambda) = \frac{1}{2\, p_f\, \overline{W}(\lambda)} \left[1 - \sqrt{1 - 4p_f(1-p_f)\overline{W}(\lambda)}\right], \tag{7.47}$$

where $p_f = \Sigma_f/\Sigma_a = k/2$ is the fission probability and k is the multiplication factor. Thus the system is critical if $p_f = 0.5$. To proceed further it is necessary to specialize to a specific form of $W(\phi)$. For illustrative purposes it proves convenient and informative to use the following one-parameter normalized gamma distribution which has a simple image function:

$$W(\phi) = \frac{4}{E_f^2}\, \phi\, \exp\left(-\frac{2\phi}{E_f}\right), \tag{7.48a}$$

$$\overline{W}(\lambda) = \frac{4}{E_f^2} \frac{1}{(\lambda + \frac{2}{E_f})^2}, \tag{7.48b}$$

where E_f is the average energy deposited in a fission reaction:

$$E_f = \int_0^\infty \mathrm{d}\phi\, \phi\, W(\phi). \tag{7.49}$$

The Laplace transform in Eq. 7.47 can then be inverted to yield the steady state probability density of the deposited fission energy in closed form:

$$P(\phi) = (1-p_f)\, \delta(\phi) + 2(1-p_f) \frac{1}{\phi} \exp\left\{-\frac{2}{E_f}\, \phi\right\}\, I_2\left(\frac{4}{E_f^2}\, \sqrt{\gamma}\, \phi\right), \tag{7.50}$$

where $\gamma = 4p_f(1-p_f)$ and $I_2(\cdot)$ is the modified Bessel function of order 2. The first term describes the event in which the initial neutron is absorbed at the first collision, with probability $(1-p_f)$, in which case no fission energy is deposited, while the second term gives the distribution of cumulative energy deposited in fission reactions caused by the initial neutron and all its progeny. The normalization of the FPDF is very simply obtained by setting $\lambda = 0$ in Eq. 7.47 to get:

$$\begin{aligned} G(\lambda = 0) &= \int_0^\infty \mathrm{d}\phi\, P(\phi) \\ &= \frac{1}{2p_f}\left(1 - \left|2p_f - 1\right|\right) \\ &= \frac{1}{k}\left(1 - \left|k - 1\right|\right), \end{aligned} \tag{7.51}$$

a result that can also be obtained with considerably more algebra by integrating the FPDF given in Eq. 7.50 over all ϕ. For $p_f \leq 0.5$ or $k \leq 1$ Eq. 7.51 gives unit normalization, an obvious and unsurprising result. The supercritical case, $k > 1$, however is less obvious and will be discussed below.

The problem was also solved by time dependent event-based Monte Carlo simulation in a subcritical medium for which it was possible to simulate to steady state. In Fig. 7.8a, simulation results for the distribution plotted against the normalized energy deposition variable $\psi = \phi/E_f$, are compared with the exact solution in Eq. 7.50 for various fission probabilities approaching critical. The agreement is seen to be within statistical noise. The figure demonstrates a trend towards longer tailed distributions as the system approaches critical, made clearer in Fig. 7.8b for $p_f = 0.49$, $k = 0.98$ where the probability of significant cumulative energy deposition is observed to be high.

To analyze this result, we consider $\psi \gg 1$, for which the exact solution Eq. 7.50 has the asymptotic form:

$$P(\psi) \sim \frac{1-p_f}{\sqrt{\pi}\sqrt[4]{\gamma}}\,\frac{1}{\psi^{3/2}}\,\exp\left\{-2\left(1-\sqrt{\gamma}\right)\psi\right\}. \tag{7.52}$$

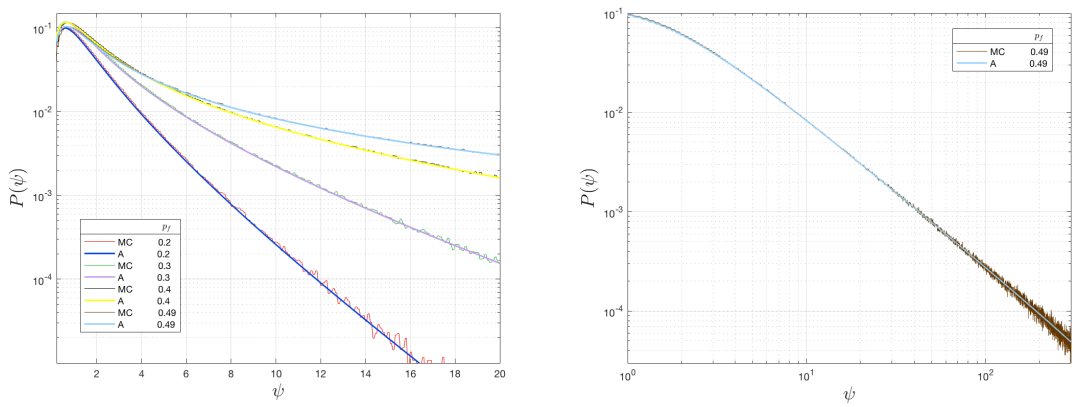

(a) **(b)**

Figure 7.8: Deposited fission energy probability density for (a) subcritical systems and (b) near critical systems.

It is clear that as $p_f \to 0.5$ so that $\gamma \to 1$ the exponent in Eq. 7.52 gets smaller which slows the decay of the distribution with increasing ψ, consistent with the simulation results. The physical reason is that near critical neutron chains can survive for very long times before becoming extinct, resulting in larger numbers of fission reactions and consequently greater cumulative deposited fission energy. The question as to what happens when the system is exactly critical naturally arises and can be addressed by noting that at critical, when $p_f = 1/2$, $\gamma = 1$, the exponential factor vanishes and the distribution reduces to:

$$P(\psi) \sim \frac{1}{2\sqrt{\pi}} \frac{1}{\psi^{3/2}}, \tag{7.53}$$

displaying an algebraic rather than an exponential decay of density. This means that although the distribution remains normalized, all moments of the distribution of order one or higher diverge, i.e., $\int_0^\infty \mathrm{d}\phi\, \phi^n\, P(\phi, t|s) \to \infty$, $n \geq 1$. The conclusion is that the amount of deposited energy in a single chain can be significant and strongly fluctuating near critical.

The single chain FPDFs for a supercritical system with p_f in the range $0.506 - 0.90$, or k in the range $1.012 - 1.8$, are shown in Fig. 7.9, obtained using the analytic

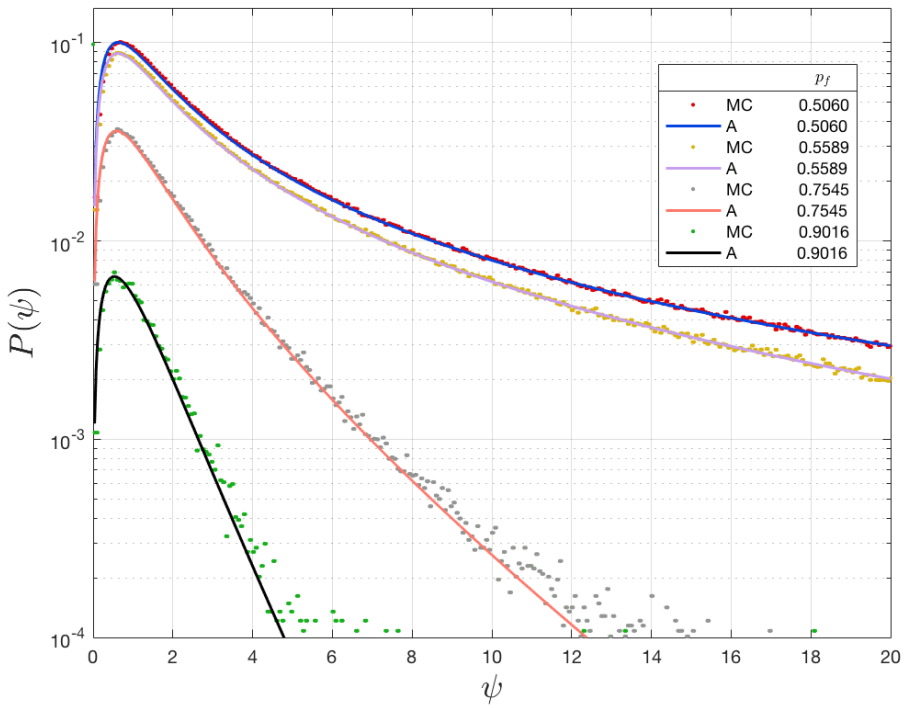

Figure 7.9: Deposited Fission Energy Probability Density: Supercritical

solution in Eq. 7.50 as well as Monte Carlo simulation. Recall, the binary fission approximation has been assumed for the multiplicity distribution. There are a number of interesting aspects to these results that we address first with reference to the analytic solution. Although the distribution shows the expected long tailed behavior for the weakly supercritical case $k = 1.012$, very rapid fall-off is observed to occur as the system becomes more supercritical. Moreover, the distribution clearly loses mass with increasing k. That is, the normalization deviates increasingly from unity, in contrast to the subcritical case where unit normalization was preserved regardless of the level of subcriticality. In fact, it follows from Eq. 7.51 that $p_f > 0.5$ gives $\int_0^\infty \mathrm{d}\phi\, P(\phi, t|s) = 1/p_f - 1 = 2/k - 1$ for the normalization, which is less than unity. There is in fact a perfectly reasonable explanation for what at first blush is a puzzling result, and to understand this result it is necessary to refer to the time

asymptotic behavior of the neutron chain itself.

For a supercritical system it is known [3, 11] that as $t \to \infty$ a neutron chain will either diverge, i.e., the population will grow to infinity, with some probability P_∞ or become extinct, i.e., the population will vanish, with probability $(1 - P_\infty)$. There is zero probability of a finite neutron population existing. For the binary fission multiplicity model in lumped geometry, the divergence probability is given by $P_\infty = 2(1 - 1/k)$ so that the extinction probability is just $2/k - 1$ [3, 11], which we note is the normalization factor above. Random variables (the neutron population in our case) that can have a nonzero probability of assuming infinite values are known as defective random variables [66] for which the infinite state probability must be included to obtain a properly normalized distribution. Against this backdrop, we can now understand the FPDFs in the supercritical case in Fig. 7.9. As soon as the system becomes supercritical, unbounded growth of the neutron population can occur (with probability P_∞) and obviously the cumulative amount of fission energy deposited by these diverging chains will likewise be infinite. However, for the chains that eventually become extinct (with probability $1 - P_\infty$) there will be a finite amount of fission energy deposited, although the neutron population has gone to zero in the process. It is this component of the deposited energy whose distribution is captured by the solution in Eq. 7.50 and plotted in Fig. 7.9 and the normalization is simply the chain extinction probability, as it must be. With increasing k the likelihood of chains diverging increases so a smaller mass of the distribution is captured by the extinct chains. Eventually, for $p_f = 1$ or $k = 2$ when there is no parasitic capture, $P_\infty = 1$ so that all chains diverge as will the amount of deposited fission energy.

Monte Carlo simulation of the supercritical case presents a challenge in that diverged chains will require infinite simulation time. In implementation, chains were simulated to a length of 10^6 neutrons and the fission energy deposited was accumulated only for those chains that went extinct during this time. Chains that reached the maximum length were assumed to diverge and their contribution to the deposited

fission energy was added to the diverged component. The simulated results agree with the analytical solution, although for the highly supercritical cases the chains grew very rapidly, giving poor statistics for the larger energy deposition values due to fewer realizations of the extinct chains for the same number of histories as the lower k systems.

7.4 Single Chain FPDF Results for Differing $W(\phi)$

In this section, we devise schemes for sampling the amount of energy deposited in a fission event depending on the form of the deposition distribution, $W(\phi)$; specifically, we consider three distributions: the gamma distribution, the beta distribution, and the truncated Gaussian distribution. Event Based Monte Carlo simulation results are shown to demonstrate the behavior of the single chain FPDF for these differing deposition distributions.

7.4.1 The Gamma Distribution

Using a gamma distribution to model $W(\phi)\,\mathrm{d}\phi$ was already realized in the previous section, due to the simple form of its Laplace transform, to ascertain a steady-state solution for the Binary Fission model. Replicating the distribution for ease of the reader, we may write $W(\phi)\,\mathrm{d}\phi$ as:

$$W(\phi)\,\mathrm{d}\phi = \frac{4}{E_f^2}\phi \exp\left\{-\frac{2}{E_f}\phi\right\}\mathrm{d}\phi, \tag{7.54}$$

where $\phi \in [0, \infty]$ and E_f is the average amount of energy deposited in an induced fission event given by Eq. 7.49. We may obtain a PDF for the average-normalized energy deposited per fission event by introducing the quantity $\epsilon = \phi/E_f$, and, by the conservation of probability, we find:

$$\widetilde{W}(\epsilon)\,\mathrm{d}\epsilon = W(\phi)\,\mathrm{d}\phi \qquad \rightarrow \qquad \widetilde{W}(\epsilon) = 4\,\epsilon \exp\Big\{-2\epsilon\Big\}. \tag{7.55}$$

We next wish to sample ϵ from $\widetilde{W}$ in the event of an induced fission by setting the CDF equal to a random number $\xi \in [0, 1]$:

$$\xi = \int_0^{\epsilon} \mathrm{d}\epsilon' \widetilde{W}(\epsilon') = 1 - (2\epsilon + 1) \exp\Big\{ - 2\epsilon \Big\}. \tag{7.56}$$

Equation 7.56 is transcendental in ϵ, requiring the application of the Newton-Raphson Iteration Method. We may sample a value of ϵ using the formula for the n^{th} iteration:

$$\epsilon_n = \epsilon_{n-1} + \frac{1}{2} + \frac{1}{4\epsilon_{n-1}} \left(1 - \xi \exp\Big\{2\epsilon_{n-1}\Big\}\right), \tag{7.57}$$

where we set the initial guess to be $\epsilon_0 = 0.5$. Once converged, such that ϵ_n is less than some tolerance (we use a tolerance of 10^{-9}), we accumulate the total energy deposited for all fission events in a given history as:

$$\psi = \sum \epsilon. \tag{7.58}$$

To recover the cumulative energy deposition, simply multiply Eq. 7.58 by E_f. One must be careful not to confuse induced fission and spontaneous fission values of E_f if one is accumulating ψ rather than ϕ for a given history involving sources because E_f may differ between the two types of events. For this reason, it is recommended not to accumulate ψ unless E_f is chosen to be a constant value for both induced and spontaneous deposition events. On a final note, we recall the range of ϕ is $[0, \infty]$ and this may cause unrealistically high energy deposition for select events. The next two distributions consider an upper limit on the maximum energy that may be deposited in an event.

7.4.2 The Beta Distribution

We next wish to compare the differences of the FPDF due to differing the energy deposition distribution. Using the Beta Distribution of the First Kind, or simply the Beta Distribution, the energy deposition distribution is stated as:

$$W(\phi)\,\mathrm{d}\phi = \frac{\phi_u^{1-\alpha-\beta}}{B(\alpha, \beta)} \cdot \phi^{\alpha-1} (\phi_u - \phi)^{\beta-1}\,\mathrm{d}\phi \tag{7.59}$$

Table 7.6: Case-dependent Beta Distribution parameters

Case	σ_ϕ	α	β
1	σ_Γ	$2-3\frac{E_f}{\phi_u}$	$\alpha\left(\frac{\phi_u}{E_f}-1\right)$
2	rE_f	$\frac{1}{r^2}\left(1-\frac{E_f}{\phi_u}(1+r^2)\right)$	$\frac{r^2\alpha(\alpha+1)}{1-r^2\alpha}$

where $\phi \in [0, \phi_u]$, ϕ_u is the maximum amount (upper limit) of energy deposited per fission event, and $B(\alpha,\beta) = \Gamma(\alpha)\Gamma(\beta)/\Gamma(\alpha+\beta)$ is the Beta function. The distribution given by Eq. 7.59 is a four-parameter distribution, where α and β are the shape parameters and the limits on ϕ are the remaining two. The mean and standard deviation of this Beta distribution are

$$\overline{\phi} = E_f = \frac{\alpha\,\phi_u}{\alpha+\beta} \tag{7.60a}$$

$$\sigma_\phi = \frac{\phi_u}{\alpha+\beta}\sqrt{\frac{\alpha\beta}{\alpha+\beta+1}}. \tag{7.60b}$$

The two positive shape parameters, α and β, may be determined in a myriad of ways by using knowledge of the moments of the distribution; in the following analysis we consider two cases, both of which assume the mean is known. In the first case, we equate the standard deviation with that of the gamma distribution as $\sigma_\phi = \sigma_\Gamma = \sqrt{2}E_f/2$. For the second case, we choose to scale the standard deviation to the mean, i.e., $\sigma_\phi = rE_f$ for $r \geq 0$. Table 7.6 summarizes the relationship between the shape parameters and the moments for these two cases. We note that if we set $r = \sqrt{2}/2$, the shape parameters for Cases 1 and 2 equate because the standard deviation of the gamma distribution is $\sigma_\Gamma = \sqrt{2}E_f/2$.

Regardless of the shape parameters, the CDF of the beta distribution is

$$\begin{aligned}\int_0^\phi \mathrm{d}\phi' W(\phi') &= \frac{1}{\alpha B(\alpha,\beta)}\cdot\left(\frac{\phi}{\phi_u}\right)^\alpha \cdot {}_2F_1\left(\alpha, 1-\beta; \alpha+1; \frac{\phi}{\phi_u}\right) \\ &= I_{\frac{\phi}{\phi_u}}(\alpha,\beta),\end{aligned} \tag{7.61}$$

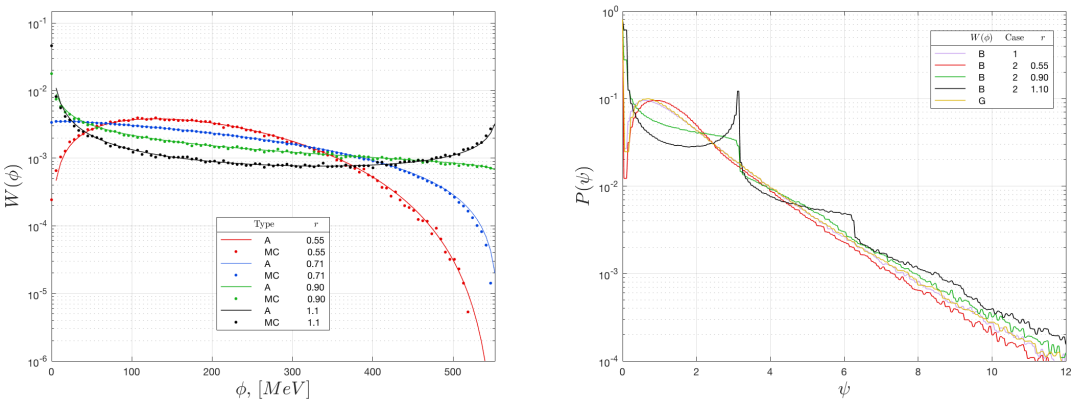

(a) A = Analytical, MC = Monte Carlo **(b)** B = Beta Dist., G = Gamma Dist.

Figure 7.10: Monte Carlo simulation results for (a) the Case 2 beta distribution $W(\phi)$ for differing r and (b) the single chain FPDF in a subcritical system ($p_f = 0.2$) for differing $W(\phi)$.

where ${}_2F_1$ is the Gaussian hypergeometric function and $I_{\phi/\phi_u}(\alpha, \beta)$ is the regularized incomplete beta function. Proceeding, we set Eq. 7.61 equal to a random number, $\xi \in [0, 1]$, and once again employ the Newton-Raphson Method to sample ϕ for a given fission event. The iteration formula, in terms of I_{ϕ/ϕ_u}, is

$$\phi_n = \phi_{n-1} + B(\alpha, \beta)\left[\xi - I_{\frac{\phi_{n-1}}{\phi_u}}(\alpha, \beta)\right]\left(\frac{\phi_{n-1}}{\phi_u}\right)^{1-\alpha}\left(1 - \frac{\phi_{n-1}}{\phi_u}\right)^{1-\beta}, \tag{7.62}$$

and once we have a converged value of ϕ_n, we calculate $\epsilon = \phi/E_f$, and we accumulate ψ values according to Eq. 7.58.

In Fig. 7.10a, we show the Case 2 beta distribution for differing r values as sampled by the given iteration scheme for 10^5 realizations of Eq. 7.62 as compared to the analytical (A in the legend) distribution, Eq. 7.59, where we set the upper energy limit to $\phi_u = 3.1E_f$. For the $r = 0.9$ case, we see $W \to \infty$ for $\phi \to 0$; this is due to $\alpha < 1 (= 0.51)$, causing the $\phi^{\alpha-1}$ factor in Eq. 7.59 to become a singularity at $\phi = 0$. For the $r = 1.1$ case, both $\alpha < 1 (= 0.24)$ and $\beta < 1 (= 0.50)$, and we see both end points of the distribution diverge. These diverging endpoint values have no bearing on our ability to sample from the CDF of the Beta distribution because

$I_{\phi/\phi_u}(\alpha, \beta)$ is bounded and normalized.

In Fig. 7.10b, we compare the FPDF for the beta distribution Cases 1 and 2 for varying r values with the gamma distribution in a subcritical system with $p_f = 0.2$, $k_\infty = 0.4$. Each of these distributions was obtained by running 10^7 histories out to $t_f = 1,250\tau$ to ensure steady-state conditions are met. It is observed that the Case 1 line deviates only slightly from the gamma distribution line due to the $W(\phi)$ sharing the first two moments. We do not expect there to be an appreciable difference for such a low multiplying system for minuscule fission energy deposition, but as $k \to 1^-$, persistent fission chains are expected to occur more frequently, causing the non-equivalent higher moments to differently affect the tails of the FPDFs.

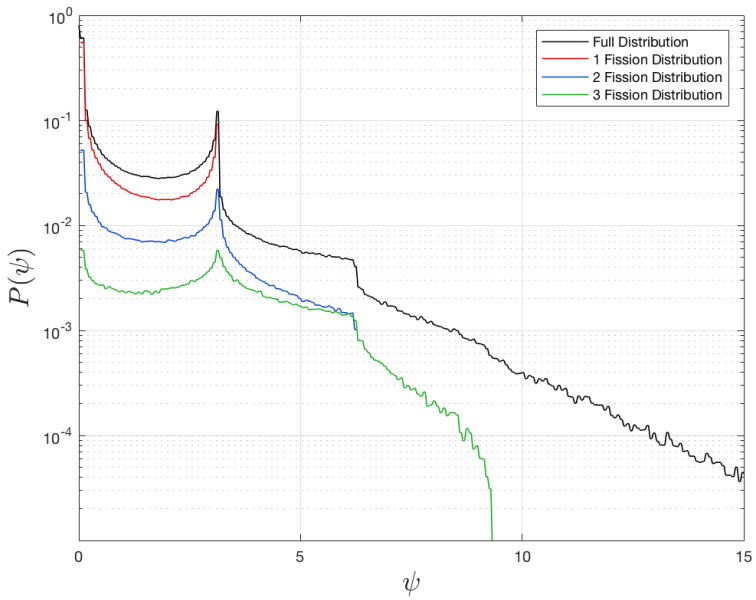

Figure 7.11: Separation of the FPDF components for Case 2 with $r = 1.1$.

As r increases, we witness a "shouldering" behavior in the FPDF and this is attributed to the increase in probability of $\phi = 0$ and $\phi = \phi_u$ for every fission event. We now affix our attention on the extreme example for Case 2 with $r = 1.1$ in Fig. 7.11, recalling that we set $\phi_u = 3.1E_f$ for this exercise. We see a clear and dramatic

increase in $P(\psi = 3.1)$, corresponding to the upper limit of the first fission that takes place in the simulated fission chain. As expected, the next shoulder occurs at $P(\psi = 6.2)$, and so on for every integer multiple of 3.1ψ. Figure 7.11 shows the single chain FPDF and the components of the distribution for which histories concluded with exactly one, two, or three fission events. As more fission events occur per history, the distinctive inverted shape of W diminishes due to the overlapping of possible successive ϕ combinations as well as an increase in the statistical noise in tandem with the decreasing magnitude of the probability for increasing ψ. These component distributions are obtained by adding to a separate designated histogram at the end of each history if the condition that the number of fissions that occurred is met.

7.4.3 The Truncated Gaussian Distribution

The beta distribution provides interesting results and allows insight into the behavior of the FPDF for increasingly exotic shapes of the fission energy deposition distribution, $W(\phi)$; another form worth investigating is the truncated Gaussian distribution. We choose to truncate the upper and lower bounds of a general Gaussian distribution with mean $\overline{\phi}_p$ and standard deviation σ_p. Here, the subscript p refers to the *parent*, general Gaussian distribution. The truncated bounds of the energy deposition distribution are set to a minimum value ϕ_ℓ, and maximum value ϕ_u, such that $\phi \in [\phi_\ell, \phi_u]$. With this, the truncated Gaussian form of the fission energy deposition distribution is defined as

$$W(\phi)\,\mathrm{d}\phi = \frac{\omega\left(\frac{\phi-\overline{\phi}_p}{\sigma_p}\right)}{\sigma_p\left[\Omega\left(\frac{\phi_u-\overline{\phi}_p}{\sigma_p}\right) - \Omega\left(\frac{\phi_\ell-\overline{\phi}_p}{\sigma_p}\right)\right]}\,\mathrm{d}\phi, \tag{7.63}$$

where ω is the probability density function of the standard normal distribution,

$$\omega(\chi) = \frac{1}{\sqrt{2\pi}}\exp\left(-\frac{1}{2}\chi^2\right), \tag{7.64}$$

and Ω is the CDF of ω:

$$\Omega(\chi) = \frac{1}{2}\left[1 + \text{erf}\left(\frac{\chi}{\sqrt{2}}\right)\right]. \tag{7.65}$$

Also, erf is the error function:

$$\text{erf}(\chi) = \frac{2}{\sqrt{\pi}}\int_0^{\chi} \text{d}t \exp\left\{-t^2\right\}. \tag{7.66}$$

By setting the CDF equal to a uniformly distributed random number, ξ, we may invert the CDF to sample an amount of energy deposited in the event of an induced fission using the formula:

$$\phi = \overline{\phi}_p + \sigma_p\sqrt{2}\,\text{erf}^{-1}\left\{\xi\left[\text{erf}\left(\frac{\phi_u - \overline{\phi}_p}{\sigma_p\sqrt{2}}\right) + \text{erf}\left(\frac{|\phi_\ell - \overline{\phi}_p|}{\sigma_p\sqrt{2}}\right)\right] - \text{erf}\left(\frac{|\phi_\ell - \overline{\phi}_p|}{\sigma_p\sqrt{2}}\right)\right\}, \tag{7.67}$$

where we have assumed $\phi_\ell < \overline{\phi}_p$. In the next subsection, we discuss a methodology for obtaining the moments of the parent distribution based on assumptions and restrictions imposed on the truncated distribution's moments- allowing us to then sample deposition values from Eq. 7.67.

7.4.4 Prerequisites for the Truncated Gaussian Distribution

Although the truncated Gaussian distribution provides a simplification in the sampling of ϕ using Eq. 7.67 because we do not need to iterate, other complications arise. The first issue is made apparent when one wishes to compare the truncated Gaussian to the previous beta distribution and gamma distribution- we may immediately equate the moments of the truncated Gaussian to

$$\overline{\phi} = E_f \tag{7.68a}$$

$$\sigma_\phi = rE_f, \tag{7.68b}$$

but Eq. 7.67 requires knowledge of the moments of the parent Gaussian distribution, $\overline{\phi}_p$ and σ_p. The truncation of the parent distribution is a mean-preserving contraction

combined with a mean-changing rigid shift, and hence the variance of the truncated distribution is less than the variance of the parent normal distribution. We may relate the first two moments using the formulae:

$$\overline{\phi} = \overline{\phi}_p + \sigma_p \left[\frac{\omega(a) - \omega(b)}{\Omega(b) - \Omega(a)} \right] \tag{7.69a}$$

$$\sigma_\phi = \sigma_p \sqrt{1 + \frac{a\omega(a) - b\omega(b)}{\Omega(b) - \Omega(a)} - \left[\frac{\omega(a) - \omega(b)}{\Omega(b) - \Omega(a)} \right]^2} \tag{7.69b}$$

where

$$a = a\left(\overline{\phi}_p, \sigma_p\right) = \frac{\phi_\ell - \overline{\phi}_p}{\sigma_p}, \tag{7.70a}$$

$$b = b\left(\overline{\phi}_p, \sigma_p\right) = \frac{\phi_u - \overline{\phi}_p}{\sigma_p}. \tag{7.70b}$$

In order to compute $\overline{\phi}_p$ and σ_p such that $\overline{\phi} = E_f$ and $\sigma_\phi = rE_f$, we must determine the roots of Eq. 7.69. This is accomplished by, once again, employing the Newton-Raphson method to iteratively solve the transcendental-in-$\overline{\phi}_p$ and -σ_p system of equations:

$$f\left(\overline{\phi}_p, \sigma_p\right) = 0 = \overline{\phi}_p - \overline{\phi} + \sigma_p A(a, b) \tag{7.71a}$$

$$g\left(\overline{\phi}_p, \sigma_p\right) = 0 = \sigma_p - \frac{\sigma_\phi}{\sqrt{1 + B(a, b) - [A(a, b)]^2}}, \tag{7.71b}$$

where we have defined A and B as:

$$A\left(a\left(\overline{\phi}_p, \sigma_p\right), b\left(\overline{\phi}_p, \sigma_p\right)\right) = \frac{\omega(a) - \omega(b)}{\Omega(b) - \Omega(a)} \tag{7.72a}$$

$$B\left(a\left(\overline{\phi}_p, \sigma_p\right), b\left(\overline{\phi}_p, \sigma_p\right)\right) = \frac{a\omega(a) - b\omega(b)}{\Omega(b) - \Omega(a)}. \tag{7.72b}$$

We may then iterate on $\overline{\phi}_p$ and σ_p until convergence is achieved; for the n^{th} iteration, the system of updating equations is

$$\begin{bmatrix} \overline{\phi}_{p,n} \\ \sigma_{p,n} \end{bmatrix} = \begin{bmatrix} \overline{\phi}_{p,n-1} \\ \sigma_{p,n-1} \end{bmatrix} - \mathbf{J}_{n-1}^{-1} \begin{bmatrix} f(\overline{\phi}_{p,n-1}, \sigma_{p,n-1}) \\ g(\overline{\phi}_{p,n-1}, \sigma_{p,n-1}) \end{bmatrix}, \tag{7.73}$$

Table 7.7: Jacobian matrix entries for the parent Gaussian distribution iterative scheme.

	y	
	$\overline{\phi}_p$	σ_p
$\frac{\partial f}{\partial y}$	$1+\sigma_p\frac{\partial A}{\partial\overline{\phi}_p}$	$A+\sigma_p\frac{\partial A}{\partial\sigma_p}$
$\frac{\partial g}{\partial y}$	$\frac{\sigma_\phi}{2(1+B-A^2)^{3/2}}\left(\frac{\partial B}{\partial\overline{\phi}_p}-2A\frac{\partial A}{\partial\overline{\phi}_p}\right)$	$1+\frac{\sigma_\phi}{2(1+B-A^2)^{3/2}}\left(\frac{\partial B}{\partial\sigma_p}-2A\frac{\partial A}{\partial\sigma_p}\right)$
$\frac{\partial A}{\partial y}$	$\frac{1}{\sigma_p}\left(B+A^2\right)$	$\frac{1}{\sigma_p}\left(\frac{a^2\omega(a)-b^2\omega(b)}{\Omega(b)-\Omega(a)}+AB\right)$
$\frac{\partial B}{\partial y}$	$\frac{1}{\sigma_p}\left(\frac{(a^2-1)\omega(a)-(b^2-1)\omega(b)}{\Omega(b)-\Omega(a)}+AB\right)$	$\frac{1}{\sigma_p}\left(\frac{(a^2-1)a\omega(a)-(b^2-1)b\omega(b)}{\Omega(b)-\Omega(a)}+B^2\right)$

where $\mathbf{J}_{n-1}$ is the Jacobian matrix of the previous iteration, defined as

$$\mathbf{J}_{n-1}=\begin{bmatrix}\left.\frac{\partial f}{\partial\overline{\phi}_p}\right|_{(\overline{\phi}_{p,n-1},\sigma_{p,n-1})} & \left.\frac{\partial f}{\partial\sigma_p}\right|_{(\overline{\phi}_{p,n-1},\sigma_{p,n-1})}\\ \left.\frac{\partial g}{\partial\overline{\phi}_p}\right|_{(\overline{\phi}_{p,n-1},\sigma_{p,n-1})} & \left.\frac{\partial g}{\partial\sigma_p}\right|_{(\overline{\phi}_{p,n-1},\sigma_{p,n-1})}\end{bmatrix}, \tag{7.74}$$

and the entries of the Jacobian matrix are listed in Table 7.7 for convenience.

We may assess the convergence status of the iterative scheme by comparing the set values $\overline{\phi}=E_f$ and $\sigma_\phi=rE_f$ with the truncated moments computed with Eqs. 7.69a and 7.69b using $\overline{\phi}_{p,n}$ and $\sigma_{p,n}$. Once a prescribed tolerance in the relative error has been satisfied, we declare the iteration process to be complete. In Fig. 7.12a, we demonstrate the effect on the mean of the parent distribution due to the scaling factor of the standard deviation of the truncated Gaussian distribution, r, for varying upper limit energy values, ϕ_u. These results are for a convergence tolerance of 10^{-9}, $\phi_\ell=0$, $\overline{\phi}=180$, and initial guesses of $\overline{\phi}_{p,0}=180$ and $\sigma_{p,0}=180r$. It is apparent that $\overline{\phi}_p$ dramatically decreases over small ranges of r, causing the number of iterations to diverge, as seen in Fig. 7.12b. Also of note, we observe that $\overline{\phi}_p$ approaches an asymptotic value for increasing ϕ_u (the $\phi_u/E_f=5$ and 10 lines are nearly indistinguishable); this is due to the diminishing mass in the higher-ϕ region of the parent distribution, causing a lessening effect on the truncated distribution's profile.

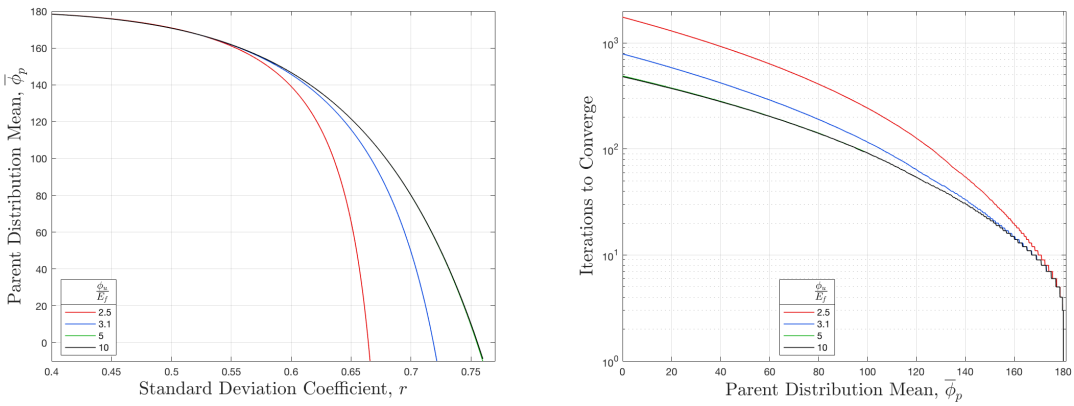

(a) **(b)**

Figure 7.12: (a) Parent Gaussian distribution mean as a function of truncated Gaussian's standard deviation scaling factor, r. (b) The number of iterations required to converge for varying parent distribution mean, where the initial guesses are $\overline{\phi}_{p,0} = E_f$ and $\sigma_{p,0} = rE_f$.

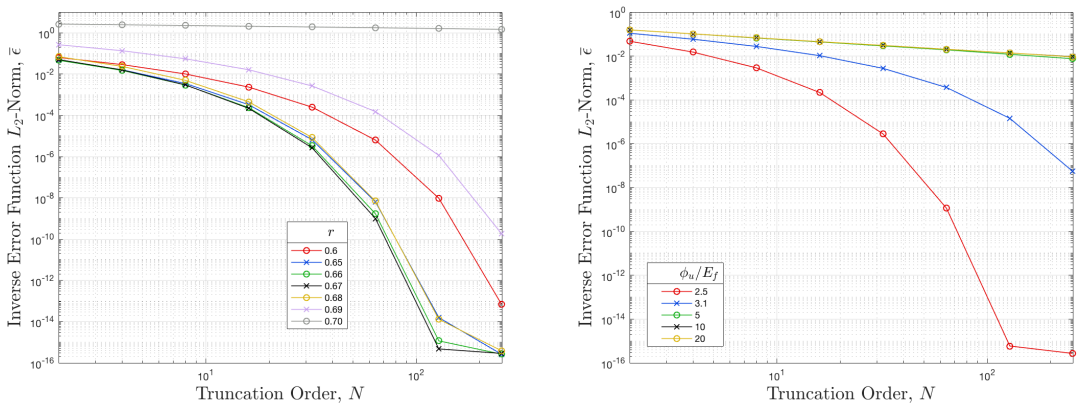

(a) **(b)**

Figure 7.13: L_2-norm error in the approximated inverse error function for (a) the $\phi_u/E_f = 2.5$ case and varying r, and (b) for varying ϕ_u/E_f where $\overline{\phi}_p = 0$.

The second issue concerns the evaluation of the inverse error function in the sampling formula Eq. 7.67, $\text{erf}^{-1}(x)$, for $\{x \in \mathbb{R} | x \in (-1, 1)\}$. It is approximated

using the N-order truncated Maclaurin series:

$$\text{erf}^{-1}(x) = \sum_{k=0}^{N} \frac{c_k}{2k+1} \left(\frac{\sqrt{\pi}}{2} x \right)^{2k+1}, \tag{7.75}$$

where $c_0 = 1$, and

$$c_k = \sum_{m=0}^{k-1} \frac{c_m c_{k-1-m}}{(m+1)(2m+1)}. \tag{7.76}$$

The necessary truncation order may be determined by randomly selecting $\xi \in [0,1]$ and evaluating the argument of erf^{-1} in Eq. 7.67 a total of H times and calculating an L_2 error norm as

$$\varepsilon = \sqrt{\frac{1}{H} \sum_{h=1}^{H} \left(\text{erf}_T^{-1}(\xi_h) - \text{erf}^{-1}(\xi_h) \right)^2}, \tag{7.77}$$

where erf_T^{-1} is the assumed true, accurate calculation, and erf^{-1} is determined by Eq. 7.75. If we then run H simulations a total of B times, we will obtain a distribution of error norms, and that distribution of ε approaches a Gaussian distribution in accordance with the Law of Large Numbers. We then determine the average L_2 error norm, $\overline{\varepsilon}$, from the distribution of B ε values:

$$\overline{\varepsilon} = \frac{1}{B} \sum_{b=1}^{B} \varepsilon_b. \tag{7.78}$$

In Fig. 7.13a, we show $\overline{\varepsilon}$ as a function of the series truncation order, N, for the $\phi_u / E_f = 2.5$ case for $r \in [0.6, 0.7]$, corresponding to the region of strongly varying $\overline{\phi}_p$ (see Fig. 7.12a). These results were obtained for $H = 10^5$, $B = 20$, and erf_T^{-1} was calculated using MATLAB's intrinsic inverse error function. We see that $\overline{\varepsilon}$ drops to the machine precision limit for $N > 100$ and $r = 0.67$, corresponding to $\overline{\phi}_p \to 0^+$, but once $\overline{\phi}_p < 0$, $\overline{\varepsilon}$ quickly diverges. This supports the need to prevent $\overline{\phi}_p$ from taking on negative values.

A final analysis regarding the accuracy of the inverse error function approximation is shown in Fig. 7.13b, where we have chosen to determine the L_2-norm error at

Table 7.8: Neutron multiplicity distributions used.

Method	q_0^f	q_1^f	q_2^f	q_3^f	q_4^f	q_5^f	q_6^f
Full	0.0222	0.200	0.306	0.307	0.136	0.0248	0.0004
Bounded Integer	0.0	0.0	0.575	0.425	0.0	0.0	0.0
Binary Fission	0.0	0.0	1.0	0.0	0.0	0.0	0.0

$\overline{\phi}_p = 0$ for varying upper bounds, ϕ_u. The value of r that provides $\overline{\phi}_p = 0$ was determined by iterating on r_n and $\sigma_{p,n}$ (and setting $\overline{\phi}_p = 0$) from a similar system derived from Eqs. 7.69a and 7.69b, covered in Appendix E. It can be seen that the error saturates for increasing ϕ_u, and to minimize the error, one should reduce ϕ_u. Unfortunately, ϕ_u is a parameter with physical significance, thus reducing it to numbers near or below $\overline{\phi}$ will provide unrealistic distributions. To remain consistent with the maximum energy deposited per fission with $\phi_u = 3.1\overline{\phi}$, we choose to set $N = 200$ to have an L_2 error of $\overline{\epsilon} \approx 3 \cdot 10^{-7}$.

7.4.5 Truncated Gaussian Distribution Results

With the numerical considerations of the Sec. 7.4.4 in mind, we are now prepared to perform Monte Carlo simulations of systems with varying criticality in order to determine the FPDF with an induced fission energy deposition distribution taking the form of a truncated Gaussian distribution. Figure 7.14 shows several truncated Gaussian distributions as determined through Monte Carlo sampling and compared to the analytical distribution, Eq. 7.63, for $\phi_\ell = 0$, $\phi_u = 3.1E_f = 558\ MeV$, and the parent moments are determined using the Newton-Raphson iteration scheme previously discussed.

Figure 7.15a shows the single chain FPDF profiles for a subcritical system with $k = 0.4$, $\overline{\nu} = 2.4245$, and multiplicity data is given in Table 7.8 for the full multiplicity

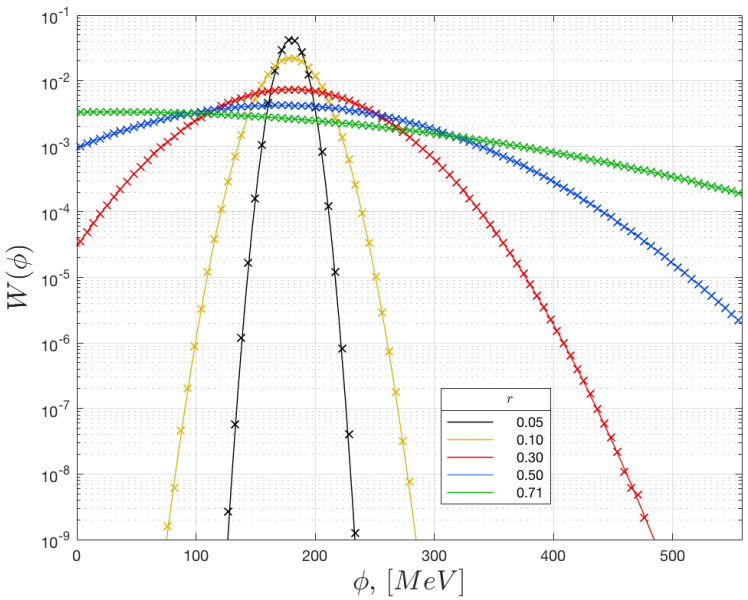

Figure 7.14: The truncated Gaussian energy deposition distribution; analytical (-) and Monte Carlo (x) results.

distribution. We vary the width of $W(\phi)$ by scaling r in $\sigma_\phi = rE_f$. As was observed with the beta distribution for varying values of r, the FPDF displays shoulders for wide deposition distributions corresponding to high values of r, and highly concentrated consecutive peaks for lower r values. In the Monte Carlo simulations, we construct the component distributions of the FPDF for which precisely a single fission, two fissions, or three fissions occurred throughout the history, shown in Fig. 7.15b. For the prominently-peaked FPDF with $r = 0.3$, we see the component distributions centered about integer values of ψ with a positive skew corresponding to the higher energy tail of $W(\phi)$. For the FPDF with $r = 0.71$, because W is more broad, the shoulders appear near the $\psi = \phi_u/E_f = 3.1$- in accordance with a higher frequency of occurrence of the maximum energy deposited in a fission.

Next, we demonstrate the effect of the standard deviation coefficient of the energy deposition distribution, r, for varying system criticality. In the limit of $r \to 0$, we

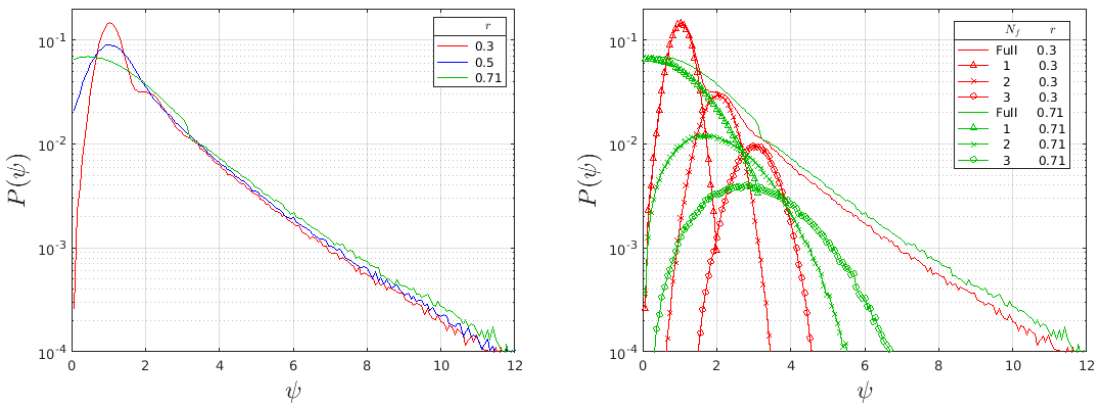

(a) **(b)**

Figure 7.15: The FPDF in a subcritical system ($k = 0.4$) for (a) differing r values and (b) the separation of the FPDF components where precisely $1, 2$, or 3 fissions occur. N_f is the total number of fissions to have occurred.

see from Eqs. 7.68a and 7.68b that the moments of the truncated distribution are $\overline{\phi} = E_f$ and $\sigma_\phi = 0$. For these limits to hold in Eqs. 7.69a and 7.69b, the limits of the moments of the parent Gaussian distribution must be $\overline{\phi}_p = \overline{\phi} = E_f$ and $\sigma_p = 0$ for $r \to 0$. From this, we may determine the limit of $W(\phi)$ as:

$$\begin{aligned}\lim_{r\to 0^+} W(\phi) =& \lim_{\overline{\phi}_p \to E_f} \lim_{\sigma_p \to 0^+} W(\phi) \\ =& 2\left\{\lim_{\sigma_p\to 0^+} \frac{1}{\operatorname{erf}\left(\frac{\phi_u - E_f}{\sqrt{2}\sigma_p}\right) + \operatorname{erf}\left(\frac{|\phi_\ell - E_f|}{\sqrt{2}\sigma_p}\right)}\right\}\left\{\lim_{\sigma_p\to 0^+} \frac{\exp\left(-\frac{\left[\phi - E_f\right]^2}{2\sigma_p^2}\right)}{\sqrt{2\pi\sigma_p^2}}\right\},\end{aligned}$$

where we have enforced that $\phi_\ell < E_f$, which allows us to apply the identity $\operatorname{erf}(-|a|) = -\operatorname{erf}(|a|)$. The first bracketed limit is evaluated using the identity $\lim_{x\to 0} \operatorname{erf}(1/x) = 1$, thus the first limit is equal to $1/2$. The second bracketed limit equals 0 whenever $\phi \neq E_f$, and it equals ∞ when $\phi = E_f$; thus, by also recalling that $W(\phi)$ is normalized, this limit satisfies the criterion of the Dirac delta function as having infinite magnitude at a singular point with unit area. This provides us with the result:

$$\lim_{r\to 0^+} W(\phi) = \delta(\phi - E_f). \tag{7.79}$$

Unfortunately, for what appears to be an intuitively simple-in-form distribution given by Eq. 7.79, there does not appear to be an attainable analytic form of $P(\phi)$ due to the non-invertible expression of the generating function. However, we may still employ the Monte Carlo method to study lumped systems and the consequences of reducing r.

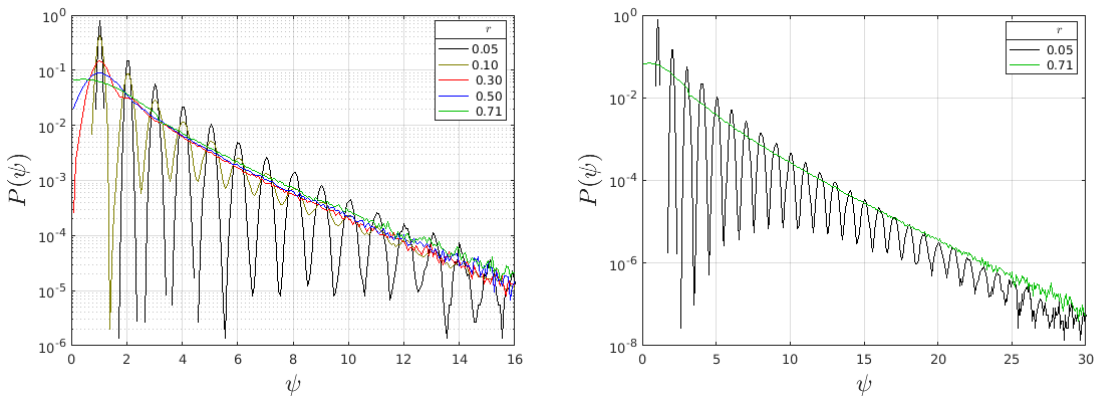

(a) **(b)**

Figure 7.16: The FPDF in a subcritical system ($k = 0.4$) (a) for several differing r values and (b) for $r = 0.05, 0.71$, to demonstrate the separation of the FPDF tails as a function r.

Figure 7.16a shows the FPDF as attained by Monte Carlo simulation of a subcritical system with $k = 0.4$ for a variety of standard deviations of $W(\phi)$. It is clear that the FPDF undergoes a drastic qualitative change in the limit of $r \to 0$, where it can be seen that the energy deposited by successive fissions of a propagating chain become separated to the point they appear to be an array of Dirac delta functions of diminishing magnitude. For the two extremes of $r = 0.05, 0.71$, we show in Fig. 7.16b that the tails of $P(\psi)$ become noticably separate for increasing values of ψ, confirming the intuition that the probability of more cumulative energy being deposited within the system will occur for a more broad $W(\phi)$.

For the near-critical case of $k = 0.98$, where non-divergent fission chain reactions have the potential to persist for uncharacteristically long time periods, we see in Fig.

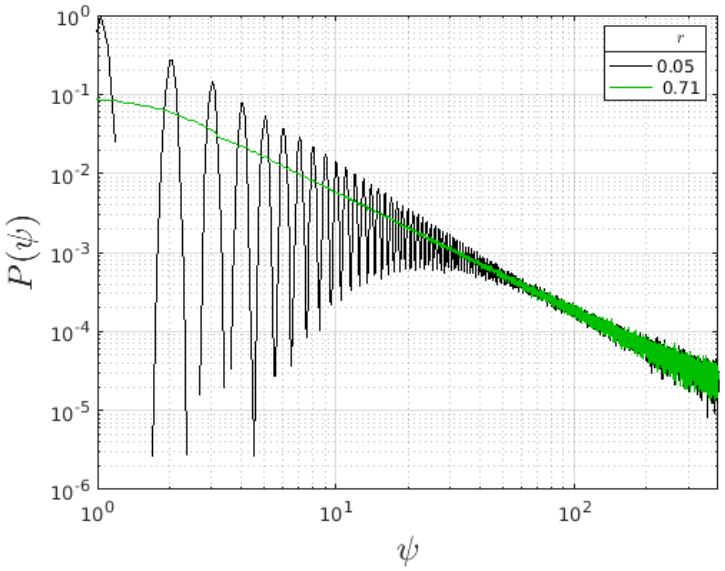

Figure 7.17: Per Fig. 7.16, but for $k = 0.98$ with varying r values.

7.17 that the tail of the FPDF tends to converge regardless r. This is to be expected because the longer-lived chains occur with greater frequency (compared to the $k = 0.4$ case), increasing the average cumulative energy deposited, $\overline{\phi}$, and thus the difference in the tails of the distributions are not apparent for this suite of simulations. It is true, however, that if one were to refine the statistics to this calculation, there would be a clear difference in the distributions at much higher ψ than is currently feasible.

Figure 7.18 shows the FPDF for varying r in a supercritical system with $k = 1.1$. We see that the distributions tend toward a common asymptote. As we saw with the subcritical case, we expect there to be a difference in the higher energy deposition tails, but for supercritical systems this becomes unfeasible to simulate with analog Monte Carlo. The reason for this lack of feasibility is that the supercritical system does not have a steady-state distribution, except for the infinite future where the FPDF has a diverged component and a finite distribution corresponding to the chains that happen to go extinct but still deposit energy when they were propogating. In order to obtain this extinct component, we must run the MC simulation to long

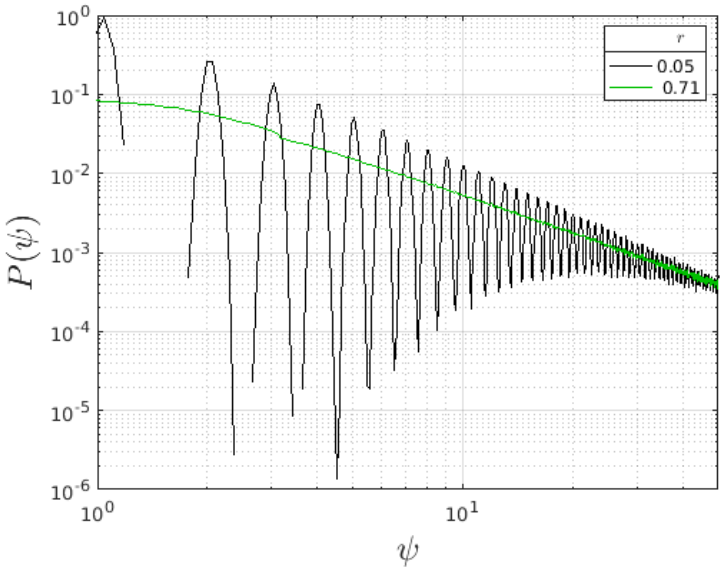

Figure 7.18: Per Fig. 7.16, but for $k = 1.1$ with varying r values.

enough times that we may then discern a diverged chain from an extinct one, this is where the difficulty arises. For the case presented in Fig. 7.18, we could run the MC to longer final times in an attempt to resolve the higher energy tails of the respective FPDFs, or we could increase the multiplication factor to mirror the subcritical case, both of which require more computational power than is available at the time of this writing, but it is expected that we would see a separation of the distributions in either case.

Finally, we wish to compare the FPDF for differing $W(\phi)$, namely the gamma distribution and the truncated Gaussian distribution. We compare the case where both distributions have the same standard deviation (all $W(\phi)$ presented thus far have had the same mean, $E_f = 180\ MeV$). The standard deviation of the gamma distribution is given by $\sigma_\Gamma = \sqrt{2}E_f/2 \approx 0.71E_f$, which by design corresponds to the $r = 0.71$ cases we have considered in this section. Figure 7.19 shows a comparison of the FPDF for the different $W(\phi)$ at several criticality regimes. For the low energy deposition region, we see an expected difference in the FPDF profiles due to the

fact that this region is only affected by the single-fission outcomes, and thus the shape of the FPDF mimics that of W. We immediately witness a convergence of the distributions once we surpass the $\psi = 3.1$ limit of the first fission (recall $\phi_u = 3.1E_f$ for the TG). This behavior suggests that two functionally different energy deposition distributions will produce the same high-energy tails of the FPDF, given those W distributions have the same mean and standard deviation.

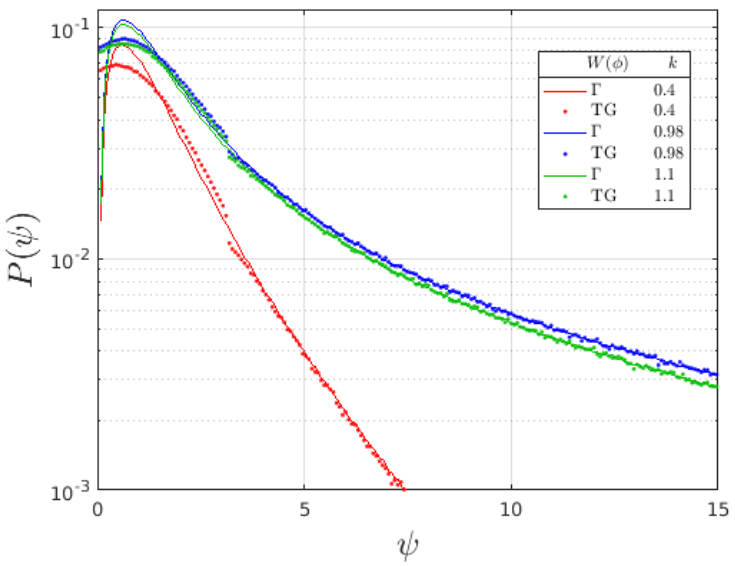

Figure 7.19: Comparison of the FPDF as given by $W(\phi)$ being a gamma distribution (Γ) and a truncated Gaussian distribution (TG) for varying k.

7.5 Effects of the Multiplicity Distribution

The previous analysis has restricted the neutron multiplicity to the binary case. We now consider two less restrictive neutron emission possibilities, introducing an additional element of stochasticity to the problem space. We compare the natural full distribution of ^{238}U taken from [67] for $\overline{\nu} = 2.45$ with the bounded integer sampling method used in the MCNP code [68]. For completion, Table 7.8 displays

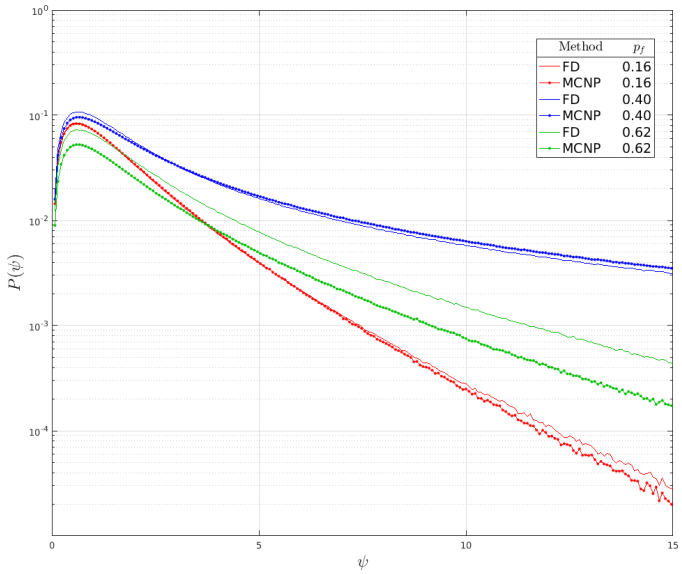

Figure 7.20: The FPDF for $W(\phi)$ being a gamma distribution and comparing the full emission distribution (FD) with the bounded integer emission method.

the multiplicity distributions. With the bounded integer method, the distribution is decided by enforcing there to be either 2 or 3 neutrons emitted per induced fission event and the probabilities are then determined via the first two moments of the multiplicity distribution, i.e.,

$$1 = q_2^f + q_3^f \tag{7.80a}$$

$$\overline{\nu} = 2q_2^f + 3q_3^f. \tag{7.80b}$$

Solving the system of Eq. 7.80 results in the probabilities seen in Table 7.8. It is expected that the PDFs produced will differ from the BFM analytical solution, and we do not show a comparison. In Fig. 7.20, we show for the case where $W(\phi)$ is a gamma distribution and several differing fission probabilities of $p_f = [0.16, 0.40, 0.62]$, corresponding to multiplication factors of $k = [0.392, 0.98, 1.519]$, respectively. It is clear that the system criticality has an effect on the PDF produced depending on the multiplicity model employed. For the highly subcritical case, the lines begin to

show non-negligible separation for $\psi > 10$, where the neutron muliplets emerging from the full distribution simulation cause a greater deposition of energy into the system. For the highly supercritical case, the separation of the lines is immediate and dramatic, showing how the bounded integer method is wholly insufficient in modeling such a stochastic system. This is to be expected, as the bounded integer method preserves only the first two moments of the multiplicity distribution and any underlying randomness of a given fission event is neglected. This is not as important in the near-critical case, where the branches of the fission chain are not as crucial to the behavior of the energy deposition distribution, and the mean tends to dominate the higher order moments. A final observation concerns the runtime of these simulations, where the bounded integer method took, on average, twice as long to complete. This is due to the fact that the bounded integer method must simulate an additional two or three neutrons for every fission event while the full distribution has the opportunity to simulate more lesser-emitting fission events, causing the simulation to be substantially less costly. With these observations, it is recommended that a consideration of the full distribution is tantamount in attaining the true FPDF, with the added benefit of computational efficiency as compared to the bounded integer method.

7.6 Lumped Results of the FPDF with a Source

Up to this point, we have only considered the probability distributions of the cumulative energy deposition from a single neutron chain reaction. This has its usefulness in that one may assess the safety regime a particular system exists within, and if a single neutron chain has the potential of diverging, precautions must be engineered into place to prevent such circumstances. A more realistic situation actually involves systems which contain randomly emitting sources which, primarily, are intrinsic to the multiplying medium itself. In this section, we consider lumped geometry systems

Table 7.9: Some parameters and data for the source simulations.

k	t_f	τ $[ns]$	$\chi_2' \cdot 10^{-8}$ $[s^{-1}]$	$Q(0)$ with $S = \cdots$ $[s^{-1}]$		
				10^2	10^4	10^6
0.40	60τ	4.4469	1.7441	0.9999734	0.9973379	0.7658057
0.98	30τ	3.1815	5.9498	0.9999905	0.9990476	0.9089590
1.10	30τ	2.9012	7.3777	0.9999913	0.9991313	0.9166428

with sources of strength S, defined as the probability per unit time that a source event will occur. From any given event, a stochastic amount of energy is deposited as well as an emission of a random set of neutron multiplets, each one then propagating their own branches of the chain reaction. From this, it is clear why we began our investigation of the single chain to develop an intuition of multifold chain behavior.

As we are interested in the cumulative energy deposited, we may sample from the source energy deposition distribution, $W_S(\phi)$, before following the neutrons emitted from the collection of source events. Upon accumulating the fission energy deposited from the source events, the simulation of each source fission chain proceeds in a typical manner, where we accumulate the induced fission energy that is deposited within the system. We continue our analysis of a ^{238}U system with the spontaneous fission multiplicity distribution taken from [69], which has the first two moments: $\overline{\nu}_S = 2.1538$ and $\overline{\nu_S^2} = 5.9450$. Figure 7.21 displays the FPDF due to the presence of a source, $Q(\psi)$, for several source strengths and multiplication factors. We set $W(\phi)$ and $W_S(\phi)$ to be gamma distributions for both induced fission and spontaneous fission, each with $E_f = 180\ MeV$, and some other quantities are displayed in Table 7.9.

For the $S = 10^2\ 1/s$ cases for each k, we ran 10^{10} total histories to resolve such low-probability distributions out to t_f; note that the majority of the probability mass is contained in the singular $Q(\psi = 0)$ value (shown in Table 7.9) corresponding to simulations where no source events occur. For the $S = 10^4$, $10^6\ 1/s$ cases, 10^9 total histories were performed. As the source strength increases, corresponding to an

increase in the probability of source events occurring per unit time, the distributions increase in magnitude equivalent to the increase in the magnitude of the source strength, as seen in Fig. 7.21. For the $k = 1.1$ case, we would expect the tails to decrease in magnitude if we simulated the system to a later final time, this would be due to the increase in chains that have reached the divergence criteria, which we have set to be 10^5 neutrons per chain, which would then not contribute to the finite ψ portion of the distribution.

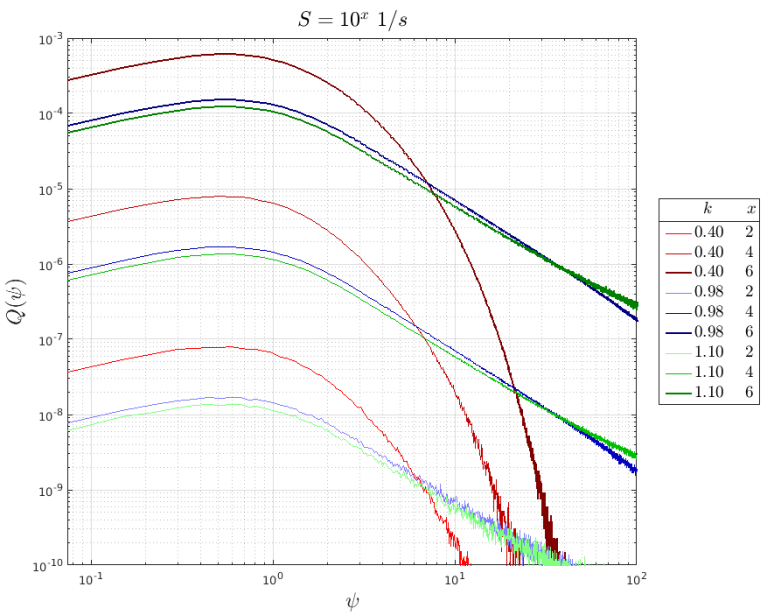

Figure 7.21: The FPDF in the presence of a source for systems of varying criticality. Here, x determines the magnitude of S, such that $S = 10^x\ 1/s$.

As was observed by Prinja and Souto, the neutron number probability distribution in the presence of a source, P_n, will transition from a monotonically decreasing distribution to a unimodal distribution as the source strength is increased [11, 12]. This transition may be quantified by the magnitude of Bell's η parameter (originating in [3]), defined as

$$\eta = \frac{2S}{\chi_2'} = \frac{2S}{\lambda_f \left(\overline{\nu^2} - \overline{\nu}\right)}, \tag{7.81}$$

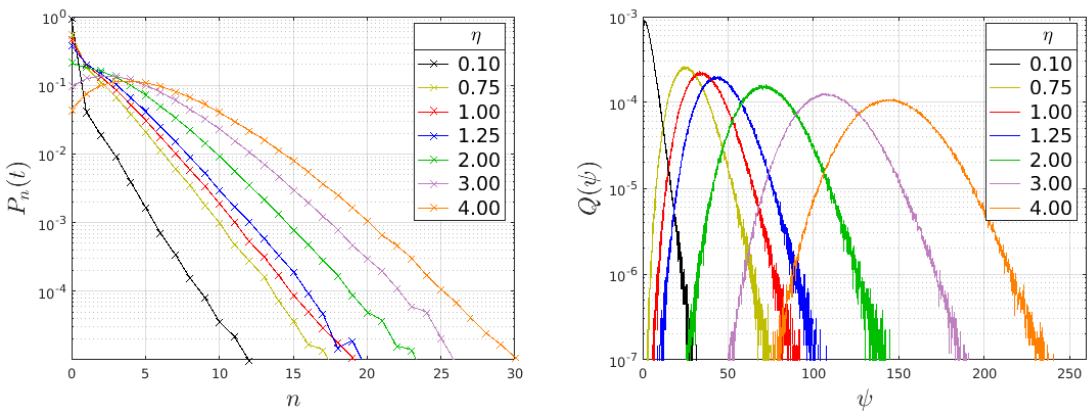

(a) **(b)**

Figure 7.22: In the presence of a constant randomly emitting source, (a) the neutron number distribution as it transitions from a stochastic to a deterministic system and (b) the accompanying FPDFs.

where $\lambda_f = p_f/\tau$ is the induced fission reaction rate and $p_f = k/\overline{\nu}$ is the probability of fission. We see, then, that for a set material and criticality, η is only a function of S. Prinja and Souto observed that the aforementioned transition occurs when $\eta < 1 \rightarrow \eta > 1$, corresponding to a transition of the neutron number distribution from a stochastic quantity to a deterministic one. Every line in Fig. 7.21 pertains to a source that is too weak to make $\eta > 1$, thus these systems are still behaving stochastically with regards to the neutron number distribution.

For the $k = 0.4$ example, we have $\chi_2' = 1.7441 \cdot 10^8$ $1/s$, and from this $\eta = 1.1467 \cdot 10^{-8} \cdot S$. If we then select source strengths such that we may set η to values near unity, we may study the effects of the FPDF with a source as the neutron number distribution undergoes its transition. Figure 7.22 shows the neutron number distribution undergoing this change for increasing η, and the accompanying FPDFs. Although the FPDF in the presence of a source (and the single chain FPDF, for that matter) is always a unimodal distribution for $\psi \neq 0$ for the $W(\phi)$ we have studied, we see that the transition from $\eta < 1 \rightarrow \eta > 1$ corresponds to the $Q(\psi = 0) \rightarrow 0$ and

thus the distribution 'flattens' as the mass motivates toward $\psi = \infty$.

We next contrast the single chain FPDF, $P(\psi)$, with the source FPDF, $Q(\psi)$, for the case where the neutron number distribution in the presence of a source is stochastic as well as deterministic. Figure 7.23 shows the single chain FPDF superimposed onto Fig. 7.22b, illustrating the vast difference in energy deposition for the $k = 0.4$ system. This result implies that, even if a system has low multiplication properties, if a source in strength enough, there may still be a significant amount of energy deposited within the system in a relatively short time. Figures 7.24 and 7.25 show the same contrast, but for the $k = 0.98$ and $k = 1.10$ systems. In these higher k simulations, we increased the cumulative energy cutoff from 10^5 MeV up to 10^6 MeV in order to capture the breadth of these distributions. The single chain distributions were run to 10^8 histories, while all the source distributions were run to 10^7 histories.

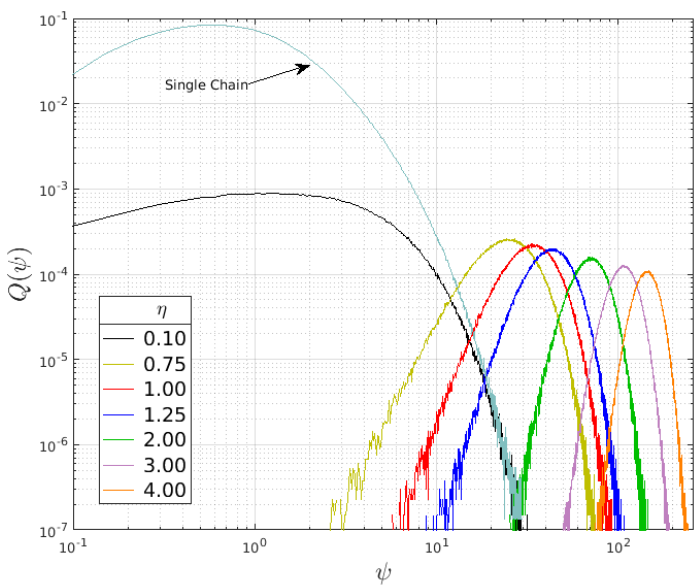

Figure 7.23: Comparison of $P(\psi)$ with differing $Q(\psi)$ for a $k = 0.4$ system.

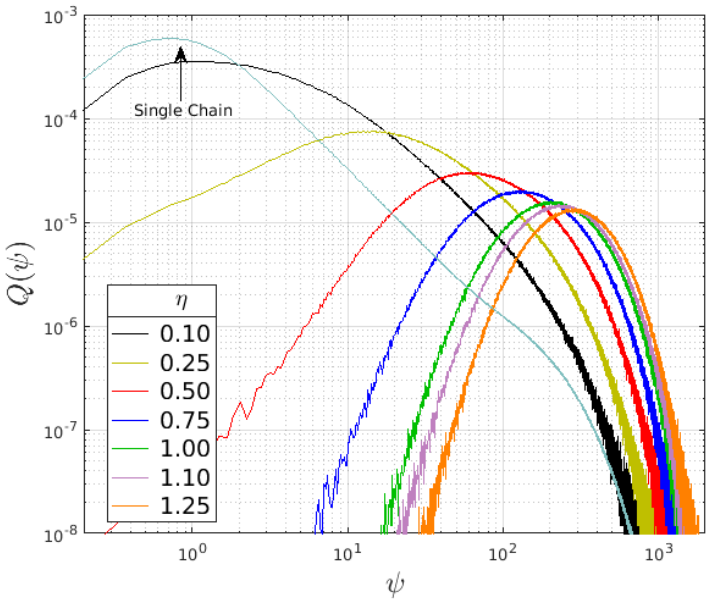

Figure 7.24: As for Fig. 7.23 but for a $k = 0.98$ system.

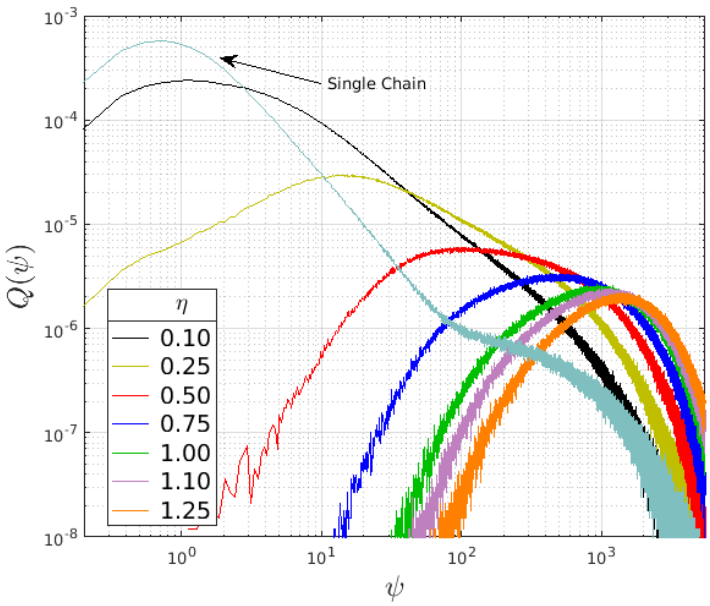

Figure 7.25: As for Fig. 7.23 but for a $k = 1.10$ system.

Chapter 8

The Boltzmann Master Equation Formulation

The topics and methods that have been discussed in this document allow us to now introduce recent research that permit one to obtain, in principle, the neutron number distribution in unlumped (full phase-space) systems. In short, this is accomplished by treating the neutron population as a continuous variable and thus the discrete probability distribution function becomes a continuous probability density function in n; for example, in the lumped setting, the transition is made: $P_n(t) \to P(n,t)\,\mathrm{d}n$. The presented methodology circumvents the traditional difficulties in obtaining the full distribution, whether it be by propagated error through numerical inversion of the generating function solution [40] or cumbersome and labor-intensive numerical solution of the set of coupled Master equations investigated by Saxby et. al [41].

We show a derivation of the equations for the single neutron chain and the separate equations with intrinsic sources for the PDFs. We then show a reduction to point models so as to demonstrate preliminary work that has been completed and benchmarked against Monte Carlo and analytical lumped model equations. As it stands, this chapter proves inconclusive in our attempt at treating the neutron

number as a phase-space variable and thus allowing us to perform standard numerical discretization schemes on n to quickly obtain the number distribution. In that sense, the reader should interpret this chapter as a laying of the groundwork of this novel formulation and, in that vain, there are many future work aspects worth pursuing which we will discuss in Chapter 9.

8.1 Derivation of the Principle Equations

We begin this section by reminding the reader of the Pál-Bell equation, derived in Chapter 5, whose solution is $P_n(\mathcal{R}, t_f|\vec{r}, \hat{\Omega}, t)$: the probability of there being n neutrons in $\mathcal{R}$, a subvolume of $(\vec{r}, \hat{\Omega})$, at a final time of observation t_f due to the appearance of a single neutron at the location $\vec{r}$ moving in direction $\hat{\Omega}$ at an earlier time $t < t_f$:

$$\begin{aligned} P_n\left(\mathcal{R}, t_f|\vec{r}, \hat{\Omega}, t\right) = &\int_0^{\ell(s_b,s_t)} \mathrm{d}s\Sigma_t\left(\vec{r}+s\hat{\Omega}, t+\frac{s}{v}\right) \mathrm{e}^{-\int_0^s \mathrm{d}s'\Sigma_t\left(\vec{r}+s'\hat{\Omega}, t+\frac{s'}{v}\right)} \Bigg[\\ &+\sum_{\nu=0}^{\nu_m^f} c_\nu\left(\vec{r}+s\hat{\Omega}, t+\frac{s}{v}\right) \sum_{n_1+\cdots+n_\nu=n} \prod_{k=1}^{\nu} \int_{4\pi} \frac{\mathrm{d}\Omega_k}{4\pi} P_{n_k}\left(\mathcal{R}, t_f|\vec{r}+s\hat{\Omega}, \hat{\Omega}_k, t+\frac{s}{v}\right) \Bigg] \\ &+\sum_{j=1}^{3} A_j, \end{aligned} \tag{8.1}$$

where the A_j terms account for the possibility that the neutron does not interact with the material before leaving the system or before time t_f, defined by Eq. 5.2. Next, we introduce the discrete moment generating function (DMGF),

$$M_d(z, \mathcal{R}, t_f|\vec{r}, \hat{\Omega}, t) = \sum_{n=0}^{\infty} e^{-nz} P_n(\mathcal{R}, t_f|\vec{r}, \hat{\Omega}, t), \tag{8.2}$$

with the aim of applying it to Eq. 8.1. In doing so, and then taking the difference between $M_d(z|\vec{r}+\Delta s\hat{\Omega}, \hat{\Omega}, t+\Delta s/v) - M_d(z|\vec{r}, \hat{\Omega}, t)$ and take the limit as $\Delta s \to 0$, we find a nonlinear partial differential equation describing the behavior of M_d near

the point $\vec{r}$. If we now assume that the neutron population is large enough such that the discrete neutron number variable may be treated as a continuous variable, we may make the conversion from a discrete PDF to a probability density function:

$$P_n(\mathcal{R}, t_f|\vec{r}, \hat{\Omega}, t) \rightarrow P(n, \mathcal{R}, t_f|\vec{r}, \hat{\Omega}, t)\,\mathrm{d}n, \tag{8.3}$$

then we may simultaneously convert the DMGF from a summation over n into a continuous moment generating function (CMGF), M_c, defined as:

$$\begin{aligned} M_c(z, \mathcal{R}, t_f|\vec{r}, \hat{\Omega}, t) &= \int_0^\infty \mathrm{d}n e^{-nz} P(\mathcal{R}, t_f, n|\vec{r}, \hat{\Omega}, t), \\ &= \mathcal{L}_{n\rightarrow z}\{P(\mathcal{R}, t_f, n|\vec{r}, \hat{\Omega}, t)\}, \end{aligned} \tag{8.4}$$

which we immediately recognize as the Laplace Transform of $P(n)$. We may formally obtain $P(n)$ by the inverse Laplace Transform of the CMGF as

$$P(n) = \mathcal{L}^{-1}_{z\rightarrow n}\{M_c(z)\}. \tag{8.5}$$

Further, it proves expedient and favorable in obtaining numerical and analytical solutions to define the complementary CMGF:

$$\mathcal{M}_c(z, \mathcal{R}, t_f|\vec{r}, \hat{\Omega}, t) = 1 - M_c(z, \mathcal{R}, t_f|\vec{r}, \hat{\Omega}, t), \tag{8.6}$$

and, upon applying the inverse Laplace Transform to Eq. 8.6, we find a quantity henceforth referred to as the neutron number PDF pseudo-density:

$$\widetilde{P}(n, \mathcal{R}, t_f|\vec{r}, \hat{\Omega}, t) = \delta(n) - P(n, \mathcal{R}, t_f|\vec{r}, \hat{\Omega}, t). \tag{8.7}$$

Equation 8.7 provides an identity to obtain $P(n)$ given the pseudo-density is known. By applying the inverse Laplace Transform to the PDE satisfied by $\mathcal{M}_c$, an equation satisfied by the pseudo-density is obtained:

$$\begin{aligned} \left[-\frac{1}{v}\frac{\partial}{\partial t} - \hat{\Omega}\cdot\vec{\nabla} + \Sigma_t(\vec{r}, t)\right]\widetilde{P}(n|\vec{r}, \hat{\Omega}, t) &= \Big(\Sigma_s(\vec{r}, t) + \overline{\nu}\Sigma_f(\vec{r}, t)\Big)\int_{4\pi}\frac{\mathrm{d}\Omega'}{4\pi}\widetilde{P}(n|\vec{r}, \hat{\Omega}', t) \\ &\quad - \Sigma_f(\vec{r}, t)\sum_{j=2}^{J}\frac{(-1)^j\chi_j(\vec{r})}{j!}\left[\int_{4\pi}\frac{\mathrm{d}\Omega'}{4\pi}\widetilde{P}(n|\vec{r}, \hat{\Omega}', t)\right]^{\circledast j-1} \end{aligned}$$

(8.8)

where we have suppressed the explicit dependence on $\mathcal{R}$ and t_f and the j-way autoconvolution operator is defined as [71]:

$$\left[\widetilde{P}(n)\right]^{\circledast j} = \int_0^n \mathrm{d}n_j \widetilde{P}(n_j) \int_0^{n-n_j} \mathrm{d}n_{j-1} \widetilde{P}(n_{j-1}) \cdots \\ \cdots \int_0^{n-\sum_{k=2}^{j} n_k} \mathrm{d}n_1 \widetilde{P}\left(n - \sum_{k=1}^{j} n_k\right) \widetilde{P}(n_1). \tag{8.9}$$

The final condition for Eq. 8.8 is

$$\lim_{t_f \leftarrow t} \widetilde{P}(n, \mathcal{R}, t_f | \vec{r}, \hat{\Omega}, t) = \delta(n) - \delta(n-1) \quad \text{for } \vec{r}, \hat{\Omega} \in \mathcal{R} \tag{8.10}$$

and the boundary condition is given by

$$\widetilde{P}(n, \mathcal{R}, t_f | \vec{r}, \hat{\Omega}, t) = 0 \quad \text{for } \vec{r} \in \partial V, \hat{n}_b \cdot \hat{\Omega} > 0, \tag{8.11}$$

where ∂V is the convex surface of the system and $\hat{n}_b$ is the corresponding unit surface normal vector.

Of significance is that in Eq. 8.8 we have an equation for the pseudo-density wherein the neutron number appears as a continuous independent variable in the range $0 < n < 1$. This equation inherits features of the moment generating function equation but crucially it is in "real" space form with respect to the neutron number n that make direct numerical computation feasible. This is in contrast to the moment generating function equation with its dependence on an unphysical transform variable that must be continued into the complex plane and relying on numerical inversion techniques for its solution. Equation 8.8 is a novel nonlinear transport equation (in adjoint form) with the phase-space extended to contain the neutron number and the branching process represented explicitly through convolutions of the pseudo-density. As such, standard numerical and other approximation techniques for solving the linear transport equation can be adapted to solve Eq. 8.8 for the pseudo-density, with the true PDF obtained from Eq. 8.7. Finally, in view of the connection to the underlying

Master equation and the similarity to a transport equation, we refer to Eq. 8.8 as the Boltzmann Master Equation or BME. Generalizing the BME to include energy dependence would not change the functional form of Eq. 8.8, as the linear adjoint operators for scattering and fission would simply adopt their customary general forms [51], while the autoconvolution terms would, in addition to the angle integral, include an energy integral weighted by the fission energy spectrum.

In the next section, we simplify the form of the BME by applying the Quadratic Approximation to the nonlinear autoconvolution terms, but first we present the auxiliary equations for the number distribution in the presence of a neutron source.

We now consider the auxiliary equation for a system with an intrinsic randomly emitting source. Let $\Theta_n(t_f|t_o)$ be the probability that n neutrons exist within the system at time t_f due to the introduction of a volumetric source, $S(\vec{r},t_o)$, at some earlier time t_o. Allowing for separability of the source, $S(\vec{r},t_o)=\omega(\vec{r})\mathcal{S}(t_o)$, with $\int_V \mathrm{d}\vec{r}\omega(\vec{r})=1$, it can be shown that $\Theta_n(t_f|t_o)$ satisfies the partial differential equation:

$$-\frac{\partial\Theta_n(t_f|t_o)}{\partial t_o}=-\mathcal{S}(t_o)\Theta_n(t_f|t_o)+\mathcal{S}\sum_{k=1}^{\nu_m^{\mathcal{S}}}\int_V \mathrm{d}\vec{r}\omega(\vec{r})q_k^{\mathcal{S}}(\vec{r})\Bigg\{ \sum_{n_1+\ldots+n_k+m_k=n}\Theta_{m_k}(t_f|t_o)\prod_{j=1}^{k}\left[\int_{4\pi}\frac{\mathrm{d}\Omega'}{4\pi}P_{n_j}(\mathcal{R},t_f|\vec{r},\hat{\Omega},t_o)\right]\Bigg\}, \tag{8.12}$$

with final condition $\lim_{t_f\leftarrow t_o}\Theta_n(t_f|t_o)=\delta_{n,0}$.

We proceed by defining the discrete moment generating function for the source case as

$$M_d^{\mathcal{S}}(z,t_f|t_o)=\sum_{n=0}^{\infty}e^{-nz}\Theta_n(t_f|t_o), \tag{8.13}$$

which we may apply to Eq. 8.12. We now elect to convert the discrete generating function transform into a continuous one by treating P_n and Θ_n as probability density functions; then, $\Theta_n\rightarrow\Theta(n)\,\mathrm{d}n$, and we write the continuous moment generating

function transform as

$$\begin{aligned}\mathcal{M}_c^{\mathcal{S}}(z,t_f|t_o) &= \int_0^\infty \mathrm{d}n e^{-nx}\Theta(n,t_f|t_o),\\ &= \mathcal{L}_{n\to z}\{\Theta(n,t_f|t_o)\}\end{aligned} \tag{8.14}$$

where it is immediately clear that this definition has the form of the Laplace transform, and we use the formal shorthand as before. This provides a means of determining the continuous PDFs by inverting the Laplace transform:

$$\Theta(n,t_f|t_o) = \mathcal{L}_{z\to n}^{-1}\{\mathcal{M}_c^{\mathcal{S}}(z,t_f|t_o)\}. \tag{8.15}$$

We ultimately find

$$\begin{aligned}-\frac{\partial\Theta(n,t_f|t_o)}{\partial t_o} =& -\mathcal{S}(t_o)\Theta(n,t_f|t_o) + \mathcal{S}(t_o)\sum_{k=1}^{\nu_m^{\mathcal{S}}}\int_V \mathrm{d}\vec{r}\omega(\vec{r})q_k^{\mathcal{S}}(\vec{r})\Bigg\{\\ &\Theta(n,t_f|t_o) * \Big[\int_{4\pi}\frac{\mathrm{d}\Omega'}{4\pi}P(n,t_f|\vec{r},\hat{\Omega}',t_o)\Big]^{\circledast k-1}\Bigg\},\end{aligned} \tag{8.16}$$

with final condition $\lim_{t_f\leftarrow t_o}\Theta(n,t_f|t_o) = \delta(n)$; this is consistent with the discrete PDF's final condition, being that there are zero neutrons in the system if the observation time, t_f, is also the time the source is introduced into the system. We note that the solution convolved with the j-way autoconvolution is defined as

$$\begin{aligned}\Theta(n) * \Big[P(n)\Big]^{\circledast j-1} =& \int_0^n \mathrm{d}n_j P(n_j)\int_0^{n-n_j}\mathrm{d}n_{j-1}P(n_{j-1})\cdots\\ &\cdots\int_0^{n-\sum_{k=2}^{j}n_k}\mathrm{d}n_1 P\left(n-\sum_{k=1}^{j}n_k\right)\Theta(n_1).\end{aligned} \tag{8.17}$$

By convention, we may only be concerned with a singlet emitting neutron source, such that $q_\nu^{\mathcal{S}} = \delta_{\nu,1}$, and Eq. 8.16 reduces to

$$\begin{aligned}-\frac{\partial\Theta(n,t_f|t_o)}{\partial t_o} =& -\mathcal{S}\Theta(n,t_f|t_o)\\ &+\mathcal{S}\int_0^n \mathrm{d}n'\Theta(n',t_f|t_o)\int_V\mathrm{d}\vec{r}\omega(\vec{r})\int_{4\pi}\frac{\mathrm{d}\Omega'}{4\pi}P(n-n',t_f|\vec{r},\hat{\Omega}',t_o).\end{aligned} \tag{8.18}$$

We will consider Eq. 8.18 in the following sections where we present a discretization framework for numerically solving Eqs. 8.29 and 8.18.

8.1.1 The Quadratic Approximation

Assuming that the Quadratic Approximation holds, we truncate the nonlinear terms at second order and Eq. 8.8 simplifies to

$$-\frac{1}{v}\frac{\partial \widetilde{P}}{\partial t} - \hat{\Omega}\cdot\vec{\nabla}\widetilde{P} + \Sigma_t \widetilde{P}(n|\vec{r},\hat{\Omega},t) = \Big(\Sigma_s + \overline{\nu}\Sigma_f\Big)\widetilde{P}_o(n|\vec{r},t) - \frac{\Sigma_f \chi_2}{2}\int_0^n \mathrm{d}n' \widetilde{P}_o(n-n'|\vec{r},t)\widetilde{P}_o(n'|\vec{r},t), \tag{8.19}$$

where $\widetilde{P}_o(n|\vec{r},t) = \int_{4\pi}\mathrm{d}\Omega' \widetilde{P}(n|\vec{r},\hat{\Omega}',t)/4\pi$ and the final and boundary conditions are given by Eqs. 8.10 and 8.11.

By now introducing the decomposition of $\widetilde{P}$ into a singularity appended with a continuous function of n:

$$\widetilde{P}(n,\mathcal{R},t_f|\vec{r},\hat{\Omega},t) = \gamma(\mathcal{R},t_f|\vec{r},\hat{\Omega},t)\delta(n) - Q(n,\mathcal{R},t_f|\vec{r},\hat{\Omega},t), \tag{8.20}$$

it can be shown that by inserting Eq. 8.20 into Eq. 8.8, we have two nonlinear adjoint equations for γ and Q:

$$\left[-\frac{1}{v}\frac{\partial}{\partial t} - \hat{\Omega}\cdot\vec{\nabla} + \Sigma_t\right]\gamma(\vec{r},\hat{\Omega},t) = \Big(\Sigma_s + \overline{\nu}\Sigma_f\Big)\gamma_o(\vec{r},t) - \frac{\Sigma_f\chi_2}{2}\Big[\gamma_o(\vec{r},t)\Big]^2, \tag{8.21}$$

and

$$\left[-\frac{1}{v}\frac{\partial}{\partial t} - \hat{\Omega}\cdot\vec{\nabla} + \Sigma_t\right]Q(n|\vec{r},\hat{\Omega},t) = \Big(\Sigma_s + \overline{\nu}\Sigma_f\Big)Q_o(n|\vec{r},t) - \Sigma_f\chi_2\gamma_o(\vec{r},t)Q_o(n|\vec{r},t) + \frac{\Sigma_f\chi_2}{2}\int_0^n \mathrm{d}n' Q_o(n-n'|\vec{r},t)Q_o(n'|\vec{r},t), \tag{8.22}$$

where $\gamma_o(\vec{r},t) = \int_{4\pi}\mathrm{d}\Omega\gamma(\vec{r},\hat{\Omega},t)/4\pi$, and $Q_o(n|\vec{r},t) = \int_{4\pi}\mathrm{d}\Omega Q(n|\vec{r},\hat{\Omega},t)/4\pi$. The final conditions are $\lim_{t_f\leftarrow t}\gamma(\vec{r},\hat{\Omega},t) = 1$, and $\lim_{t_f\leftarrow t} Q(n|\vec{r},\hat{\Omega},t) = \delta(n-1)$ and the boundary conditions are both 0 for $\vec{r}\in\partial V$, $\hat{n}_b\cdot\hat{\Omega} > 0$.

It can be shown that the quantity γ is equivalent to the survival probability, P_S, to which we dedicated much effort in determining in Chapter 6. Thus, in order

to determine the full neutron distribution, we must solve the survival probability equation and then supplement that solution into the determining the remainder of the distribution contained within the quantity Q. Similarly, equations are obtained for the source as is common in literature, which are functions of the solution $\widetilde{P}$.

Once the the survival probability and the quantity related to the extant population distribution, γ and Q, respectively, are obtained we may determine the neutron number PDF as

$$P(n|\vec{r},\hat{\Omega},t) = \Big[1-\gamma(\vec{r},\hat{\Omega},t)\Big]\delta(n) + Q(n|\vec{r},\hat{\Omega},t), \tag{8.23}$$

where it is clear that $1-\gamma = P(0)$ is the extinction probability, and $P(0)\delta(n)$ only contributes in the realization of the limit as $n \to 0$, thus $Q(n=0)=0$ for all time. Integrating Eq. 8.23 over all n and enforcing normalization on P yields

$$\int_0^\infty \mathrm{d}n P(n|\vec{r},\hat{\Omega},t) = 1 = 1-\gamma(\vec{r},\hat{\Omega},t) + \int_0^\infty \mathrm{d}n Q(n|\vec{r},\hat{\Omega},t),$$

from which we prove that Q is normalized to the survival probability:

$$\int_0^\infty \mathrm{d}n Q(n|\vec{r},\hat{\Omega},t) = \gamma(\vec{r},\hat{\Omega},t). \tag{8.24}$$

From Eq. 8.24, it is clear that Q gives the unnormalized neutron number PDF for the finite but non-extinct portion of the particle population. The condition Eq. 8.24 is easily confirmed by integrating Eq. 8.22 over all n, which reduces to Eq. 8.21, as does the final condition.

In the next section, we consider lumped systems to aide in our numerical investigation of the convolution integral of Eq. 8.22, which is the only term in the equation which contains explicit dependence on n.

8.2 Lumped Equations Considered

We now consider the lumped description of the neutron number PDF for the single neutron chain with the Quadratic Approximation applied as well as for the case when a random source is present. Lumped equations are easily obtained by striking the streaming operator from Eqs. 8.21 and 8.22 for the survival probability and the extant number distribution. Further, by assuming the reactivity is constant, then the probability density is time-translation invariant and we apply the change in variables $t \to -t$. With some rearranging, the lumped equation may be written in a forward-in-time setting as

$$\frac{\partial Q}{\partial t} = -\left[\alpha - \frac{\chi_2 p_f}{\tau}\gamma(t)\right] Q(n|t) + \frac{\chi_2 p_f}{2\tau}\int_0^n \mathrm{d}n' Q(n-n'|t)Q(n'|t), \tag{8.25}$$

with the initial condition $Q(n|0) = \delta(n-1)$, and the lumped equation for the survival probability satisfies the initial value problem

$$\frac{\partial \gamma}{\partial t} = \alpha\gamma(t) - \frac{\chi_2 p_f}{2\tau}\Big[\gamma(t)\Big]^2, \tag{8.26}$$

with initial condition $\gamma(0) = 1$. Recognizing the POI for lumped systems is $\lim_{t\to\infty}\gamma(t) = p_\infty = 2\alpha\tau/(\chi_2 p_f)$, the survival probability equation may be simplified to

$$\frac{\partial \gamma}{\partial t} = \alpha\gamma(t) - \frac{\alpha}{p_\infty}[\gamma(t)]^2, \tag{8.27}$$

with initial condition , which has the solution:

$$\gamma(t) = P_S(t) = \frac{e^{\alpha t}}{1 + \frac{1}{p_\infty}\Big(e^{\alpha t} - 1\Big)}. \tag{8.28}$$

We may also write Eq. 8.25 more compactly as

$$\frac{\partial Q(n|t)}{\partial t} = -\frac{\hat{\alpha}(t)}{p_\infty}Q(n|t) + \frac{\alpha}{p_\infty}\int_0^n \mathrm{d}n' Q(n'|t)Q(n-n'|t), \tag{8.29}$$

where $[n,t] \in (0,N] \times [0,t_f]$, and the time-dependent coefficient is

$$\hat{\alpha}(t) = \alpha\left(2\gamma(t) - p_\infty\right) = \alpha\left(2P_S(t) - p_\infty\right). \tag{8.30}$$

The lumped equation for the source distribution is attained from Eq. 8.18 by pulling $P(n)$ out of the volume and angle integrals (for which $\int_V \mathrm{d}\vec{r}\omega(\vec{r}) = 1$) to find:

$$-\frac{\partial\Theta(n,t_f|t_o)}{\partial t_o} = -\mathcal{S}\Theta(n,t_f|t_o) + \mathcal{S}\int_0^n \mathrm{d}n'\Theta(n',t_f|t_o)P(n-n',t_f|t_o). \tag{8.31}$$

By now inserting Eq. 8.23 ($P(n) = \gamma\delta(n) + Q(n)$) into Eq. 8.31, we find:

$$-\frac{\partial\Theta(n,t_f|t_o)}{\partial t_o} = -\mathcal{S}\gamma(t_f|t_o)\Theta(n,t_f|t_o) + \mathcal{S}\int_0^n \mathrm{d}n'\Theta(n',t_f|t_o)Q(n-n',t_f|t_o), \tag{8.32}$$

which has the final condition: $\lim_{t_f \leftarrow t_o}\Theta(n|t_f|t_o) = \delta(n)$.

Equation 8.29 is a nonlinear in n Volterra-type integro-differential equation which we choose to solve numerically. To solve this equation, we choose to discretize the neutron population into M bins and to truncate the domain of n at some upper population N. Once Q is known, the distribution in the presence of a source may be determined by integrating Eq. 8.32 in time.

8.3 Discretization of the Neutron Number Distribution

In this section, we introduce a general numerical discretization scheme for the neutron number, which results in obtaining systems of coupled ODEs, presented in Sec. 8.3.1. In Sec. 8.3.2, we then discuss different combinations of test functions and basis functions and test their efficacy in accurately computing the convolution for the quadratic approximation case. Based on the results of Sec. 8.3.2, we then present numerical results for lumped systems for single chains and sources in Sec. 8.3.2, and

we then compare these numerical solution methods to an satz solution of the number distribution which we derive in Sec. 8.3.3.

8.3.1 A General Numerical Framework

In this section we demonstrate a general discretization method for solving the extant neutron number distribution equation, Eq. 8.29, by introducing $\{\phi_m(n)\}_{1\leq m\leq M}$, a continuous set of basis functions [73, 72]. In doing so, we may expand our solution as

$$Q(n|t) = \sum_{m=1}^{M} q_m(t)\phi_m(n). \tag{8.33}$$

By inserting Eq. 8.33 into Eq. 8.29, we find

$$\sum_{m=1}^{M}\left(\frac{\mathrm{d}q_m}{\mathrm{d}t} + \frac{\hat{\alpha}(t)}{p_\infty}q_m\right)\phi_m = \frac{\alpha}{p_\infty}\sum_{j=1}^{M}\sum_{k=1}^{M} q_j q_k \int_0^n \mathrm{d}n'\phi_j(n')\phi_k(n-n'). \tag{8.34}$$

Next, we multiply by a test function, $\xi_i(n)$ and integrate over all n to obtain M ordinary differential equations

$$\sum_{m=1}^{M}\left(\frac{\mathrm{d}q_m}{\mathrm{d}t} + \frac{\hat{\alpha}(t)}{p_\infty}q_m\right)\int_0^\infty \mathrm{d}n\xi_i(n)\phi_m(n) = \frac{\alpha}{p_\infty}\sum_{j=1}^{M}\sum_{k=1}^{M} q_j q_k \times \int_0^\infty \mathrm{d}n\xi_i(n)\int_0^n \mathrm{d}n'\phi_j(n')\phi_k(n-n'). \tag{8.35}$$

Proceeding, we define the integral coefficient matrix, $\mathbf{A}$, whose $A_{i,m}$ element is

$$A_{i,m} = \int_0^\infty \mathrm{d}n\xi_i(n)\phi_m(n). \tag{8.36}$$

The right-hand side of Eq. 8.35 can be simplified by defining

$$h^i_{j,k} = \int_0^\infty \mathrm{d}n\xi_i(n)\int_0^n \mathrm{d}n'\phi_j(n')\phi_k(n-n'), \tag{8.37}$$

which is the $(j,k)^{th}$ element of $\mathbf{H}^i$. We may write the system of equations in matrix-vector form as

$$\mathbf{A}\left(\frac{\mathrm{d}\vec{q}(t)}{\mathrm{d}t}+\frac{\hat{\alpha}(t)}{p_\infty}\vec{q}(t)\right)=\frac{\alpha}{p_\infty}\begin{bmatrix}\vec{q}^\top(t)\mathbf{H}^1\vec{q}(t)\\ \vdots \\ \vec{q}^\top(t)\mathbf{H}^M\vec{q}(t)\end{bmatrix}, \tag{8.38}$$

where $\vec{q}(t)=\langle q_1(t),\ldots,q_M(t)\rangle^\top$, and, by defining a vector of the test functions as $\vec{\xi}(n)=\langle\xi_1(n),\ldots,\xi_M(n)\rangle^\top$, we may determine the initial condition as

$$\vec{q}(0)=\mathbf{A}^{-1}\vec{\xi}(1). \tag{8.39}$$

Note that if the test functions are the Dirac delta, $\{\xi_i(n)=\delta(n-N_i)\}$, with N_i being the collocation points, $A_{i,m}=\phi_m(N_i)$, and $h^i_{j,k}=\int_0^{N_i}\mathrm{d}n'\phi_j(n')\phi_k(N_i-n')$, significantly reducing the number of integrals to be computed in constructing the matrices of Eq. 8.38. A similar set of equations may be obtained for the source equations by defining the expansion:

$$\Theta(n|t)=\sum_{m=1}^{M}\theta_m(t)\phi_m(n), \tag{8.40}$$

which provides

$$\mathbf{A}\left(\frac{\mathrm{d}\vec{\theta}(t)}{\mathrm{d}t}+\mathcal{S}\gamma(t)\vec{\theta}(t)\right)=\mathcal{S}\begin{bmatrix}\vec{\theta}^\top(t)\mathbf{H}^1\vec{q}(t)\\ \vdots \\ \vec{\theta}^\top(t)\mathbf{H}^M\vec{q}(t)\end{bmatrix}, \tag{8.41}$$

with the initial condition $\vec{\theta}(0)=\mathbf{A}^{-1}\vec{\xi}(0)$. We next explore different basis functions that are commonly employed for numerically solving such systems of equations.

8.3.2 Test Functions and Basis Functions

In this section, we consider several combinations of test functions and basis functions that will most accurately compute the first-order autoconvolution integral defined

Table 8.1: Test and basis functions analyzed for computing an exponential autoconvolution.

Case	Test Function, $\xi_\ell(n)$	Basis Function, $\phi_i(n)$	Compare To
0	Simpson's	-	$C_{A,1}$
1	Unity	Dirac	$C_{A,1}$
2	Dirac	Constant	$C_{A,1}$
3	Constant	Constant	$C_{A,2}$
4	Dirac	Linear	$C_{A,1}$
5	Constant	Linear	$C_{A,2}$
6	Linear	Linear	$C_{A,3}$

by Eq. 8.37. In order to assess which combination is best, we make the assumption that the solution decays exponentially in n, say $Q(n) = \mathrm{e}^{-n}$, in accordance with the functional form of Bell's single chain solution given by Eq. 2.48. Thus the autoconvolution of e^{-n} will have an analytical solution given by:

$$C_A(n) = \int_0^n \mathrm{d}n' \mathrm{e}^{-n'} \mathrm{e}^{-n+n'} = n\mathrm{e}^{-n}. \tag{8.42}$$

It is then the goal to determine which representation of Q will compute the result of Eq. 8.42 with the highest degree of precision.

For brevity in presenting the results below, we show the cases we consider in Table 8.1. For every case, we define a uniform grid of N_b bins and $N_m = N_b + 1$ mesh points such that the i^{th} cell is defined as $c_i = [n_i, n_{i+1}]$ with midpoint $n_{i+\frac{1}{2}}$. For the functions listed in Table 8.1, we define both the basis and test functions to be localized within a given cell and null when n is out of the bounds of the cell. When numerically computing the integrals given by Eq. 8.37, we appropriately break the integral with respect to n into a sum over the cells leading to the final cell containing

a chosen n. If the chosen n is within cell i, each of the given functions is defined as:

$$\text{Dirac: } \delta(n-\eta_i) \tag{8.43a}$$

$$\text{Constant: } \frac{1}{\Delta n_j}\delta_{j,i} \tag{8.43b}$$

$$\text{Linear: } \frac{n-n_j}{\Delta n_j}\delta_{j,i}, \quad \frac{n_{j+1}-n}{\Delta n_j}\delta_{j,i}. \tag{8.43c}$$

We note that Case 0 corresponds to the Composite Simpson's Rule and allows us to compare a relatively accurate numerical integration scheme with the typical shape functions we have selected. The "Compare To" column of Table 8.1 refers to the analytical expression that corresponds to the discretization scheme, these expressions are simply stated below for a given $n \in c_i$:

$$C_{A,1} = n_{i+1}\mathrm{e}^{-n_{i+1}} \tag{8.44a}$$

$$C_{A,2} = \frac{1}{\Delta n_i}\Big[(n_i+1)\mathrm{e}^{-n_i} - (n_{i+1}+1)\mathrm{e}^{-n_{i+1}}\Big] \tag{8.44b}$$

$$C_{A,3} = \frac{\mathrm{e}^{-n_i}}{\Delta n_i}\Big[-n_i^2 + n_i(n_{i+1}-2) + n_{i+1} - 2\Big] + \frac{\mathrm{e}^{-n_{i+1}}}{\Delta n_i}\Big[n_{i+1}+2\Big] \tag{8.44c}$$

To determine which method is most appropriate to use moving forward, we note the obvious, that it is expected for each case to increase in accuracy for a given n when the number of bins is increased. For a numerical method to be useful, we need to relax the limit of $N_b \to \infty$ and select the method for which the smallest N_b provides the highest accuracy. In essence, we will have as many equations to solve as there are bins, so it is our goal to limit $N_b \leq \lceil n \rceil$. For this reason, we show in Fig. 8.1 the absolute error between the analytical and numerical computation of the convolution integral. Clearly, the greatest error occurs for lower n because the bin resolution is more coarse. It is the desire of this study to determine the lower order probability values with highest precision, then it follows that Cases 1 and 2 will provide the most consistent and accurate computation, especially for the lowest bin numbers. In the proceeding sections, we will then use the Case 1 combination for its overall simplicity. On a final observation, we see that the Composite Simpson's

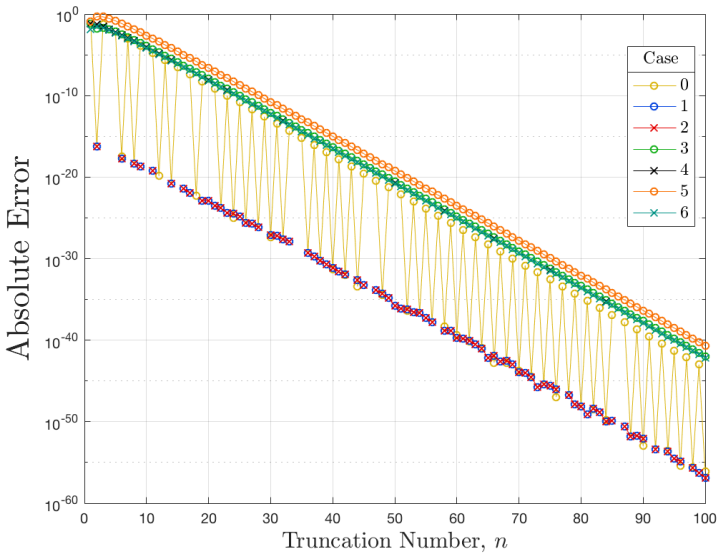

Figure 8.1: Comparison of relative error between analytical and numerical computation of exponential autoconvolution where $N_b = \lceil n \rceil$.

Rule (CSR) computation effectively oscillates between the high-error and low-error Cases. This is due to the requirement that the CSR be uniformly computed on a mesh with an even number of bins, thus the high error corresponds to meshes with odd bin numbers.

8.3.3 The Exponential Ansatz

In the previous section, we explored numerical methods for basis functions with compact support, i.e., locally defined, we now consider an example for a global basis function in n. If one were to attempt to insert Bell's single chain solution, Eq. 2.48, into the Q equation given by Eq. 8.29, one would discover that Bell's distribution is not a solution. We know, however, that the solution to Eq. 8.29 will asymptotically approach Bell's distribution in time for systems where the quadratic approximation holds, and it should also agree with the Prinja-Souto distribution given by Eq. 2.42b

for earlier times. It is then natural to attempt to obtain an analytical solution to Eq. 8.29, and we therefore make the ansatz that the solution obeys the following form:

$$Q(n|t) = A(t)\mathrm{e}^{-\lambda(t)n}. \tag{8.45}$$

We note that an identity for A in terms of λ is immediately available from the normalization of Q given by Eq. 8.24, $\int_0^\infty \mathrm{d}nQ(n|t) = P_S(t)$, to give

$$A(t) = \lambda(t)P_S(t), \tag{8.46}$$

for which we note the terminal condition: $A(0) = \lambda(0)(1)$. Inserting Eq. 8.45 into Eq. 8.29 and rearranging provides:

$$\frac{\mathrm{d}A}{\mathrm{d}t} + \frac{\hat{\alpha}(t)}{p_\infty}A = \left[A\frac{\mathrm{d}\lambda}{\mathrm{d}t} + \frac{\alpha}{p_\infty}A^2\right]n, \tag{8.47}$$

which to be true for $\forall n$, both sides of Eq. 8.47 must equal zero; two equations are then obtained:

$$\frac{\mathrm{d}A(t)}{\mathrm{d}t} = -\frac{\hat{\alpha}(t)}{p_\infty}A(t) \tag{8.48a}$$

$$\frac{\mathrm{d}\lambda(t)}{\mathrm{d}t} = -\frac{\alpha}{p_\infty}A(t). \tag{8.48b}$$

Solving Eq. 8.48a provides

$$A(t) = \lambda(0)\exp\left\{-\frac{1}{p_\infty}\int_0^t \mathrm{d}t'\hat{\alpha}(t')\right\}. \tag{8.49}$$

Inserting Eq. 8.49 into Eq. 8.48b gives

$$\lambda(t) = \lambda(0)\left[1 - \frac{\alpha}{p_\infty}\int_0^t \mathrm{d}t'\exp\left\{-\frac{1}{p_\infty}\int_0^{t'} \mathrm{d}t''\hat{\alpha}(t'')\right\}\right]. \tag{8.50}$$

Noting Eqs. 8.28 and 8.30 for systems with static reactivity, the integrals of Eqs. 8.49 and 8.51 are easily computed to yield:

$$\lambda(t) = \lambda(0)P_S(t)\mathrm{e}^{-\alpha t} = \lambda(0)\frac{P_S(t)}{\overline{n}(t)}, \tag{8.51}$$

where $\overline{n}(t)$ is the average neutron number for a single chain.From this, our ansatz solution is

$$Q(n|t) = \lambda(0)\frac{[P_S(t)]^2}{\overline{n}(t)}\exp\left\{-\lambda(0)\frac{P_S(t)}{\overline{n}(t)}n\right\}. \tag{8.52}$$

The initial condition of $Q(n|0) = \delta(n-1)$, which would require us to set $\lambda(0) = \delta(n-1)$, which would invalidate the solution given by Eq. 8.52 for $n \neq 1$. As we are interested in times for which the neutron chain has potentially evolved to populations far from $n = 1$, and can therefore be treated as a continuum, we may simply set $\lambda(0) = 1$. In doing so, we find an expression that is essentially a generalization of Bell's single chain solution by simply replacing the POI with the survival probability. We note that in the limit of $t \to \infty$, Eq. 8.52 $\to$ Eq. 2.48, and this solution is essentially a bridge between the Prinja-Souto distribution and its asymptotic counterpart, the Bell distribution.

Performing the ansatz on the source distribution, in-line with the functional form of Bell's gamma solution given by Eq. 2.49, is then:

$$\Theta(n|t) = B(t)n^b\mathrm{e}^{-\xi(t)n}. \tag{8.53}$$

Inserting into Eq. 8.32 and assuming that the exponential shape of the source solution is that same as the single chain solution, i.e. $\xi(t) = \lambda(t)$, we arrive at a system of equations:

$$\frac{\mathrm{d}B(t)}{\mathrm{d}t} = SP_S(t)B(t) \tag{8.54a}$$

$$\frac{\mathrm{d}\lambda(t)}{\mathrm{d}t} = \frac{\mathrm{d}\xi(t)}{\mathrm{d}t} = -\frac{SA(t)}{b+1}. \tag{8.54b}$$

We then solve for $B(t)$ by integrating over time, and we then use Eq. 8.54b to solve for b:

$$B(t) = B(0)\mathrm{e}^{S\int_0^t \mathrm{d}t' P_S(t')} \tag{8.55a}$$

$$b = \frac{Sp_\infty}{\alpha} - 1 = \eta - 1, \tag{8.55b}$$

We eliminate $B(0)$ using the normalization:

$$\int_0^\infty \mathrm{d}n\Theta(n) = 1 = B(0)\mathrm{e}^{-S\int_0^t \mathrm{d}t' P_S(t')}\Gamma(\eta)\lambda^{-\eta}, \tag{8.56}$$

which provides the final solution for the number distribution in the presence of a source:

$$\Theta(n|t) = \Big[\lambda(t)n\Big]^{\eta-1}\frac{\lambda(t)}{\Gamma(\eta)}\mathrm{e}^{-\lambda(t)n}, \tag{8.57}$$

which is a gamma distribution. It is again advised to set $\lambda(0) = 1$ to avoid issues with the singular initial condition of $\Theta(n|0) = \delta(n)$.

8.3.4 Numerical Results

We first compare the single chain ansatz solution from the previous section, given by Eq. 8.52, with the analytical distributions for the discrete distribution, the Prinja-Souto distribution given by Eq. 2.42b, and the continuous distribution, the Bell distribution given by Eq. 2.48. For a supercritical system of $k = 1.136$ with $P_\infty = 0.122$, we see in Fig. 8.2 that the ansatz solution is bounded by the two other solutions, and the solutions eventually converge by $t_f = 20\tau$. We also note that the ansatz solution converges to the Prinja-Souto distribution before it converges with the Bell distribution, suggesting that the ansatz solution can be used within a few lifetimes to accurately assess the number distribution.

As was demonstrated in Sec. 8.3.2, the most accurate basis-test function combination for the lowest resolution cell is the case for which the test function is set to unity and the basis function is the Dirac delta with a single collocation point per population cell. Specifically, to solve Eq. 8.29, we begin by collocating $Q(n|t)$ in, say, population cell m, denoted as c_m, at a single pivot point N_m. Doing so, we may write

$$Q(n|t) = \sum_{m=1}^{M} q_m(t)\delta(n - N_m). \tag{8.58}$$

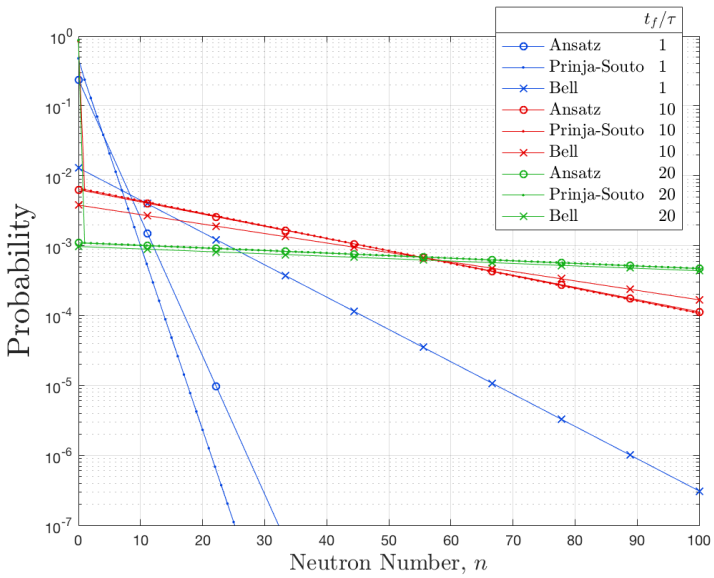

Figure 8.2: Comparison of the ansatz distribution with the Prinja-Souto and Bell distributions over time.

Table 8.2: Parameters used to compare the discrete analytical solutions with the numerical results.

$\mathcal{S}$ $[n^0/s]$	$\overline{\nu}$	$\overline{\nu^2}$	k	α $[1/s]$	η
56.6	2.5416	7.5406	1.0074	$1.1216 \cdot 10^{6}$	$3.7577 \cdot 10^{-7}$
v $[cm/s]$	τ $[s]$	χ_2'	N $[1/(cm \cdot b)]$	σ_f $[b]$	σ_c $[b]$
$1.0351 \cdot 10^{9}$	$6.5772 \cdot 10^{-9}$	$3.0125 \cdot 10^{8}$	0.0478	1.2180	1.8550

And upon inserting Eq. 8.58 into Eq. 8.29, integrating over a single bin i, c_i, such that $n \in [n_i, n_{i+1}]$, and invoking the definition of the Dirac delta function, we find with some work [70]:

$$\frac{\mathrm{d}q_i}{\mathrm{d}t} = -\frac{\hat{\alpha}(t)}{p_\infty} q_i(t) + \frac{\alpha}{p_\infty} \sum_{j=1}^{i} q_j(t) \sum_{N_j + N_k \in c_i} q_k(t), \tag{8.59}$$

with $i = 1, \ldots, M$ and the initial condition is $q_h(0) = 1$ such that $N_h = 1$.

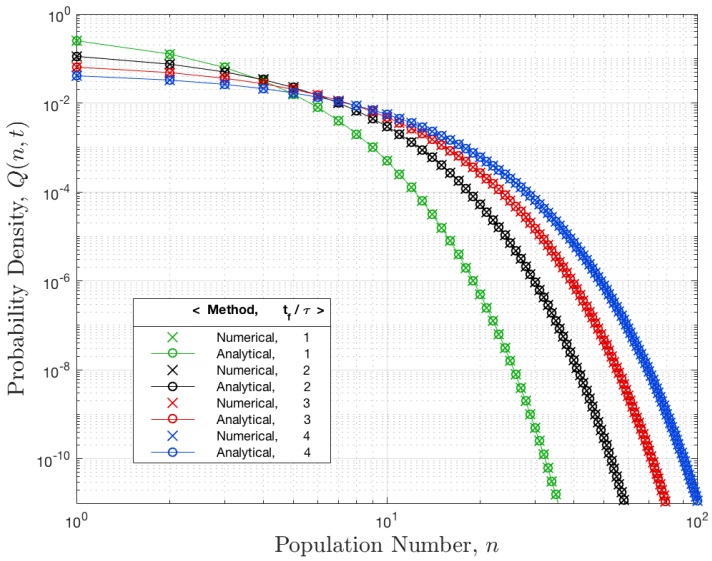

Figure 8.3: Comparison of the analytical with the numerical neutron numbers for different final times scaled by the neutron lifetime.

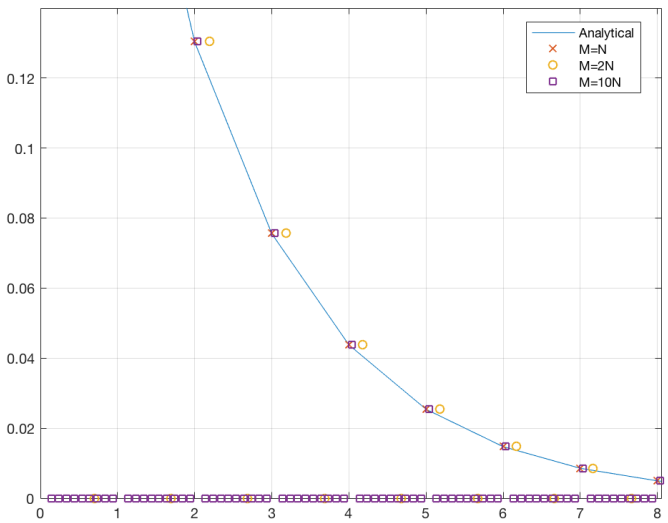

Figure 8.4: Demonstration of increasing mesh refinement on single chain solution.

We proceed in comparing the numerical solution of the set of Eqs. 8.59 to the Prinja-Souto distribution using the data in Table 8.2, shown in Fig. 8.3. The numerical solutions are solved linearly in this case and we set the number of population bins equal to the population truncation number, that is $M = N$. The corresponding extinction probabilities are $Q(0,\tau) = 0.4974$, $Q(0,2\tau) = 0.6635$, $Q(0,3\tau) = 0.7441$, $Q(0,4\tau) = 0.7949$. We also note in Fig. 8.4 that the solution using collocation requires the bin width to be $\Delta n_i = 1$, such that each bin contains a single integer value of n. This phenomenon occurs because the initial condition of Eq. 8.59 occurs at $n = 1$, and therefore the solution for bins corresponding to cells with $0 < n < 1$ will always be zero because $Q(n = 0) = 0$ for all time and thus the calculation of these coupled terms via the convolution operator will also always be zero. Once the upward bin-sweep has reached $n = 1$, we arrive at the initial condition cell which is the first non-zero probability and by continuing to the next cell, all other q_i values will equal zero and the only non-zero q_i for the cell with $n = 1$ will be multiplied by a q_j that equals zero, nullifying its contribution. This continues until the next integer bin, and will do so for all bins containing integer n. Similarly, by decreasing the bin width, the error becomes too large. For this reason, we proceed by setting the number of bins equal to the truncation population.

Clearly for supercritical systems, having the requirement that the bin number be equivalent to the truncation population will cause the system of coupled ODEs to grow to an unmanageable size for population regimes greater than $n = 10^4$. This is especially troublesome when we shift our focus to unlumped systems, which will then require us to solve a transport equation for each population size. An optional remedy is to have the initial size of the system to be a set and small and to then add equations for higher order populations as the population grows in time. This would be best accomplished by following the growth of the average of the distribution compared to the growth of the average as calculated from the moment equation. To elaborate, one would need to calculate the average from the distribution using $\overline{n}_{dist}(t) = \sum_{i=1}^{N_b} iq_i(t)$

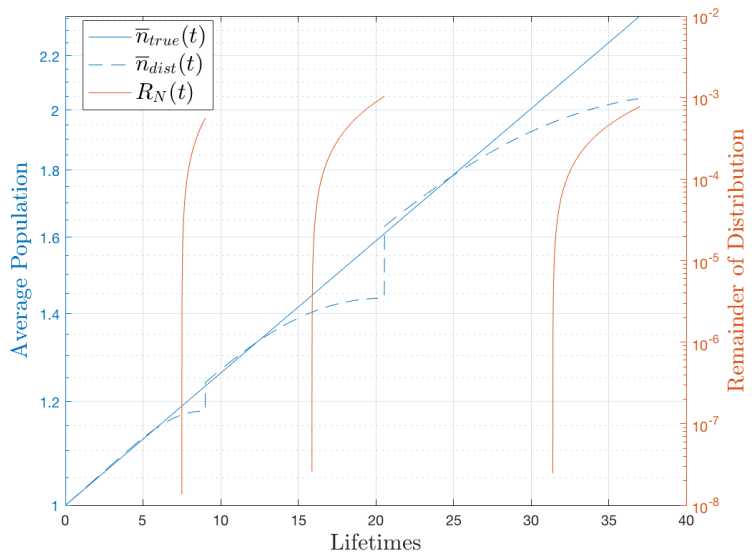

Figure 8.5: Remesh example based on the calculation of the remainder of the distribution.

for every time step and to compare it to the solution of the ODE: $\mathrm{d}\overline{n}_{true}(t)\,\mathrm{d}t = \alpha\overline{n}(t)$. Once the numerically computed average reaches a prescribed threshold relative to the analytical true average, say $\overline{n}_{dist}(t) = 0.1\overline{n}_{true}(t)$, we append more equations to the system and solve accordingly. This is accomplished by calculating the remainder of the distribution:

$$R_N(t) = 1 - \sum_{i=1}^{N_b} q_i(t)\delta(n - N_i), \tag{8.60}$$

then if $R_N(t)$ exceeds a threshold, a non-negligible quantity of the distribution is amassing for $N' > N$. In Fig. 8.5, we show such a scenario for a supercritical system of $k = 1.023$ over a range of lifetimes. We set the initial $N_b = 50$ and once the remainder equates to 10^{-3}, we increase the number of bins by a factor of 1.5.

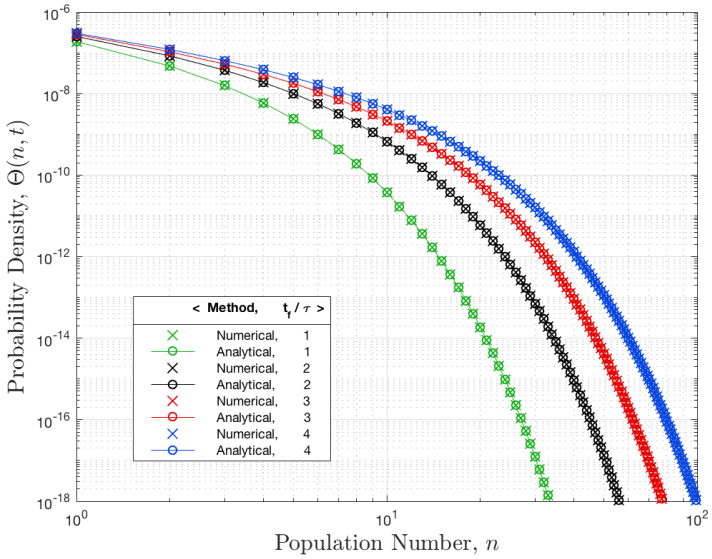

Figure 8.6: Comparison of the analytical and numerical neutron numbers in the presence of a source.

Singlet Emitting Source Equations

By performing the process that has been just described to the equation for a system with an intrinsic randomly emitting source, we define the expansion of $\Theta(n,t)$ as

$$\Theta(n|t) = \sum_{m=1}^{M} \theta_m(t)\delta(n - N_m), \tag{8.61}$$

where we have changed the notation for t to represent t_o. Note that the pivots, $\{N_m\}$, are treated as the same set of pivots used for the single chain equations. With the expansions defined by Eqs. 8.58 and 8.61, we find for the singlet emitting source case:

$$-\frac{\mathrm{d}\theta_i(t)}{\mathrm{d}t} = -\mathcal{S}\gamma(t)\theta_i(t) + \mathcal{S}\sum_{j=1}^{i} q_j(t) \sum_{N_j+N_k\in c_i} \theta_k(t), \tag{8.62}$$

with the final condition being $\theta_h(0) = 1$, such that $N_h = 0$. We show in Fig. 8.6 the numerical solution compared with the Prinja-Souto distribution for a source, given by

Eq. 2.45. This numerical solution method is forced to have the same bin widths as the single chain solution due to the computation issues we observed in the previous subsection.

In the next section, we expand our consideration of the Boltzmann Master equation into a phase-space setting and compare two solution methods. The first solves the system of equations by collocation of the neutron number which, as was elucidated in this section, requires solving as many transport equations as the truncation population.

8.4 Unlumped Systems Solution Methods

In this section, we introduce numerical solution methods of the Boltzmann Master Equation for single neutron chains and in the presence of sources that we have investigated and then show numerical results. Keeping in mind the results for the lumped system setting, we are restricted to considering two discretization methods for the neutron number variable. The first being the vastly inefficient solution by collocation which requires truncating to some finite population number and we must then solve a transport equation for every integer value of the population leading up to the truncated population number. The other method, solution by eigenfunction expansion, involves an identical process employed in Sec. 6.2. We then compare the two methods in Sec. 8.4.3, concluding the chapter. In either solution method, we begin with the BME for the single initiating neutron with the Quadratic Approximation applied, restated in operator notation as:

$$\left[-\frac{1}{v}\frac{\partial}{\partial t}+T^{\dagger}\right]Q(n|\vec{r},\hat{\Omega},t)=\Big(S^{\dagger}+F^{\dagger}-W\Big)Q(n|\vec{r},\hat{\Omega}',t)+C(Q_o,Q_o), \quad (8.63)$$

the various operators in the above equation are defined as:

$$T^{\dagger}\equiv-\hat{\Omega}\cdot\vec{\nabla}+\Sigma_t\left(\vec{r},t\right), \quad (8.64a)$$

$$S^{\dagger}\equiv\int_{4\pi}\frac{\mathrm{d}\Omega'}{4\pi}\Sigma_s\left(\vec{r},\hat{\Omega}\cdot\hat{\Omega}',t\right), \quad (8.64b)$$

$$F^{\dagger} \equiv \overline{\nu}\Sigma_f\left(\vec{r},t\right)\int_{4\pi}\frac{\mathrm{d}\Omega'}{4\pi}, \tag{8.64c}$$

$$W \equiv \Sigma_f\left(\vec{r},t\right)\chi_2\left(\vec{r},t\right)P_{S,o}(\mathcal{R},t_f|\vec{r},t)\int_{4\pi}\frac{\mathrm{d}\Omega'}{4\pi}, \tag{8.64d}$$

$$C\left(Q_o,Q_o\right) \equiv \frac{\Sigma_f\chi_2}{2}\int_0^n \mathrm{d}n' Q_o(n-n'|\vec{r},t)Q_o(n'|\vec{r},t), \tag{8.64e}$$

where $P_{S,o}(\vec{r},t) = \int_{4\pi}\frac{\mathrm{d}\Omega'}{4\pi}P_S(\vec{r},\hat{\Omega}',t)$ and $Q_o(n|\vec{r},t) = \int_{4\pi}\frac{\mathrm{d}\Omega'}{4\pi}Q(n|\vec{r},\hat{\Omega}',t)$. The final condition is $\lim_{t_f\leftarrow t}Q(n|\vec{r},\hat{\Omega},t) = \delta(n-1)$ and the boundary condition $Q(n|\vec{r},\hat{\Omega},t) = 0$ for $\vec{r}\in\partial V$, $\hat{n}_b\cdot\hat{\Omega} > 0$.

8.4.1 Solution by Collocation

The solution by collocation requires expanding the solution in the following manner:

$$Q(n,\mathcal{R},t_f|\vec{r},\hat{\Omega},t) = \sum_{m=1}^{N_b} Q_m(\mathcal{R},t_f|\vec{r},\hat{\Omega},t)\delta(n-N_m), \tag{8.65}$$

where N_m is the collocation point of cell m, where cell m is defined as $c_m = \{n|n\in(n_m,n_{m+1}]\}$. Inserting the expansion of Eq. 8.65 into Eq. 8.63 and integrating over cell ℓ allows us to isolate Q_ℓ for all linear operators to find

$$\begin{aligned}\left[-\frac{1}{v}\frac{\partial}{\partial t}+T^{\dagger}\right]Q_\ell(\vec{r},\hat{\Omega},t) = &\Big(S^{\dagger}+F^{\dagger}-W\Big)Q_\ell(\vec{r},\hat{\Omega}',t)\\ &+\frac{\Sigma_f\chi_2}{2}\sum_{j=1}^{\ell}Q_{j,o}(\vec{r},t)\sum_{N_j+N_k\in c_\ell}Q_{k,o}(\vec{r},t),\end{aligned} \tag{8.66}$$

for $\ell = 1,2,\ldots N_b$. The final condition and boundary condition are:

$$\lim_{t_f\leftarrow t}Q_\ell(\mathcal{R},t_f|\vec{r},\hat{\Omega},t) = \delta_{\ell,i} \text{ for } 1\in c_i \tag{8.67a}$$

$$Q_\ell(\mathcal{R},t_f|\vec{r},\hat{\Omega},t) = 0 \qquad \text{for } \vec{r}\in\partial V,\ \hat{n}_b\cdot\hat{\Omega} > 0. \tag{8.67b}$$

The system of equations is further discretized using a standard discrete ordinates in angle, diamond difference in space discretization [51], as well as semi-implicit backward-Euler time discretization [35]. We commence the solution by starting at

$\ell = 1$, solve with source-iteration by assuming the lagging the right-hand side of Eq. 8.66, converging, and then advancing $\ell \to \ell + 1$. We note that the convolution operator vanishes for $\ell = 1$ for reasons described in Sec. 8.3.4.

Similarly, the number distribution in the presence of a source may be collocated as

$$\Theta(n, t_f|t_o) = \sum_{m=1}^{N_b} \theta_m(t_f|t_o)\delta(n - N_m), \tag{8.68}$$

which provides an ODE for cell i

$$\begin{aligned} -\frac{\mathrm{d}\theta_i}{\mathrm{d}t_o} =& -\mathcal{S}(t_o)\theta_i(t_f|t_o)\int_V \mathrm{d}\vec{r}\,\omega(\vec{r})P_{S,o}(t_f|\vec{r}, t_o) \\ &+ \mathcal{S}(t_o)\sum_{j=1}^{i}\left(\int_V \mathrm{d}\vec{r}\,\omega(\vec{r})\int_{4\pi}\frac{\mathrm{d}\Omega'}{4\pi}Q_j(t_f|\vec{r}, \hat{\Omega}', t_o)\right)\sum_{N_j+N_k\in c_i}\theta_k(t_f|t_o), \end{aligned} \tag{8.69}$$

with the final condition $\theta_h(t_f|t_f) = \delta_{h,\ell}$ where $1 \in c_\ell$.

8.4.2 Solution by Eigenfunction Expansion

In solving the BME by means of the Eigenfunction Expansion Method, we begin by expanding the solution into adjoint eigenfunctions:

$$Q(n, \mathcal{R}, t_f|\vec{r}, \hat{\Omega}, t) = \sum_{m=1}^{\infty}\hat{Q}_m(n, t_f|t)\Psi_m^\dagger(\mathcal{R}|\vec{r}, \hat{\Omega}). \tag{8.70}$$

Inserting Eq. 8.70 into Eq. 8.63 and following the procedure outlined in Sec. 6.2, we obtain a system of equations for the time-population dependent amplitudes:

$$-\frac{\partial\hat{Q}_m(n|t)}{\partial t} = \sum_{\ell=1}^{\infty}\Delta_{m,\ell}(t)\hat{Q}_\ell(n|t) + \sum_{j=1}^{\infty}\sum_{k=1}^{\infty}D_{m,j,k}\int_0^n \mathrm{d}n'\hat{Q}_j(n'|t)\hat{Q}_k(n-n'|t) \tag{8.71}$$

where the coefficients defined above are

$$\begin{aligned} \Delta_{m,\ell}(t) = \frac{v}{\gamma_m}\Bigg\{&\left(1 - \frac{1}{k_\ell}\right)\int_V \mathrm{d}\vec{r}\,\Phi_m(\vec{r})\left[\overline{\nu}\Sigma_f(\vec{r})\right]^2\Phi_\ell^\dagger(\vec{r}) \\ &- \int_V \mathrm{d}\vec{r}\,\Phi_m(\vec{r})\overline{\nu}(\vec{r})\left[\Sigma_f(\vec{r})\right]^2\chi_2(\vec{r})P_{s,o}(\vec{r}, t)\Phi_\ell^\dagger(\vec{r})\Bigg\} \end{aligned} \tag{8.72a}$$

$$D_{m,j,k} = \frac{v}{\gamma_m}\int_V \mathrm{d}\vec{r}\,\Phi_m(\vec{r})\overline{\nu}(\vec{r})\left[\Sigma_f(\vec{r})\right]^2\frac{\chi_2(\vec{r})}{2}\Phi_j^\dagger(\vec{r})\Phi_k^\dagger(\vec{r}), \tag{8.72b}$$

and $\Phi_\ell^\dagger(\vec{r}) = \int_{4\pi}\mathrm{d}\Omega'\Psi_\ell^\dagger(\vec{r},\hat{\Omega}')/4\pi$ and similarly for the forward scalar eigenfunctions, $\Phi_\ell(\vec{r})$. The final condition and normalization constant are:

$$\lim_{t_f\leftarrow t}\hat{Q}_m(n,t_f|t) = \delta(n-1)\frac{1}{\gamma_m}\int_V \mathrm{d}\vec{r}\,\overline{\nu}\Sigma_f(\vec{r})\Phi_m(\vec{r}) \tag{8.73a}$$

$$\gamma_m = \int_V \mathrm{d}\vec{r}\,\overline{\nu}\Sigma_f(\vec{r})\Phi_m(\vec{r})\Phi_m^\dagger(\vec{r}). \tag{8.73b}$$

We are now required to discretize $\hat{Q}_m$ in n and t. Based on the success of the ansatz solution for the lumped model of Sec. 8.3.3, we choose to make the same assumption on the functional form of the modes, such that

$$\hat{Q}_m(n,t_f|t) = A_m(t_f|t)\mathrm{e}^{-\lambda_m(t_f|t)n}. \tag{8.74}$$

Inserting this ansatz solution into Eq. 8.71 and integrating over all n, we obtain a coupled system of equations:

$$\frac{\partial A_m}{\partial t} = \lambda_m\left\{\sum_{\ell=1}^{\infty}\Delta_{m,\ell}(t)\frac{A_\ell}{\lambda_\ell} + \sum_{j=1}^{\infty}\sum_{k\neq j}D_{m,j,k}\frac{A_jA_k}{\lambda_j\lambda_k}\right\} \tag{8.75a}$$

$$\frac{\partial \lambda_m}{\partial t} = -\frac{\lambda_m}{A_m}\sum_{\ell=1}^{\infty}D_{m,\ell,\ell}\frac{A_\ell^2}{\lambda_\ell}. \tag{8.75b}$$

The final conditions are obtained using the normalization of Q to P_S and the first moment ($\int_0^\infty \mathrm{d}n\,nQ(n) = \overline{n}$) to find $\lambda_m(t_f|t_f) = 1$ and $A_m(t_f|t_f) = \frac{1}{\gamma_m}\int_V \mathrm{d}\vec{r}\,\overline{\nu}\Sigma_f\Phi_m$. On a final note, if we are interested in final times for which the solution has converged to the fundamental mode (recall this occurs by one lifetime, seen in Fig. 6.9), we may truncate the expansion of Eq. 8.70 at $m = 1$. In doing so, and by converting to forward time, we find closed-form solutions for the shape functions:

$$A(t) = A(0)\exp\left\{\int_0^t \mathrm{d}t'\Delta_{1,1}(t')\right\} \tag{8.76a}$$

$$\lambda(t) = \lambda(0)\left[1 - \frac{D_{1,1,1}}{\gamma_1}\left(\int_V \mathrm{d}\vec{r}\overline{\nu}\Sigma_f\Phi_1\right)\int_0^t \mathrm{d}t'\exp\left\{\int_0^{t'}\mathrm{d}t''\Delta_{1,1}(t'')\right\}\right], \tag{8.76b}$$

where $A(0) = \lambda(0)\frac{1}{\gamma_1}\int_V \mathrm{d}\vec{r}\vec{\nu}\Sigma_f\Phi_1$ and $\lambda(0) = 1$. In essence, by reducing to the fundamental mode, we have essentially obtained the space-generalized form of the ansatz solution given by Eq. 8.52.

Under the same assumption, the closed-form solution for the number distribution in the presence of a source is given by

$$\Theta(n|t) = \Big(\lambda(t)n\Big)^{\eta-1}\frac{\lambda(t)}{\Gamma(\eta)}\mathrm{e}^{-\lambda(t)n}, \tag{8.77}$$

where

$$\eta = \frac{\mathcal{S}}{D_{1,1,1}}\int_V \mathrm{d}\vec{r}\omega(\vec{r})\Phi_1^\dagger(\vec{r}). \tag{8.78}$$

In the next section, we compare numerical solution results for the two methods discussed in this section.

8.4.3 Numerical Results

As the collocation method is cumbersome, computationally expensive, and provides no clear advantage aside from being more accurate for earlier times, we begin by simply comparing it to the fundamental mode result obtained in Sec. 8.4.2. We consider an isolated slab system composed of pure ^{235}U metal that is 5.75 cm thick, with a fundamental k-mode of $k = 1.157$. The system is divided into 100 spatial points and we restrict the time step width to $\Delta t = 10^{-3}$ s. The survival probability is calculated with the Quadratic Approximation in place using the λAM described in Sec. 6.1; we use the same survival probability for both methods to reduce the possibility of a disagreement arising from a difference in computing the W operator of Eq. 8.64d. In principle, one would compute the survival probability using the same numerical method, but this would most certainly require a higher number of modes to accurately compute the spatial integrals of the EFE.

Figure 8.7 shows the single chain solutions and their convergent agreement between the two solution methods for differing final times for $n = 1$. As was demonstrated

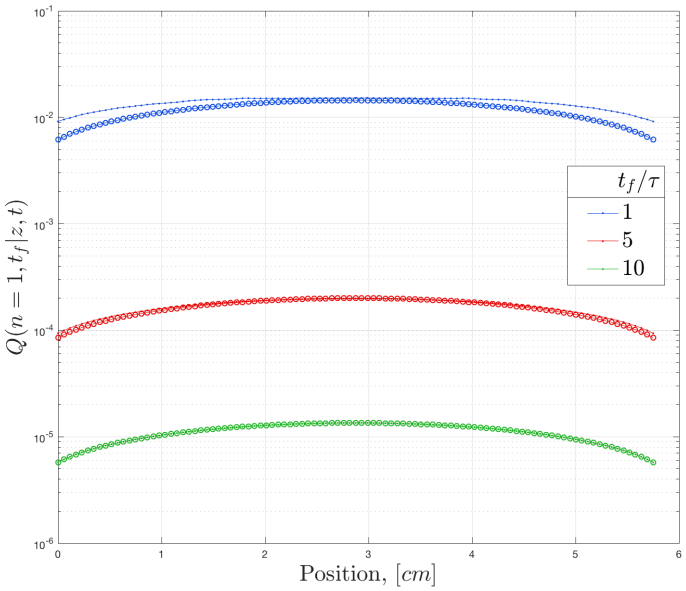

Figure 8.7: Comparison of collocation results (dotted lines) with the EFE fundamental mode results ($\circ$) in a ^{235}U slab for $n = 1$ for varying final times.

for the survival probability, the solutions settle into the fundamental mode relatively quickly and this proves to be an acceptable assumption to make. We also note that the $n = 1$ solutions agree in the center of the system for all final times shown. If we then consider Fig. 8.8, for which we are now comparing the number distribution in the center spatial cell, $z_{1/2}$. It can be seen that the same convergence occurs within the first 10 lifetimes of the introduction of the initiating neutron. This is promising and permits us to proceed to more complicated geometries if we so choose.

We conclude this section and chapter by considering the number distribution with a source for the single slab system at a final time of $t_f = 20\tau$. By altering the source strength, we can change the η value given by Eq. 8.78. It can be seen that the collocation method agrees well with the EFE method for the fundamental mode for any source strength, whether it be weak ($\eta < 1$) or strong ($\eta > 1$).

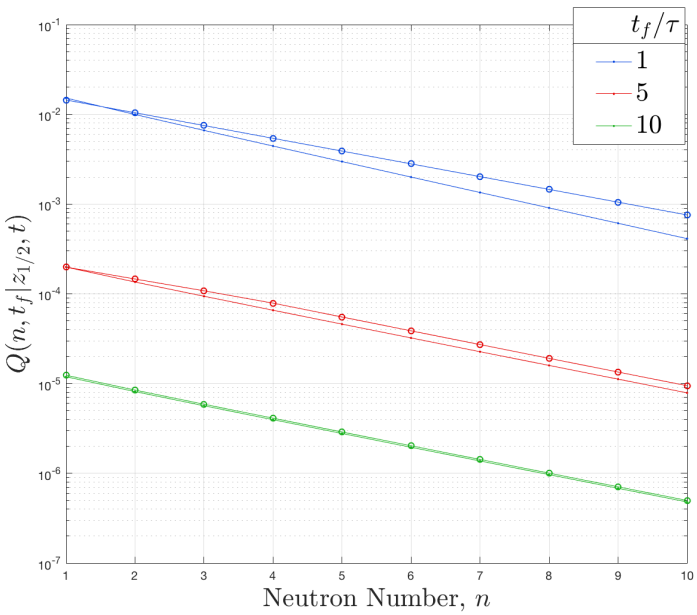

Figure 8.8: Per Fig. 8.7, but for all n in the center cell of the slab system.

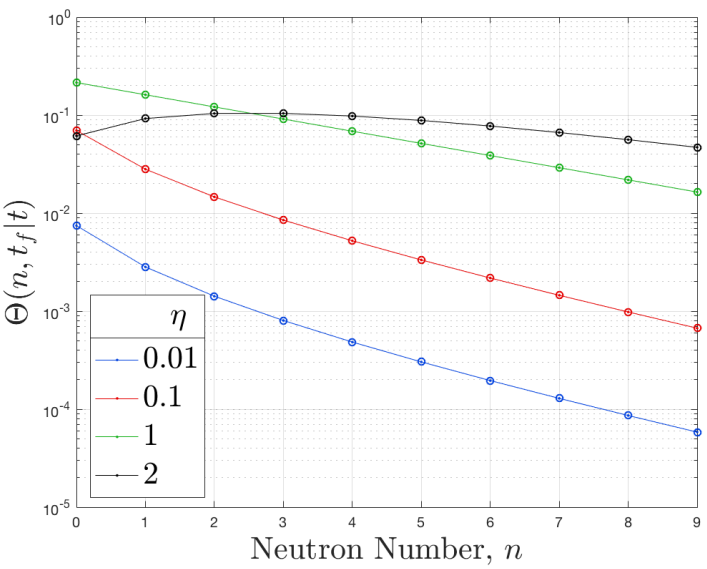

Figure 8.9: Comparison of number distributions in the presence of a source for the collocation method (dotted lines) and the fundamental mode results (∘) for varying source strengths at $t_f = 20\tau$.

Chapter 9

Conclusions & Future Work

In this chapter, we conclude the findings of this dissertation and discuss future work that would further benefit the application space of stochastic neutron transport problems. In proceeding, we discuss the primary take-aways of each chapter and then propose ideas on future work for the subject matter of each chapter.

In Chapter 2, we presented the primary results given by Prinja and Souto [11] and how those distributions asymptotically converge to Bell's distributions. Further, we developed a unique analytical solution by restricting the neutron multiplicity distribution for the emission of 0, 1, or 2 neutrons per induced fission event. This result would be more appropriately generalized to include the possibility of the emission of three neutrons in an event. Recent work has shown that a third-order nonlinear first order ODE (Abel's nonlinear ODE of the First Kind) has a general solution [10], if one is able to solve this form of the relevant characteristic equation and then invert the generating function solution, such a PDF would prove beneficial in characterizing zero-dimensional systems and benchmarking codes for which $\overline{\nu} > 2$.

In Chapter 3, we introduced the two Monte Carlo algorithms we use throughout this document. The event-based Monte Carlo (EBMC) method is widely used in large-scale codes, but the Stochastic Simulation Algorithm (SSA) is relatively new

to this application space. We showed that the SSA outperforms the EBMC for the restrictive parameter space we are interested in. In particular, we showed that by reducing the neutron multiplicity distribution to the Binary Fission Model and considering system multiplication factors within the range of $k \in [0.70, 1.30]$, the EBMC tends to take, at a minimum, 2.5 times longer to simulate the same system as the SSA. Future work would include performing a more computer-science oriented study on the efficiency of one algorithm over the other. As an example, the SSA clearly outperforms the EBMC because the SSA does not require one to save information of event times to follow all the progeny of a single initiating neutron.

In Chapter 4, we investigated systems composed of, at-most, two spherical regions with neutrons that could occupy either a fast or thermal energy group with weak fast neutron sources. Forward Master equations were derived and, from which, systems of coupled linear ODEs satisfied by the population moments were obtained. We then developed two methods for calculating the geometry-dependent transfer probabilities, the View Factor Approximation and the Sphere Point Picking Monte Carlo Method, and compared the parametric space for which the computationally superior VF approximation holds. We proceeded to apply the SSA in analyzing coupled regions of increasingly complexity while benchmarking the code with the numerical solution of the moment equation ODEs. It was shown that, for a one-group setting, a supercritical region has the capability of driving the neutron number distribution of a subcritical region to behave like a gamma distribution within a few decades of the region's neutron lifetimes. Then, by incorporating two energy groups and considering a thermal system, it was shown that the fast neutrons (born from source events and induced fission) independent distribution decays monotonically and behaves stochastically while the thermal neutron populations accumulate and their independent distribution appears unimodal and may more quickly transition to a deterministic regime. We concluded the chapter by introducing a time-dependent reactivity insertion and showing that the approach to gamma-like distributions occurs,

unsurprisingly, more abruptly. Future work may easily include a larger range of types of systems analyzed, such as a system with more than two regions, a system that requires higher energy group resolution, systems with non-multiplying barriers (for shielding calculations), or systems with different energy group sources. A possible increase in efficiency of the SSA worth exploring would be to restrict the time-step width when the population has increased to such a size that the sampled times to event occurrences becomes unmanageably small. If we force the time-step to a constant value for such situations, we would need to alter our sampling scheme to include the possibility that no event occurs in said time-interval. The choice in the size of the set time-step would be system-specific, but would certainly require knowledge of the time-dependent neutron lifetime, which would inform one of a "center of mass" that a population evolves about in a given time interval.

In Chapter 6, we discussed the primary numerical solution methods that have been developed for solving the nonlinear adjoint transport equation satisfied by the neutron survival probability. We showed the primary competitive direct solution referred to as the λ-Acceleration Method (λAM), and introduced a new indirect solution method called the Eigenfunction Expansion Method (EFE). The λAM proves to be a superior numerical scheme compared to the most direct solution method of Picard iteration, especially for marginally supercritical systems. It was then shown that the neutron chain survival and divergence probabilities in a static supercritical medium can be efficiently calculated using an expansion in k-eigenmodes. The space-angle shape of the solutIon in a nonhomogeneous planar medium equilibrates very rapidly after the initiation of the chain and for practical purposes 3 modes are sufficient to accurately capture the time variation of the survival probability, with a full fission neutron multiplicity distribution, while just 1 mode gives acceptable accuracy in steady state, i.e., for the divergence probability or POI. The order of the nonlinearity, correlated to the induced fission chain branching, has a larger effect on the solution than the number of modes retained in the expansion. In particular, the quadratic

approximation, corresponding to truncation order 2 in the nonlinear fission branching terms, is accurate for near critical systems but nonlinearity orders of 4 to 5 are necessary for more strongly supercritical media. Comparison of numerical results against the λAM, which itself was benchmarked with the MMS method, established the quantitative accuracy and computational efficiency achievable with the eigenmode expansion approach.

The eigenmode expansion has a physically appealing construct and the conclusion that as few as 2 modes are sufficient for weakly and strongly supercritical systems, suggests that more general point kinetic models may be developed for the description of strongly stochastic neutron populations. In particular, by introducing the expansion in the equation for the generating function itself, it may be possible to obtain the neutron number distribution as well, thereby generalizing the classical infinite medium solutions such as Bell's gamma distribution [3]. An obvious extension of this work is to multidimensional geometries and to energy dependent problems, both of which impact only the calculation of the eigenmodes and not the computation of the mode amplitudes. A less obvious generalization, that would greatly increase the utility of this approach, is to allow time dependent reactivity. This would be feasible if, for instance, the temporal variation of the reactivity is piecewise constant with time between step changes in reactivity being one neutron lifetime or longer to allow the modal expansion to equilibrate and hence be updated adiabatically when necessary.

In Chapter 7, we derived space, angle, and time-dependent single chain a source equations for the cumulative energy deposition distribution (the FPDF) in a system via the backward Master equation formulation; from which, equations of the moments were also derived. This new formulation has the benefit of not requiring knowledge of the neutron number distribution. We then compared results of the EBMC method with the direct numerical solution of the moment equations and showed excellent agreement. We then showed that by altering the induced fission energy deposition distribution, $W(\phi)$, the first four moments are virtually the same for supercritical

systems. We later showed that the FPDF itself does indeed have noticeable alterations in the high energy deposition tails of the distribution, suggesting that one may need to consider higher order moments in order to witness a noticeable difference in the respective profile. It was also shown that the multiplicity distribution model being used, where we compared the full distribution with the MCNP mean-preserving model, has an effect on the higher energy deposition region of the single chain FPDF. Finally, we then considered the effects of a source, where it was shown that cumulative energy deposited will eventually diverge for a source that is continuously emitting neutrons. Future work would include looking at the effects of subregions of a system to aide in the determination of potential 'hot-spots' in a given assembly. Ultimately, one would use this formulation to inform the design of a system where the temperature changes as a result of the fission energy deposition could negatively affect the integrity of the system. This would require supplementing either the FPDF or the moments into a model for the system of interest, perhaps a backward Master equation formulation for the temperature distribution of a system may be feasible. Finally, it would prove beneficial to consider using fission energy deposition distributions derived from data, which is readily available in codes such as FREYA [74].

In Chapter 8, we formulated the Boltzmann Master equation- a nonlinear adjoint transport equation satisfied by the neutron number density distribution. In a lumped system setting, we considered several numerical discretization schemes for the number distribution, which showed that typical basis and test functions used in transport methods are not as robust as we had hoped. It was found that the best results occur for the collocation method as well as by deriving an analytical generalization of Bell's distribution via an exponential solution ansatz. We then expanded our scope to include space and angle dependence, derived systems of equations for the aforementioned discretization schemes, and compared the results, showing excellent agreement for long enough times in supercritical systems for which the Quadratic Approximation is applicable. Future work would involve solving the BME for higher orders of

nonlinearity, as it is expected that for highly sub- and supercritical systems the number distribution solution will rely more heavily on the higher order autoconvolution terms. Further, one would be most interested in determining a numerical scheme that follows the collocation method, but allows one to discretize the neutron number variable to larger than unity bin widths while retaining precision. If such a scheme exists, it would be advantageous to then parallelize, as is done with the transport solver in PARTISN. Finally, if one is interested in the long-time behavior of the distribution for Quadratic Approximation applicable systems, one may consider implementing a continuous distribution function initial condition rather than the singularity initial condition that is the Dirac delta function; this will allow for one to use a basis function other than the collocation method.

Appendices

Appendix A

Mathematical Identities

Pochhammer Notation

The Pochhammer symbol, introduced by by Leo August Pochhammer, is the notation $(x)_n$, where n is a non-negative integer. It may represent either the rising or the falling factorial, with different articles and authors using different conventions. In this document, we use the convention $(x)_n$ to define the falling factorial and $x^{(n)}$ for the rising factorial. These are defined as follows:

$$\text{Falling Factorial: } (x)_n = x(x-1)(x-2)\cdots(x-n+1) = \prod_{k=0}^{n-1}(x-k) \quad \text{(A.1a)}$$

$$\text{Rising Factorial: } x^{(n)} = x(x+1)(x+2)\cdots(x+n-1) = \prod_{k=0}^{n-1}(x+k) \quad \text{(A.1b)}$$

The Gamma function

The gamma function was originally derived by Daniel Bernoulli, for complex numbers with a positive real part the gamma function is defined via a convergent improper integral:

$$\Gamma(z) = \int_0^\infty \mathrm{d}x\, x^{z-1}\mathrm{e}^{-x}, \qquad \mathbb{R}(z) > 0. \quad \text{(A.2)}$$

The gamma function is a natural extension of the factorial function to complex numbers; for any positive integer,

$$\Gamma(n) = (n-1)!. \tag{A.3}$$

Another important identity used throughout this document concerns the rising factorial of a real number x, defined by Eq. A.1b, which may be written in terms of the Gamma function:

$$x^{(n)} = x(x+1)\cdots(x+n-1) = \frac{\Gamma(x+n)}{\Gamma(x)}, \tag{A.4}$$

as well as the falling factorial given by Eq. A.1a:

$$(x)_n = x(x-1)\cdots(x-n+1) = \frac{\Gamma(x+1)}{\Gamma(x-n+1)}. \tag{A.5}$$

Finally, for large z, the gamma function asymptotically approaches a value given by Stirling's Formula:

$$\Gamma(z+1) \sim \sqrt{2\pi z}\left(\frac{z}{\mathrm{e}}\right)^z \tag{A.6}$$

Stirling Numbers of the First Kind

Stirling numbers of the first kind are the coefficients $s_1(n,k)$ in the expansion of the falling factorial, $(x)_n = x(x-1)\cdots(x-n+1)$, into powers of the variable x:

$$(x)_n = \sum_{k=0}^{n} s_1(n,k)x^k, \tag{A.7}$$

thus it is no surprise that they appear in expressions involving expansions of multitudes of derivatives.

Leibniz Integral Rule

The derivative of a definite integral is given by the formula:

$$\frac{\mathrm{d}}{\mathrm{d}x}\int_{a(x)}^{b(x)} \mathrm{d}x' f(x,x') = f(x,b(x))\frac{\mathrm{d}b(x)}{\mathrm{d}x} - f(x,a(x))\frac{\mathrm{d}a(x)}{\mathrm{d}x} + \int_{a(x)}^{b(x)} \mathrm{d}x' \frac{\partial f(x,x')}{\partial x} \tag{A.8}$$

Binomial Theorem

A polynomial of order n may be rewritten as a summation of products of the polynomial sum, x and y, such that the sum of their powers is equal to n with coefficients given by the binomial coefficient:

$$(x+y)^n = \sum_{k=0}^{n} \binom{n}{k} x^{n-k} y^k, \tag{A.9}$$

where $\binom{n}{k}$ is the binomial coefficient, defined by:

$$\binom{n}{k} = \frac{n!}{(n-k)!k!} = \frac{\Gamma(n+1)}{\Gamma(k+1)\Gamma(n-k+1)}. \tag{A.10}$$

Multinomial Theorem

The Multinomial Theorem is a generalization of the Binomial Theorem and gives the expansion of a power of a sum in terms of powers of the terms of that sum as:

$$\left(\sum_{k=1}^{K} x_k\right)^n = \sum_{j_1+j_2+\cdots+j_K=n} \binom{n}{j_1, j_2, \ldots, j_K} \prod_{k=1}^{K} x_k^{j_k} \tag{A.11}$$

where

$$\binom{n}{j_1, j_2, \ldots, j_K} = \frac{n!}{j_1! j_2! \cdots j_K!} \tag{A.12}$$

is the Multinomial Coefficient.

The Gaussian Hypergeometric Function

The Gaussian or ordinary hypergeometric function has a power series representation for $|z| < 1$ given by:

$${}_2F_1(a, b; c; z) = \sum_{k=0}^{\infty} \frac{a^{(k)} b^{(k)}}{c^{(k)}} \frac{z^k}{k!} \tag{A.13}$$

where $x^{(k)}$ is the rising factorial function using the Pochhammer notation. It is undefined (or infinite) if c equals a non-positive integer and the series terminates

if either a or b is a non-positive integer, in which case the function reduces to a polynomial.

In the text, we utilize an identity relating the Gaussian hypergeometric function to the regularized incomplete beta function, $I_z(a,b)$, for the special form of the arguments we encounter:

$$ {}_2F_1(a, 1-b; a+1; z) = aB(a,b)z^{-a}I_z(a,b), \tag{A.14}$$

where $B(a,b) = \Gamma(a)\Gamma(b)/\Gamma(a+b)$ is the Beta function.

Kummer's Confluent Hypergeometric Function

Kummer's confluent hypergeometric function, also referred to as the confluent hypergeometric function of the first kind, has a hypergeometric series given by

$$ {}_1F_1(a; b; z) = 1 + \frac{a}{b}z + \frac{a(a+1)}{b(b+1)}\frac{z^2}{2!} + \cdots = \sum_{k=0}^{\infty} \frac{a^{(k)}}{b^{(k)}}\frac{z^k}{k!}, \tag{A.15}$$

where $x^{(k)}$ is the rising factorial function using the Pochhammer notation. There is an integral representation given by:

$$ {}_1F_1(a; b; z) = \frac{\Gamma(b)}{\Gamma(b-a)\Gamma(a)} \int_0^1 \mathrm{d}t\, \mathrm{e}^{zt} t^{a-1}(1-t)^{b-a-1}, \tag{A.16}$$

where $\Gamma(z)$ is the gamma function.

Appendix B

Calculation of the Reaction Rates

The rates of interaction are inputs into all of the algorithms and methods discussed and are assumed to be known. Further, it is crucial to define quantities, such as the mean neutron lifetime and the reaction rates, in a consistent manner for a lumped model description to be accurate. To obtain general expressions for the rates, we solve the time-dependent homogeneous neutron transport equation. In doing so, we make the assumption that the system is sufficiently isolated, allowing us to apply vacuum boundary conditions. The neutron transport equation may be stated as:

$$\left[\frac{1}{v(E)}\frac{\partial}{\partial t} + \hat{\Omega}\cdot\nabla + \Sigma_t(\vec{r},E,t)\right]\psi(\vec{r},E,\hat{\Omega},t) = \frac{1}{2}\int_0^\infty \mathrm{d}E'\Sigma_s(\vec{r},E'\rightarrow E,t)\phi(\vec{r},E',t) + \frac{\chi(E)}{2}\int_0^\infty \mathrm{d}E'\nu(E')\Sigma_f(\vec{r},E',t)\phi(\vec{r},E',t). \tag{B.1}$$

In Eq. B.1, we have assumed that scattering events are isotropic, and we allow for energy dependence as we occasionally consider multigroup neutrons in this document. Initially, we simply solve Eq. B.1 using traditional numerical solution methods-namely we employ the standard discrete ordinates in angle, diamond difference in space discretization with source-iteration [51] at every time step to obtain the solution, $\psi(r,E,\mu,t)$, in one-dimensional spheres.

With the angular flux distribution in-hand, we may then determine the lifetime and reaction rates; to obtain expressions for said quantities, we perform a global balance of Eq. B.1 by integrating over the entire system volume, all energies, and all angles to yield a conservation equation of the neutron population. Evidently, in order to more accurately describe the quantities of interest, we must perform an adjoint-weighting of the transport equation [57], which is accomplished by multiplying Eq. B.1 by the adjoint flux, $\psi^{\dagger}(\vec{r}, E, \hat{\Omega})$. The adjoint-weighted conservation equation is then

$$\frac{\mathrm{d}N(t)}{\mathrm{d}t} = P(t) - L(t), \tag{B.2}$$

where N is the adjoint-weighted total neutron population, P is the adjoint-weighted production rate, and L is the adjoint-weighted loss rate, respectively defined as

$$N(t) = \int_V \mathrm{d}^3 r \int_0^{\infty} \mathrm{d}E \int_{4\pi} \mathrm{d}^2\Omega\, \psi^{\dagger}(\vec{r}, E, \hat{\Omega}) \frac{1}{v(E)} \psi(\vec{r}, E, \hat{\Omega}, t) \tag{B.3a}$$

$$P(t) = \int_V \mathrm{d}^3 r \int_0^{\infty} \mathrm{d}E \phi^{\dagger}(\vec{r}, E) \frac{\chi(E)}{2} \int_0^{\infty} \mathrm{d}E' \nu(E') \Sigma_f(\vec{r}, E', t) \phi(\vec{r}, E', t) \tag{B.3b}$$

$$\begin{aligned} L(t) = &\int_0^{\infty} \mathrm{d}E \int_{\hat{n}\cdot\hat{\Omega}>0} \mathrm{d}^2\Omega \oiint_{\partial V} \mathrm{d}A \psi^{\dagger}(\vec{r}, E, \hat{\Omega}) \left(\hat{n}\cdot\hat{\Omega}\right) \psi(\vec{r}, E, \hat{\Omega}, t) \\ &+ \int_V \mathrm{d}^3 r \int_0^{\infty} \mathrm{d}E \int_{4\pi} \mathrm{d}^2\Omega\, \psi^{\dagger}(\vec{r}, E, \hat{\Omega}) \Bigg\{ \Sigma_t(\vec{r}, E, t) \psi(\vec{r}, E, \hat{\Omega}, t) \\ &- \frac{1}{2} \int_0^{\infty} \mathrm{d}E' \Sigma_s(\vec{r}, E' \to E, t) \phi(\vec{r}, E', t) \Bigg\}, \end{aligned} \tag{B.3c}$$

where the volume and surface of the region are V and ∂V, respectively. Further, if $P(t) \neq L(t)$ and the shape function has reached its asymptotic form, the total adjoint-weighted neutron population will increase or decrease at an exponential rate given by

$$N(t) = N(0) \exp\{\alpha t\}. \tag{B.4}$$

Inserting Eq. B.4 into Eq. B.2, we find the time-dependent equation

$$\alpha N(t) = P(t) - L(t),$$

and by dividing through by the loss rate, $L(t)$, we arrive at a well-known equation:

$$\alpha\,\tau(t) = k(t) - 1, \tag{B.5}$$

where we recognize the ratio of the production rate to the loss rate as being the definition of the fundamental k-eigenmode and we have come to define the neutron lifetime as

$$\tau(t) = \frac{N(t)}{L(t)}. \tag{B.6}$$

As a consequence of this formulation of the neutron lifetime, one must solve the forward time-dependent neutron transport equation and the steady-state adjoint neutron transport equation. Once the solutions, $\psi(\vec{r}, E, \hat{\Omega}, t)$ and $\psi^{\dagger}(\vec{r}, E, \hat{\Omega})$, are known, the computation of the integrals of N and L is straight-forward and the minimalization of error is left to the discretion of one's choice in the discretization schemes of the transport equations as well as the numerical integration method used.

Equation B.6 has an intuitive interpretation as being the ratio of the total number of neutrons in the system to that of the rate of disappearance of neutrons from the system- this is simply a statement that the neutron population has a probability of disappearing which is inversely proportional to the total loss rate. We surmise that these quantities should be adjoint-weighted to provide a more realistic global balance of the rates pertaining to their true effects on the system. This adjoint-weighting scheme is a way of assessing the effects the neutron flux at a location within the system has on the entirety of the system. To provide an example, consider that a neutron born in the center of the system will, on average, live longer than a neutron born near the surface (leakage being a dominant factor in the depletion of near-surface particles), and that center-born neutron has a higher likelihood of inducing fission and thus has a greater importance to the time-evolution of the system.

Next we consider the probabilities of particular events occurring per neutron interaction. When a single neutron interacts with the system, there is an associated

probability that in that interaction the neutron is either captured, induces fission, or leaks, given by p_c, p_f, and p_ℓ, respectively. We do not consider scattering events as they do not remove neutrons from the system, nor have we allowed for multiplicative scattering events, such as $(n, 2n)$, but these types of reactions are readily incorporated into the production term, Eq. B.3b (see [57] for insightful details). These probabilities may be determined by calculating the ratio of the respective annihilation rate with that of the total annihilation rate of the system, which can be interpreted as the sum of the leakage, fission, and capture rates. Defining these rates as R_y, where $y = \{c, f, \ell, t\}$, we have

$$R_c(t) = \int_V \mathrm{d}^3 r \int_0^\infty \mathrm{d}E \int_{4\pi} \mathrm{d}^2\Omega\, \psi^\dagger(\vec{r}, E, \hat{\Omega}) \Sigma_c(\vec{r}, E, t) \psi(\vec{r}, E, \hat{\Omega}, t) \tag{B.7a}$$

$$R_f(t) = \int_V \mathrm{d}^3 r \int_0^\infty \mathrm{d}E \int_{4\pi} \mathrm{d}^2\Omega \psi^\dagger(\vec{r}, E, \hat{\Omega})\, \Sigma_f(\vec{r}, E, t) \psi(\vec{r}, E, \hat{\Omega}, t) \tag{B.7b}$$

$$R_\ell(t) = \int_0^\infty \mathrm{d}E \int_{\hat{n}\cdot\hat{\Omega}>0} \mathrm{d}^2\Omega \oiint_{\partial V_j} \mathrm{d}A \psi^\dagger(\vec{r}, E, \hat{\Omega}) \left(\hat{n} \cdot \hat{\Omega}\right) \psi(\vec{r}, E, \hat{\Omega}, t), \tag{B.7c}$$

where the sum of these rates is denoted by $R_t(t)$ and we see that $\sum_y R_y = L$. The aforementioned probabilities may then be determined with

$$p_y(t) = \frac{R_y(t)}{L(t)}. \tag{B.8}$$

In-line with the logic of our definition of $\tau(t)$, we may now determine the mean time per neutron between events of a particular event type y, τ_y, as

$$\tau_y(t) = \frac{N(t)}{R_y(t)}, \tag{B.9}$$

where it is clear that the harmonic sum of these constituent lifetimes gives

$$\frac{1}{\tau(t)} = \sum_y \frac{1}{\tau_y(t)}. \tag{B.10}$$

Finally, we may define the reciprocal of the consitutent lifetime of event y to be the probability per unit time that a neutron will undergo a collision, resulting in the effects of event y:

$$\lambda_y(t) = \frac{1}{\tau_y(t)}, \tag{B.11}$$

which are appropriately referred to as the reaction rate lifetime of event y. If one wishes to know a reaction rate within a given portion of space, energy range, and or angle distribution, one simply needs to alter the appropriate integration limits of the rates. As an example, the adjoint-weighted total neutron population within group g, E_g, would be determined as

$$N_g(t) = \int_V \mathrm{d}^3 r \int_{E_g} \mathrm{d}E \int_{4\pi} \mathrm{d}^2\Omega \, \psi^\dagger(\vec{r}, E, \hat{\Omega}) \frac{1}{v(E)} \psi(\vec{r}, E, \hat{\Omega}, t), \tag{B.12}$$

and the total population would be obtained by $N = \sum_g N_g$. As was described before, we must then solve the pair of time-dependent forward and steady-state adjoint neutron transport equations to then calculate N, the adjoint-weighted total neutron population, and the set of $R_y(t)$, the adjoint-weighted collisional outcome rates.

On a final note, one may be interested in asymptotic behavior of the system, or time-independent distributions, to which one may remove the time-dependence on the solution to the forward transport equation by striking the time derivative in Eq. B.1; in doing so, one must then solve the k-eigenvalue form of the transport equation by means of iteration.

Appendix C

Time-Dependent Reaction Rate Coefficient Tables

Table C.1: Coefficients of polynomial fits (see Eq. 4.50) for $t_{in} = 0.01\tau_2^1(0)$.

	c_4	c_3	c_2	c_1	c_0
$k_{eff,1}$	0	$5.60968 \cdot 10^{11}$	$-1.34235 \cdot 10^{7}$	$3,836.37$	0.498436
ϱ	$1.73644 \cdot 10^{17}$	$-1.47160 \cdot 10^{13}$	$1.10706 \cdot 10^{9}$	$5.27407 \cdot 10^{4}$	9.02805
$\lambda^1_{f,1}$	$4.14887 \cdot 10^{19}$	$-4.04047 \cdot 10^{15}$	$2.24620 \cdot 10^{11}$	$2.65780 \cdot 10^{6}$	374.621
$\lambda^1_{f,2}$	$2.24811 \cdot 10^{19}$	$-2.18978 \cdot 10^{15}$	$1.21667 \cdot 10^{11}$	$1.42945 \cdot 10^{6}$	200.835
$\lambda^1_{c,1}$	$1.79797 \cdot 10^{16}$	$-1.75100 \cdot 10^{12}$	$9.73429 \cdot 10^{7}$	$1,151.80$	0.162347
$\lambda^1_{c,2}$	$3.79270 \cdot 10^{18}$	$-3.69430 \cdot 10^{14}$	$2.05260 \cdot 10^{10}$	$2.41157 \cdot 10^{5}$	33.8821
$\lambda^1_{\ell,1}$	$1.54619 \cdot 10^{19}$	$-4.52878 \cdot 10^{14}$	$1.63787 \cdot 10^{11}$	$2.09524 \cdot 10^{7}$	$3,717.77$
$\lambda^1_{\ell,2}$	$1.23407 \cdot 10^{16}$	$-4.65227 \cdot 10^{11}$	$1.46661 \cdot 10^{4}$	$1.22141 \cdot 10^{8}$	2.73307
$\lambda^1_{s,1\to2}$	$2.62997 \cdot 10^{19}$	$-2.56126 \cdot 10^{15}$	$1.42387 \cdot 10^{11}$	$1.68478 \cdot 10^{6}$	237.472

Table C.2: Coefficients of polynomial fits (see Eq. 4.50) for $t_{in} = 0.1\tau_2^1(0)$.

	c_4	c_3	c_2	c_1	c_0
$k_{eff,1}$	0	$5.60968 \cdot 10^8$	$-1.34235 \cdot 10^5$	383.637	0.498436
ϱ	$1.736444 \cdot 10^{13}$	$-1.47160 \cdot 10^{10}$	$1.10706 \cdot 10^7$	$5,274.07$	9.02805
$\lambda_{f,1}^1$	$4.14887 \cdot 10^{15}$	$-4.04047 \cdot 10^{12}$	$2.24620 \cdot 10^9$	$2.65780 \cdot 10^5$	374.6218
$\lambda_{f,2}^1$	$2.24811 \cdot 10^{15}$	$-2.18978 \cdot 10^{12}$	$1.21667 \cdot 10^9$	$1.42945 \cdot 10^5$	200.835
$\lambda_{c,1}^1$	$1.79797 \cdot 10^{12}$	$-1.75100 \cdot 10^9$	$9.73429 \cdot 10^5$	115.180	0.162347
$\lambda_{c,2}^1$	$3.7927 \cdot 10^{14}$	$-3.69430 \cdot 10^{11}$	$2.05260 \cdot 10^8$	$2.41157 \cdot 10^4$	33.8821
$\lambda_{\ell,1}^1$	$1.54619 \cdot 10^{15}$	$-4.52878 \cdot 10^{11}$	$1.63787 \cdot 10^9$	$2.09524 \cdot 10^6$	$3,717.77$
$\lambda_{\ell,2}^1$	$1.23407 \cdot 10^{12}$	$-4.65227 \cdot 10^8$	$1.22141 \cdot 10^6$	$1,466.61$	2.73307
$\lambda_{s,1\to2}^1$	$2.62997 \cdot 10^{15}$	$-2.56126 \cdot 10^{12}$	$1.42387 \cdot 10^9$	$1.68478 \cdot 10^5$	237.472

Appendix D

Fortran Fission Subroutine Example

Below is an example Fortran code that was implemented to simulate a fission chain and all of its resultant progeny. The parameter `gen_cutoff` defines when one considers a single fission chain to have diverged or grown to a point that it will not extinguish within the observation interval based on the number of successive generations that have occurred in the chain. This number is normally set to 10^6, because if we have a slightly supercritical system of, say $k = 1.0001$, then if 10^6 generations have propagated the population has likely grown to a level that it will most likely not extinguish. The subroutine `BANK_NS` sorts the induced fission neutrons into the appropriate `fission_bank` and `time_bank` arrays. It also allows for dynamic array allocation so that we do not need to preallocate an unnecessarily large array at the beginning of the chain simulation. On a final note, we also follow the total population of the fission chain using the `chain_pop` value. The chain population begins at 1 due to the initial particle and we only add to the population for every time there is a fission event. From this, we specifically define a chain's population as being the total number of fissions that that chain produces and once the chain grows to a value

greater than `diverged_pop`, we terminate the fission chain simulation.

```
subroutine FISSION(t, persistent_ns)
implicit none
real(dp), intent(in) :: t
integer(sik), intent(inout) :: persistent_ns
integer(sik), allocatable :: fission_bank(:,:,:)
real(dp), allocatable :: time_bank(:,:,:)
integer(sik) :: current, next, h, i, j, k, m
integer(sik) :: gen, Num_in_step, ns, chain_pop
real(dp) :: xi, s, tt, orig_t
!Fission_bank & time_bank are partitioned into # of rows =
!t_steps, # of columns = fission locations w/in that t_step,
!2 sheets for current & next generation of neutrons
allocate(fission_bank(t_steps, 1000, 2), &
         time_bank(t_steps, 1000, 2))
fission_bank(:,:,:) = 0_sik; time_bank(:,:,:) = 0.0_dp
!As we enter this subroutine, the fission occurs at some time
!t, which we call orig_t
orig_t = t
chain_pop = 1_sik
!Start with generation 0
gen = 0_sik
mloop:do m = 1,gen_cutoff !Chain has diverged if m=gen_cutoff
   !Determine the "current" gen fission_bank column:
   if (mod(gen,2) .eq. 0_sik) then
      current = 1_sik; next = 2_sik
   else
      current = 2_sik; next = 1_sik
    end if
    fission_bank(:,:,next) = 0_sik
```

```
30      time_bank(:,:,next)     = 0.0_dp
31  !Banking time of ORIGINAL n that induced a fission chain:
32  !Note: these emitted neutrons are considered 'current' gen
33  !Note: we consider a single SF n at a time in this subroutine
34      if (gen .eq. 0_sik) then
35  tscan1:do j = 1, t_steps
36             if ((orig_t .ge. time_grid(j)) .and. &
37                 (orig_t .lt. time_grid(j+1))) then
38                 !Sample IF mult. distribution and bank # emitted
39                 call IFMD_SAMPLER(ns)
40                 if (ns .eq. 0_sik) then !No ns were emitted
41                    exit mloop !Chain dies
42                 else
43                    time_bank(j,1:ns,current)    = orig_t
44                    fission_bank(j,1:ns,current) = 1_sik
45                    exit tscan1
46                 end if
47             end if
48          end do tscan1
49      end if
50  !At this point, we have the time & # of neutrons emitted from
51  !the ORIGINAL IF event. Now track each new particle individu-
52  !ally to determine the next gen and all ensuing gens.
53
54  !Essence of the following procedure:
55  !1. Follow each n that was produced, determine if it persists,
56  !gets captured, or induces yet another fission.
57  !a. If persistent, add it to the Pn, move to next particle.
58  !b. If captured, move to next particle.
59  !c. If fission, sample IFMD and add these ns to the next gen.
```

```
60
61 tscan2:do k = 1, t_steps
62         Num_in_step = sum(fission_bank(k,:,current))
63         if (Num_in_step .eq. 0) then
64            cycle tscan2
65         else !We have ns to track
66 ncounter:do j = 1, Num_in_step
67               tt = time_bank(k,j,current)
68               call random_number(xi)
69               s  = -log(xi)/XS_a
70               tt = tt + s/vel
71               !Determine if n "leaks" from time interval
72               if (tt .ge. tf) then
73                  call BIN_POP(persistent_ns)
74                  cycle ncounter
75               end if
76               call random_number(xi)
77               if (xi .le. micro_c/micro_a) then
78                  !Captured:
79                  cycle ncounter
80               else
81                  !Fissioned:
82                  chain_pop = chain_pop + 1
83                  call IFMD_SAMPLER(ns)
84                  if (ns .eq. 0) then
85                     cycle ncounter
86                  else
87                     call BANK_NS(ns,time_bank,fission_bank)
88                  end if
89               end if
```

```
90            end do ncounter
91         end if !(Num_in_step .eq. 0) then
92      end do tscan2
93      !Updating current gen to next gen:
94      gen = gen + 1
95      fission_bank(:,:,current) = fission_bank(:,:,next)
96      time_bank(:,:,current)    = time_bank(:,:,next)
97
98      if (chain_pop .gt. diverged_pop) then
99         exit mloop
100     end if
101     if (sum(fission_bank(:,:,next)) .eq. 0) then
102        exit mloop
103     end if
104  end do mloop
105
106  deallocate(fission_bank)
107  deallocate(time_bank)
108
109  return
110  end subroutine FISSION
```

Appendix E

Iteration Scheme for the Truncated Gaussian $W(\phi)$

We wish to determine r such that $\overline{\phi}_p = 0$, the mean value of the parent/general Gaussian distribution. This is accomplished by setting $\phi_\ell = 0$ and $\overline{\phi}_p = 0$ in Eqs. 7.69a - 7.70b, which simplify to:

$$\overline{\phi} = E_f = 2\sigma_p \cdot \frac{\omega(0) - \omega(b)}{2\Omega(b) - 1} \tag{E.1a}$$

$$\sigma_\phi = rE_f = \sigma_p \sqrt{1 - \frac{2b\omega(b)}{2\Omega(b) - 1} - 4\left[\frac{\omega(0) - \omega(b)}{\Omega(b) - 1}\right]^2}, \tag{E.1b}$$

where $a = 0$, $b = \phi_u/\sigma_p$, and $\omega(0) = 1/\sqrt{2\pi}$. In order to compute r and σ_p such that $\overline{\phi} = E_f$, $\sigma_\phi = rE_f$, and $\overline{\phi}_p = 0$, we must determine the roots of Eqs. E.1a and E.1b. Employing the Newton-Raphson method to iteratively solve the transcendental-in-r and -σ_p system of equations:

$$f\left(r, \sigma_p\right) = 0 = \sigma_p A(0, b) - E_f \tag{E.2a}$$

$$g\left(r, \sigma_p\right) = 0 = r - \frac{\sigma_p}{E_f}\sqrt{1 + B(0, b) - \left[A(0, b)\right]^2}, \tag{E.2b}$$

where A and B are defined by Eq. 7.72, but we replicate them below for convenience:

$$A\left(0, b\left(\overline{\phi}_p, \sigma_p\right)\right) = \frac{\omega(0) - \omega(b)}{\Omega(b) - 1/2} \tag{E.3a}$$

Table E.1: Jacobian matrix entries for the parent Gaussian distribution iterative scheme.

	y	
	r	σ_p
$\frac{\partial f}{\partial y}$	0	$A + \sigma_p \frac{\partial A}{\partial \sigma_p}$
$\frac{\partial g}{\partial y}$	1	$-\frac{1}{E_f}\left(\sqrt{1+B-A^2} + \frac{\sigma_p}{2\sqrt{1+B-A^2}}\left(\frac{\partial B}{\partial \sigma_p} - 2A\frac{\partial A}{\partial \sigma_p}\right)\right)$
$\frac{\partial A}{\partial y}$	0	$\frac{1}{\sigma_p}\left(AB - \frac{2b^2\omega(b)}{2\Omega(b)-1}\right)$
$\frac{\partial B}{\partial y}$	0	$\frac{1}{\sigma_p}\left(B^2 - \frac{(b^2-1)b\omega(b)}{\Omega(b)-1/2}\right)$

$$B\left(0, b\left(\overline{\phi}_p, \sigma_p\right)\right) = -\frac{b\omega(b)}{\Omega(b) - 1/2}. \tag{E.3b}$$

We then iterate on r and σ_p until convergence is achieved; for the n^{th} iteration, the system of updating equations is

$$\begin{bmatrix} r_n \\ \sigma_{p,n} \end{bmatrix} = \begin{bmatrix} r_{n-1} \\ \sigma_{p,n-1} \end{bmatrix} - \mathbf{J}_{n-1}^{-1} \begin{bmatrix} f(r_{n-1}, \sigma_{p,n-1}) \\ g(r_{n-1}, \sigma_{p,n-1}) \end{bmatrix}, \tag{E.4}$$

where $\mathbf{J}_{n-1}$ is the Jacobian matrix of the previous iteration, defined as

$$\mathbf{J}_{n-1} = \begin{bmatrix} \left.\frac{\partial f}{\partial r}\right|_{(r_{n-1},\sigma_{p,n-1})} & \left.\frac{\partial f}{\partial \sigma_p}\right|_{(r_{n-1},\sigma_{p,n-1})} \\ \left.\frac{\partial g}{\partial r}\right|_{(r_{n-1},\sigma_{p,n-1})} & \left.\frac{\partial g}{\partial \sigma_p}\right|_{(r_{n-1},\sigma_{p,n-1})} \end{bmatrix}, \tag{E.5}$$

and the entries of the Jacobian matrix are listed in Table E.1 for convenience.

Bibliography

[1] PÁZSIT, I. and PÁL, L., *Neutron Fluctuations*, Elsevier, Oxford, UK (2008).

[2] ROSS, S.M. *Introduction to Probability Models* (11th ed.). (2014).

[3] BELL, G.I., "Probability Distribution of Neutrons and Precursors in a Multiplying Assembly," *Annals of Physics*, **21**, 243-283 (1963).

[4] WILLIAMS, M.M.R., *Random Processes in Nuclear Reactors*, Pergamon Press, Oxford & UK (1974).

[5] PAPOULIS, A., *Probability, Random Variables, and Stochastic Processes*, 2nd ed. New York: McGraw-Hill, 1984.

[6] PÁZSIT, I., "Theory and Use of Branching Processes in Nuclear Applications" Presentation given during the Miniworkshop on Stochastic Processes and Transport at Chalmers University. May, 2008.

[7] WEBER, M.F. and FREY, E., "Master Equations and the Theory of Stochastic Path Integrals," *Rep. Prog. Phys.*, **80**, 046601 (2017).

[8] EDDY, S.R., "A Probabilistic Model of Local Sequence Alignment That Simplifies Statistical Significance Estimation" *PLoS Computational Biology*, **4**(5): e1000069. DOI:10.1371/journal.pcbi.1000069. (2008).

[9] JOHNSON, N.L., KOTZ, S., KEMP, A.W., *Univariate Discrete Distributions* (2nd edition). Wiley. ISBN 0-471-54897-9 (Section 1.B9) (1993) .

[10] PANAYOTOUNAKOS, D.E. and ZARMPOUTIS, T.I., "Construction of Exact Parametric or Closed Form Solutions of Some Unsolvable Classes of Nonlinear ODEs (Abel's Nonlinear ODEs of the First Kind and Relative Degenerate Equations)," *International Journal of Mathematics and Mathematical Sciences*, **2011**, Article ID 387429, DOI:10.1155/2011/387429

[11] PRINJA, A., and SOUTO, F., " Probability Distributions for Neutron Multiplying Systems without Delayed Neutrons," Los Alamos National Laboratory report LA-UR 09-07886 (2009).

[12] PRINJA, A., and SOUTO, F., "Some Considerations on Stochastic Neutron Populations," *Trans. Am. Nucl. Soc.*, **102**, 255-257 (2010).

[13] PRINJA, A., " Notes on the Lumped Backward Master Equation for the Neutron Extinction/Survival Probability," Los Alamos National Laboratory report LA-UR-12-22638.

[14] O'ROURKE, P., PRINJA, A., and FICHTL, E., "Neutron Number Probability Distributions in a Subcritical System Using the Forward Master Equation," *Trans. Am. Nucl. Soc.* (2016).

[15] PRINJA, A. "Fission Number Distributions," Letter to Patrick O'Rourke. N.d. MS. Albuquerque, New Mexico.

[16] O'ROURKE, P., "Benchmarking PARTISN with Analog Monte Carlo: Moments of the Neutron Number and the Cumulative Fission Number Probability Distributions," Los Alamos National Laboratory report LA-UR 16-28191 (2016).

[17] HARRIS, D.R., *Naval Reactors Handbook*, Vol. 1, "Selected Basic Techniques," Chapter 5 (1964).

[18] BELL, G., "On the Stochastic Theory of Neutron Transport," *Nuclear Science and Engineering*, **21**, 390-401, (1965).

[19] PÁL, L., *On the Theory of Stochastic Processes in Nuclear Reactors*, *Nuovo Cim.* supp VII. 25-42 (1958).

[20] PÁL, L., *Statistical Theory of Neutron Chain Reactors*, I, II, III. Acta Physica Hungar., **14**, 345 (1962). Translation by V. Shibayev, NP-TR-951 Harwell (1962).

[21] LEWINS, J., "Linear Stochastic Neutron Transport Theory," *Proc. Royal Soc. London A*, **362**, 537 (1978).

[22] STACEY, W.M., "Stochastic Kinetic Theory for a Space- and Energy-Dependent Zero Power Nuclear Reactor Model," *Nuclear Science and Engineering*, **36**, 389-401, 1969.

[23] FEYNMAN, R., Los Alamos Scientific Laboratory, private communication, (1946).

[24] CARLSON, B., "Solution of the Transport Equation by the Sn Method," Los Alamos Scientific Laboratory Report LA-1891 (1955).

[25] CARLSON, B., LEE, C., and WORLTON, W., "The DSN and TDC Neutron Transport Codes," Los Alamos Scientific Laboratory Report LAMS-2346 (1959).

[26] BELL, G., and LEE, C., " On the Probability of Initiating a Persistent Fission Chain," LA-2608, Los Alamos National Laboratory, 1976.

[27] BAKER, R., "Probability of Initiation." Presentation. LA-UR-04-6589. 2005.

[28] BAKER, R., "Deterministic Methods for Time-Dependent Stochastic Neutron Transport," *International Conference on Mathematics and Computational Methods Applied to Nuclear Science & Engineering*, 2009.

[29] BROCKWAY, D., SORAN, P., and WHALEN, P., "Monte-Carlo Eigenvalue Calculation." Los Alamos National Laboratory, 1985.

[30] LARSEN, E.W. and ZWEIFEL, P.F., "On the Spectrum of the Linear Transport Operator," *Journal of Mathematical Physics*, **15**, 1987-1997, 1974.

[31] BETZLER, B.R. "Calculating Alpha Eigenvalues and Eigenfunctions with a Markov Transition Rate Matrix Monte Carlo Method." PhD Dissertation. University of Michigan, 2014.

[32] ATHREYA, K.B., and NEY, P.E., *Branching Processes*, Dover, New York (1972).

[33] MÉCHITOUA, B., "Monte Carlo Estimation of Nonextinction Probabilities," *Trans. Am. Nucl. Soc.*, **82**, 2000.

[34] GREGSON, M., "Time Dependent Non-Extinction Probability for Fast Burst Reactors." PhD Dissertation. University of New Mexico, 2009.

[35] ALCOUFFE, R.E., BAKER, R.S., DAHL, J.A., TURNER, S.A., and WARD, R., "PARTISN: A Time-Dependent, Parallel Neutral Particle Transport Code System," LA-UR-08-07258 (Revised 2008).

[36] BROWN, F.B., "Fundamentals of Monte Carlo Transport – Variance Reduction – Lecture 9," September 2014.

[37] GILLESPIE, D.T., "A General Method for Numerically Simulating the Stochastic Time Evolution of Coupled Chemical Reactions," *J. Comput. Phys.*, **22**(4), 403-434, 1976. DOI:10.1016/0021-9991(76)90041-3.

[38] BARTLETT, M.S., "Stochastic Processes or the Statistics of Change," *J. R. Stat. Soc. C*, **2**(1), 44-64, 1953. DOI:10.2307/2985327.

[39] FICHTHORN, K.A. and WEINBERG, W.H., "Theoretical Foundations of Dynamical Monte Carlo Simulations," *J. Chem. Phys.*, **95**(2), 1090-1096, 1991.

[40] ABATE, J. and WARD, W., "Numerical Inversion of Probability Generating Functions," *Operations Research Letters*, **12**(4), 245-251, 1992.

[41] SAXBY, J. E. M., PRINJA, A. K., and EATON, M. D., "Energy Dependent Transport Model of the Neutron Number Probability Distribution in a Subcritical Multiplying Assembly," *Nuclear Science and Engineering*, DOI: 10.1080/00295639.2017.1367569 (2017).

[42] PEARSON, K., "Contributions to the Mathematical Theory of Evolution. II. Skew Variation in Homogeneous Material," *Philosophical Transactions of the Royal Society on London A*, **186**, 343-414 (1895).

[43] FICHTL, E. and BAKER, R., "Computing the Moments of the Neutron Population Using Deterministic Neutron Transport." *International Conference on Mathematics and Computational Methods Applied to Nuclear Science & Engineering* (M&C 2013).

[44] FICHTL, E., and PRINJA, A., "The Asymptotic Probability Distribution of Fission Numbers in a Multiplying System," *Trans. Am. Nucl. Soc.* (2014).

[45] PRINJA, A., "A Stochastic Theory of Number Distributions of Fissions in a Multiplying Assembly." Letter to Erin Fichtl. N.d. MS. Albuquerque, New Mexico (2015).

[46] DUDERSTADT, J., and HAMILTON, L., *Nuclear Reactor Analysis, Nuclear Reactor Kinetics*, Wiley & Sons, pp. 257-267 (1976).

[47] PATEL, S.B., *Nuclear Physics: An Introduction.* New Delhi: New Age International. pp. 62-72. (2000).

[48] ENQVIST, A., PAZSIT, I., and POZZI, S., "The Number Distribution of Neutrons and Gamma Photons Generated in a Multiplying Sample," *Nuclear Instruments and Methods: Accelerators, Spectrometers, Detectors and Associated Equipment*, **566.2**, 598-608, (2006).

[49] KAMM, R.J. and PRINJA, A.K., "Eigenfunction Expansion of the Space-Time Dependent Neutron Survival Probability," *Trans. Am. Nucl. Soc.*, **109**, 1354 (2013).

[50] KAMM, R., "Eigenfunction Expansion of the Time and Space-Dependent Neutron Survival Probability Equation." Master's Thesis. University of New Mexico, 2005.

[51] LEWIS, E. E., and MILLER, W. F., *Computational Methods of Neutron Transport*, New York: Wiley, 1984.

[52] "GCC Releases– GNU Project– Free Software Foundation (FSF)," GNU Project. Retrieved 28-10-2019.

[53] SALARI, K., and KNUPP, P., " Code Verification by the Method of Manufactured Solutions," SAND2000-1444, Sandia National Laboratory, 2000.

[54] PAUTZ, S., "Verification of Transport Codes by the Method of Manufactured Solutions: The ATTILA Experience," LA-UR-01-1487, Los Alamos National Laboratory, 2001.

[55] MACHORRO, E., "Discontinuous Galerkin Finite Element Method applied to the 1-D Spherical Neutron Transport Equation," UCRL-JRNL-216956, Lawrence Livermore National Laboratory, 2005.

[56] SUTTON, T.M., LaCHARITE, A.D., PRINJA, A.K. "Marduk: A Monte Carlo Code for Analyzing Stochastic Neutron Population Dynamics," *International Conference on Mathematics & Computational Methods Applied to Nuclear Science & Engineeering*, 2017.

[57] SPRIGGS, G.D., BUSCH, R.D., "On the Definition of Neutron Lifetimes in Multiplying and Non-multiplying Systems," Los Alamos National Laboratory report LA-13260-MS, 1997.

[58] CENGEL, Y.A. and GHAJAR, A.J. *Heat and Mass Transfer*, 4^{th} Edition (2011).

[59] JONES, L.R., "Diffuse Radiation View Factors Between Two Spheres," *Journal of Heat Transfer*, **87(3)**, 421-422, 1965.

[60] FELSKE, J.D., "Approximate Radiation Shape Factors Between Two Spheres," *Journal of Heat Transfer*, **100(3)**, 547-548, 1978.

[61] MILLER, J.R., "Geometric Approaches to Nonplanar Quadric Surface Intersection Curves," *ACM Trans. on Graphics*, **6**(4), 274-307, 1987.

[62] LEEMIS, L.M. and MCQUESTION, J.T., "Univariate Distribution Relationships," *American Statistician*, **62**(1), 45-53, 2008.

[63] SHAMPINE, L.F., and GORDON, M.K., *Computer Solution of Ordinary Differential Equations: The Initial Value Problem* Freeman, San Francisco, 1975.

[64] O'ROURKE, P.F. and PRINJA, A.K., "Solution of the Neutron Survival Probability Equation Using k-Eigenmode Expansion," *Annals of Nuclear Energy*, **134**, 178-192, 2019.

[65] PRINJA, A.K. and O'ROURKE, P.F., "A Stochastic Theory of Deposited Fission Energy in Neutron Chains," *Proceedings of The International Conference on Mathematics and Computational Methods applied to Nuclear Science and Engineering* (M&C 2019) (2019).

[66] FELLER, W., *An Introduction to Probability Theory and Its Applications* Vols. 1 & 2, Wiley (1968).

[67] LESTONE, J., "Energy and Isotope Dependence of Neutron Multiplicity Distributions," Los Alamos National Laboratory report, LA-UR-05-0288 (2005).

[68] RISING, M., and SOOD, A., "Using the MCNP6.2 Correlated Fission Multiplicity Models, CGMF and FREYA," Los Alamos National Laboratory report, LA-UR-17-20799 (2017).

[69] LESTONE, J., "A Comparison Between Two Evaluations of Neutron Multiplicity Distributions," Los Alamos National Laboratory report, LA-UR-08-1084 (2008).

[70] RAMKRISHNA, D., *Population Balances: Theory and Applications to Particulate Systems in Engineering*, Academic Press, 2000.

[71] CIRNU, M., "Initial-Value Problems for First-Order Differential Recurrence Equations with Auto-Convolution", *Electronic Journal of Differential Equations*, **2011**(2), 1-13 (2011).

[72] SANDU, A., and BORDEN, C., "A Framework for the Numerical Treatment of Aerosol Dynamics", *Applied Numerical Mathematics*, **45**(4), 475-497 (2005).

[73] SANDU, A., "Piecewise Polynomial Solutions of Aerosol Dynamic Equation", *Aerosol Sci. and Tech.*, **40**(4), 261-263 (2004).

[74] HAGMANN, C.A., RANDRUP, J., and VOGT, R.L., "FREYA- A New Monte Carlo Code for Improved Modeling of Fission Chains", Lawrence Livermore National Laboratory report, LLNL-PROC-561431 (2012).